

**Glycan-based biomarkers for the quality assurance
in stem cell therapy**

—
**Cell surface N-glycosylation of human stem cells
and its changes during the process of differentiation**

Dissertation zur Erlangung des akademischen Grades
des Doktors der Naturwissenschaften (Dr. rer. Nat.)

eingereicht im Fachbereich Biologie, Chemie, Pharmazie
der Freien Universität Berlin

vorgelegt von
Houda Montacir
aus Berlin, Deutschland

Dezember 2013

Die vorliegende Arbeit wurde in der Arbeitsgruppe von Dr. Véronique Blanchard in der Zeit von November 2010 bis Dezember 2013 am Institut für Laboratoriumsmedizin, Klinische Chemie und Pathobiochemie der Charité-Universitätsmedizin Berlin, Campus Virchow Mitte, angefertigt.

1. Gutachterin: Dr. Véronique Blanchard

2. Gutachter: Prof. Dr. Rudolf Tauber

Disputation am: 20.05.2014

Wissenschaftliche Beiträge

Publikationen

D. M. M. Jaradat, H. Hamouda, C. P. R. Hackenberger, *Eur. J. Org. Chem.* **2010**, *Solid-phase synthesis of phosphoramidate-linked glycopeptides*

M. Ullah, H. Hamouda, S. Stich, M. Sittinger, and J. Ringe, *BioResearch Open Access* **2012**, *A Reliable Protocol for the Isolation of Viable, Chondrogenically Differentiated Human Mesenchymal Stem Cells from High-Density Pellet Cultures*

H. Hamouda, M. Ullah, M. Berger, M. Sittinger, R. Tauber, J. Ringe, and V. Blanchard, *Stem Cells and Development* **2013**, *N-Glycosylation Profile of Undifferentiated and Adipogenic Differentiated Human Bone Marrow Mesenchymal Stem Cells - Towards a Next Generation of Markers for Regenerative Medicine*

H. Hamouda, M. Kaup, M. Ullah, M. Berger, V. Sandig, R. Tauber, and V. Blanchard, *Journal of Proteome Research*, *Rapid analysis of cell surface N-glycosylation of living cells using mass spectrometry*, **in Revision**

Poster

H. Hamouda, M. Kaup, A. Kamalakumar, R. Tauber, M. Berger and V. Blanchard, *N-glycosylation status of alpha-1 antitrypsin in sera of patients suffering from ovarian cancer*, The 5th Glycan Forum **2011**, Berlin

H. Hamouda, M. Kaup, A. Kamalakumar, R. Tauber, M. Berger and V. Blanchard, *N-glycosylation status of alpha-1 antitrypsin in sera of patients suffering from ovarian cancer*, IFCC-WorldLab **2011**, Berlin

H. Hamouda, M. Ullah, M. Kaup, V. Blanchard, R. Tauber, J. Ringe, M. Sittinger and M. Berger, *The N-glycome as a potential marker to differentiate human mesenchymal stem cells from adipocytes*, The 6th Glycan Forum **2012**, Berlin

H. Hamouda, M. Ullah, M. Berger, M. Sittinger, R. Tauber, J. Ringe and V. Blanchard, *N-Glycosylation Profile of Undifferentiated and Adipogenic Differentiated Human Bone Marrow Mesenchymal Stem Cells - Towards a Next Generation of Markers for Regenerative Medicine*, The 7th Glycan Forum **2013**, Berlin

Die Dissertation wurde in englischer Sprache verfasst.

Danksagung

Ich bedanke mich bei Dr. Markus Berger und Dr. Véronique Blanchard für die Aufnahme in die Arbeitsgruppe, die Überlassung des sehr interessanten Projektes sowie der wissenschaftlichen Betreuung meiner Doktorarbeit. Frau Dr. Véronique Blanchard danke ich zusätzlich für die Übernahme des ersten Gutachters. Zudem bedanke ich mich bei Prof. Dr. Rudolf Tauber für das stete Interesse an meiner Arbeit sowie der Übernahme des zweiten Gutachters. Weiterhin möchte ich mich bei Dr. Matthias Kaup für die wissenschaftliche Betreuung und immer gewährte fachliche Hilfe während des ersten Jahres meiner Doktorarbeit bedanken.

Mein großer Dank gilt den Kooperationspartnern dieses Projektes, der AG Ringe (Charité-Universitätsmedizin Berlin, BCRT, Labor für Tissue Engineering/ Klinik für Rheumatologie) sowie der AG Zeilinger (Charité-Universitätsmedizin Berlin, BCRT, Biomedizinisches Forschungszentrum). Ich bedanke mich sehr bei Dr. Jochen Ringe sowie Mujib Ullah für die Überlassung aller wertvollen Stammzellproben, der immer gewährten fachlichen Diskussionen sowie sehr guten Zusammenarbeit während dieses Projektes. Mein Dank gilt Dr. Katrin Zeilinger, Dr. Fanny Knöspel sowie Thomas Urbaniak für die Übergabe der Stammzellen sowie Hepatozyten. Ich bedanke mich zudem bei der Investitionsbank Berlin, die dieses Projekt finanziell unterstützt hat.

Ich bedanke mich ganz herzlich bei den ehemaligen und derzeitigen Mitgliedern der Arbeitsgruppe „Glycodesign und Glykoanalytik“ für die kompetente Zusammenarbeit und angenehme Arbeitsatmosphäre während meiner Doktorarbeit. Insbesondere möchte ich mich hier nochmals namentlich bei Elena Frisch, Julia Rosenlöcher, Zemra Skenderi, Nilgün Neziroglu, Aji Kandeepan, Detlef Grunow, Astrid Lusch, Xi Liu, Karina Biskup, Christina und Peter Hoffmann, Christian Schwedler und Dominique Petzold bedanken.

Ich bedanke mich bei all meinen lieben Freunden und Verwandten, die mich immer unterstützt haben und mir immer Wärme und Freude geschenkt haben, insbesondere meiner Oma Zoubeyda, meinem Onkel Mohammed und meiner Tante Nadja, meinen lieben Freunden Fatimah, Samiha, Taybet, Aref, Zena, Asmaa, Nour und Saskia.

Mein großer Dank gilt meinen liebevollen Eltern Hédi und Moufida Hamouda sowie meinen Geschwistern Imen, Ferdaus und Hamza, die mich während dieser Zeit immer unterstützt haben und denen ich den Erfolg dieser Arbeit zu verdanken habe. Zudem danke ich meinem Schwager Rabie Ben Meftah, vor allem für die zwei wundervollen Wonnepoppen Takoia und Zahra, die stets Licht und Freude in mein Leben strahlen lassen.

Ich bedanke mich ganz herzlich bei meinem Ehemann Othman Montacir für die liebevolle Unterstützung, sowohl im privaten als auch im wissenschaftlichen Bereich.

Elhamdulillah Wa-Shoukro Lillah Rabbi El3alamin, Era7man, Era7im, Wa La 7awla Wa La Quwwata Illa Billah.

بِسْمِ اللّٰهِ الرَّحْمٰنِ الرَّحِیْمِ

والصَّلَاةِ وَالسَّلَامِ عَلٰی اَشْرَفِ الْمُرْسَلِیْنَ

اللهم انفعني بما علمتني، وعلمي ما ينفعني، وزدني علماً

Table of contents

ZUSAMMENFASSUNG	14
ABSTRACT	16
1 INTRODUCTION	18
1.1 Stem cells	18
1.1.1 Embryonic stem cells	19
1.1.2 Adult stem cells	21
1.1.2.1 Mesenchymal stem cells	21
1.1.3 Embryonic and mesenchymal stem cells in regenerative medicine and tissue engineering	22
1.2 Glycosylation	24
1.2.1 Glycocalyx	25
1.2.2 N-Glycosylation	26
1.2.3 O-Glycosylation	30
1.2.4 Function of glycans in stem cells and stem cell markers	32
1.3 Profiling of cell surface glycosylation	33
1.3.1 Lectin staining of the cell surface	33
1.3.2 Cell membrane extraction	35
1.3.3 Release of N- and O-glycans	36
1.3.4 MALDI-TOF-MS	37
1.3.5 CE-LIF	38
1.4 Aim of the work	41
2 RESULTS	42
2.1 Design and optimisation of a rapid analysis method to profile cell surface N-glycosylation of living cells	42
2.1.1 Analysis of cell surface N-glycosylation using the cell membrane preparation protocol	42

2.1.2	Analysis of cell surface N-glycosylation using the new method that releases only cell surface N-glycans from living cells	43
2.1.3	Reproducibility of the new method	45
2.1.4	Analysis of the N-glycome by membrane preparation protocol after cell surface digestion of living cells with trypsin	46
2.1.5	Cell surface N-glycosylation of AGE1.HN, CHO-K1 and Hep G2 cells	48
2.1.6	CE-LIF analysis of cell surface N-glycosylation of HEK 293, AGE1.HN, CHO-K1 and Hep G2 cells	50
2.1.7	Verification of identified N-glycan structures of HEK 293, AGE1.HN, CHO-K1 and Hep G2 with MALDI-TOF/TOF sequencing and exoglycosidase digestions	52
2.1.8	Verification of Neu5Gc in CHO-K1 cells using HPLC	57
2.2	N-Glycosylation profile of mesenchymal stem cells and its changes during adipogenic, chondrogenic and osteogenic differentiation	58
2.2.1	N-Glycosylation profile of undifferentiated and adipogenically differentiated human bone marrow mesenchymal stem cells	58
2.2.1.1	Analysis strategy for N-glycans derived from undifferentiated and adipogenically differentiated human bone marrow mesenchymal stem cells	58
2.2.1.2	N-Glycome of mesenchymal stem cells and its changes during adipogenic differentiation	58
2.2.1.3	CE-LIF analysis of N-glycans from undifferentiated and adipogenically differentiated human bone marrow mesenchymal stem cells	64
2.2.1.4	Verification of identified N-glycan structures of undifferentiated and adipogenically differentiated mesenchymal stem cells with MALDI-TOF/TOF sequencing and exoglycosidase digestions	66
2.2.1.5	Gene expression analysis of undifferentiated and adipogenically differentiated mesenchymal stem cells	69
2.2.2	N-Glycosylation profile of undifferentiated and chondrogenically differentiated human bone marrow mesenchymal stem cells	70
2.2.2.1	N-Glycome of mesenchymal stem cells and its changes during chondrogenic differentiation	70
2.2.2.2	CE-LIF analysis of N-glycans from undifferentiated and chondrogenically differentiated human bone marrow mesenchymal stem cells	75
2.2.2.3	Verification of identified N-glycan structures in undifferentiated and chondrogenically differentiated mesenchymal stem cells with MALDI-TOF/TOF sequencing and exoglycosidase digestions	75
2.2.2.4	N-Glycosylation profile of chondrogenically differentiated mesenchymal stem cells with their extracellular matrix	78
2.2.2.5	CE-LIF analysis of N-glycans from chondrogenically differentiated mesenchymal stem cells with their extracellular matrix	82

2.2.3	N-Glycosylation profile of undifferentiated and osteogenically differentiated human bone marrow mesenchymal stem cells	83
2.2.3.1	N-Glycome of mesenchymal stem cells and its changes during osteogenic differentiation	83
2.2.3.2	CE-LIF analysis of N-glycans from undifferentiated and osteogenically differentiated human bone marrow mesenchymal stem cells	87
2.2.3.3	Verification of identified N-glycan structures in undifferentiated and osteogenically differentiated mesenchymal stem cells with MALDI-TOF/TOF sequencing and exoglycosidase digestions	88
2.2.3.4	N-Glycosylation profile of osteogenically differentiated mesenchymal stem cells with their extracellular matrix	90
2.2.4	Glycan-based biomarkers of adipogenically, chondrogenically and osteogenically differentiated mesenchymal stem cells	94
2.3	N-Glycosylation profile of mesenchymal stem cells depends on the passage number	98
2.4	N-Glycosylation profile of chondrogenic dedifferentiated cells	100
2.5	N-Glycosylation profile of undifferentiated embryonic stem cells and its changes during endoderm differentiation into hepatocyte-like cells	104
2.5.1	N-Glycosylation profile of embryonic stem cells before and after differentiation into hepatocyte-like cells	104
2.5.2	CE-LIF analysis of N-glycans from undifferentiated embryonic stem cells and hepatocyte-like cells	108
2.5.3	Verification of identified N-glycan structures in undifferentiated embryonic stem cells and hepatocyte-like cells with MALDI-TOF/TOF sequencing and exoglycosidase digestions	109
2.5.4	Glycan-based biomarkers of undifferentiated embryonic stem cells and hepatocyte-like cells	111
3	<u>DISCUSSION</u>	113
3.1	Rapid analysis of cell surface N-glycosylation of living cells	113
3.2	N-Glycosylation profile of undifferentiated and adipogenically, chondrogenically and osteogenically differentiated human bone marrow mesenchymal stem cells	116
3.2.1	Adipogenic differentiation of human mesenchymal stem cells	116
3.2.2	Chondrogenic differentiation of human mesenchymal stem cells	120
3.2.3	Osteogenic differentiation of human mesenchymal stem cells	122

3.3 N-Glycosylation profile of undifferentiated embryonic stem cells and hepatocyte-like cells	123
3.4 Conclusion	126
4 MATERIAL AND METHODS	128
4.1 Devices	128
4.1.1 Electrophoresis	128
4.1.2 Cell culture	128
4.1.3 Centrifuges	128
4.1.4 Other devices	128
4.2 Consumables	129
4.2.1 Chemicals	129
4.2.2 Enzymes	130
4.2.3 Standards	131
4.2.4 Other consumables	131
4.2.5 Cell culture	131
4.2.6 Cell lines	132
4.3 Cell biological methods	132
4.4 Cell culture	132
4.4.1 Cell culture of HEK 293, CHO-K1, AGE1.HN and Hep G2	132
4.4.2 Generation of cryocultures	133
4.5 Protein biochemical methods	133
4.5.1 Isolation of cell membrane glycoproteins	133
4.5.2 Protein concentration determination by BCA assay	134
4.5.3 SDS polyacrylamid gel electrophoresis (SDS-PAGE)	134
4.5.3.1 Peparation of stacking and separation gels	134
4.5.3.2 Sample preparation and application on the gel	134
4.5.4 Coomassie staining	135
4.6 Analytical methods for glycan analysis	135
4.6.1 Tryptic digestion of cell membrane (glyco)proteins	135

4.6.2	Release of N-glycans from cell membrane (glyco)proteins by PNGase F	135
4.6.3	Release of N-glycans from cell membrane (glyco)proteins by Endo H followed by PNGase F	135
4.6.4	Enzymatic release and isolation of cell surface N-glycans	136
4.6.5	Purification of N-glycans	136
4.6.5.1	Calbiosorb	136
4.6.5.2	C18 reversed phase chromatography	136
4.6.5.3	Carbograph	137
4.6.5.4	C18 reversed phase chromatography of permethylated N-glycans	137
4.6.5.5	Self-made graphite micro column	137
4.6.5.6	Lyophilisation of samples	138
4.6.6	Exoglycosidase digestions of N-glycans	138
4.6.7	Desialylation of N-glycans	139
4.6.8	Derivatisation of N-glycans	139
4.6.8.1	Permethylation	139
4.6.8.2	2AB-labeling	139
4.6.8.3	APTS-labeling	139
4.6.9	MALDI-TOF-MS	139
4.6.10	CE-LIF	140
4.6.11	Sialic acid determination using HPLC	140
4.7	Statistical analysis	141
4.8	Softwares	141
5	REFERENCES	142
6	APPENDIX	154

List of abbreviations

2AB	2-Aminobenzamide
A1AT	alpha-1-antitrypsin
ACCA	α -Cyano-4-hydroxycinnamic acid
ACN	Acetonitrile
AEM	Adenovirus Expression Medium
APS	Ammonium persulfate
APTS	8-aminopyrene-1,3,6-trisulfonic acid
Asp	Aspartic acid
Asn	Asparagine
ATT	6-Aza-2-thiothymine
BCA	Bicinchoninic acid
BSA	Bovine serum albumin
CE-LIF	Capillary electrophoresis laser-induced fluorescence
CHO	Chinese hamster ovary
CID	Collision induced dissociation
CMP	Cytidine monophosphate
Cys	Cysteine
DH	Dextran hydrolysate
DHB	2,5-dihydroxybenzoic acid
DMB	1,2-diamino-4,5-methylenedioxybenzene
DMSO	Dimethyl sulfoxide
Dol-PP	Dolichol phosphate
DTE	1,4-Dithioerythriol
ECM	Extracellular matrix
EDTA	Ethylenediaminetetraacetic acid
EGCs	Embryonic germ cells
EGF	Epidermal growth factor
Endo H	Endo- β -N-acetylglucosaminidase H
ER	Endoplasmic reticulum
ESCs	Embryonic stem cells
FA	Formic acid
FAC	Frontal affinity chromatography
FACS	Fluorescence-activated cell sorting
FCS	Fetal calf serum
FGF	Fibroblast growth factor

Fuc	Fucose
FUT8	Fucosyltransferase 8 (alpha (1,6) fucosyltransferase)
Gal	Galactose
GalNAc	N-Acetylgalactosamine
GDP	Guanosin diphosphate
Glc	Glucose
GlcNAc	N-Acetylglucosamine
GU	Glucose units
HEK 293	Human Embryonic Kidney 293
Hep G2	Hepatocellular carcinoma human cell line
HPAEC-PAD	High Performance Anion-Exchange Liquid Chromatography with Pulsed Amperometric Detection
HPLC	High Performance Liquid Chromatography
HSCs	Hematopoietic stem cells
ICM	Inner cell mass
KDN	2-keto-3-deoxy-D-glycero-D-galacto-nononic acid
LacNAc	N-Acetylglucosamine
LC-ESI-MS	Liquid Chromatography-Electrospray Ionization-Mass Spectrometry
Man	Mannose
MALDI-TOF-MS	Matrix-Assisted Laser Desorption Ionization Time-of-Flight Mass spectrometry
MSCs	Mesenchymal stem cells
Neu5Ac	N-Acetylneuraminic acid
Neu5Gc	N-Glycolylneuraminic acid
NMR	Nuclear Magnetic Resonance
NSC	Neuronal stem cell
OA	Osteoarthritis
Oct	Octamer binding transcription factor
OST	Oligosaccharyl-transferase
PBS	Phosphate buffered saline
PCR	Polymerase chain reaction
PEO	Polyethylene oxide
PGCs	Primordial germ cells
PNGase F	Peptide-N ⁴ -(N-acetyl-β-D-glucosaminyI)-asparagin amidase F
Pro	Proline
PSA-NCAM	Polysialylated neuronal cell adhesion molecule
PVA	Polyvinyl alcohol

SCs	Stem cells
SDS	Sodium dodecyl sulfate
SEM	Standard error of mean
Ser	Serine
SRY-box 2	Sex determining region Y
SSEA	Stage specific embryonic antigen
ST3Gal1	<i>Beta</i> -galactoside alpha-2,3-sialyltransferase 1
TEMED	N,N,N',N'-Tetramethylethylenediamine
TFA	Trifluoroacetic acid
THF	Tetrahydrofurane
Thr	Threonine
Trp	Tryptophan
TRA	Tumor rejection antigen
Tyr	Tyrosine
UDP	Uridin diphosphate
UV	Ultraviolet

Zusammenfassung

Die Glykokalyx ist eine dichte Schicht an der Zelloberfläche, die sich aus komplexen Kohlenhydratstrukturen zusammensetzt. Qualitative und quantitative Veränderungen des Glykosylierungsmusters der Zelloberfläche können genutzt werden, um bestimmte Stammzellpopulationen zu identifizieren, um die Differenzierung einer Stammzelle (SZ) zu verfolgen sowie den Verlust des SZ-Status festzustellen, was von großer Bedeutung auf dem Gebiet der regenerativen Medizin sowie des *Tissue Engineerings* ist.

In der vorliegenden Arbeit wurde eine einfache, schnelle, reproduzierbare und sensitive Methode zur Charakterisierung des N-Glykosylierungsprofils der Zelloberfläche etabliert und optimiert. Die häufig genutzte Methode zur Analyse der N-Glykosylierung von Zellen besteht aus der Isolierung von Membranglykoproteinen, der einer enzymatischen N-Glykanfreisetzung folgt. Jedoch ist bei Anwendung dieser Methode der Anteil der N-Glykane vom High-Mannose-Typ relativ hoch, wobei diese vorwiegend aus intrazellulären Proteinen des endoplasmatischen Retikulums (ER) stammen können. Für die neu etablierte Methode, die direkt Glykopeptide der Zelloberfläche freisetzt, konnte mittels MALDI-TOF-MS eine Erniedrigung des Anteils an N-Glykanen vom High-Mannose-Typ von 90 % auf 10 % bestätigt werden. Zudem konnte die Sensitivität der Detektion sowie Quantifizierung der N-Glykane vom Komplex-Typ stark verbessert werden. Die Selektivität der neuen Methode wurde am Beispiel der Zelllinien HEK 293, CHO-K1, AGE1.HN und Hep G2 getestet. Die Ergebnisse zeigten, dass die N-Glykosylierung der Zelloberfläche der untersuchten Zelllinien strukturell die Hauptmerkmale der Glykoproteine aufwies, welche rekombinant in ihnen produziert werden.

Unter Verwendung der neu etablierten Methode, wurde das N-Glykosylierungsmuster der Zelloberfläche von aus Knochenmark isolierten humanen mesenchymalen Stammzellen (MSZn) und den aus ihnen adipogen, chondrogen sowie osteogen differenzierten Zellen mittels MALDI-TOF-MS und CE-LIF untersucht. Darüberhinaus wurden zur Bestätigung der gefundenen Strukturen Exoglykosidaseverdaus des Gesamt-N-Glykanpools sowie Fragmentierungen der N-Glykansignale über MALDI-TOF/TOF-MS Analysen durchgeführt. Analog wurde verfahren, um das N-Glykosylierungsmuster der Zelloberfläche von humanen embryonalen Stammzellen (ESZn) vor und nach ihrer Differenzierung in Hepatozyten-ähnliche Zellen zu untersuchen.

Die Ergebnisse zeigten, dass das N-Glykom von adipogen differenzierten MSZn im Vergleich zu undifferenzierten MSZn eine deutlich geringere Fucosylierung sowie Antennarität aufweist. Aufgrund eines signifikant erhöhten Anteils werden die N-Glykane H6N5F1 und H7N6F1 als potentielle Glykan-basierte Stammzellmarker für undifferenzierte MSZn sowie H3N4F1 und H5N4F3 für adipogen differenzierte MSZn vorgeschlagen.

Das N-Glykosylierungsprofil der Zelloberfläche von chondrogen differenzierten MSZn vor und nach Isolierung aus ihrer extrazellulären Matrix (EZM) wurde untersucht und mit dem Profil undifferenzierter MSZn verglichen. Die Ergebnisse zeigten einen erhöhten Anteil von High-Mannose-Typ Strukturen sowie einen geringeren Anteil von Komplex-Typ N-Glykanen in chondrogen differenzierten MSZn mit EZM. Im Falle des Nichtvorhandenseins der EZM wird die Differenzierung von einem erhöhten Anteil biantennärer N-Glykane begleitet. Im Vergleich zu den undifferenzierten MSZn wies das N-Glykanprofil chondrogen differenzierter MSZn eine geringere Antennarität auf. Es wurden N-Glykane mit Fucosen (Fuc) detektiert, die am N-Acetylglucosamin des reduzierenden Endes der Kernstruktur (*core*-Fucosylierung) oder an den Antennen gebunden vorlagen (Lewis^x Epitope). Die triantennären N-Glykane H6N5F1 und S1H6N5F1 sowie tetraantennären Strukturen H7N6F1, S1H7N6F1 und S2H7N6F1 werden als potentielle Glykan-basierte Biomarker für undifferenzierte MSZn vorgeschlagen. Zudem werden die biantennären N-Glykane S1H5N4F2 und S2H5N4F1 als potentielle Glykan-basierte Biomarker für chondrogen differenzierte MSZn vorgeschlagen, die aus ihrer EZM isoliert waren. Die biantennären Strukturen H3N4F1, H4N4F1 und H4N4F2 werden als Glykan-basierte Biomarker für chondrogen differenzierte MSZn mit EZM vorgeschlagen.

Die osteogene Differenzierung von MSZn wurde begleitet von einem erhöhten Anteil biantennärer N-Glykane. Zudem war die Antennarität der N-Glykosylierung der Zelloberfläche osteogen differenzierter MSZn geringer. Der Anteil fucosylierter Strukturen war nach der Differenzierung erhöht und bestand hauptsächlich aus *core*-fucosylierten N-Glykanen. Als potentielle Glykan-basierte Biomarker für osteogen differenzierte MSZn werden die biantennären Strukturen H4N4F2, H5N4, H5N4F1, S1H5N4 und S1H5N4F1 vorgeschlagen.

Das N-Glykosylierungsprofil undifferenzierter ESZn und den aus ihnen differenzierten Hepatozyten-ähnlichen Zellen war signifikant unterschiedlich. ESZn enthielten einen höheren Anteil an N-Glykanen vom High-Mannose-Typ wohingegen N-Glykane vom Komplex-Typ, wie zum Beispiel bi- und triantennäre Strukturen, dominant vertreten waren in Hepatozyten-ähnlichen Zellen. Zudem waren in den Hepatozyten-ähnlichen Zellen vollgalactosylierte Strukturen viel häufiger vertreten als in undifferenzierten ESZn. Das GalNAc Epitop konnte als strukturell charakteristisch in Hepatozyten-ähnliche Zellen nachgewiesen werden. Basierend auf den Ergebnissen wurden die High-Mannose-Typ N-Glykane H6-9N2 und die Komplex-Typ N-Glykane H4N4F1 und H3N5F1 als potentielle Glykan-basierte Biomarker für humane ESZn vorgeschlagen. Die biantennären N-Glykane H5N4, H5N4F1, H5N4F2, S1H5N4, S1H5N4F1 und S2H5N4F2 sowie die triantennären Strukturen H6N5F1 und S1H6N5F1 wurden als potentielle Biomarker für Hepatozyten-ähnliche Zellen vorgeschlagen.

Abstract

The glycocalyx is a dense cell surface layer composed of complex carbohydrate structures. Qualitative and quantitative changes of the cell surface N-glycosylation pattern can be used to identify stem cell (SC) populations, to monitor SC differentiation as well as the loss of the SC status, which is of high relevance in the field of regenerative medicine and tissue engineering.

In this study, a simple, rapid, reproducible and sensitive method to profile cell surface N-glycosylation was established and optimised. The common procedure involves the isolation of membrane (glyco)proteins, which is then followed by an enzymatic N-glycan release. However, this method yields a major proportion of high-mannose N-glycans that may stem from intracellular proteins derived from the endoplasmic reticulum (ER). With the new method, that directly releases cell surface (glyco)peptides, a decrease of the amount of high-mannose N-glycans from 90 % to 10 % was verified using MALDI-TOF-MS. At the same time, the detection sensitivity and quantification of complex-type N-glycans was drastically improved. The selectivity of the new method was tested by applying it to the cell lines HEK 293, CHO-K1, AGE1.HN and Hep G2. The data revealed that the cell surface N-glycosylation of these cells displays the main glycan features that are found on recombinant glycoproteins produced from these cell lines.

Using the new method, the cell surface N-glycosylation pattern of human bone marrow mesenchymal stem cells (MSCs) and their adipogenically, chondrogenically as well as osteogenically differentiated progeny was investigated and verified using MALDI-TOF-MS and CE-LIF in combination with exoglycosidase digestions and MALDI-TOF/TOF fragmentation analysis. The same was done to profile the cell surface N-glycosylation pattern of human embryonic stem cells (ESCs) before and after their differentiation into hepatocyte-like cells.

The results showed that the N-glycome of adipogenically differentiated MSCs was clearly less fucosylated and branched than the one of undifferentiated MSCs. Due to their significantly increased amount, N-glycans like H6N5F1 and H7N6F1 are proposed as candidate MSC markers for undifferentiated MSCs and N-glycans like H3N4F1 and H5N4F3 as potential markers for adipogenically differentiated MSCs.

The N-glycosylation profile of chondrogenically differentiated MSCs was investigated before and after isolation from their extracellular matrix (ECM) and compared to the profile of undifferentiated MSCs. The data revealed that they contained more high-mannose and less complex N-glycans when their ECM was present. Differentiation was accompanied by an increased amount of biantennary N-glycans when the ECM was absent. Cell surface N-glycosylation of chondrogenically differentiated MSCs was generally less branched than the

one of undifferentiated MSCs. N-glycans were found to contain core-linked fucose (Fuc) as well as Lewis^x epitopes. The triantennary N-glycans H6N5F1 and S1H6N5F1 as well as tetraantennary structures H7N6F1, S1H7N6F1 and S2H7N6F1 were proposed as glycan-based biomarkers for undifferentiated MSCs. The biantennary structures S1H5N4F2 and S2H5N4F1 are proposed as glycan-based biomarkers for chondrogenically differentiated cells without ECM and the biantennary N-glycans H3N4F1, H4N4F1 and H4N4F2 for chondrogenically differentiated cells with ECM.

Osteogenic differentiation of MSCs was accompanied by an increased amount of biantennary structures. In addition, cell surface N-glycosylation was less branched in osteogenically differentiated MSCs. Furthermore, the amount of fucosylated structures increased with differentiation and contained mainly core-linked Fuc residues. The biantennary structures H4N4F2, H5N4, H5N4F1, S1H5N4 and S1H5N4F1 were proposed as glycan-based biomarkers for osteogenically differentiated cells.

The N-glycosylation profiles of undifferentiated ESCs and hepatocyte-like cells were qualitatively and quantitatively significantly different. ESCs contained a high amount of high-mannose N-glycans. In contrast, complex-type N-glycans such as biantennary and triantennary N-glycans were dominant in hepatocyte-like cells and fully-galactosylated structures were much more abundant than in undifferentiated ESCs. In addition, the GalNAc epitope was detected in hepatocyte-like cells. High-mannose-type N-glycans of the form H6-9N2 and the complex-type N-glycans H4N4F1 as well as H3N5F1 were proposed as glycan-based biomarkers for human undifferentiated ESCs. The biantennary N-glycans H5N4, H5N4F1, H5N4F2, S1H5N4, S1H5N4F1 and S2H5N4F2 as well as the triantennary structures H6N5F1 and S1H6N5F1 were proposed as glycan-based biomarkers for hepatocyte-like cells.

1 Introduction

1.1 Stem cells

Stem cells (SCs) are basically unspecialised cells and defined functionally as cells that have the ability to self-renew as well as to generate differentiated cells (Fig.1.1) (1, 2). Self-renewal is the process in which a SC generates daughter cells identical to their mother. During differentiation the SCs are capable of producing progeny with more restricted potential (more specialised cells) (3).

SCs are identified and named according to the function of their descendants or their place in development. The diversity of differentiated descendants that vary among SCs is dependent on their potency to generate specific cell types. The potency of a SC is categorised into totipotent, pluripotent, multipotent, omnipotent and unipotent. Totipotent SCs are able to give rise to all cell types including the embryonic membranes such as trophoctoderm (e.g. the zygote). Pluripotent SCs are able to differentiate into almost all cell types of the three germ layers (e.g. embryonic SCs). Multipotent SCs can generate multiple types of differentiated cells, which possess distinct morphologies and gene expression patterns (e.g. hematopoietic SCs). Omnipotent SCs are able to give rise to a more restricted subset of cell lineages than multipotent SCs (e.g. adult myeloid SCs) and unipotent SCs are able to generate only one mature cell type (e.g. adult muscle SCs).

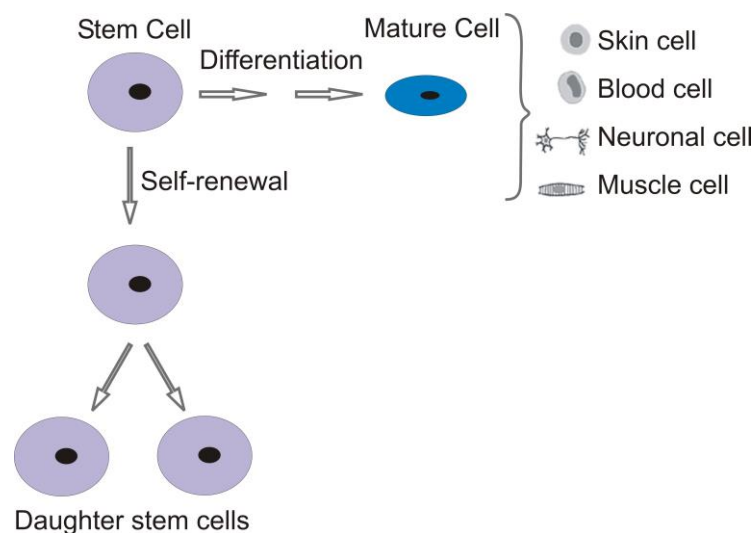


Fig. 1.1. Graphical illustration of the ability of stem cells to self-renew (generation of identical daughter cells) as well as to differentiate into progeny with more restricted potential.

Due to their restoration ability, human SCs offer a powerful source for the application in future regenerative medicine, whereupon the main goal of research is to find methods to

repair and regenerate diseased or damaged tissue and organs, and to prevent diseases from occurring. However, research with human pluripotent embryonic stem cells (ESCs) faces complex ethical and technical issues. Hence, adult multipotent SCs are a remarkable alternative to fulfill the therapeutic expectations (4, 5).

1.1.1 Embryonic stem cells

Mouse and human embryonic stem cells (ESCs) are derived from the inner cell mass of embryos after the formation of a cystic blastocyst (Fig.1.2) (2). This was shown more than 30 years ago for mouse ESCs (6, 7). This cell population is capable of producing the epiblast (a tissue type found in the blastocyst, which is able to give rise to all three germ layers through gastrulation) and all adult tissues, explaining the developmental plasticity of ESCs.

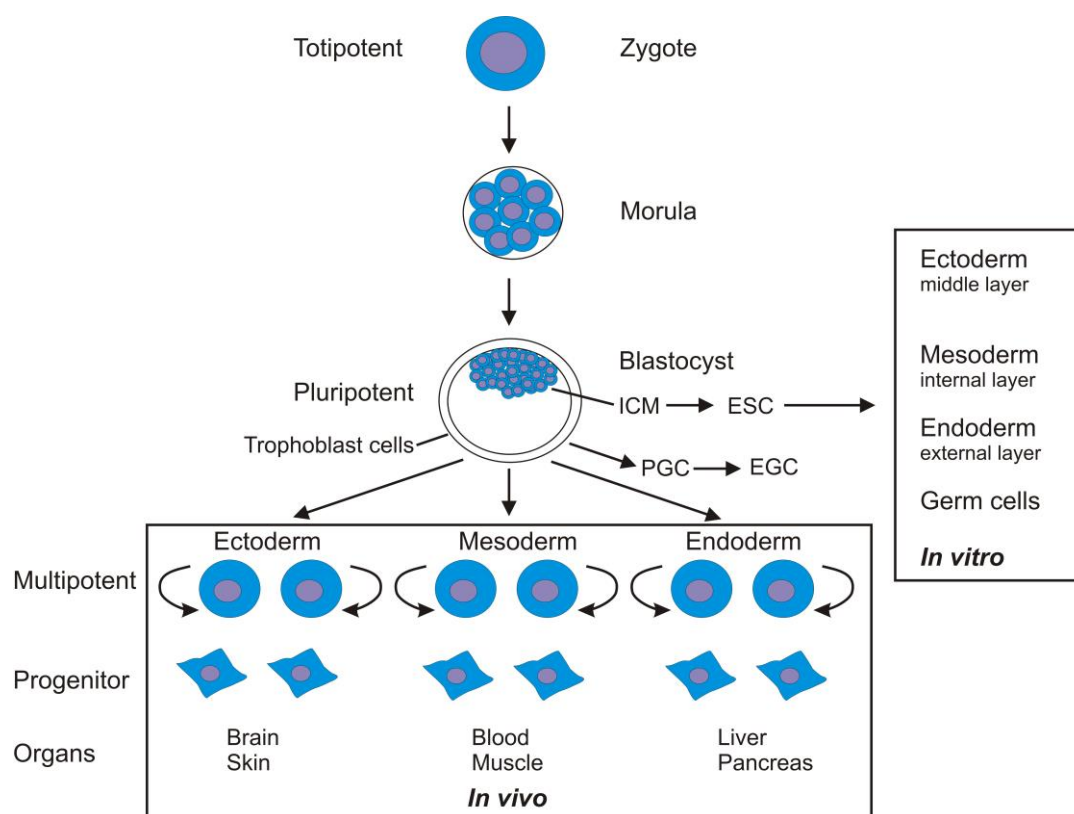


Fig. 1.2. Hierarchy of stem cells. Zygote and early cell division stages till the morula stage are totipotent, since they can generate a complex organism. At the blastocyst stage, the cells of the inner cell mass (ICM) are able to build up all three primary germ layers; endoderm, mesoderm and ectoderm as well as the primordial germ cells (PGC), which are the founder cells of male and female gametes. Multipotent stem and progenitor cells exist in tissues and organs of adult tissues and are responsible for the replacement of lost or injured cells. Embryonic stem cells (ESCs) are derived from the ICM of the blastocyst, and have the developmental capacity to differentiate *in vitro* into cells of all three somatic cell lineages (endoderm, mesoderm and ectoderm) as well as into male and female germ cells.

In vitro, ESCs appear to be equivalent to the epiblast, due to their ability to contribute to the formation of all somatic lineages (8). By the time the zygote has reached the blastocyst stage whereupon the developmental potential of certain cells has been restricted. The outer cells of the embryo have begun to differentiate to form trophectoderm, which contains embryonic trophoblast SCs with the ability to generate all cell types of the trophectoderm lineage (8).

At the egg cylinder stage of embryonic development, which is embryonic day 6.5 in mice, a cell population near the epiblast can be identified as primordial germ cells (PGCs). These cells are subsequently excluded from somatic specification or restriction (9). When cultured with suitable factors *in vitro*, they can produce embryonic germ cells (EGCs) (8). EGCs possess many common characteristics as ESCs with respect to their differentiation potential and their contribution to the germ line (8).

The property of ESCs to develop into all three primary germ layer derivatives, namely ectoderm, mesoderm and endoderm, and their almost unlimited proliferation capacity is achieved by a high telomerase activity in the cell lines over approximately 300 population doublings (10). In addition, ESCs express characteristic stem cell markers such as stage specific embryonic antigen (SSEA) 3 and 4, octamer binding transcription factor (Oct) 3/4, sex determining region Y (SRY)-box 2 (Sox2) and Rex-1, also referred to as zinc-finger protein 42, or nanog, which are down-regulated upon differentiation (11). SSEA3 and SSEA4 are globoseries glycolipids located on the cell surface and sensitive markers of the undifferentiated state of human ESCs (11). Oct 4 as well as nanog are located in the nucleus and are pluripotency associated transcription factors (11). Sox2 is also a transcription factor and maintain or protect self-renewal as well as the pluripotent state of ESCs (12).

Besides stem cell markers, that ensure pluripotency of ESCs, it is necessary to confirm their ability to differentiate into all germ layers. This is achieved by *in vitro* differentiation into embryoid bodies (13, 14) and/ or by testing the *in vivo* teratoma formation of ESCs in immunodeficient mice (15, 16).

In this study, the cell surface N-glycosylation of ESCs and thereof differentiated hepatic cells was analysed. Hepatocytes constitute the primary cells of the liver and are essential for many crucial functions such as metabolizing dietary molecules, detoxifying compounds and glycogen storage. Patients with acute hepatic failure or end-stage liver disease have to be treated by transplantation of the liver or hepatocytes (17). The transplantation of hepatocytes has shown to be efficient, but the availability of human hepatocytes is limited. Thus, human ESCs have been proposed as an appropriate alternative source of hepatocytes for transplantation (11). Due to their ability to proliferate indefinitely in culture, ESCs are an unlimited source of cells. In addition, the differentiation of ESCs into hepatocytes may be helpful to study the processes involved in embryonic development of the liver. Furthermore,

the understanding of the developmental processes may play a key role for the diagnosis and treatment of liver-associated congenital pathologies (11).

1.1.2 Adult stem cells

Application of pluripotent cells, such as ESCs or induced pluripotent progenitor cells faces complex difficulties like the formation of teratoma. Multipotent stem and progenitor cells are therefore a remarkable alternative to fulfill the therapeutic expectations (18). Most of the adult SCs are multipotent. Thus they are able to differentiate into multiple cell types that are restricted to a given tissue.

Adult SCs are generated during development beyond the stage of gastrulation. During the gastrulation process, pluripotent SCs become mesoderm, endoderm and ectoderm. Afterwards tissue-specific decisions according to the fate of the SC are made. Thus, adult SCs have lost their pluripotency and adopt tissue-specific and restricted differentiation abilities (19).

Adults SCs are found in a number of tissues and are capable of differentiating into a multiple number of other cell types. The term “adult SCs” is not always correct, because these cells are also found in infants, in umbilical cord and placenta. Thus, other terms have been proposed as tissue SCs, somatic SCs or post-natal SCs.

Adult SCs are involved in the growth of the organism by increasing the dimension of the organs. Their main role is to renew cells and/ or to regenerate cells of damaged tissues, which takes place in tissues and organs by adult SC depots. They are able of responding to different physiological and pathological tissue requests due to their very dynamic proliferative and differentiative plasticity. In adult organisms, numerous types of multipotent SCs are able to trans-differentiate, to fuse with other cells as well as to promote new genetic reprogramming processes (20). Adult SCs have been isolated from numerous adult tissues such as umbilical cord and other non-embryonic sources (such as bone marrow, muscle, peripheral blood, skin, brain, liver) (5).

1.1.2.1 Mesenchymal stem cells

Bone marrow contains at least two SC populations. Besides the hematopoietic stem cells (HSCs), which differentiate into blood cell progeny, mesenchymal stem cells (MSCs) are also present in bone marrow. MSCs provide support for hematopoietic and other cells in the marrow. The bone marrow is a complex tissue and comprises numerous cell types. It maintains the undifferentiated state of HSCs and MSCs and supports differentiation of different SCs (21). Bone marrow MSCs, presently also referred to as mesenchymal stromal cells, are non-hematopoietic adult multipotent cells (22). Flow cytometry using different

surface markers revealed that the expanded bone marrow MSCs population is >98 % homogeneous (22).

MSCs are easy to isolate and expand and develop *in vitro* as well as *in vivo* into a variety of tissues including fat, bone and cartilage (22). In addition, human MSCs have been shown to differentiate into neuronal cells (23). MSCs are also able to migrate to diseased organs, they possess strong immunosuppressive properties and they secrete regenerative factors (24-26). Therefore, MSCs are of great interest for application in cell-based therapies. In clinical therapies they are administered to patients with hematological pathologies, cardiovascular diseases, osteogenesis imperfecta, musculoskeletal disorders, lung diseases and diabetes (27).

The primary source of mesenchymal stem cells is bone marrow, but adipose tissue, synovium, periosteum, amniotic fluid, placenta and umbilical cord blood also contain MSCs and can therefore be used as alternative cell sources (28).

However, all known MSC markers, among them the most prominent ones like the cell surface proteins CD73 (5'-nucleotidase), CD90 (thy-1), CD105 (endoglin), CD166 (alcam) (22) and Stro-1 (29), are not specific. For instance, MSCs are usually identified as colony-forming unit-fibroblasts and Stro-1 negative cells are not capable of forming colonies (30). In contrast, Stro-1 positive cells are capable to become hematopoietic stem cell-supporting fibroblasts, smooth muscle cells, adipocytes, osteoblasts and chondrocytes, which support the functional role of MSCs. In addition, Stro-1 is not only expressed from MSCs and its expression is gradually lost during culture. Several other useful but unspecific markers for MSCs and their differentiated progeny have been identified in molecular profiling approaches for example focusing on the adipogenic lineage (31).

1.1.3 Embryonic and mesenchymal stem cells in regenerative medicine and tissue engineering

SCs are of great interest in regenerative medicine, since their properties makes them ideal to replace defective body parts by *in vivo* infusion or by the creation of bioartificial tissues. However, at the moment, they are extensively used to study self-renewal and differentiation (19). The pluripotent potential and unlimited availability of human ESCs makes them an appropriate candidate for diverse cell replacement therapies and organ transplantation programs. ESC-based therapies are of significant interest for the treatment of diseases in which a single cell type is destroyed or lost its function.

The potential of ESCs have been studied in neurodevelopmental biology with the aim to treat neurological defects caused by degeneration of neural lineages. Studies discuss the potential of neurons derived from human ESCs in the treatment of Parkinson's (32-36) and

Alzheimer's (37), where for example ESCs are described as a source of neurons to replace the degenerating nerve cells in Parkinson disease looming [32]. Application of ESCs research is of great interest in the field of degenerative liver disease due to the fact that the ability to regenerate liver tissue without transplanting donor organs would be a step forward in the treatment of severe diseases such as cirrhosis (38, 39). Similarly, studies with ESC-based techniques for heart repair have been encouraging, too. Cardiomyocytes derived from human ESCs were efficiently integrated into the heart of pigs. In addition, the implantation of ESCs into injured myocardium led to an improvement of contractility and reduction of myocardial wall thinning (39, 40).

Many studies deal with differentiation of SCs into pancreatic tissue with the aim to establish a cell replacement therapy for type 1 diabetes mellitus. Recent studies demonstrated the use of mouse and human ESCs to produce insulin secreting cells (39). However, it was shown that *in vitro* derived cells release insulin not only due to *de novo* synthesis but also because of an uptake from the medium (39, 41). Furthermore, the differentiation of ESCs into diverse types of blood cells is relatively well established. They were successfully differentiated into hematopoietic progenitor cells and were shown to be able to engraft in sheep. In addition, ESCs were directed to differentiation into CD34+ cells with genotypic and phenotypic similarities to hematopoietic SC, into B cells, natural killer cells, macrophages, granulocytes and functional T lymphocytes, making them very appropriate for replacement and regeneration of diverse blood cell types (39, 42).

The applications of ESCs in regenerative therapies are versatile; however their use faces two main problems; their haphazard differentiation and ability to give rise to tumor cells as well as the possible rejection of ESC-derived tissue graft by the immune system. Therefore, clinical transplantation remains unsafe (39). Multipotent stem and progenitor cells are therefore a better alternative to fulfill the therapeutic expectations (18).

Multipotent MSCs are of great interest in the field of cell-based therapy. They may be used in bone regeneration. Studies revealed that culture-expanded marrow MSCs are capable of regenerating structurally sound bone (19). In cartilage repair, chondrocytes have been used to repair large cartilage defects; however it is difficult to integrate the tissue with that of the host. In this case, hyaluronan scaffolds were shown to facilitate the integration due to the high content of hyaluronan in the embryonic mesenchyme of precartilaginous tissues (19, 43). MSCs can help in marrow regeneration, since injected MSCs are able to migrate back to the bone marrow to refabricate injured marrow stroma (19). MSCs were successfully injected into a mouse muscle, where they differentiated into skeletal myoblasts, then fused with the host myotubes and induced synthesis and distribution of dystrophin (sub-membrane cytoskeletal protein found in the muscle fiber membrane) (44, 45). Thus, MSCs are an important tool in the field of muscle regeneration.

Moreover, MSCs and their adipogenically differentiated progeny also play a role in the regenerative treatment of burn and tumor patients and in cosmetic surgery (46). In addition, they have been induced into the adipocyte pathway and thereby were shown to accumulate fat droplets (19). Furthermore, MSCs were used for repair of tendons (19). They may be used in a variety of gene therapy applications (polysaccharide storage diseases, osteogenesis imperfect) and are clinically relevant as growth factor pumps in neural environments, where they can facilitate axonal reconnection and neuronal stem cell (NSC) growth, migration and differentiation (19). Thus, MSCs have great potential to be used in tissue engineered regeneration and repair of a variety of tissues.

1.2 Glycosylation

Protein glycosylation is besides phosphorylation and sulfation one of the most common post-translational protein modifications. Glycans are often covalently attached to proteins or lipids and constitute a significant amount of the mass in glycoconjugates, in which they are able to influence intramolecular and intermolecular functions (47, 48). Consequently, they play a crucial role in various key biological processes such as cell adhesion, molecular trafficking and clearance, receptor activation, signal transduction and endocytosis (48).

In contrast to DNA, RNA and proteins, glycans are able to form complex branched structures. Therefore glycans possess great structural diversity. Despite the theoretically huge structural diversity of glycans (49), only the monosaccharides N-acetylglucosamine (GlcNAc), N-acetylgalactosamine (GalNAc), mannose (Man), galactose (Gal), N-acetylneuraminic acid (Neu5Ac) and Fuc are typically found in human systems (50).

In general, protein-bound glycans are classified into two main groups, namely the N- and O-glycans. N-glycosylation is a protein cotranslational modification occurring on asparagine (Asn) residues of the consensus sequence Asn-X-Ser/Thr, where X may be any amino acid except proline (Pro) (51-53). In O-glycans the carbohydrate moiety is connected via GalNAc to a serin (Ser)- or threonine (Thr) residue of the protein chain. In addition to N- and O-glycosylation, the C-mannosylation is another type of glycosylation, in which one α -Man is bonded to the first tryptophan (Trp) residue of the consensus sequence Trp-X-X-Trp (51, 54).

Protein N-glycosylation takes place in the endoplasmic reticulum as well as in the Golgi apparatus, where the extent and type of glycosylation is determined by the cell type and species (47, 51, 55). N-glycans share a common branched core structure that consists of three Man residues and two GlcNAc units of the form $\text{Man}\alpha 1-6(\text{Man}\alpha 1-3)\text{Man}\beta 1-4\text{GlcNAc}\beta 1-4\text{GlcNAc}\beta 1-\text{Asn}$ (56). In addition, so-called antennae may be bonded to the terminal Man residues of the core structure. In contrast to N-glycans, O-glycans are smaller and less branched and share no common core structure. Their synthesis starts in the cis-Golgi and is

a post-translational process (57). N- and O-glycans are characterised by a wide structural diversity, which is due to the saccharide type, sequence, position, linkage type as well as the degree of branching.

Glycans are able to increase the solubility of the protein in aqueous media, to maintain correct folding and orientation of the protein, to protect the protein from proteolysis and to regulate its functions (58-60). The structures of oligosaccharides found on many cell surface glycoproteins significantly change upon the occurrence of inner or outer cellular environmental modifications such as cell development and differentiation, inflammation, malignant transformations, tumor progression and metastasis (47, 55, 61-64). Structural changes are caused by altered expressions of glycosyltransferases, which may modulate cellular functions (64-66). Structural alterations have been described in several diseases such as cancer, where the glycan epitopes sialyl-Lewis^x and sialyl-Lewis^a represent epitope markers for tumor progression (67-69).

Complex glycan structures cover all cellular surfaces to form a dense layer named glycocalyx and are therefore involved in many aspects of stem cell biology and technology. As an example, the proliferation or differentiation of a SC into specific cell types requires a complex and glycan-dependent modulation of signal molecules (26) (see section 1.2.4). In addition, cell surface glycans are ideal biomarker candidates due to their prominent cell-surface position and cell lineage-specific nature (70).

1.2.1 Glycocalyx

Carbohydrates are referred to as glycans that are covalently linked to membrane proteins or lipids and form a dense glycocalyx on the extracellular side of the surface of all cells found in multicellular animals, including SCs. Cell surface glycans are optimally positioned to help the cell to communicate with its extracellular environment and are the main components of the glycocalyx (71, 72). Since they form the outermost layer of the cell, cell surface glycans act as recognition elements and binding sites. Thus, they are the first molecules that are encountered by antibodies, hormones, viruses, bacteria, toxins and other cells. In addition to their receptor function, glycans play an important role in regulating the immune response since the majority of cell surface receptor proteins involved in antigen recognition by T cells are glycosylated. Therefore, glycosylation ensures correct functioning of receptor proteins by stabilising their conformation, regulating their cell-surface clustering, and increasing protease resistance (73). Moreover, cell surface glycans are capable of orienting the binding faces of cells to facilitate cell adhesion and they can prevent non-specific protein-protein interactions (74, 75). Besides the fact that glycans are involved in the regulation and control of protein

folding and trafficking, cell surface glycans play important roles in the interaction of SCs with their niche and are able to modulate the growth and differentiation of SCs *in vitro* (76, 77).

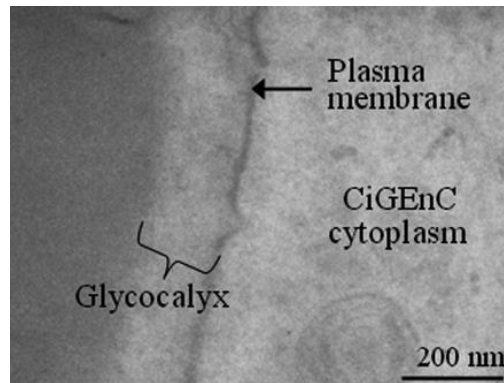


Fig. 1.3. Transmission electron micrograph shows the presence of a 200 nm-thick layer coating the surface of the human glomerular endothelial cells (CiGEnC). This layer was enhanced by Alcian blue staining and represents the glycocalyx (78).

The endothelial glycocalyx (Fig. 1.3) was already described before 75 years as a layer of the endothelial cells composed of proteoglycans, glycosaminoglycans and glycoproteins (79). It was thought that this layer was only a few nanometers thick (80). In the last years studies revealed that the glycocalyx has a thickness of about 0.5 μm and plays besides the function as a vascular barrier also many physiological roles (81-83). The glycocalyx forms together with attached plasma proteins a cell surface layer named the endothelial surface layer (ESL), which possess a height of about 1 μm and is often thicker than the endothelial cells itself (84, 85). Changes of the endothelial glycocalyx are clinically relevant because the decrease of the glycocalyx thickness results in an increased permeability of the vessel wall for macromolecules (81, 82, 86). In addition, the glycocalyx plays important roles in different diseases such as diabetes (87), sepsis (88), arteriosclerosis (49) and metastatic cancer (89).

1.2.2 N-Glycosylation

N-Glycans are attached via a GlcNAc residue through a β -glycosidic bond to a nitrogen atom of an Asn residue of a polypeptide. N-glycans are divided into three subgroups (Fig.1.4), namely the high-mannose-type, the complex-type and the hybrid-type N-glycans (90, 91). All three subgroups have a common core structure, consisting of two GlcNAc and three Man residues. In the high-mannose-type N-glycans, additional Man units are added to the pentasaccharide core whereas in the complex-type N-glycans different combinations of GlcNAc, Gal, Neu5Ac and Fuc are added to the terminal Man units of the core.

Depending on the number of GlcNAc units bond to the three mannosyl residues of the core, the resulting glycan is named for example mono-, bi-, tri- or tetraantennary N-glycan (92, 93).

The terminal GlcNAc residues can carry Gal units resulting in galactosylated N-glycans. The GlcNAc of the antennae, the reducing GlcNAc of the core structure and the Gal can be fucosylated with Fuc units. The structural diversity of the complex N-glycans may be expanded through possible sialylation of the Gal units. The third subgroup, the hybrid-type N-glycans, possess characteristics of both, high-mannose- and complex-type N-glycans (90). Complex-type N-glycans can carry a bisecting GlcNAc residue, which is attached to the $\beta(1-4)$ -linked Man of the core. Although the structural diversity of N-glycans is tremendous, the resulting oligosaccharide structure is dependent on the cell type and its stage of development, on the availability of monosaccharides as well as pathological changes (94).

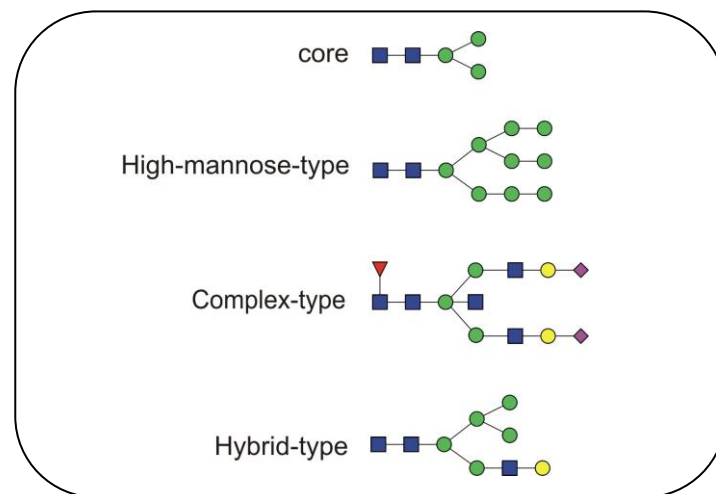


Fig. 1.4. The three subgroups found in N-glycans. The core structure consists of three mannose and two N-acetylglucosamine units. In the high-mannose-type additional mannose units are added, whereas in the complex-type N-acetylglucosamine, galactose, fucose and sialic acids form the antennae. The hybrid-type possesses characteristics of the two other subgroups. Blue square represents N-acetylglucosamine, green circle mannose, yellow circle galactose, red triangle fucose and pink diamond N-acetylneuraminic acid.

The biosynthesis of N-glycans starts in the cytosolic ER with the transfer of a preassembled lipid-linked oligosaccharide to the polypeptide (Fig.1.5). The lipid-linked oligosaccharide is synthesised on the membrane-bound dolichol phosphate (Dol-PP) starting with the transfer of GlcNAc-P from UDP-GlcNAc to form dolichol pyrophosphate-N-acetylglucosamine (Dol-PP-GlcNAc), which is catalysed by the enzyme GlcNAc-1-phosphotransferase. Afterwards one additional GlcNAc and five Man units were stepwisely transferred from UDP-GlcNAc and GDP-Man to Dol-PP-GlcNAc with the help of specific glycosyltransferases to yield $\text{Man}_5\text{GlcNAc}_2\text{-PP-Dol}$ (52, 53). This precursor is then translocated to the ER lumen through a flippase. Then the transfer of four Man units through Dol-P-Man and three glucose (Glc) units through Dol-P-Glc to the precursor $\text{Man}_5\text{GlcNAc}_2\text{-PP-Dol}$ takes place to form the mature N-

In the next steps, the N-glycan precursor, which is linked to the Asn residue, undergoes first extensive trimming then elongation reactions (Fig.1.6). First, the Glc units are sequentially cleaved in the ER lumen by α -glucosidase-I and -II. The terminal $\alpha(1-2)$ -linked Man unit is cleaved by α -mannosidase I and the glycoprotein exits the ER (95). The trimming of Glc and Man units is associated with the folding of the glycoprotein, which is supported by the lectins calnexin and calreticulin.

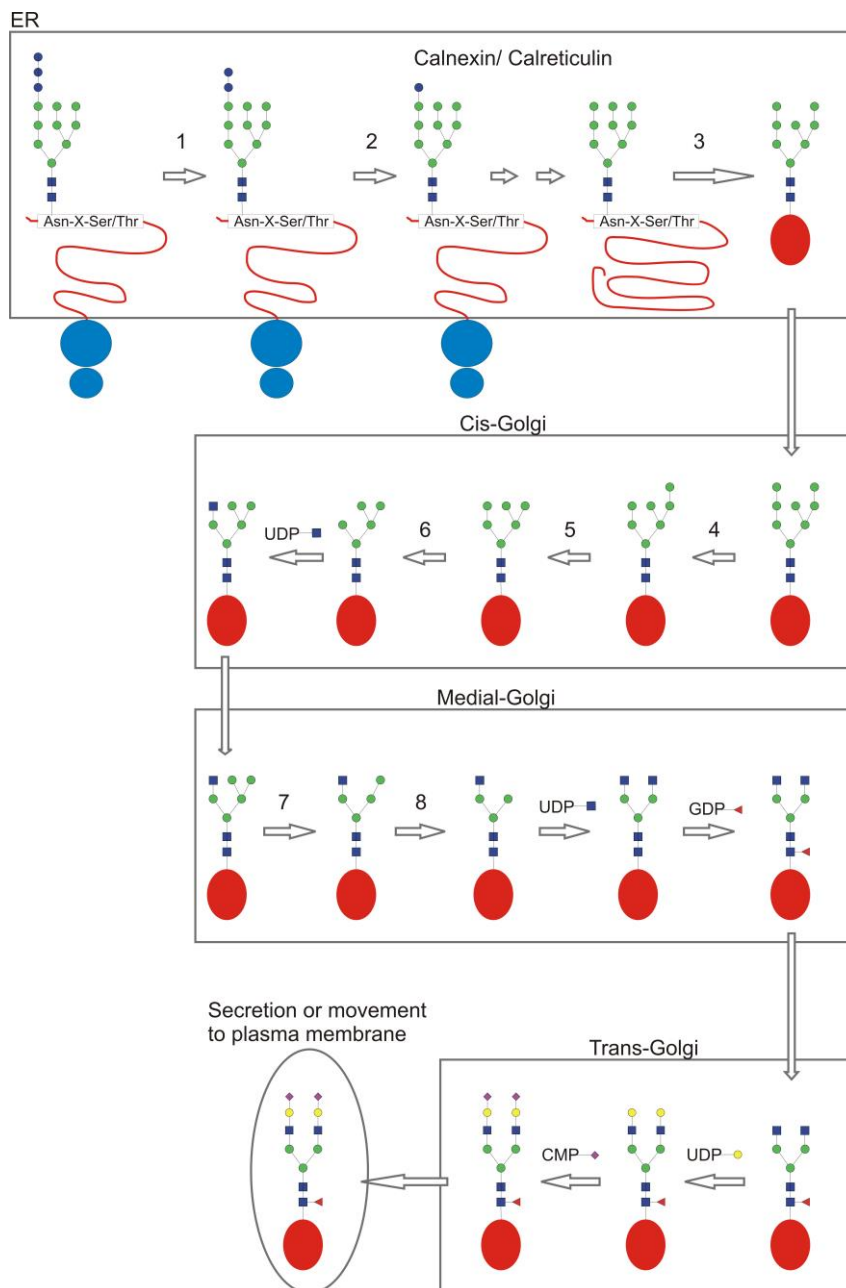


Fig. 1.6. N-glycan processing and maturation. The mature Dol-PP-glycans are transferred to Asn-X-Ser/Thr sequons during protein synthesis. 1/ 2: α -glucosidases I and II, 3/ 4/ 5/ 6: $\alpha(1-2)$ -mannosidases I/ IA/ IB/ IC, 7/ 8: $\alpha(1-3/6)$ -mannosidase II, red oval: mature and folded protein (53).

These lectins determine whether the glycoprotein will enter the Golgi apparatus, which is the case when it is correctly folded (96). Further trimming of the protein-bound oligosaccharide $\text{Man}_8\text{GlcNAc}_2$ takes place in the cis-Golgi. The $\alpha(1-2)$ -linked Man units are cleaved by the $\alpha(1-2)$ -mannosidases IA, IB and IC (95). The resulting protein-bound oligosaccharide $\text{Man}_5\text{GlcNAc}_2$ is an important glycan precursor, which will be modified to hybrid-type and complex-type N-glycans. Some of the N-glycan precursors will not be modified (52, 53). In this case mature glycoproteins bearing high-mannose N-glycans of the form $\text{Man}_{5-9}\text{GlcNAc}_2$ will be generated. The biosynthesis of hybrid and complex N-glycans continues in the medial-Golgi. A N-acetylglucosaminyltransferase-I called GlcNAcT-I transfers GlcNAc to the C2 carbon atom of $\alpha(1-3)$ -linked Man of the core structure of the precursor $\text{Man}_5\text{GlcNAc}_2$ (52, 53). At this point hybrid-type N-glycans can be generated and further modification will lead to complex-type N-glycans. In case of complex-type N-glycans the terminal $\alpha(1-3)$ - and $\alpha(1-6)$ -linked Man is cleaved by α -mannosidase II in the medial-Golgi. The resulting $\text{GlcNAcMan}_3\text{GlcNAc}_2$ is then further elongated through action of GlcNAcT-II, which will transfer one additional GlcNAc unit to the C2 carbon atom of $\alpha(1-6)$ -linked Man of the core structure (52, 53). Thereby the precursor of biantennary complex-type N-glycans is generated. Additional antennae are formed through addition of GlcNAc to the $\alpha(1-6)$ - and $\alpha(1-3)$ -linked Man residues of the core, which will give rise to tri- and tetraantennary complex-type N-glycans. In addition, further modification with addition of Fuc, Gal and sialic acid units will take place in the trans-Golgi (90, 95). Differences in N-glycan structures are due to cell type-specific expression patterns of glycosylation enzymes but are also dependent on the glycoproteins themselves.

1.2.3 O-Glycosylation

O-linked glycans (O-glycans) are α -glycosidically linked to the oxygen atom of Ser or Thr residues through GalNAc. In addition, O-glycans are also found on hydroxyl groups of hydroxyproline and hydroxylysine residues. In contrast to N-glycosylation, O-glycan biosynthesis is a post-translational process and no general consensus sequence has been identified so far. However, a series of general rules have been proposed and an algorithm has been developed to predict O-glycosylation sites (97). In addition, only Ser and Thr residues that are exposed on the surface of the molecule will be glycosylated, suggesting the conformational role of the protein (52, 98). The most abundant O-glycosidic linkage is the mucin-type GalNAc- α -Ser/Thr, which is found in mucins. Mucins are glycoproteins with a high molecular weight (> 200 kDa) whereby the carbohydrates constitute about 50-80 % of the molecular weight. Mucin-type O-glycosylation is divided into eight different core structures (Table 1.1) (53).

The biosynthesis of O-glycans starts in the Golgi-apparatus. Monosaccharides are stepwisely added to the protein. The transfer of the first monosaccharide GalNAc to Ser and Thr residues in mucin-type O-glycans takes place in the cis-Golgi (99, 100). This step is catalysed by a family of about 20 ppGaNtases (52). These transferases specifically detect acceptor Ser or Thr residues in the protein and whether they are already substituted by GalNAc or not. Then addition of GlcNAc or/ and Gal results in the generation of one of the eight possible core structures which will then be sialylated and/ or fucosylated or further extended with monosaccharides (GlcNAc, Gal, Man, Glc) to form linear or branched O-glycans. O-glycans may exist as mono- or disaccharides to form small structures but they can be extended to much more complex structures through the addition of polylactosamine sequence Gal β (1-4)GlcNAc β (1-3)Gal. In addition, sulfation of Gal, GlcNAc and GalNAc and O-acetylation of sialic acids are possible events in O-glycans (52).

core-type	Structure
<i>core 1</i>	Gal(β 1-3)GalNAc- α -Ser/Thr
<i>core 2</i>	GlcNAc(β 1-6)[Gal β 1-3]GalNAc- α -Ser/Thr
<i>core 3</i>	GlcNAc(β 1-3)GalNAc- α -Ser/Thr
<i>core 4</i>	GlcNAc(β 1-6)[GlcNAc(β 1-3)]GalNAc- α -Ser/Thr
<i>core 5</i>	GalNAc(α 1-3)GalNAc- α -Ser/Thr
<i>core 6</i>	GlcNAc(β 1-6)GalNAc- α -Ser/Thr
<i>core 7</i>	GalNAc(α 1-6)GalNAc- α -Ser/Thr
<i>core 8</i>	Gal(α 1-3)GalNAc- α -Ser/Thr

Table 1.1. Core structures of mucin-type O-glycans. Their structure starts with a GalNAc unit that is α -linked to Ser or Thr.

Further O-glycosidically linked glycans are known such as O- β -GlcNAc, O-Man, O-Fuc or O-Glc (51). The GlcNAc- β -Ser/Thr O-glycosylation is typically found in nuclear and cytoplasmic proteins and is not modified with further monosaccharides (51, 101).

The functions of protein-linked O-glycans are diverse. O-glycans play crucial roles in recognition phenomena such as cell growth and proliferation, cell fate determination, differentiation, glycoprotein clearance and trafficking, immunological recognition, signaling pathways and regulation of proteolysis. In addition, they stabilise the conformation of the protein, their tertiary and quaternary structure and they confer protease and heat resistance (52).

1.2.4 Function of glycans in stem cells and stem cell markers

The unique characteristics of SCs to self-renew through cell division as well as to generate a progeny of specialised cells make them ideal in the field of tissue formation, regeneration and repair. The optimal position of glycans at the cell surface grants them important roles in the control of stem cell maintenance, proliferation and differentiation. The fibroblast growth factor (FGF) is responsible for regulation of growth and differentiation factors in stem cells. The first fibroblast growth factor was isolated and characterised over 30 years ago (102). Since that time the FGF family was shown to comprise a family of 22 molecules in mammals (103), which is involved in numerous processes such as proliferation, differentiation, cell migration, tissue repair, wound healing, as well as tumor angiogenesis. FGF-2 plays crucial roles in the regulation of self-renewal and proliferation of SCs. Thereby FGFs bind to high-affinity FGF receptors as well as to lower-affinity to heparan sulfate proteoglycans at the cell surface. The binding-affinity of FGF is regulated by the substitution profile such as sulfation (52, 70).

Proteoglycans are a family of molecules consisting of a core protein (aggrecan, glypican, perlecan or syndecan) to which long chains of repeating sulfated disaccharide units are bonded such as heparan sulfate. Proteoglycans are either secreted molecules or found on the cell surface. Besides proteoglycans, Cystatin C was shown to modulate the mitogenic properties of FGF-2 signalling in neural SCs. Cystatin C is a secreted N-glycosylated polypeptide and acts as a cysteine proteinase inhibitor (104). Studies in rats revealed that the single N-glycosylation site of Cystatin C plays crucial roles in its autocrine/ paracrine cell signaling effect (105).

The Wnt proteins are growth and differentiation factors and secreted glycoproteins in the extracellular matrix (ECM). They induce intracellular signaling through binding to heparan sulfate proteoglycans (70).

In addition, Notch is a large transmembrane glycoprotein which is essential in stem cell fate determination. The signaling event of Notch is dependent on the glycosylation of its extracellular epidermal growth factor (EGF) domains, which can bear numerous N-linked as well as O-linked glycans. The two following glycan modifications are essential in the Notch signaling pathway; one describes the addition of fucose by O-fucosyltransferase enzyme to the hydroxy groups of Ser or Thr residues in specific Notch EGF repeats (106). The glycan is then further elongated by addition of a GlcNAc residue (107). These glycan modifications were demonstrated to modulate Notch binding to its ligands (108), which automatically makes them participating in cell fate determination.

Both carbohydrate specific antibodies and lectins were used for the analysis of stem cell surface N-glycans and showed that each SC type possess a distinct glycan decoration at the

cell surface (70). Thus, the cell-specific glycosylation is a potential appropriate tool for SC lineage characterisation and beneficial for applications in regenerative medicine.

Most of the known molecular markers of cells are cell surface proteins or lipids. In addition to proteins and lipids, carbohydrates are the next major class of cellular macromolecules and are at the same time abundant components of the cell surface. Indeed, many stem cell markers possess a crucial carbohydrate epitope, which is involved in many aspects of stem cell biology such as proliferation and differentiation (77). Moreover, the cell surface position and lineage-specific nature of glycans makes them ideal to identify and isolate specific cell types (77).

Several studies revealed stem cell markers mainly for embryonic, hematopoietic and neural SCs that are identified through their carbohydrate antigens (109-111). For instance, the stage-specific embryonic antigen (SSEA) glycolipids SSEA-3 and SSEA-4, which are typically used as embryonic stem cell markers, were originally identified through monoclonal antibodies recognising carbohydrate epitopes that are part of globoseries glycosphingolipids (77, 111). In addition to that, the tumor-rejectin antigens (TRA) are a family of ESC markers. They have been shown to recognise a keratan-sulfated proteoglycan in neuraminidase-sensitive (TRA-1-60) and neuraminidase-insensitive (TRA-1-82) fashion (112).

PSA-NCAM (polysialylated neuronal cell adhesion molecule) is considered to be a neural cell surface stem cell marker, which is modified with a linear homopolymer consisting of $\alpha(2-8)$ -linked sialic acid molecules and is mainly expressed in the developing nervous system (113, 114). CD34 is a type 1 transmembrane sialomucin and a glycan marker of human hematopoietic SCs. It is heavily glycosylated and clinically relevant since it is extensively used to separate bone marrow cells for transplantation (70). CD133 is a stem cell marker used for the identification and purification of human neural SCs. It is a five-transmembrane-domain cell surface glycoprotein and also called prominin-1 (70).

1.3 Profiling of cell surface glycosylation

1.3.1 Lectin staining of the cell surface

Due to the great structural diversity of glycans, glycan profiling with antibodies is difficult since it is impossible to generate antiglycan antibodies against each epitope. Glycoproteins, glycolipids and glycosaminoglycans of mammalian and non-mammalian origin comprise together more than 10^4 structures when bacterial glycans such as those from lipopolysaccharides are not included (52). Thus, the size of the glycome is tremendous. In addition to that, glycan structures are influenced by the structures of the protein or lipid backbone as well as by their own density and their position on the cell surface.

Lectins are a good alternative since they can discriminate between diverse structures through lectin-glycan interaction machineries. Lectins are mostly obtained from plants and are proteins that recognise and bind to glycans in a specific manner without modifying its structure. For example, they have been successfully used for glycan profiling as well as to study bioactivity and biomarker status of cells (115). Lectins are widely used in combination with common techniques like flow cytometry, western blottings, microarrays and immunohistochemistry to study cell surface glycan structures (55, 116).

Lectin microarrays, which use a combination of multiple lectins having different specificities, can also be used for glycan profiling. The main advantage is that glycan release is not necessary prior to use (117-119). In addition, the method can be applied to purified glycan samples such as glycoproteins or even to crude samples that contain diverse glycoconjugates such as cell lysates or body fluids (120, 121). Structural analysis can be directly obtained from the resulting signal pattern on the lectin microarray, which is very useful for quality control of glycoprotein products such as antibody drugs or in the analysis of clinical samples with respect to glycan-related biomarkers. A disadvantage of lectin microarrays is the washing step, which is required to remove unbonded fluorescence material. The affinity between lectin and glycan is weak (in terms of K_d , 10^{-4} to 10^{-7} M) in comparison to antigen-antibody interaction (10^{-6} to 10^{-9} M). As a result, the lectin-glycan complex dissociates easily during the washing process of the microarray and thus leads to a significant reduction of the signal intensity (52).

The interaction between lectins and glycans is usually analysed by frontal affinity chromatography (FAC) which is a quantitative method used to determine affinity constants. The lectin is immobilised on an affinity support and the glycan sample is added to the immobilised lectin. If the glycan binds to the immobilised lectin, the elution will be decelerated and the binding specificity of the lectin can be determined (52). Another technique is fluorescence-activated cell sorting (FACS), a flow cytometric approach, that enables sorting of cells based on their specific fluorescent characteristic.

Besides plants, lectins are also found in bacteria, viruses as well as animals or humans. The following plant lectins are typically used to study glycosylation: *Canavalia ensiformis* (ConA recognises Man and Glc), *Artocarpus integrifolia* (JAC, recognises Gal and GalNAc) or *Griffonia simplicifolia II* (GSA II recognises GlcNAc) (52). However, lectins possess limited specificity which may hinder accurate profiling and can lead to the loss of important structural information.

1.3.2 Cell membrane extraction

A frequent method used to analyse the N-glycome of cells is membrane (glyco)protein isolation followed by denaturation and/ or tryptic digestion of the (glyco)proteins and an enzymatic release of the N-glycans (122-125). In order to extract cell membrane (glyco)proteins cells have to be lysed for example by mechanical disruption. Cell lysis is the first step used in cell fractionation, isolation of organelles and protein extraction and purification. Cell lysis has to be applied after addition of protease inhibitors in order to prevent proteolysis. Several methods are possible, such as liquid homogenisation, sonication, freeze and thaw cycles or manual grinding. Sonication is achieved by a sonicator, in which high frequency sound waves shear the cells resulting in cell lysis. The application of repeated freeze and thaw cycles disrupt the cells through ice crystal formation. In the manual grinding, mortar and pestle are used to grind cells in liquid nitrogen. In this study, cell lysis was performed by a combination of the freezing/ thawing method and liquid homogenisation. In the liquid homogenisation method, which is the most widely used cell disruption technique for cultured cells, a French Press, a potter or a homogeniser is used to force the cells through a narrow space. Thereby, the cells are in suspension and cell membranes are sheared. This can also be achieved by passing the cell suspension through a syringe with a narrow needle.

After cell lysis, membrane (glyco)proteins have to be separated from cell debris and organelles. One very simple method to enrich (glyco)proteins from cell lysates is (ultra)centrifugation using sequentially increasing centrifugal forces which enables separation of cellular (glyco)proteins from cell debris as well as from membranes, mitochondria, nuclei or other cell organelles. In the first centrifugation steps, which are performed at low centrifugal forces, the heaviest fragments such as cell organelles are removed and soluble (glyco)proteins remain in the supernatant. In the last centrifugation step the centrifugal force is the highest and results in the formation of a pellet which includes membrane (glyco)proteins but also (glyco)lipids.

This pellet is soluble in water and (glyco)proteins can then be precipitated through the addition of a combination of organic solvents such as chloroform and methanol, in which (glyco)lipids are soluble. (Glyco)lipids can be extracted from the (glyco)proteins using an organic solvent such as ethanol in which the hydrophobic membrane (glyco)proteins are insoluble. Due to the hydrophobic character of membrane proteins, non-ionic detergents such as sodium dodecyl sulfate (SDS) are required for their solubilisation to induce the formation of protein-detergent micelle complexes. In addition, solubilisation can be facilitated with sonication. Once (glyco)proteins are in solution, they can be denatured and/ or

tryptically digested to facilitate subsequent glycan release. N-glycans are classically released with peptide-N⁴-(N-acetyl- β -D-glucosaminyI)-asparagin amidase F (PNGase F).

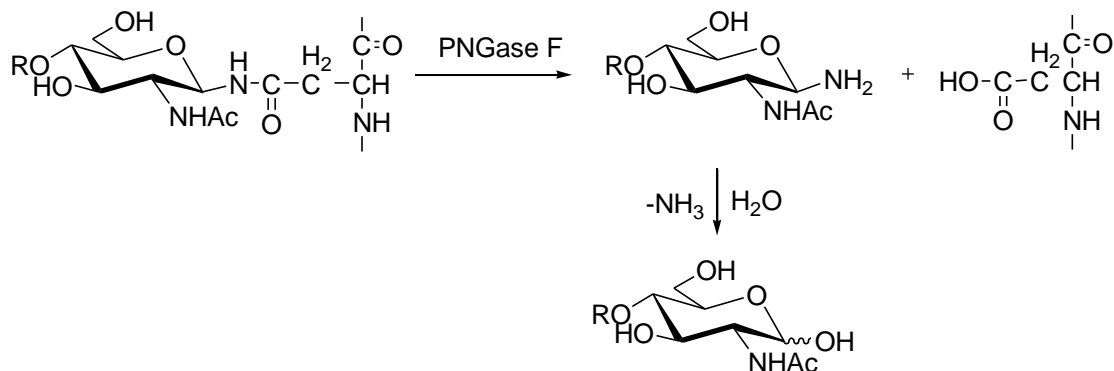
However, the protocol of membrane (glyco)protein isolation requires many time-consuming steps and the resulting N-glycan pool contains intra- and extracellular proteins. In addition, it was found that the N-glycans obtained by this method have a high proportion of high-mannoses, which may originate from intracellular proteins derived from the ER (122, 124, 126). This hinders accurate detection and quantification of the complex-type N-glycans. We recently developed a protocol to overcome the problem of complex-type N-glycan quantification using Endo H to detach and isolate high-mannose and hybrid-type N-glycans (127) (section 2.2.1). Complex-type N-glycans were subsequently released by PNGase F digestion. This protocol resulted in improved detection and quantification of the complex N-glycans in the investigation of the change in N-glycome during mesenchymal SC differentiation (127).

1.3.3 Release of N- and O-glycans

In order to investigate the structures of glycans, they have to be detached from the protein through cleavage of the glycosidic bond between the glycan and polypeptide. One method is the enzymatic deglycosylation, where several glycosidases stemming from bacteria and plants are used (51). A frequently used glycosidase is PNGase F, also known as N-glycanase. PNGase F was first isolated from the bacteria *Flavobacterium meningosepticum* but is commercially available as a recombinant protein expressed in *Escherichia coli*. Three acidic amino acid, two glutamic acid residues as well as one aspartic acid (Asp) residue are involved in the catalytic activity of the enzyme and are located in a cleft between the two domains of the protein (128). PNGase F cleaves the β -glycosidic amide bond between the Asn side chain and the first GlcNAc unit of the N-glycan (GlcNAc-Asn), whereupon the Asn residue is converted into Asp (128, 129). This results in the generation of the 1-amino-oligosaccharide-intermediate, which will hydrolyses to ammonia and the free intact oligosaccharide (128).

Denaturation of the glycoprotein prior to the PNGase F-digestion increases the efficiency of the carbohydrate cleavage and requires significant lower amounts of the enzyme (128, 130). PNGase F possesses high substrate specificity and is able to cleave complex di-, tri- and tetraantennary carbohydrate structures, which may be polysialylated, sulfated or phosphorylated (128-131). In addition, the enzyme is able to cleave N-glycans of the high-mannose- and hybrid-type (132). However, some N-glycosylation sites in native structures of protein are inaccessible (129). PNGase F is able to cleave α (1,6)-fucosylated N-glycans whereas it is not able to release N-glycans having α (1,3)-linked core-Fuc residues (128,

133). In this case PNGase A, which was first discovered in almonds, is used to cleave $\alpha(1,3)$ -fucosylated N-glycans. In addition, PNGase A can detach N-glycans of the high-mannose, hybrid- as well as complex-type (128, 133).



Scheme 1.1: General scheme of the enzymatic deglycosylation of a N-glycan by PNGase F. The enzymatic cleavage takes place when the GlcNAc-Asn region is accessible for the active side of PNGase F (129). In addition, the oligosaccharide has to consist of at least two GlcNAc units, which are $\beta(1-4)$ -linked to each other and attached at the Asn residue of the peptide. In addition the peptide backbone plays important structural roles, since the carboxyl as well as the amine group of the Asn have to be part of the peptide bond (128, 130).

In contrast to PNGase F, the endo- β -N-acetylglucosaminidases H, L, D and F cleave the bond between the GlcNAc- $\beta(1,4)$ -GlcNAc disaccharide of the core structure leaving one GlcNAc at the Asn residue of the peptide (134). Alternatively, N-glycans are chemically cleaved by hydrazinolysis but this leads also to a side reaction in which N-acetyl groups of the glycan are deacetylated and have to be reacylated afterwards.

There is no universal enzyme that cleaves O-glycans due to their numerous core-structures. O-glycans are detached from the protein backbone by β -elimination using chemical bases (135, 136). Many soft bases are used such as ammonia, methylamine, ethylamine and dimethylamine but degradation of the protein moiety is possible (136).

1.3.4 MALDI-TOF-MS

Matrix Assisted Laser Desorption/Ionization-time-of-flight mass spectrometry (MALDI-TOF-MS) is a popular mass spectrometry technique, for which samples are mixed with a UV-absorbing auxiliary compound named matrix and cocrystallised on a ground steel target. For the analysis of glycans the matrices 2,5-dihydroxybenzoic acid (DHB) or arabinosazone are often classically used. The laser beam reaches the matrix crystals and triggers acceleration of the ions under vacuum in an electric field, which are then detected after a flight route.

Because of the pulsed ion generation, a TOF-analysator is used for mass analysis. Ions are accelerated towards the detector with the same amount of kinetic energy. Ions with the same energy but different masses possess different speeds and reach the detector at different times. Thus, each molecule produces its own signal (129). The ionised species are mainly single charged molecule ions such as $[M+H]^+$, $[M+Na]^+$ and $[M+K]^+$.

MALDI-TOF-MS is able to detect and characterise biomolecules such as proteins, peptides, lipids, oligosaccharides and oligo-nucleotides. At the same time it is a very sensitive method, which enables analysis of low sample amounts (10^{-15} bis 10^{-18} mol) with very high accuracy. The advantages of this method are the short measuring time and the small sample consumption. In addition, a high mass range can be covered.

Collision induced dissociation (CID) fragmentation is a method used in MALDI-TOF-MS, which allows detailed analysis of the sequence and linkage-type of the monosaccharides in glycans (137). Through high-energy collision-induced activation, specific ion fragments are generated, which deliver important informations about the degree of branching, the substitution and a hint about the linkage-type of monosaccharides (138).

1.3.5 CE-LIF

Capillary electrophoresis (CE) is an analytical separation technique, which uses a thin capillary (20-200 μm inner diameter) to separate small and large molecules with high efficiency. The separation of the molecules occurs through the application of high voltages, which induce an electroosmotic flow (EOF) of the buffer solution inside the capillary.

The phenomenon of electroosmosis plays crucial roles in CE and is caused by the charge found on the surface of the capillary wall. Fused silica-capillaries, which possess ionisable silanol groups are used for CE analysis. The capillary is in contact with the buffer and its pH value determines the degree of ionization. The EOF is defined through the following equation, in which ϵ is the dielectric constant, η the viscosity of the buffer and ζ the zeta-potential. The zeta-potential is measured on the moving surface near to the solid-liquid barrier. Positively charged ions of the buffer are attracted by the negatively charged silanol groups of the capillary wall resulting in an electric double layer.

$$v_{eo} = \frac{\epsilon \zeta}{4\pi\eta} E$$

Electroosmotic flow

When a voltage is applied along the capillary, cations of the double layer start to migrate to the cathode and thereby transporting water molecules. This results in a flow of the buffer solution in direction to the negatively charged electrode. The EOF is dependent on the pH

value, temperature, concentration of the electrolyte as well as on the electrophoretic mobility of the ions. The latter represents the migration speed of the ions, which is dependent on their charge, shape, effective size, temperature, pH value, solvent system and from the strength of the electric field. Thus, ions with different electrophoretic mobilities can be separated from each other.

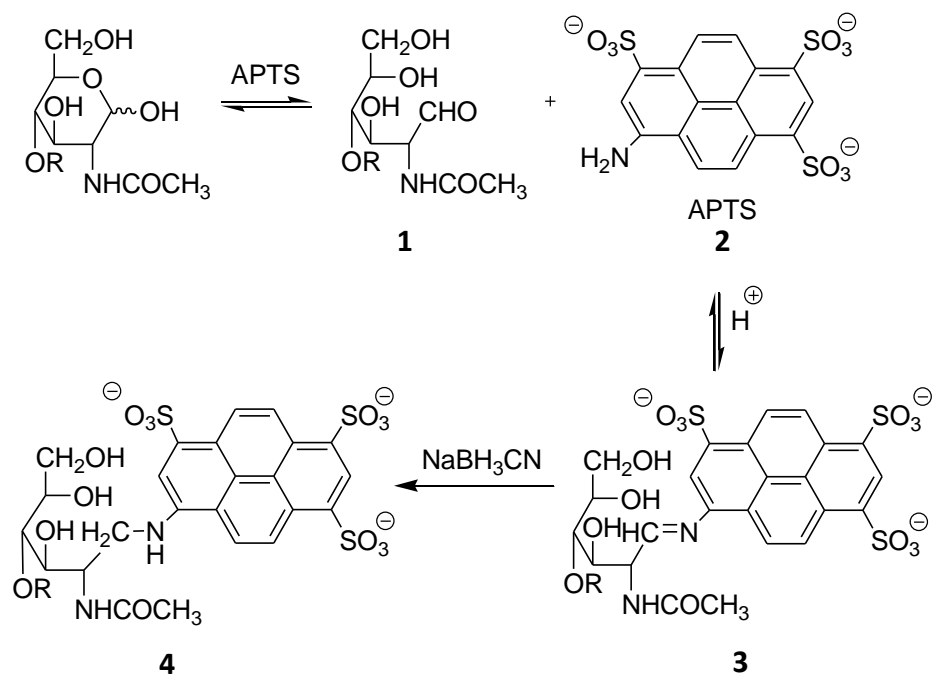
The CE instrument is easy to handle, efficient and can be automated for precise and quantitative analyses. In addition, small sample amounts and volumina (nl) as well as low amounts of reagents are required. Therefore, CE is an adequate method for the analysis of oligosaccharides and oligosaccharide mixtures. Moreover, CE is capable to separate and distinguish between carbohydrate isomers (139-141).

For structural analyses of carbohydrates, the instrumental set-up of the CE consists of a fused-silica capillary with a detector window, an adjustable high-voltage source, two electrodes, two buffer reservoirs and an UV-detector. The silica capillary is coated with polyvinyl alcohol and minimizes on the one hand the EOF and at the other hand reactions between the sample and the capillary wall. The ends of the capillary reside in the buffer reservoirs and the optical detector window is connected with the detector. After the capillary is rinsed with the buffer, the sample is electrokinetically injected or through application of pressure. Both capillary ends reside in the buffer and a voltage of about 30 kV will be applied. The sample components will migrate with different speed in the electrical field in direction to the capillary outlet and will cross the detector as well as the detector window enabling qualitative and quantitative analysis.

The detection of the analyte can be achieved through UV-absorption or laser-induced fluorescence (LIF), which requires labeling with an appropriate fluorophore. The triply charged fluorophore 8-aminopyrene-1,3,6-trisulfonic acid (APTS, $\lambda_{exc}= 488$ nm, $\lambda_{em}= 520$ nm) is widely used for carbohydrate analysis performed with CE-LIF (139, 140). It allows the detection of glycans in low attomole range (142).

The labeling of the glycans occurs through reductive amination at the reductive end of the carbohydrate. The mechanism of reductive amination through which the carbohydrate is converted to a glycamine is depicted in Scheme 1.2. The labeling proceeds via two steps. First the oligosaccharide (**1**) and the primary amine (**2**) form compound **3** by a condensation reaction. Then **3** is reduced by sodium cyanoborohydride (130). Stoichiometrically one APTS molecule binds to each oligosaccharide molecule, resulting in a second order reaction (141). The reaction of APTS-labeling through reductive amination is complete when APTS is applied with excess (142). Studies revealed that APTS is an excellent fluorophore, which enables the separation of neutral carbohydrates through CE (139, 142). However, APTS is not suitable for analysis of sialylated carbohydrates because the increasing negative charge

causes a strong increase in migration speed (139). The use of an internal standard such as maltose, enables quantitative analysis.



Scheme 1.2: Reductive amination of oligosaccharides using 8-aminopyrene-1,3,6-trisulfonic acid (APTS). The reductive amination proceeds via two steps; a condensation reaction between the oligosaccharide and the primary amine followed by a reduction using sodium cyanoborohydride.

1.4 Aim of the work

Due to the unique characteristics of stem cells (SCs) to self-renew as well as to differentiate into specialised cells with more restricted potential, they are of great interest in the field of regenerative medicine and tissue engineering.

In order to apply SCs therapeutically, they first have to be isolated and well characterised as pure cell populations thereby confirming their SC status. In addition, the process of differentiation has to be monitored to determine their differentiation status as well as to exclude teratoma formation of embryonic SCs (ESCs). This can be achieved by controlling their morphology, immunohistochemistry in combination with FACS analysis, cell staining and/ or quantitative real time PCR. Some of these methods are not reliable enough, time-consuming or require the use of high cell amounts, which will increase the costs drastically. Thus, it is of utmost importance to find reliable SC biomarkers that can identify SC populations and their differentiated progeny fast and accurately.

The glycocalyx is a dense cell surface layer, which is composed of glycans with great structural diversity. These glycans are connected to proteins or lipids through a post- or cotranslational process, which is called glycosylation. Cell surface glycosylation varies in different cell-types as well as species and is sensitive towards biological processes such as differentiation. Cell surface glycans may therefore serve as a powerful tool for the identification and isolation (quality control) of SCs and hold great potential to be used as SC biomarkers.

The main goal of this study is to determine glycan-based biomarkers for mesenchymal SCs (MSCs) and ESCs and their differentiated progeny. Therefore, the aim is to investigate the cell surface N-glycosylation pattern of MSCs and its quantitative and qualitative changes during adipogenic, chondrogenic and osteogenic differentiation as well as the cell surface N-glycosylation of ESCs and its alteration during hepatogenic differentiation into hepatocyte-like cells.

To fulfill these tasks, a rapid and reproducible protocol to analyse cell surface N-glycosylation has to be established and optimised. Qualitative and quantitative changes of N-glycan structures during SC differentiation will be analysed using MALDI-TOF mass spectrometry and CE-LIF. Verification of N-glycans will be done using mass spectrometric fragmentation (MALDI-TOF/TOF-MS) and exoglycosidase digestion experiments.

2 Results

2.1 Design and optimisation of a rapid analysis method to profile cell surface N-glycosylation of living cells

2.1.1 Analysis of cell surface N-glycosylation using the cell membrane preparation protocol

The conventional protocol used to investigate the N-glycome of a cell line is the isolation of its cell membrane by cell lysis followed by purification of membrane proteins (see 1.3.2). First, this protocol was used to characterise the N-glycosylation pattern of HEK 293 cells. Thus, about 4×10^6 HEK 293 cells were used to investigate the N-glycome by the conventional membrane preparation protocol used in our laboratory. Using this protocol, membrane (glyco)proteins were isolated from cell lysates by membrane extraction after three centrifugation steps and a lipid separation step. Afterwards, the resulting pellet was redissolved in phosphate buffer containing the detergents Nonidet P-40 and SDS to ensure solubilisation (see 1.3.2 and 4.5.1). Membrane glycoproteins were subsequently digested with trypsin and N-glycans were then released using peptide-N4-(N-acetyl- β -glucosaminyl) asparagine amidase F (PNGase F). After purification using reversed-phase C18 and carbograph cartridges, N-glycans were permethylated prior to MALDI-TOF-MS to neutralise the negative charge of sialic acids. This allows the simultaneous detection of both acidic and neutral N-glycans in the positive-ionization mode of MALDI-TOF-MS. (126, 143) A representative MALDI-TOF mass spectrum is shown in Fig. 2.2 A and the relative abundances are presented in Table 1 (see appendix). The mass spectrometric data revealed about 80 different N-glycan structures; the most abundant N-glycan fraction was the high-mannose-type, which comprised about 83 % of the N-glycan pool. Next, the complex-type N-glycans represented 15 % of the N-glycan pool and trace amounts of hybrid-type N-glycans (2 %) were detected as well. Complex-type N-glycans predominantly bore two antennae, however, tri- and tetraantennary complex N-glycans were detected as well. Moreover, complex-type N-glycans were found to contain 0-3 Fuc residues, in which at least one of them was connected to the reducing GlcNAc of the core structure. In most of the cases N-glycans were only partially sialylated. The high amount of high-mannose N-glycans obtained by the membrane preparation protocol prevents accurate detection and precise quantification of complex-type N-glycans that contain important structural informations about the degree of antennarity, fucosylation and sialylation. Therefore, a new method was established, that fulfill these criteria and at the same time is able to profile only cell surface glycosylation.

2.1.2 Analysis of cell surface N-glycosylation using the new method that releases only cell surface N-glycans from living cells

With the aim of releasing only cell surface N-glycans, living HEK 293 cells were treated with trypsin in order to digest solely cell surface (glyco)proteins. The methodical steps of the new approach were depicted in Fig. 2.1. About 4×10^6 cells were harvested and washed three times with phosphate buffered saline (PBS). Afterwards, the cell pellet was resuspended in 500 μ l of a freshly prepared 2.5 mg/mL trypsin solution in PBS. This trypsin concentration is usually used to detach adherent cells from cell culture dishes. The trypsin digestion was carried out for 15 min at 37 °C under slight agitation. For the cell lines used in this study, it was found that lower trypsin concentrations showed less efficiency regarding N-glycan yield: N-glycans of higher molecular weights were gradually lost with decreasing trypsin concentrations. After tryptic digestion, the sample was centrifuged and the supernatant, which contains cell surface (glyco)peptides, was separated from the pellet. N-glycans were released from glycopeptides using PNGase F, purified using reversed-phase C18 then carbograph cartridges and permethylated prior to mass spectrometry. N-glycans were measured by MALDI-TOF-MS in the positive ionization mode. A representative mass spectrum of cell surface N-glycans of HEK 293 is shown in Fig. 2.2 B and the relative abundance of each detected structure is summarised in Table 1 (see appendix).

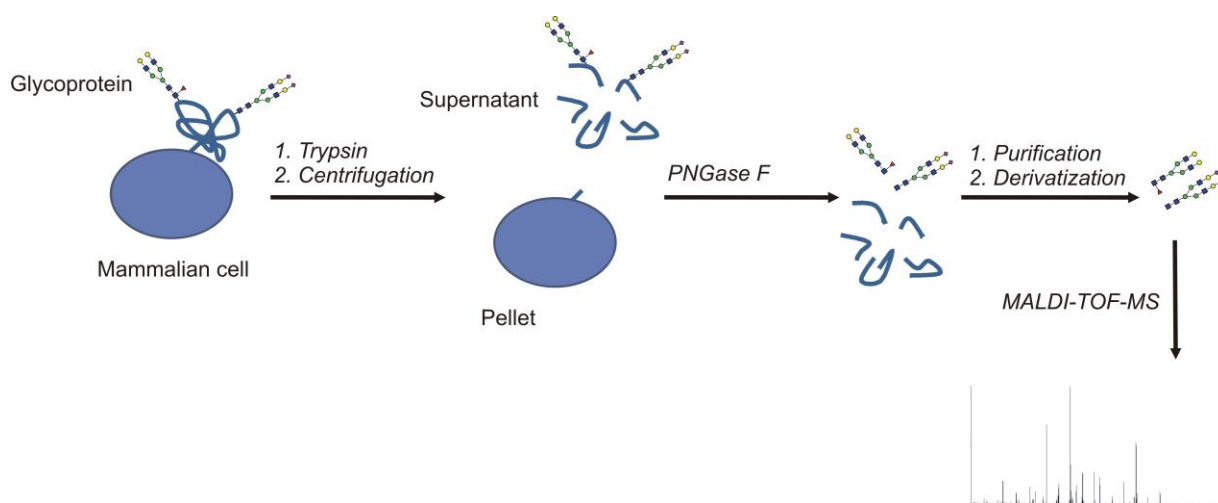


FIG. 2.1. Approach of direct digestion of cell surface (glyco)proteins on living cells. Cell surface (glyco)peptides were directly released from HEK-293 cells using trypsin and were separated from the cells by centrifugation. N-glycans were enzymatically cleaved from tryptic glycopeptides with PNGase F, permethylated and measured by MALDI-TOF-MS.

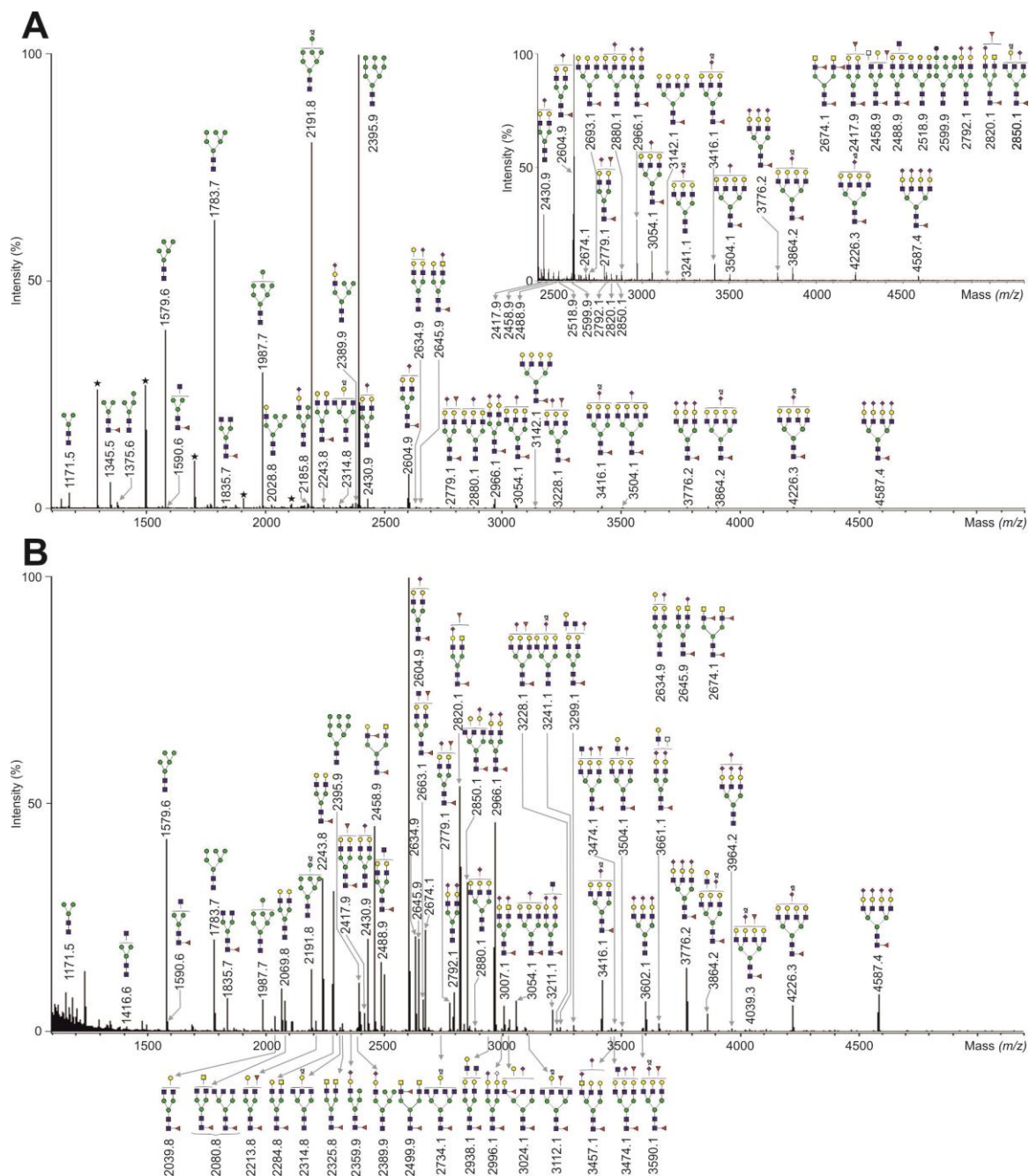


FIG. 2.2. MALDI-TOF-MS of PNGase F-released N-glycans from HEK 293 cells. (Glyco)proteins were isolated from HEK 293 using membrane extraction (A) or cell surface glycoproteins were directly tryptic digested from the cells (B). N-glycans were enzymatically cleaved from tryptic glycopeptides with PNGase F, permethylated and measured by MALDI-TOF-MS. A representative mass spectrum of PNGase F-released N-glycans of HEK 293 is shown together with the 60 most abundant structures. * Polyhexose contaminations are negligible. Blue square represents N-acetylglucosamine, yellow square N-acetylgalactosamine, white square N-acetylhexosamine, green circle mannose, yellow circle galactose, red triangle fucose, white diamond N-glycolylneuraminic acid and pink diamond N-acetylneuraminic acid.

In total, 95 different N-glycan signals were detected. The relative amount of high-mannose N-glycans dropped drastically to 14 % when compared with the amount found in the N-glycan profile of HEK 293 derived from membrane extraction method. In contrast, the amount of complex N-glycans increased to 85 % and the amount of hybrid-type N-glycans remained almost the same (1 %). High-mannose N-glycans of the composition H3-9N2 were detected. Biantennary N-glycans were the most abundant complex-type structures (70 %), but tri- and tetraantennary N-glycans were detected as well. Regarding fucosylation, fucosylated biantennary N-glycans represented about 60 % of the N-glycan pool and carried 0-3 Fuc residues. In addition, biantennary N-glycans were predominantly partially sialylated with 0-2 Neu5Ac units. Triantennary N-glycans comprised about 10 % of the N-glycan pool and contained 0-3 Fuc as well as 0-3 Neu5Ac residues. About 4 % of the N-glycan pool were tetraantennary N-glycans and were all fucosylated (1-2 Fuc). Neutral as well as sialylated or/and fucosylated hybrid-type N-glycans were detected.

With the new method the cell surface N-glycosylation profile of HEK 293 contained the following 25 additional signals, which were assigned to complex-type structures and accounted for about 7 % of the N-glycan pool: S1H4N4 (*m/z* 2226.8), H6N4 (*m/z* 2273.8), S1H4N4F1 (*m/z* 2400.9), S1H4N5 (*m/z* 2471.9), H3N6F2 (*m/z* 2499.9), H4N6F1 (*m/z* 2529.9), H4N5F3 (*m/z* 2632.9), S1H5N5 (*m/z* 2676.1), S1H3N6F1 (*m/z* 2687.1), H5N6F1 (*m/z* 2734.1), H5N5F3 (*m/z* 2837.1), S1H3N6F2 (*m/z* 2861.1), H5N6F2 (*m/z* 2908.1), S2H4N5F1 (*m/z* 3007.1), S1H5N5F2 (*m/z* 3024.1), S2H5N5 (*m/z* 3037.1), S2H3N6F1 (*m/z* 3048.1), H6N6F2 (*m/z* 3112.1), S1H5N6F2 (*m/z* 3269.1), S2H5N6F1 (*m/z* 3457.1), S1H6N6F2 (*m/z* 3474.1), S2H6N6F1 (*m/z* 3661.1), S1H7N7F1 (*m/z* 3749.1), S4H6N5 (*m/z* 3964.2) and S3H7N6F2 (*m/z* 4400.4). These signals were absent when the membrane preparation method was applied.

These results demonstrated that the new method led to an improved detection and therefore a better quantification of complex-type N-glycans, when compared with the membrane preparation method.

2.1.3 Reproducibility of the new method

To test the reproducibility of the new method, the cell surface protocol was repeated three and the membrane extraction protocol four times and the mean relative abundances were compared. Fig. 2.3 presents the relative amounts of the 27 most abundant structures found in the N-glycosylation profile of HEK 293 cells when membrane glycoproteins (black) and cell surface glycoproteins (grey) were digested. A high reproducibility of both N-glycan profiles was obtained as can be judged from the small deviations obtained within the observed glycan profiles. The N-glycan distribution was significantly different in the methods employed,

however, little variation was observed among biological replicates. Thus, the cell surface protocol is as reproducible as the membrane preparation protocol.

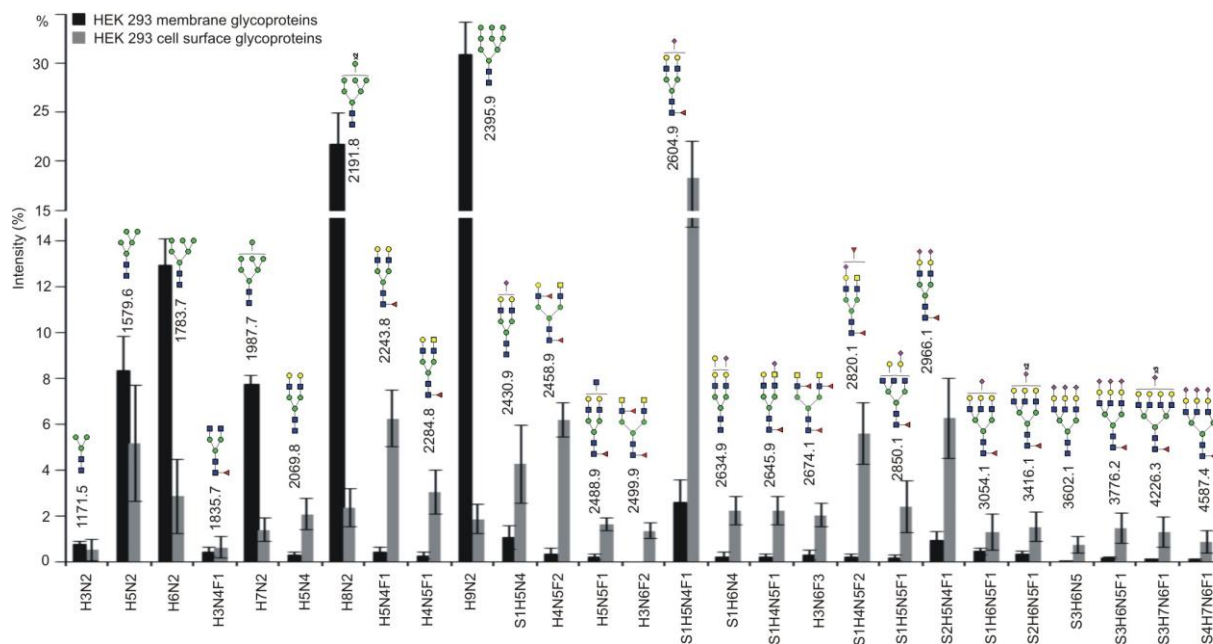


FIG. 2.3. Reproducibility of N-glycan isolation using membrane glycoprotein extraction (black) and direct digestion of cell surface glycoproteins (grey). The average relative intensity of the 27 most abundant structures from MALDI-TOF-MS are shown (n=4). Blue square represents N-acetylglucosamine, yellow square N-acetylgalactosamine, white square N-acetylhexosamine, green circle mannose, yellow circle galactose, red triangle fucose, white diamond N-glycolylneuraminic acid and pink diamond N-acetylneuraminic acid.

2.1.4 Analysis of the N-glycome by membrane preparation protocol after cell surface digestion of living cells with trypsin

The N-glycosylation profile of HEK 293 obtained from tryptic cell surface digestion of living cells comprised about 85 % of complex N-glycans, indicating that digestion was predominantly occurred on cell surface proteins. In order to confirm this assumption, cell surface (glyco)proteins were digested by trypsin. Then the pellet was separated from the supernatant that contained the (glyco)peptides, washed three times with PBS and after a freeze and thawing step, the membrane extraction protocol was applied. The isolated membrane (glyco)proteins were subsequently digested with trypsin and N-glycans were released using PNGase F. Released N-glycans were purified, permethylated and then measured by means of MALDI-TOF-MS. A representative MALDI-TOF mass spectrum is shown in Fig.2.4. High-mannose N-glycans comprised 94 % of the measured signals and were detected in the form H5-9N2 (m/z 1579.6, 1783.7, 1987.7, 2191.8 and 2395.9). In

addition, two hybrid-type N-glycans S1H5N3 (m/z 2185.8) and S1H6N3 (m/z 2389.9) were detected and comprised 1 % of the N-glycan pool.

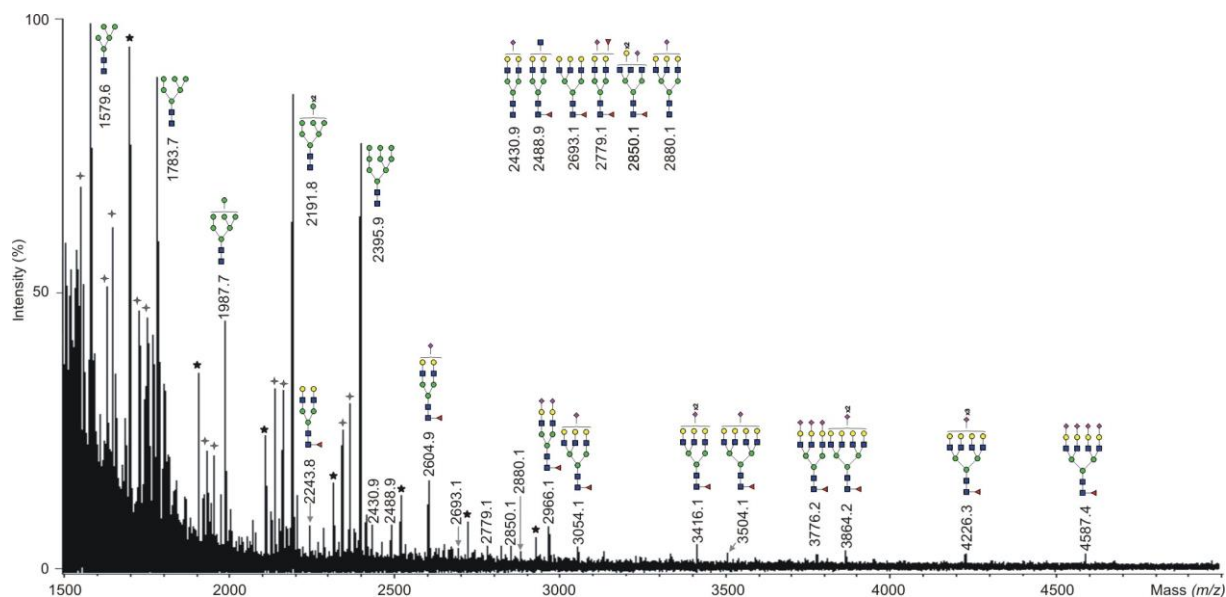


FIG. 2.4. MALDI-TOF-MS of N-glycans obtained using the membrane extraction protocol in the pellet obtained after cell surface tryptic digestion of HEK 293 cells. Cell surface (glyco)proteins were directly released from living HEK 293 cells using trypsin. The supernatant containing cell surface (glyco)peptides was separated from the pellet and the pellet was washed three times with PBS followed by a (glyco)protein isolation using membrane extraction. (Glyco)proteins were digested with trypsin and N-glycans were enzymatically cleaved with PNGase F, permethylated and measured by MALDI-TOF-MS. * Polyhexose contaminations are negligible. + Non-identified signal. Blue square represents N-acetylglucosamine, yellow square N-acetylgalactosamine, white square N-acetylhexosamine, green circle mannose, yellow circle galactose, red triangle fucose, white diamond N-glycolylneuraminic acid and pink diamond N-acetylneuraminic acid.

The remaining 5 % of detected N-glycan signals were complex N-glycans (m/z 2243.8, 2284.8, 2430.9, 2458.9, 2604.9, 2779.1, 2850.1, 2966.1, 3054.1, 3416.1, 3776.2, 3864.2, 4226.3, 4587.4 and 4675.4). From these results it can be judged that intracellular N-glycans were mainly of high-mannose type and originate very probably from the ER, where the biosynthesis of N-glycans occurs. Previous studies by An et al. [121] confirmed enrichment of plasma proteins but also contamination from ER and other membranes by proteomic analysis, which indicates that N-glycans derived from the ER were included in the N-glycan pool of glycoproteins obtained from the membrane preparation method as well. They are very likely to be the major source of high-mannose-type N-glycans in the N-glycome of cells. The use of the new established method resulted mainly in complex-type structures, which indicates the absence of nascent glycoproteins from the ER.

2.1.5 Cell surface N-glycosylation of AGE1.HN, CHO-K1 and Hep G2 cells

The sensitivity of new method was tested by applying it to the cell lines AGE1.HN (human neuronal cell line), CHO-K1 (chinese hamster ovary cell line) and Hep G2 (human liver hepatocellular carcinoma cell line). A representative MALDI-TOF mass spectrum of the cell surface N-glycosylation profile of each cell line is shown in Fig. 2.5 and the relative abundances of each detected N-glycan signal are listed in Table 1 (see appendix). About 85 different N-glycan signals were detected in the MALDI-TOF-MS spectrum of AGE1.HN cells. AGE1.HN N-glycans have a higher degree of fucosylation, when compared with HEK 293. About 43 % of the N-glycan pool was comprised by biantennary fucosylated N-glycans, which beared 1 to 3 Fuc residues. In addition, the antennarity was higher in AGE1.HN cells due to the fact that tetra- and triantennary fucosylated N-glycans (1-5 Fuc, 1-4 Fuc, respectively) comprised together 18 % of the total relative intensity, and 14% in HEK 293. The high-mannose N-glycan fraction comprised together about 18 % of the cell surface N-glycosylation profile and contained N-glycans with the composition H4-9N2. A minor amount of about 4 % of hybrid N-glycans was detected as well and contained neutral, monosialylated and/ or monofucosylated structures. The structures and relative amounts of hybrid N-glycans detected were almost similar in HEK 293, CHO-K1, AGE1.HN and Hep G2 cells.

Cell surface N-glycans of CHO-K1 cells contained a significant higher amount of high-mannose N-glycans of the form H4-9N2 (about 42 %), when compared to the three other cell lines. However, complex-type N-glycans comprised about 55 % of the N-glycan pool of CHO-K1 cells. The main part of the complex-type N-glycans found in CHO-K1 cells were biantennary monofucosylated structures, however, a minor amount of bifucosylated structures was detected as well. In addition, tri- and tetraantennary N-glycans were present, which comprised together about 5 %. Most of the complex N-glycans detected in CHO-K1 cells were present as asialylated or monosialylated structures but some fully sialylated triantennary N-glycans were detected as well. Sialylated N-glycans beared mostly Neu5Ac residues but also N-glycolylneuraminic (Neu5Gc) acid was present in the N-glycan pool of CHO-K1. The Neu5Gc-containing N-glycans represented together about 3 % of the N-glycan pool. These structures were verified by MALDI-TOF/TOF (see 2.1.7).

Cell surface N-glycosylation profiling of Hep G2 revealed about 114 different N-glycan signals by MALDI-TOF-MS. About 82 % of the detected structures were of the complex-type where biantennary N-glycans represented the majority of the N-glycan pool (55 %). Biantennary N-glycans were mostly fucosylated (1-3 Fuc) but non-fucosylated biantennary N-glycans were detected as well. The most abundant biantennary complex-type N-glycans found in Hep G2 were mono- or disialylated structures. Triantennary N-glycans constituted together 6 % of the signals and contained 0-3 Fuc residues and 0-4 terminal Neu5Ac units.

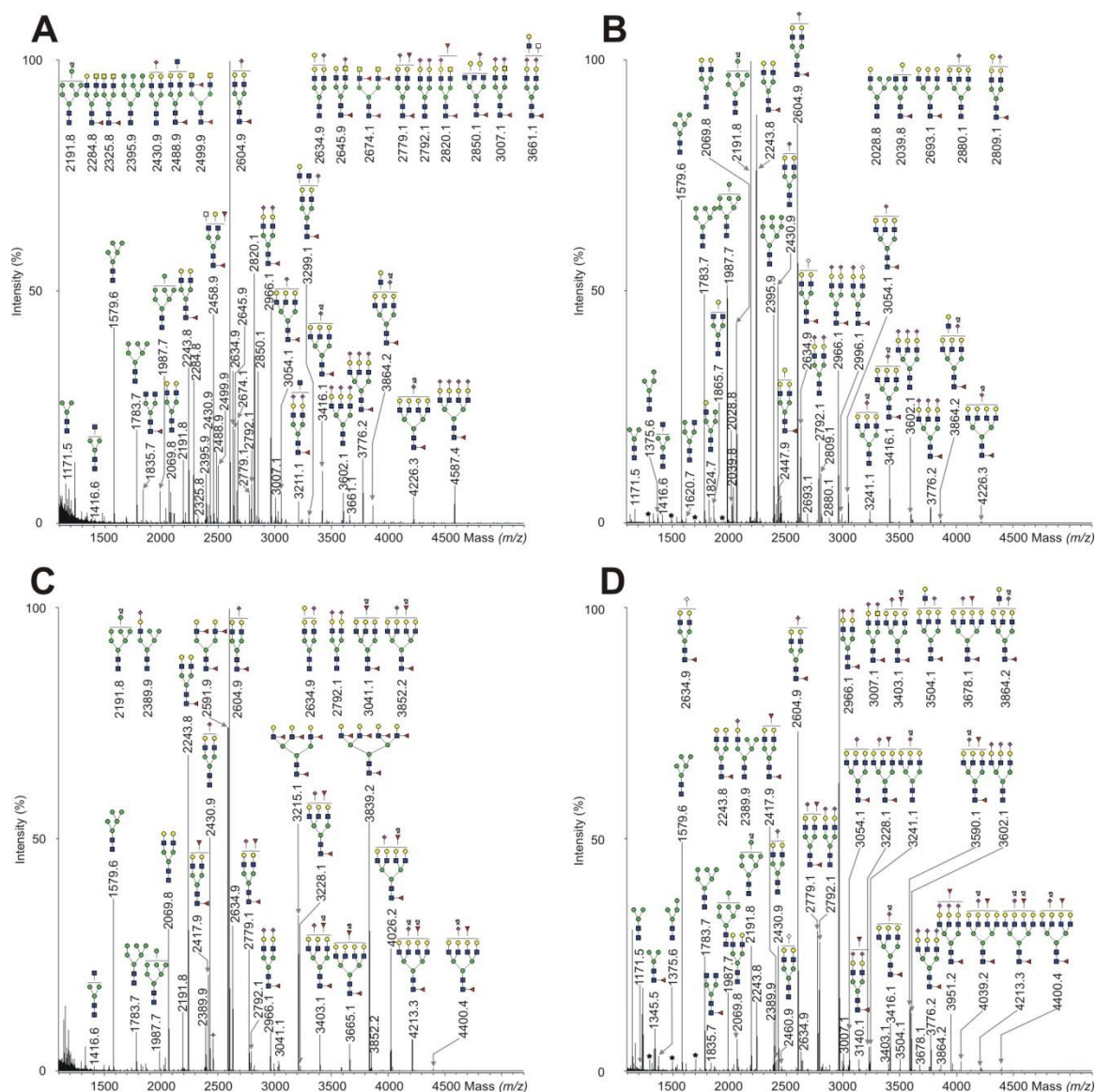


FIG. 2.5. MALDI-TOF-MS of PNGase F-released N-glycans from HEK 293 (A), CHO (B), AGE1.HN (C) and HEP G2 cells (D). Cell surface glycoproteins were directly digested from the cells. N-glycans were enzymatically cleaved from glycopeptides with PNGase F, permethylated and measured by MALDI-TOF-MS. A representative mass spectrum of PNGase F-released N-glycans of the four different cell types is shown together with the most abundant structures. * Polyhexose contaminations are negligible. † Non-identified peaks. Blue square represents N-acetylglucosamine, yellow square N-acetylgalactosamine, white square N-acetylhexosamine, green circle mannose, yellow circle galactose, red triangle fucose, white diamond N-glycolylneuraminic acid and pink diamond N-acetylneuraminic acid.

The amount of tetraantennary and larger N-glycans was about 16 % in Hep G2 cells and therefore much higher than in all the other cell lines, including AGE1.HN cells. High-mannose N-glycans of the form H4-9N2 were detected as well. In addition, two high-mannose

structures were also found to be present as monofucosylated species in Hep G2 cells, namely H4N2F1 and H5N2F1.

2.1.6 CE-LIF analysis of cell surface N-glycosylation of HEK 293, AGE1.HN, CHO-K1 and Hep G2 cells

About 40 % of the N-glycan pool was analysed by means of CE-LIF in order to confirm the structures found by MALDI-TOF-MS. Prior to the measurement, the N-glycans were labeled with APTS and chemically desialylated by acetic acid hydrolysis, in order to convert the charged sialylated N-glycans into neutral molecules, and thus making separation independent from the charge of Neu5Ac. N-Glycans were then desalted on self-made graphite micro-columns and then subjected to CE-LIF analysis. Representative CE-LIF electropherograms of PNGase F-released N-glycans of HEK 293, CHO-K1, AGE1.HN and HEP G2 cells are presented in Fig.2.6 A, B, C and D, where migration times were converted into glucose units (GU). N-glycans were assigned with the help of a standard table generated in our laboratory using N-glycan release from reference glycoproteins. In addition, MALDI-TOF-MS spectra of the desialylated N-glycan pools were used to assign the structures. The main structures were assigned to the electropherogram signals and will be presented in the next paragraphs.

In HEK 293 the high-mannose N-glycans H5N2 (6.7 GU), H6N2 (7.5 GU) and H8N2 (9.3 GU) were detected. The biantennary N-glycans H5N4 (8.9 GU) and H5N4F1 (9.8 GU) represented the majority of the N-glycan pool. In addition, triantennary N-glycans migrated between 10 and 12 GU. The tetraantennary structures H7N6 (13.0 GU) and H7N6F1 (13.8 GU) were assigned in the electropherogram as well. In addition, larger N-glycans such as H7N6F2, H7N7F1 and H8N7F1 were detected between 14.0 and 19.0 GU. The CE-LIF electropherogram of HEK 293 cell surface N-glycans confirmed the mass spectrometric data qualitatively and quantitatively.

CE-LIF analysis of CHO-K1 cell surface N-glycans revealed that the biantennary structures H5N4 (8.9 GU) and H5N4F1 (9.8 GU) comprised the main part of the N-glycan pool, followed by the triantennary N-glycans H6N5 (11.0 GU) and H6N5F1 (12.0 GU) and tetraantennary fucosylated structure H7N6F1 (13.8 GU). Furthermore, the core-fucosylated tetraantennary N-glycan with additionally one N-acetylactosamine (LacNAc) unit (H8N7F1) was detected at 16.8 GU. In addition, the high-mannose structures H5N2 (6.7 GU), H6N2 (7.5 GU), H8N2 (9.3 GU) and H9N2 (10.5 GU) were detected.

In AGE1.HN the CE-LIF data revealed the presence of high-mannose structures H5N2 (6.7 GU), H6N2 (7.5 GU) and H8N2 (9.3 GU) as well as complex biantennary N-glycans H5N4 (8.9 GU) and H5N4F1 (9.8 GU). Complex N-glycans with more than one Fuc residue were

present as well (H5N4F2 at 10.6 GU, H7N6F2 at 14.2 GU, H7N6F3 at 15.5 GU, H7N6F4 at 16.8 GU and H7N6F5 at 19.5 GU).

In HEP G2 cells high-mannose N-glycans (H5N2 at 6.7 GU, H6N2 7.5 GU) were detected but the complex biantennary N-glycans H5N4 (8.9 GU) and H5N4F1 (9.8 GU) comprised the major part of the N-glycan pool. In addition, triantennary N-glycans H6N5 (11.0 GU), H6N5F1 (12.0 GU) and H6N5F2 (12.9 GU) as well as the tetraantennary fucosylated structures H7N6F1 (13.8 GU) and H7N6F2 (14.2 GU) were detected.

The overall distribution of the N-glycans of the different cell lines is very similar to the one found with MALDI-TOF-MS. Consequently, the CE-LIF electropherograms confirmed the mass spectrometric N-glycosylation data of all four cell lines qualitatively and quantitatively.

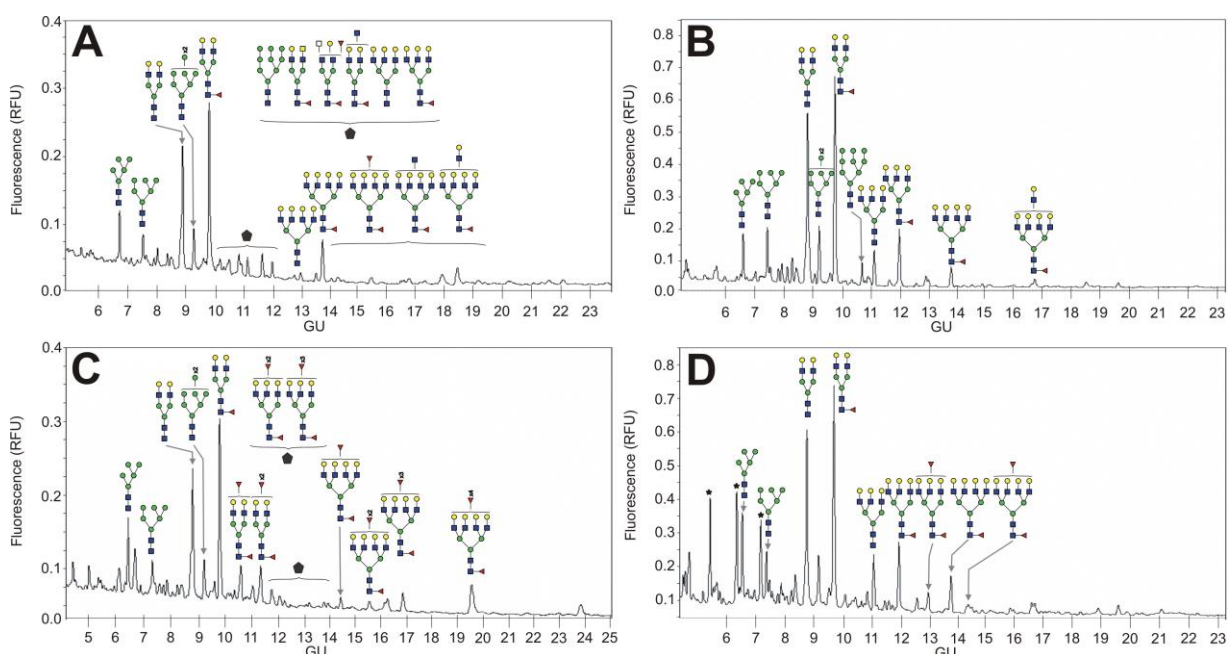


FIG. 2.6. CE-LIF electropherograms of PNGase F-released and desialylated N-glycans from HEK 293 (A), CHO-K1 (B), AGE1.HN (C) and HEP G2 cells (D). Cell surface glycoproteins were directly tryptic digested from the cells. N-glycans were enzymatically cleaved from tryptic glycopeptides with PNGase F, desialylated and measured by CE-LIF. * Polyhexose contaminations are negligible. Blue square represents N-acetylglucosamine, yellow square N-acetylgalactosamine, white square N-acetylhexosamine, green circle mannose, yellow circle galactose, red triangle fucose, white diamond N-glycolylneuraminic acid and pink diamond N-acetylneuraminic acid.

2.1.7 Verification of identified N-glycan structures from HEK 293, AGE1.HN, CHO-K1 and Hep G2 cells with MALDI-TOF/TOF sequencing and exoglycosidase digestions

Verification of the identified N-glycan structures was done with specific exoglycosidases (see exoglycosidase digestion Tables 1, 2, 3 and 4) in combination with MALDI-TOF/TOF-MS fragmentation analysis that was performed in the positive-ionisation mode. Representative MALDI-TOF/TOF mass spectra were selected from each cell line and are shown in Fig. 2.7. However, it is important to note that MALDI-TOF/TOF fragmentation was performed systematically for all detected signals before or after desialylation in order to confirm the proposed structures. The results of the most abundant signals are presented in this section. Digestion of N-glycans was performed consecutively with several enzymes in the following order: *Arthrobacter ureafaciens* neuraminidase, $\beta(1-4)$ galactosidase from *Streptococcus pneumoniae*, almond meal $\alpha(1-3,4)$ fucosidase, $\beta(1-4)$ galactosidase from *Streptococcus pneumoniae* and bovine kidney $\alpha(1-2,3,4,6)$ fucosidase. The presence of Lewis^x core-fucosylated structures was shown using the following sequence of digestions: $\beta(1-4)$ galactosidase, $\alpha(1-3,4)$ fucosidase, $\beta(1-4)$ galactosidase, and bovine kidney $\alpha(1-2,3,4,6)$ fucosidase. A representative example of exoglycosidase digestions is presented in Fig.2.9 for the cell surface N-glycans of HEK 293 cells.

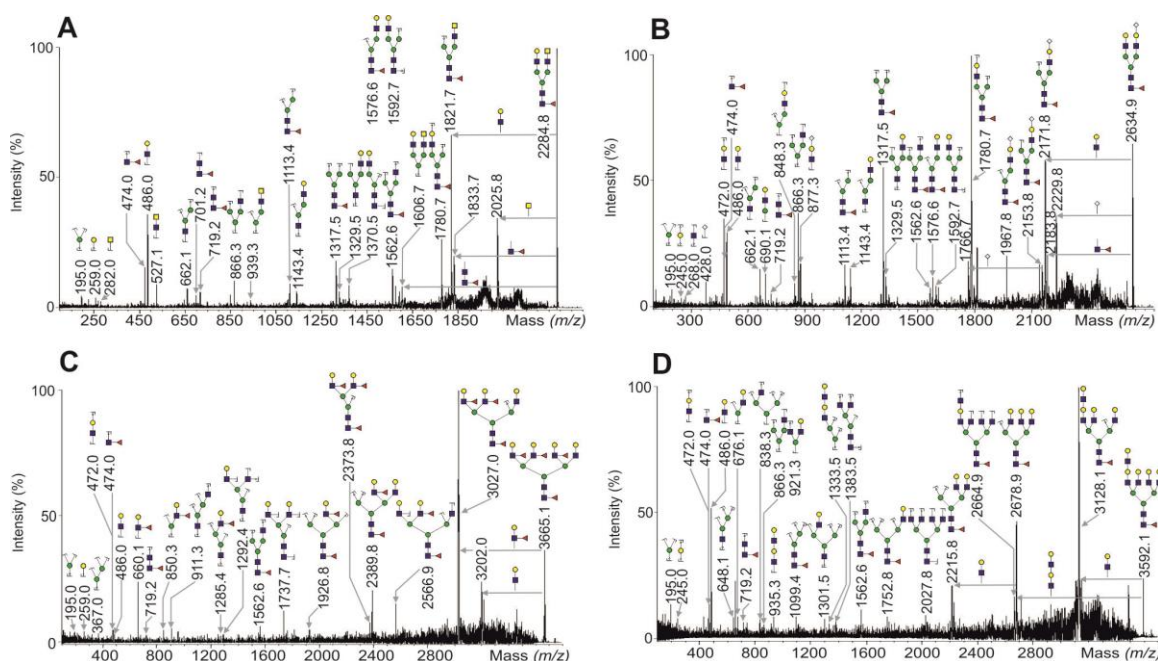


FIG. 2.7. MALDI-TOF/TOF mass spectra selected from each cell line; H4N5F1 (m/z 2284.8) for HEK 293 (A), G1H5N4F1 (m/z 2634.9) for CHO (B), H7N6F4 (m/z 3665.1) for AGE1.HN (C) and H8N7F1 (m/z 3592.1) for HEP G2 (D). Blue square represents N-acetylglucosamine, green circle mannose, yellow circle galactose, red triangle fucose and pink diamond N-acetylneuraminic acid.

Treatment of the N-glycan pool with neuraminidase resulted in the cleavage of all terminal sialic acid residues and therefore a shift of these structures to lower mass range (Fig.2.9 A). Exoglycosidase digestions revealed that the HEK 293 N-glycan signals with the composition H4N4F2 (m/z 2213.8), H5N4F2 (m/z 2417.9), H5N5F2 (m/z 2663.1), S1H5N4F2 (m/z 2779.1), S1H5N5F2 (m/z 3024.1), S1H6N5F2 (m/z 3228.1), S2H6N5F2 (m/z 3590.1), S2H7N6F2 (m/z 4039.2) and S3H7N6F2 (m/z 4400.4) contained Lewis^x epitopes (see exoglycosidase digestion Table 1). $\beta(1-4)$ Galactosidase digestion of these signals was not complete (Fig.2.9 B) but further digestion with $\alpha(1-3,4)$ fucosidase resulted in a shift (Fig.2.9 C), indicating the presence of a Lewis^x antenna. $\beta(1-4)$ Galactosidase is not able to digest $\beta(1-4)$ -linked Gal in fucosylated antennae suggesting the presence of Lewis^x motives in the respective structures. In addition, some galactosylated structures remained after $\beta(1-4)$ galactosidase (Fig.2.9 B) but were digested after following addition of a second aliquot of $\beta(1-4)$ galactosidase (Fig.2.9 D). Exoglycosidase digestion with $\alpha(1-3,4)$ fucosidase led to the removal of all antennary Fuc residues and subsequent $\beta(1-4)$ galactosidase digestion resulted in the cleavage of all remaining $\beta(1-4)$ -linked Gal residues (Fig.2.9 D), indicating that Fuc residues were $\alpha(1-3)$ -linked to GlcNAc residues of the antennae and the presence of Lewis^x. Therefore, only $\alpha(1-6)$ -linked Fuc residues remained on N-glycans. These core-fucosylated structures were digested with bovine kidney $\alpha(1-2,3,4,6)$ fucosidase (Fig.2.9 E) and shifted to lower mass range, which revealed the presence of Fuc residues linked to the reducing GlcNAc of the core. In addition, the presence of core $\alpha(1-6)$ -linked Fuc was corroborated by two MALDI-TOF/TOF fragment ions at m/z 474.0 (F1N1) and m/z 719.2 (F1N2) that were found in the respective MALDI-TOF/TOF mass spectra.

Furthermore fragmentation of desialylated N-glycans was performed after derivatisation with 2AB in order to confirm the presence of $\alpha(1,6)$ -linked core-Fuc. Derivatisation with 2AB occurs only at the reducing GlcNAc residue of the core structure. A representative MALDI-TOF/TOF mass spectrum of 2AB-H5N4F2 (m/z 2580.1) of AGE1.HN cells is shown in Fig.2.8 in which the diagnostic fragment ion 2AB-N1F1 (m/z 636.1) revealed fucosylation of the reducing GlcNAc of the core.

MALDI-TOF/TOF fragmentation analysis and exoglycosidase digestions were likewise used to analyse cell surface N-glycans of CHO-K1, AGE1.HN and Hep G2 cells. Exoglycosidase digestions (exoglycosidase digestion Tables 2, 3 and 4) revealed Lewis^x epitopes in CHO-K1 cells (H5N4F2 m/z 2417.9 and S1H5N4F2 m/z 2779.1), in Hep G2 cells (H4N4F2 m/z 2213.8, H5N4F2 m/z 2417.9, S1H4N4F2 m/z 2574.9, S1H5N4F2 m/z 2779.1, S1H4N5F2 m/z 2820.1, H6N5F2 m/z 2867.1, S1H5N5F2 m/z 3024.1, S2H5N4F2 m/z 3140.1, S1H6N5F2 m/z 3228.1, S2H5N5F2 m/z 3385.1, S1H6N5F3 m/z 3403.1, S1H6N6F2 m/z 3474.1, S2H6N5F2 m/z 3590.1, S1H7N6F2 m/z 3678.1, S2H6N5F3 m/z 3763.2, S1H7N6F3 m/z 3852.2, S3H6N5F2 m/z 3951.2, S2H7N6F2 m/z 4039.2, S3H6N5F3 m/z 4125.3,

S2H7N6F3 m/z 4213.3, S3H7N6F2 m/z 4400.4, S3H7N6F3 m/z 4574.4, S4H7N6F2 m/z 4761.5, S4H7N6F3 m/z 4935.6 and S1G3H7N6F3 m/z 5025.6) and in AGE1.HN cells (H5N4F2 m/z 2417.9, H5N4F3 m/z 2591.9, S1H5N4F2 m/z 2779.1, H6N5F2 m/z 2867.1, H6N5F3 m/z 3041.1, H6N5F4 m/z 3215.1, S1H6N5F2 m/z 3228.1, S1H6N5F3 m/z 3403.1, H7N6F3 m/z 3491.1, S2H6N5F2 m/z 3590.1, H7N6F4 m/z 3665.1, S1H7N6F2 m/z 3678.1, H7N6F5 m/z 3839.2, S1H7N6F3 m/z 3852.2, S1H7N6F4 m/z 4026.2, S2H7N6F2 m/z 4039.2, S2H7N6F3 m/z 4213.3 and S3H7N6F2 m/z 4400.4). Core-fucosylated N-glycans were confirmed using MALDI-TOF/TOF-MS, which revealed the presence of the diagnostic fragment ions F1N1 (m/z 474.0) and F1N2 (m/z 719.2).

The presence of GalNAc residues in HEK 293 cells was verified in the structures H3N5F1 (m/z 2080.8), H4N5F1 (m/z 2284.8), H3N6F1 (m/z 2325.8) and H3N6F2 (m/z 2499.9) due to the presence of the diagnostic fragment ion N2 (m/z 527.1). In addition, the diagnostic fragment ions at m/z 642.2 (N1S1) or m/z 1096.3 (H1N2S1), that were detected in the MALDI-TOF/TOF-MS spectra of S1H4N5F1 (m/z 2645.9), S2H4N5F1 (m/z 3007.1) and S2H5N6F1 (m/z 3457.1) revealed that the GalNAc in these structures was capped by a terminal Neu5Ac residue. The GalNAc-GlcNAc motif was also found in the structures H4N5F1 (m/z 2284.8), H3N6F1 (m/z 2325.8) and S2H4N5F1 (m/z 3007.1) of Hep G2 cells.

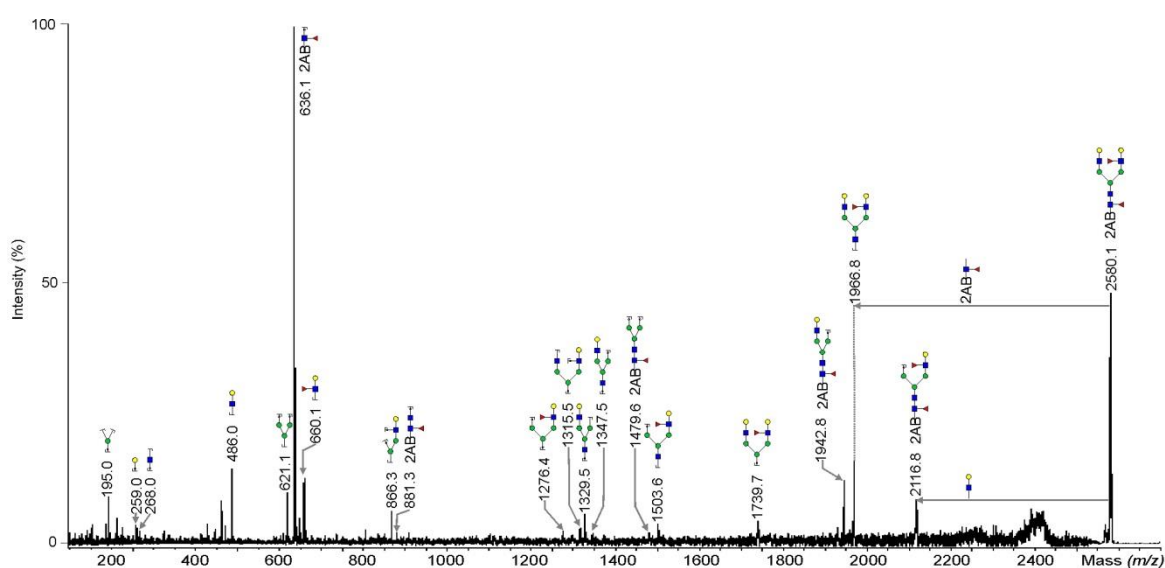


FIG. 2.8. MALDI-TOF/TOF mass spectrum of (m/z 2580.1) derived from AGE1.HN. Cell surface (glyco)peptides were directly released with trypsin, subjected to PNGase F digestion and N-glycans were purified and desalted. The N-glycans were then derivatised with 2-aminobenzamide (2AB) at their reductive end. Blue square represents N-acetylglucosamine, green circle mannose, yellow circle galactose, red triangle fucose and pink diamond N-acetylneuraminic acid.

MALDI-TOF/TOF fragmentation of the signal at m/z 1824.7 (H5N3) in HEK 293 cells revealed the presence of two isomeric hybrid structures of which one possesses a

galactosylated antenna as shown by the diagnostic fragment ions H1N1 (m/z 472.0), H1N1H1 (m/z 708.2) and N1H3 (m/z 897.2). The second isomer is not galactosylated but bears an additional Man instead, which was confirmed by a diagnostic fragment ion at m/z 693.2 (H2N1). In addition, β (1-4) galactosidase digestion was partially sensitive to the signal, which supports the finding that H5N3 (m/z 1824.7) is a mixture of two hybrid N-glycans. The same results were obtained for H5N3 (m/z 1824.7) in CHO-K1 and AGE1.HN but in CHO-K1 additionally a diagnostic fragment ion H1N1H1 (m/z 690.2) was detected, which proved the presence of the galactosylated antenna. MALDI-TOF/TOF fragmentation of the N-glycan signal H3N5F1 at m/z 2080.8 in HEK 293 cells revealed two isomeric structures as well; one was the triantennary N-glycan (diagnostic fragment ion m/z 851.2) and the second a biantennary N-glycan bearing the GalNAc-GlcNAc motif as already mentioned above.

MALDI-TOF/TOF fragmentation of signals from CHO-K1 cells revealed that H6N4 (m/z 2273.8), H6N4F1 (m/z 2447.9), S1H6N4F1 (m/z 2809.1), H7N5F1 (m/z 2897.1), S2H7N5F1 (m/z 3619.1) and S2H8N6F1 (m/z 4069.3) were structures of the form $S_xH_{y+2}N_y$ and contained a digalactosylated antenna. This was supported by the fragment ions H2 (m/z 463.0), H1N1 (m/z 472.0), N1H2 (m/z 690.2) and H1H2 (m/z 708.2). The same was found for the signal H6N4F1 (m/z 2447.9) in Hep G2 cells.

MALDI-TOF/TOF fragmentation revealed that six N-glycans in CHO-K1 cells contained Neu5Gc, namely G1H5N4 (m/z 2460.9), S1G1H4N4 (m/z 2617.9), G1H5N4F1 (m/z 2634.9), S1G1H5N4F1 (m/z 2996.1), G2H5N4F1 (m/z 3026.1) and G1H6N5F1 (m/z 3084.1). The diagnostic fragment ion N1H1G1 (m/z 877.2) proved that an antenna is sialylated with Neu5Gc. In Hep G2 cells, the two signals G1H5N4 (m/z 2460.9) and G1H5N4F1 (m/z 2634.9) were found to contain Neu5Gc, which was supported by the diagnostic fragment ion N1H1G1 (m/z 877.3).

The structures of the composition H6N6F1 (2938.1), H7N6F1 (3142.1), S1H6N6F1 (3299.1), S1H7N6F1 (3504.1), S2H6N6F1 (3661.1), S2H7N6F1 (3864.2), S2H8N7F3 (m/z 4662.4), S2H8N7F1 (4314.3), S2H8N7F3 (4662.4), S3H8N7F1 (4675.4) and S3H8N7F2 (4849.5) contained at least one LacNAc antenna. This was supported by the fragmentation results of their desialylated forms, which revealed a diagnostic fragment ion H2N2 at m/z 935.2. The LacNAc-containing signals of the desialylated N-glycan pool were mainly tri- and tetraantennary N-glycans such as H6N6F1, H7N6F1, H8N7F1, H8N7F2 and H8N7F3. In addition, some LacNAc-signals were detected in the desialylated N-glycan pool of HEK 293 (H6N7F1 and H8N7F1) and CHO-K1 (H6N5F1, H7N6 and H8N7F1) that were verified via the diagnostic fragment ion H2N2 at m/z 935.2.

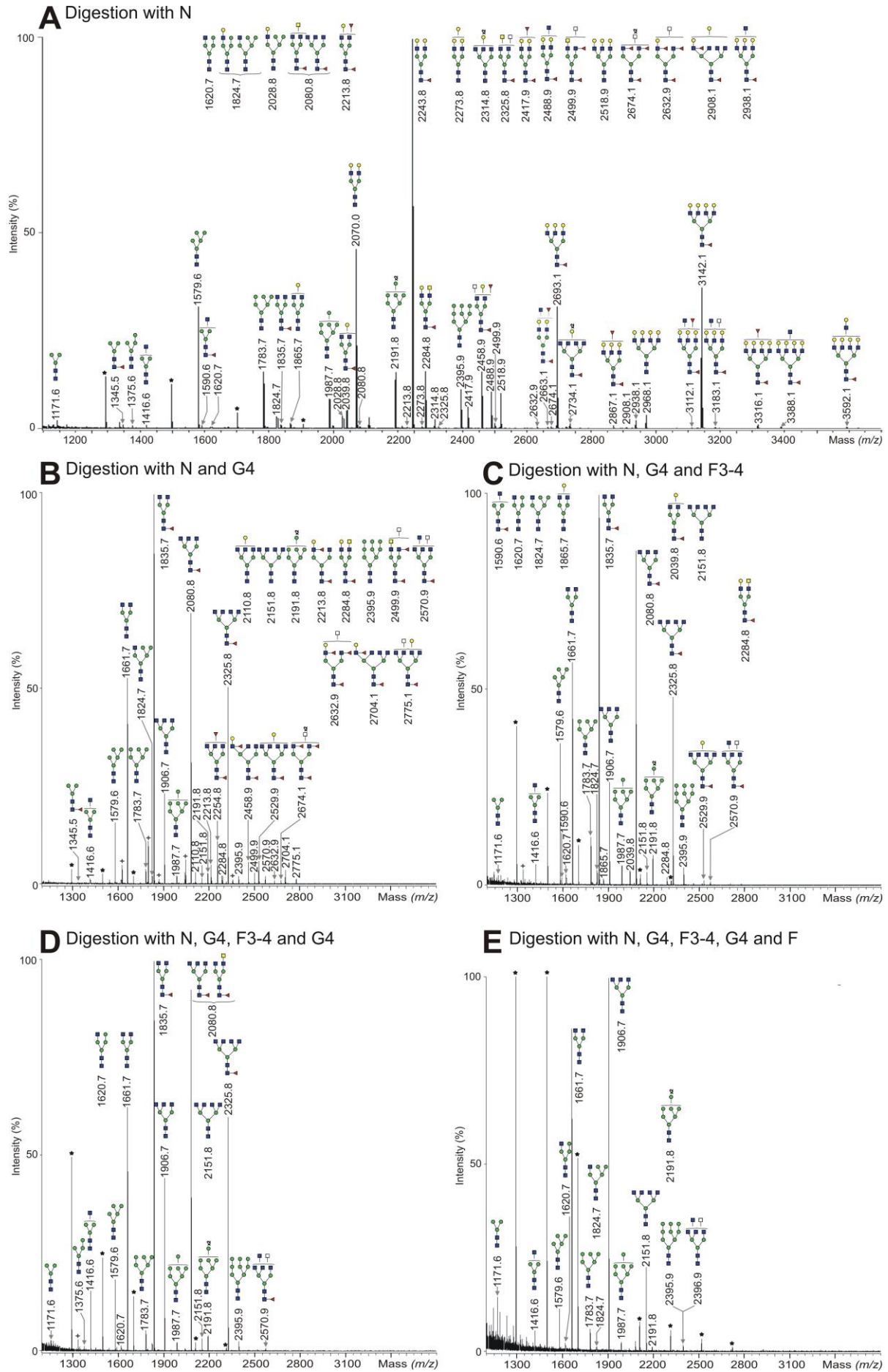


FIG. 2.9. Exoglycosidase digestions of PNGase F-released N-glycans derived from HEK 293 cells. Cell surface (glyco)peptides were directly released with trypsin, subjected to PNGase F digestion and N-glycans were purified and desalted. N: *Arthrobacter ureafaciens* neuraminidase, G4: $\beta(1-4)$ galactosidase from *Streptococcus pneumoniae*, F3-4: almond meal $\alpha(1-3,4)$ fucosidase, F: Bovine kidney $\alpha(1-2,3,4,6)$ fucosidase. * Polyhexose contaminations are negligible. † Non identified peaks.

2.1.8 Verification of Neu5Gc in N-glycans from CHO-K1 cells using HPLC

The presence of Neu5Gc was further verified using RP-HPLC. Sialic acids were hydrolysed using acetic acid and labeled with 1,2-diamino-4,5-methylendioxybenzene (DMB). Samples were then analysed using RP-HPLC. The chromatograms revealed the presence of Neu5Gc in CHO-K1 as well as in traces in HEKwt and Hep G2 (Fig.2.10). In addition, MALDI-TOF-MS data revealed that the relative amount of N-glycans bearing Neu5Gc was about 0.1 % in HEK 293 and 0.6 % in Hep G2 and therefore represent trace amounts compared to Neu5Ac (58 % in HEK 293, 25 % in CHO-K1 and 71 % in HEP G2). The abundance of Neu5Gc calculated from MALDI-TOF-MS data of CHO-K1 was higher (4 %). The observed xenoantigen contamination in HEKwt and Hep G2 most likely originated from the animal-derived components in the cell culture media as has been already reported (144, 145).

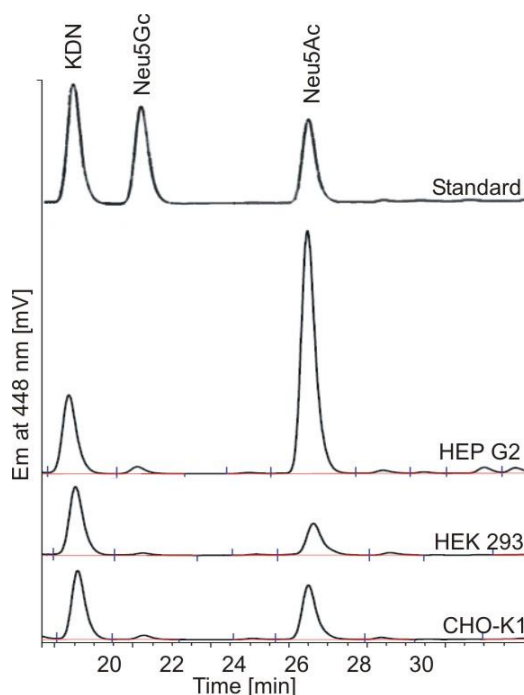


FIG. 2.10. Verification of Neu5Gc by RP-HPLC. Cell surface (glyco)peptides were released from CHO-K1, HEK 293 and HEP G2 cells using trypsin, subjected to PNGase F digestion and N-glycans were purified and desalted. Sialic acids were hydrolysed with acetic acid, labeled with DMB and subjected to RP-HPLC analysis. A standard which contains KDN, Neu5Gc and Neu5Ac was used to assign the signal peaks.

2.2 N-Glycosylation profile of mesenchymal stem cells and its changes during adipogenic, chondrogenic and osteogenic differentiation

2.2.1 N-Glycosylation profile of undifferentiated and adipogenically differentiated human bone marrow mesenchymal stem cells

2.2.1.1 Analysis strategy for N-glycans derived from undifferentiated and adipogenically differentiated human bone marrow mesenchymal stem cells

MSCs were differentiated into adipogenic, chondrogenic and osteogenic direction by the working group of Dr. Jochen Ringe (Charité-Universitätsmedizin Berlin, BCRT, Labor für Tissue Engineering/ Klinik für Rheumatologie). The N-glycome of undifferentiated and adipogenically differentiated human bone marrow-derived MSCs (n=3 donors) was investigated and compared. First, membrane glycoproteins of the respective cell pellets were isolated by membrane extraction. In order to ensure a high efficiency of the endoglycosidase digestion, membrane glycoproteins were trypsinised prior to the N-glycan release. Afterwards, high-mannose- and hybrid-type N-glycans were enzymatically released with endo- β -N-acetylglucosaminidase H (Endo H). The resulting free N-glycans were isolated from the rest of the sample by C18 solid phase extraction, which enabled separation of the N-glycan fraction (high-mannose- and hybrid-type N-glycans) and glycopeptide fraction. The glycopeptide fraction was further treated with peptide-N4-(N-acetyl- β -glucosaminy) asparagine amidase F (PNGase F) to release the remaining complex-type N-glycans. High-mannose N-glycans usually represent the majority of the N-glycan pool of cell membrane (glyco)proteins (see section 2.1) and therefore the approach of Endo H digestion followed by PNGase F digestion was chosen to ensure an improved detection and thus quantification of complex-type N-glycans. The Endo H and PNGase F digests were purified, permethylated and analysed separately in the positive ionization mode of MALDI-TOF-MS (146, 147). The N-glycan signals that were identified by MALDI-TOF-MS were verified by exoglycosidase digestions and by MALDI-TOF/TOF fragmentation.

2.2.1.2 N-glycome of mesenchymal stem cells and its changes during adipogenic differentiation

Endo H is able to cleave only asparagine-linked high-mannose- and hybrid-type N-glycans specifically between the two N-acetylglucosamine (GlcNAc) subunits of the chitobiose core. The resulting Endo H-released N-glycans were purified using reversed-phase C18 and carbograph cartridges, permethylated and measured by means of MALDI-TOF-MS. A representative mass spectrum of Endo H-released N-glycans of undifferentiated and day 15 adipogenically differentiated MSCs is shown in Fig. 2.11 A and C. Mean relative abundances

were calculated from three different biological replicates and are presented in Fig. 2.11 B and Table 2 (see appendix). The results revealed that the N-glycan profiles of the three different MSC donors were highly similar, which is supported by the small deviations observed between the glycan profiles (Fig. 2.11 B). Asterisks indicate statistical significant differences between the two sample groups undifferentiated MSCs and 15 days adipogenically differentiated MSCs according to Mann-Whitney U test ($p \leq 0.05$).

MALDI-TOF-MS profiling revealed the presence of 12 high-mannose- and hybrid-type N-glycan structures of which seven are of high-mannose-type with the composition H3-9N1 (m/z 926.4, 1130.5, 1334.6, 1538.7, 1742.8, 1946.9 and 2151.0, respectively). The relative amount of overall high-mannose-type N-glycans was 5.7 % higher in day 15 adipogenically differentiated MSCs when compared to undifferentiated MSCs. One important difference was that smaller high-mannose-type N-glycans such as H5N1 (m/z 1334.6) and H6N1 (m/z 1538.7) were particularly overexpressed in day 5 and day 15 adipogenically differentiated MSCs. Their relative amount was 14 % for H5N1 and 26 % for H6N1 in day 15 adipogenically differentiated MSCs ($p < 0.05$), which was an increase of 7 %, respectively. In contrast, larger high-mannose structures such as H9N1 (m/z 2151.0) were significantly decreased by more than 9 % in day 15 of adipogenically differentiated cells. In addition, the four hybrid-type N-glycans H5N2 (m/z 1579.7), H6N2 (m/z 1783.8), S1H5N2 (m/z 1940.9) and S1H6N2 (m/z 2145.0) constituted 2.4 % of the total N-glycome of day 15 adipogenically differentiated MSCs and decreased in relative amount during adipogenic differentiation. They were found to be 5 % underexpressed in day 15 adipogenically differentiated MSCs when compared to undifferentiated MSCs. The changes in relative amount of neutral hybrid-type N-glycans H5N2 (m/z 1579.7) and H6N2 (m/z 1783.8) were statistically significant during the process of adipogenic differentiation.

Furthermore, a glycan of the composition H10N1 was detected at m/z 2355.1 but in trace amounts. This structure was verified as the monoglucosylated precursor H10N1 high-mannose-type N-glycan that has been also reported in human blood serum by Frisch et al. (148). In general, the differences of the average relative amounts of Endo H-released N-glycans of undifferentiated and adipogenically differentiated MSCs (5 days or 15 days) were larger than those of day 5 and day 15 adipogenically differentiated MSCs (Fig. 2.11 B, Table 2). In contrast, the mass spectra of all the three groups were qualitatively almost similar but quantitatively different. As shown in the next paragraph, this was also the case for PNGase F-released N-glycans (Fig. 2.13 A and B, Table 3).

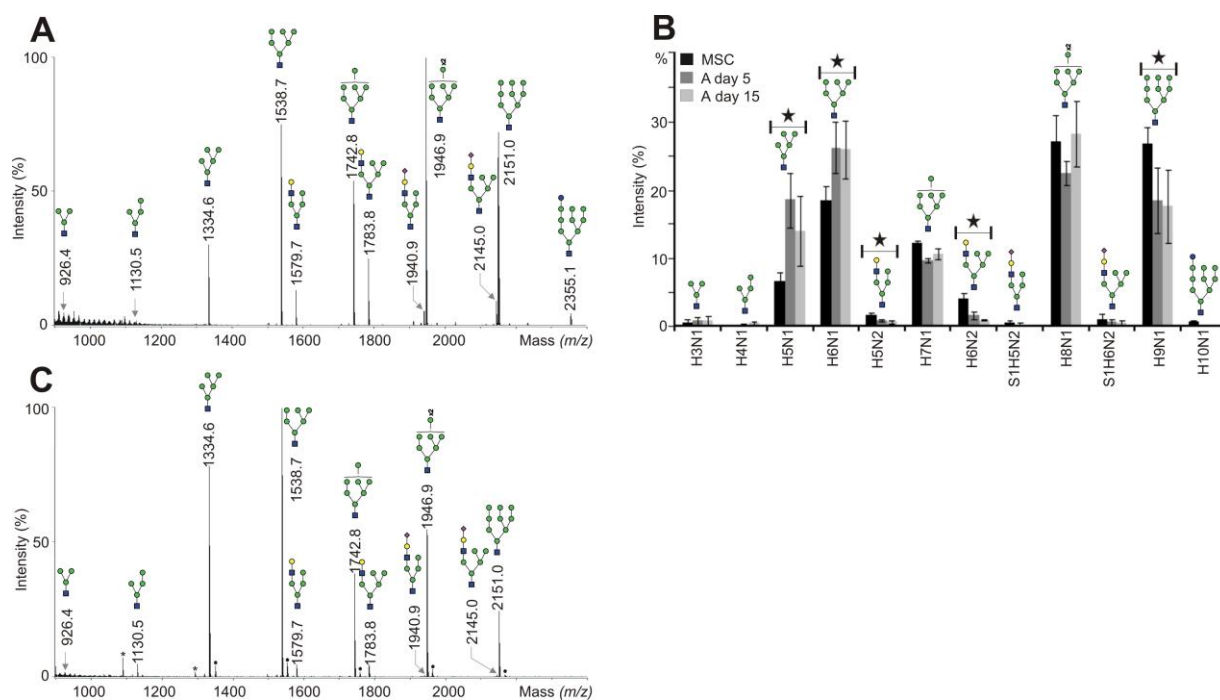


FIG. 2.11. MALDI-TOF-MS of Endo H-released N-glycans. Glycoproteins were isolated from undifferentiated and adipogenically differentiated MSCs (A) using membrane extraction. N-glycans of high-mannose- and hybrid-type were then enzymatically cleaved with Endo H, permethylated and measured by MALDI-TOF-MS. A representative mass spectrum of Endo H-released N-glycans of undifferentiated (A) and adipogenically differentiated human MSCs (C). The average relative amounts of all Endo H-released N-glycans of undifferentiated human MSCs (black) and adipogenically differentiated MSCs (A) at day 5 (dark grey) and day 15 (light grey) derived from three different preparations ($n=3$) are presented in (B). Statistical significant difference between the two sample groups undifferentiated MSCs and 15 days adipogenically differentiated MSCs was assessed using Mann-Whitney U test ($*p \leq 0.05$) and is marked with a star in (B). Blue square represents N-acetylglucosamine, green circle mannose, yellow circle galactose, red triangle fucose and pink diamond N-acetylneuraminic acid. H: hexose, N: N-acetylhexosamine, F: deoxyhexose, S: N-acetylneuraminic acid. * Polyhexose contaminations are negligible.

In order to release the remaining complex-type N-glycans, Endo H-digested glycopeptides were subjected to PNGase F-digestion. The resulting mass spectrum of the N-glycosylation profile of human undifferentiated and day 15 adipogenically differentiated MSCs after N-glycan purification and derivatisation is presented exemplary in Fig. 2.12 A and B. It was possible to detect 100 different N-glycan signals with MALDI-TOF-MS (Table 3, see appendix). The relative abundance of the 48 most abundant N-glycans is presented in Fig. 2.13 A and B in order to compare the most significant changes. It is important to note that a small amount of hybrid- and high-mannose-type N-glycans, 3 % and 2 % respectively, was detected in the pool of PNGase F-released N-glycans. This indicates that Endo H-digestion of the corresponding glycopeptides was about 95 % complete. It is probably that a low

portion of the Endo H-derived N-glycans remained bonded to the C18 column and thus eluted in the glycopeptide fraction that was then treated with PNGase F, since some of the detected structures of the PNGase F-released fraction were carrying just one core GlcNAc.

The mass spectrometric data revealed that fucosylated bi-, tri- and tetraantennary complex-type N-glycans were predominantly found in the N-glycan profiles of undifferentiated MSCs and day 5 and day 15 adipogenically differentiated MSCs.

Evaluation of fucosylation. Monofucosylation was the most abundant type of fucosylation found in undifferentiated MSCs and their adipogenic counterparts. In addition, monofucosylated structures were exclusively fucosylated at the reducing GlcNAc residue of the core structure. A key feature of day 5 and day 15 adipogenically differentiated MSCs was the increased abundance of biantennary N-glycans such as the fucosylated N-glycans H3N4F1 (m/z 1835.9), H5N4F3 (m/z 2592.3), S1H5N4F1 (m/z 2605.3) and S2H5N4F1 (m/z 2966.4) but also the non-fucosylated N-glycans S1H5N4 (m/z 2431.2) and S2H5N4 (m/z 2792.3). In addition, the relative amounts of the biantennary fucosylated N-glycans H3N4F1, H5N4F3 and S2H5N4F1 were significantly increased in day 15 adipogenically differentiated MSCs.

Evaluation of antennarity. Triantennary N-glycans were less abundant in day 5 and day 15 adipogenically differentiated cells when compared with undifferentiated MSCs. In addition, the amount of fucosylated triantennary structures like H6N5F1 (m/z 2693.3) and S1H6N5F1 (m/z 3054.5) were also decreased in the N-glycome of day 5 and day 15 adipogenically differentiated MSCs. Statistical analysis revealed that the N-glycans H6N5F1 (m/z 2693.3) and S1H6N5 (m/z 2880.4) were significantly underexpressed in day 15 adipogenically differentiated cells when compared to undifferentiated MSCs. The mass spectrometric data revealed that the amount of tetraantennary N-glycans was also decreased in the N-glycome of day 5 and day 15 adipogenically differentiated cells. It is important to note that fucosylated tetraantennary structures were at least 10 % less abundant in day 15 adipogenically differentiated MSCs than in undifferentiated MSCs. Fully galactosylated N-glycans such as H7N6F1 (m/z 3142.5), S1H7N6F1 (m/z 3503.7) and S2H7N6F1 (m/z 3864.9) were more enriched in undifferentiated MSCs. Statistical analysis revealed that the N-glycans H7N6F1 (m/z 3142.5), S1H7N6 (m/z 3329.6) and S1H7N6F1 (m/z 3503.7) were significantly underexpressed in 15 days adipogenically differentiated MSCs. Remarkably, N-glycans bearing the poly-LacNAc epitope such as H6N5 (m/z 2519.2), H6N5F1 (m/z 2693.3), H7N6F1 (m/z 3142.5) and S1H7N6F1 (m/z 3503.7) were predominantly found in human MSCs and were very minor in amount in adipogenically differentiated MSCs.

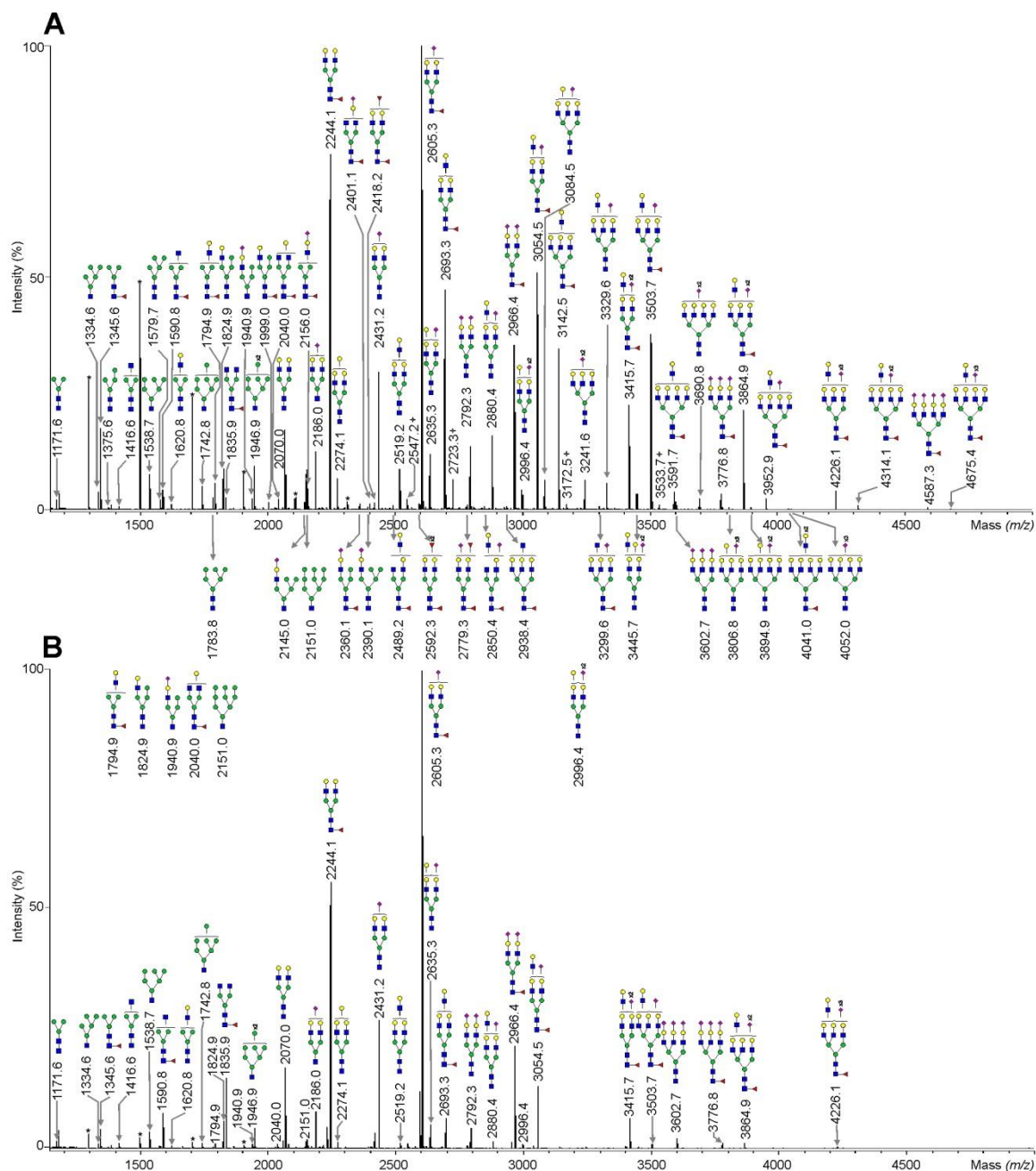


FIG. 2.12. MALDI-TOF-MS of PNGase F-released complex-type N-glycans. Glycoproteins were isolated from undifferentiated and adipogenically differentiated MSCs. After isolation of high-mannose- and hybrid-type N-glycans by Endo H digestion, digested glycopeptides were subjected to PNGase F digestion to release complex-type N-glycans, permethylated and measured by MALDI-TOF-MS. A representative mass spectrum of PNGase F-released N-glycans of undifferentiated human MSCs (**A**) and day 15 adipogenically differentiated human MSCs (**B**) is shown together with the 70 most abundant structures. Blue square represents N-acetylglucosamine, green circle mannose, yellow circle galactose, red triangle fucose and pink diamond N-acetylneuraminic acid. * Polyhexose contaminations are negligible. ✦ Non identified peaks.

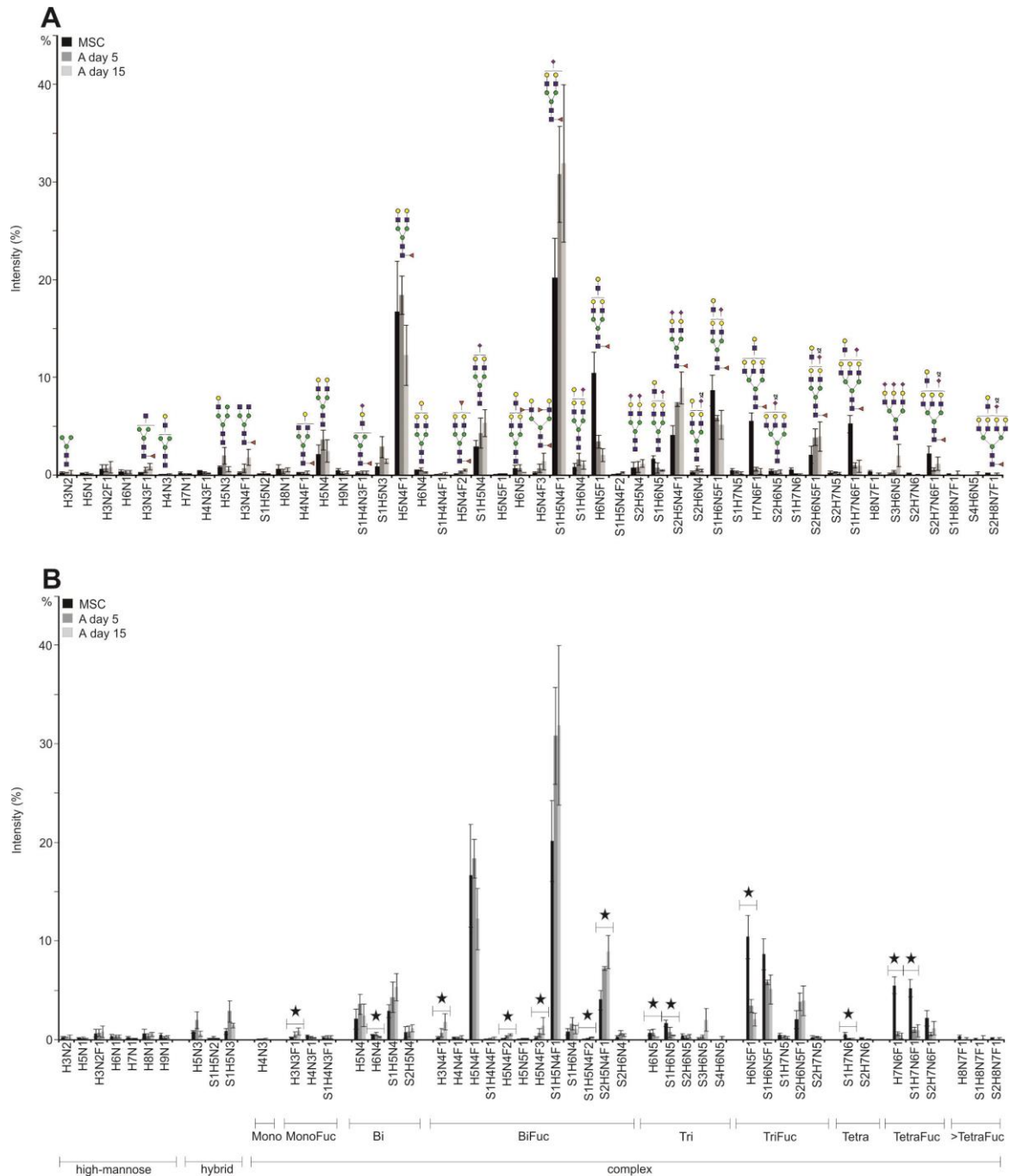


FIG. 2.13. Quantification of PNGase F-released N-glycans with MALDI-TOF-MS. **(A)** The average relative amounts of the 48 most abundant PNGase F-released N-glycans of undifferentiated human MSCs (black) and adipogenically differentiated MSCs (A) at day 5 (dark grey) and day 15 (light grey) derived from three different preparations (n=3), **(B)** grouped according to their N-glycan type, antennarity and fucosylation. Statistical significant difference between the two sample groups undifferentiated MSCs and 15 days adipogenically differentiated MSCs was assessed using Mann-Whitney U test ($p \leq 0.05$) and is marked with a star in **(B)**. Blue square represents N-acetylglucosamine, green circle mannose, yellow circle galactose, red triangle fucose and pink diamond N-acetylneuraminic acid. H: hexose, N: N-acetylhexosamine, F: deoxyhexose, S: N-acetylneuraminic acid.

Evaluation of sialylation. Quantification of the mass spectrometric data revealed that more than 50 % of the PNGase F-released N-glycans of undifferentiated MSCs were found to be sialylated. They were mainly detected as monosialylated species although di-, tri- and tetrasialylated N-glycans were verified as well. These results revealed that N-glycans bearing Neu5Ac were mostly partially sialylated and minority of them were present as fully sialylated structures. As the antennarity increased, the presence of fully sialylated structures decreased. In addition, the amount of sialylated N-glycans was 16.5 % higher in day 15 adipogenically differentiated MSCs when compared with undifferentiated MSCs. This was mainly due to the increased amount of sialylated biantennary structures, such as S1H5N4F1 (m/z 2605.3) and S2H5N4F1 (m/z 2966.4) in day 5 and day 15 adipogenically differentiated MSCs.

2.2.1.3 CE-LIF analysis of N-glycans from undifferentiated and adipogenically differentiated human bone marrow mesenchymal stem cells

In order to confirm the MALDI-TOF-MS results, 40 % of the N-glycan pool obtained after Endo H digestion was analysed by means of CE-LIF. Prior to that, the N-glycans were labeled with APTS and chemically desialylated by acetic acid hydrolysis in order to convert the charged hybrid N-glycans S1H5N2 and S1H6N2 into neutral molecules, and thus making separation independent from the charge of Neu5Ac. The N-glycans were then desalted on self-made graphite micro-columns and then subjected to CE-LIF analysis. A representative electropherogram of Endo H-released N-glycans of undifferentiated and day 15 adipogenically differentiated MSCs is shown in Fig. 2.14 A and B. N-glycans were assigned with the help of a standard table generated in our laboratory using N-glycans release from reference glycoproteins. In addition, MALDI-TOF-MS spectra of the desialylated N-glycan pools were used to assign the structures. APTS-labeled N-glycans were sequentially digested with exoglycosidases to confirm the migration times in the electropherograms. The overall distribution of the N-glycans is very similar to the one found in the MALDI-TOF mass spectrum. The high-mannose-type N-glycans comprised together the highest amount of total Endo H-released N-glycans of human MSC. The most abundant structure is H8N1 (7.0 to 7.7 GU) followed by H9N1 (8.3 GU) and H6N1 (5.9 GU). The N-glycan H7N1 migrates at a retention time between 6.4 and 6.9 GU forming three isomers of which the first isomer co-migrates together with the hybrid structure H5N2 (6.6 GU) (149). H8N1 (7.0 to 7.7 GU) forms three isomeric structures as well whereat the first isomer co-migrates together with the hybrid structure H6N2 (7.2 GU) (149). In addition, the high-mannose-type N-glycan H5N1 (4.8 GU) and the monoglucosylated structure H10N1 (9.4 GU) were detected with CE-LIF (149). Thus, the CE-LIF electropherogram confirms the mass spectrometric data.

40 % of the N-glycan pool after PNGase F-digestion was prepared as described above for Endo H-released N-glycans and subjected to CE-LIF analysis. A representative electropherogram of undifferentiated and day 15 adipogenically differentiated MSCs is shown in Fig. 2.15 A and B. It was possible to assign the 15 most abundant structures.

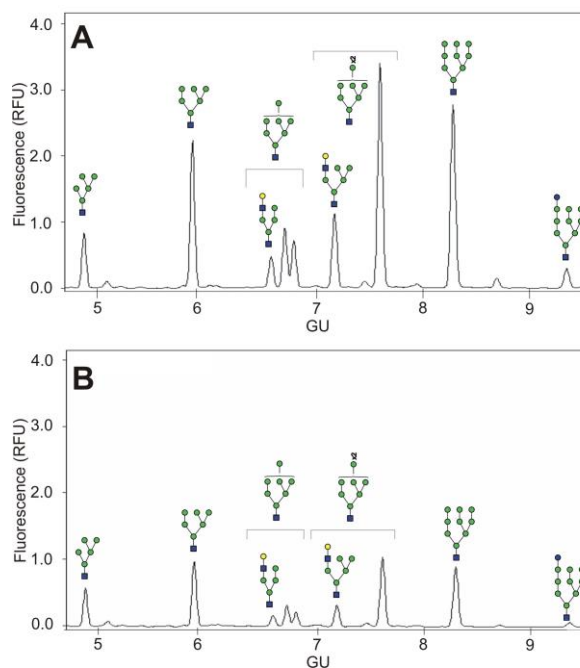


FIG. 2.14. CE-LIF electropherograms of Endo H-released and desialylated N-glycans from undifferentiated human MSCs **(A)** and day 15 adipogenically differentiated human MSCs **(B)**. Glycoproteins were isolated using membrane extraction. N-glycans of high-mannose- and hybrid-type were then enzymatically cleaved with Endo H, desialylated and measured by CE-LIF. Blue square represents N-acetylglucosamine, yellow square N-acetylgalactosamine, white square N-acetylhexosamine, green circle mannose, yellow circle galactose, red triangle fucose, white diamond N-glycolylneuraminic acid and pink diamond N-acetylneuraminic acid.

Briefly, CE-LIF revealed that the biantennary fucosylated structure H5N4F1 (9.8 GU) was the most abundant in the N-glycosylation profile of MSCs, followed by the triantennary fucosylated N-glycan H6N5F1 (11.7 and 12.0 GU) and tetraantennary fucosylated structure H7N6F1 (13.8 GU). Thus, fucosylated structures comprised together the main part of the profile as can be seen from the peak height of the detected N-glycan signals. In addition, the same non-fucosylated species were detected in the same order according to their abundance (H5N4 at 8.9 GU, H6N5 at 10.8 and 11.0 GU and H7N6 at 13.0 GU). The triantennary N-glycans H6N5F1 (11.7 and 12.0 GU) and H6N5 (10.8 and 11.0 GU) were detected as isomeric structures that differ in the linkage of the GlcNAc of the third antennae; the β 1,6-GlcNAc isomer migrates 0.25 GU faster than the β 1,4-GlcNAc isomer (150). Furthermore, tetraantennary N-glycans with additionally one and two LacNAc units were

detected as fucosylated (H8N7F1 at 16.5 GU and H9N8F1 at 19.3 GU) and to a minor extent as non-fucosylated species (H8N7 at 15.9 GU and H9N8 at 18.8 GU). The overall distribution was very similar to the one found by mass spectrometric profiling. Consequently, the CE-LIF electropherograms confirm the MALDI-TOF mass spectrometric data.

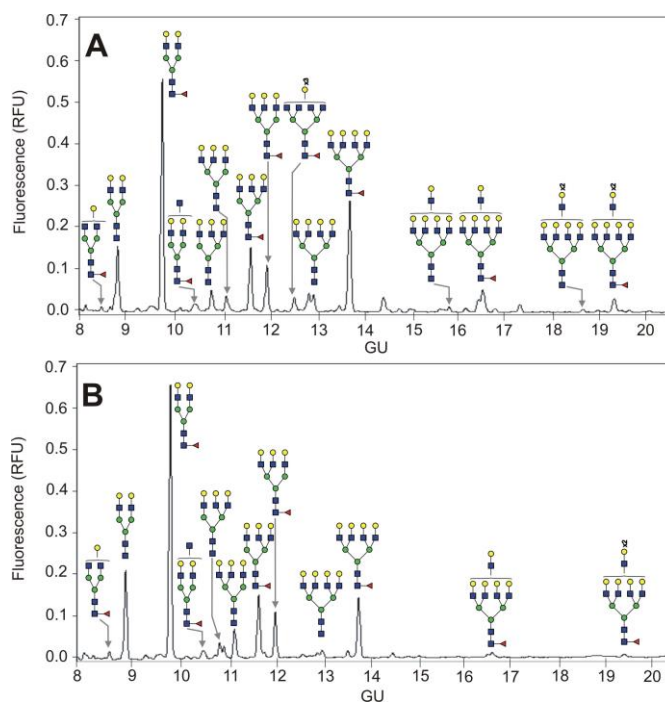


FIG. 2.15. CE-LIF electropherograms of PNGase F-released and desialylated complex-type N-glycans from undifferentiated human MSCs **(A)** and day 15 adipogenically differentiated human MSCs **(B)**. Glycoproteins were isolated using membrane extraction. After isolation of high-mannose- and hybrid-type N-glycans by Endo H digestion, digested glycopeptides were subjected to PNGase F digestion to release complex-type N-glycans, desialylated and measured by CE-LIF. Blue square represents N-acetylglucosamine, yellow square N-acetylgalactosamine, white square N-acetylhexosamine, green circle mannose, yellow circle galactose, red triangle fucose, white diamond N-glycolylneuraminic acid and pink diamond N-acetylneuraminic acid.

2.2.1.4 Verification of identified N-glycan structures from undifferentiated and adipogenically differentiated mesenchymal stem cells with MALDI-TOF/TOF sequencing and exoglycosidase digestions

Verification of the most abundant N-glycan structures was done using specific exoglycosidases (see exoglycosidase digestion Tables 5 and 6) in combination with MALDI-TOF/TOF-MS fragmentation. A representative MALDI-TOF/TOF mass spectrum of m/z 2605.3 of the composition S1H5N4F1 derived from human MSCs and of m/z 2635.3 of the composition S1H6N4 derived from day 15 adipogenically differentiated MSCs is presented in Fig. 2.16 A and B. Digestions were done with different exoglycosidases using the following

sequence of digestion: *A. ureafaciens* neuraminidase, $\beta(1-4)$ galactosidase from *S. pneumoniae*, β -N-acetylhexosaminidase recombinant from *S. pneumoniae* and expressed in *E. coli*, α -mannosidase from *C. ensiformis* (for Endo H-released N-glycans) and *A. ureafaciens* neuraminidase, bovine testes β -galactosidase, β -N-acetylhexosaminidase recombinant from *S. pneumoniae* expressed in *E. coli* and bovine kidney $\alpha(1-2,3,4,6)$ fucosidase (for PNGase F-released N-glycans).

In order to confirm the presence of sialylated antennae, Endo H-released N-glycans were digested using neuraminidase (see exoglycosidase digestion Table 5). After digestion, the mass spectrometric data revealed that the two peaks of the composition S1H5N2 (m/z 1940.9) and S2H6N2 (m/z 2145.0) shifted to H5N2 (m/z 1579.7) and H6N2 (m/z 1783.8) respectively. In addition, they further shifted after $\beta(1-4)$ -galactosidase treatment and subsequent β -N-acetylhexosaminidase digestion. Thus, the presence of hybrid-type structures at m/z 1579.7 and m/z 1783.8 and of a sialylated antenna in S1H5N2 (m/z 1940.9) and S2H6N2 (m/z 2145.0) were confirmed. In addition, a diagnostic fragment ion S1H1N1 at m/z 847.2 was detected and confirmed the sialylated antenna in S1H5N2 (m/z 1940.9) and S2H6N2 (m/z 2145.0). The structures H5N2 (m/z 1579.7) and H6N2 (m/z 1783.8) were assigned to hybrid-type structures due to the presence of a signal at m/z 486.0 (H1N1). The rest of the signals that remained after β -N-acetylhexosaminidase digestion disappeared from the MALDI-TOF mass spectrum after α -mannosidase digestion, showing that they contain Man residues. However, a signal at m/z 1334.6 corresponding to H5N1, which is a digestion product of H10N1 (m/z 2355.1), remained after α -mannosidase digestion. Therefore, H10N1 (m/z 2355.1) was assigned to the monoglucosylated N-glycan precursor Glc1Man9GlcNAc1, which was also verified with fragmentation analysis. MALDI-TOF/TOF-MS of H10N1 revealed a monoglucosylated antenna that was confirmed by the presence of the diagnostic fragment ions H4 at m/z 852.5 and H3 at m/z 649 and indicated the presence of an antenna bearing four hexoses.

PNGase F-released N-glycans were digested with neuraminidase (see exoglycosidase digestion Table 6) in order to prove the presence of sialylated antennae. Further digestion with β -galactosidase and β -N-acetylhexosaminidase led to a shift of Gal- and GlcNAc-containing structures and proved their presence in the N-glycan pool. The two structures H3N2 (m/z 1171.6) and H3N2F1 (m/z 1345.6) did not shift after digestion with β -N-acetylhexosaminidase, indicating that the fucosylated N-glycans of the pool bear one $\alpha(1-6)$ -linked Fuc at the reducing GlcNAc of the core residue. In addition, core-fucosylation was confirmed by the diagnostic fragment ions N1F1 at m/z 474.0 and N2F1 at m/z 719.2 for instance in the biantennary N-glycans H5N4F1 (m/z 2244.1) and S1H5N4F1 (m/z 2605.3) (Fig.2.16) in undifferentiated MSCs and adipogenically differentiated MSCs. The presence of sialylated antennae in S1H5N4F1 (m/z 2605.3), S2H5N4F1 (m/z 2966.4), S1H6N5F1 (m/z

3054.5), S2H6N5F1 (m/z 3415.7), S1H7N6F1 (m/z 3503.7), S3H6N5F1 (m/z 3776.8), S2H7N6F1 (m/z 3864.9) and S3H7N6F1 (m/z 4226.1) were confirmed by the diagnostic fragment ions S1H1N1 at m/z 847.2 and S1H2N1 at m/z 620.1.

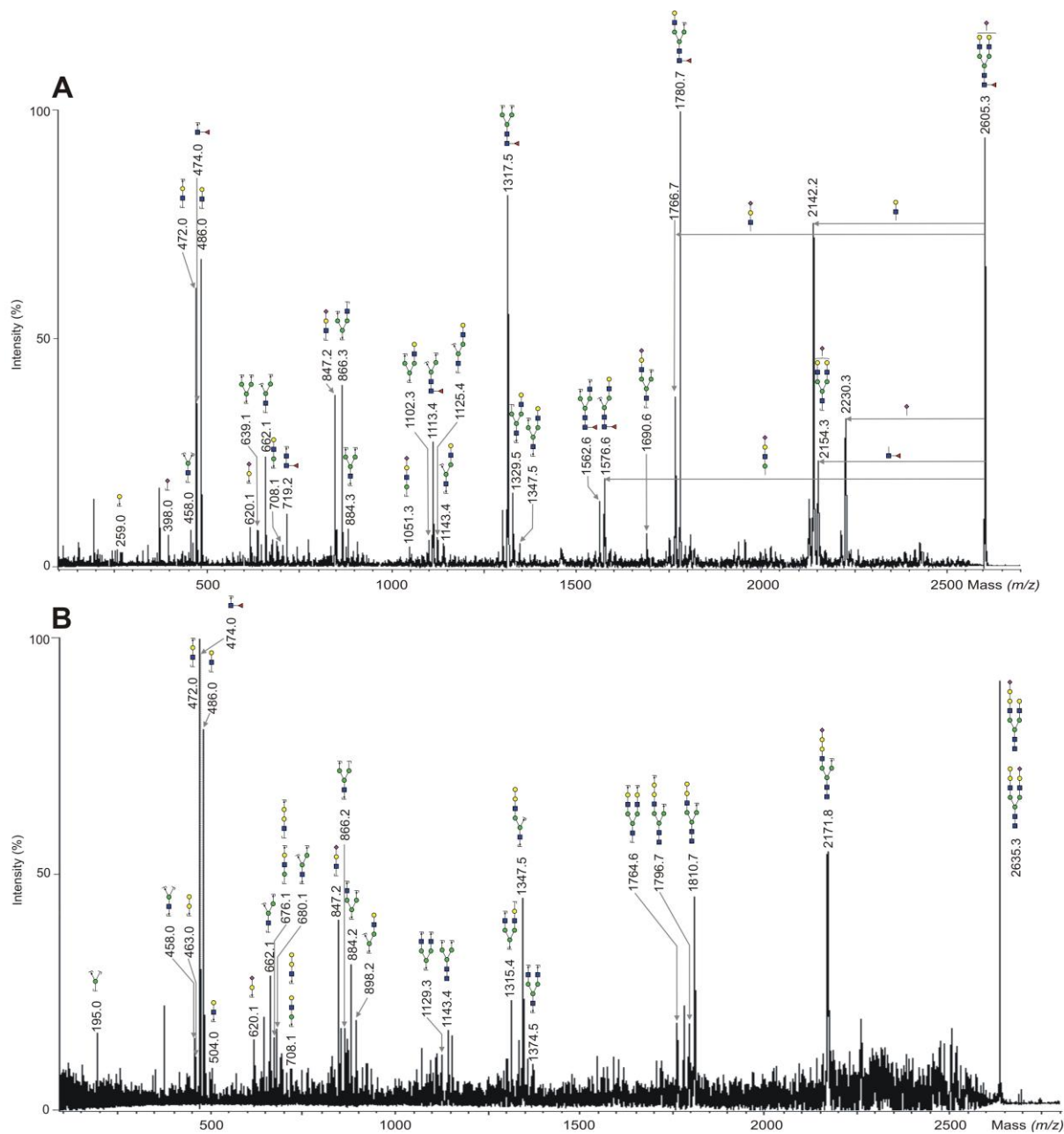


FIG. 2.16. MALDI-TOF/TOF mass spectrum of m/z 2605.3 of the composition S1H5N4F1 derived from human MSCs (**A**) and of m/z 2635.3 of the composition S1H6N4 derived from day 15 adipogenically differentiated MSCs (**B**). Blue square represents N-acetylglucosamine, green circle mannose, yellow circle galactose, red triangle fucose and pink diamond N-acetylneuraminic acid.

The signal at m/z 2461.2 corresponds to the structure G1H5N4, which contained one N-glycolyneuraminic acid residue but was only found as a trace. This structure was also

observed in a previous study by Heiskanen et al. (151) in human MSCs and is most likely stemming from the cell culture media that is displaced with animal-derived components such as fetal calf serum (FCS) (144, 152).

Exoglycosidase digestions revealed that the N-glycan structures H6N4 (m/z 2274.1) and H7N5 (m/z 2723.3) correspond to a trigalactosylated biantennary N-glycan and a tetragalactosylated triantennary N-glycan, respectively, since their signals remained after neuraminidase digestion. This was supported by the fragment ions H2 (m/z 463.0), H1N1 (m/z 472.0), N1H2 (m/z 690.2) and H1H2 (m/z 708.2). From these results it was concluded that the signals at m/z 2274.1, m/z 2635.3, m/z 2996.4, m/z 3084.5, m/z 3445.7, m/z 3806.8 and m/z 3894.9 corresponded to structures of the form $S_xH_{y+2}N_y$.

The LacNAc motif was verified in the structures H5N5F1 (m/z 2489.2), H6N5 (m/z 2519.2), H6N5F1 (m/z 2693.3), S1H5N5F1 (m/z 2850.4), S1H6N5 (m/z 2880.4), S1H6N5F1 (m/z 3054.5), H7N6F1 (m/z 3142.5), S1H7N6 (m/z 3329.6), S2H6N5F1 (m/z 3415.7), S1G1H6N5F1 (m/z 3445.7), S1H7N6F1 (m/z 3503.7), H8N7F1 (m/z 3591.7), S2H7N6F1 (m/z 3864.9), S1H8N7F1 (m/z 3952.9), S3H7N6F1 (m/z 4226.1) and S2H8N7F1 (m/z 4314.1) using MALDI-TOF/TOF fragmentation analysis. The presence of the diagnostic fragment ion H2N2 at m/z 935.2 revealed the poly-LacNAc epitope in these structures. However, the diagnostic fragment ion that indicates the presence of poly-LacNAc was predominantly found in N-glycans of undifferentiated human MSCs and was minimal in day 15 adipogenically differentiated cells. Poly-LacNAc-containing N-glycans like H8N7F1 (m/z 3591.7), S1H8N7F1 (m/z 3952.9) and S2H8N7F1 (m/z 4314.1) were also found to be core-fucosylated (diagnostic fragment ions N1F1 at m/z 474.0 and N2F1 at m/z 719.2) and the sialylated antenna in S1H8N7F1 (m/z 3952.9) and S2H8N7F1 (m/z 4314.1) was confirmed by two diagnostic fragment ions, namely S1H1N1 at m/z 847.2 and S1H1 at m/z 620.1.

2.2.1.5 Gene expression analysis of undifferentiated and adipogenically differentiated human bone marrow mesenchymal stem cells

Microarray gene expression was performed by Mujib Ullah (M. Phil), who is member of the working group of our co-operation partner Dr. Jochen Ringe (Tissue Engineering Laboratory & BCRT). On molecular level the process of sialylation and fucosylation was confirmed by the gene expression of *ST3GAL1* (*ST3 beta-galactoside alpha-2,3-sialyltransferase 1*) and *FUT8* (*fucosyltransferase 8 (alpha (1,6) fucosyltransferase)*). The expression of these two genes were selected from already submitted microarray gene data (GEO; ID: GSE36923) for similar adipogenic cultures. In adipogenic differentiated cells, the expression of *ST3GAL1* was upregulated and *FUT8* downregulated compared to MSC (Fig.2.17). On gene level, the expression of *ST3GAL1* and *FUT8* favors the process of $\alpha(2-3)$ -sialylation and $\alpha(1-6)$ -

fucosylation. According to MALDI-TOF mass spectrometric data, sialylation in adipogenic differentiated cells was increased and core-fucosylation was decreased in case of tri- and tetraantennary N-glycans. Thus, the gene expression data confirmed the MALDI-TOF-MS data.

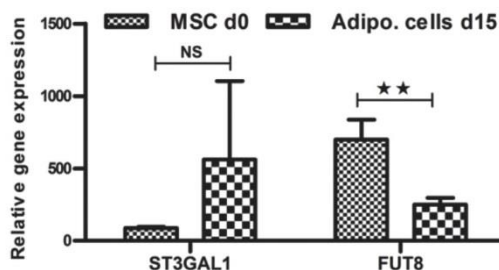


Fig. 2.17. Microarray gene expression confirmed the expression of *ST3GAL1* and *FUT8* in undifferentiated and day 15 adipogenically differentiated MSCs. Data were expressed as mean and standard error of mean (SEM). The student t-test was performed to evaluate the expressed genes for their statistical significance, (** $p < 0.01$). NS: not significant. ST3GAL1: ST3 beta-galactoside (alpha-2,3-sialyltransferase 1), FUT8: fucosyltransferase 8 (alpha (1,6) fucosyltransferase).

2.2.2 N-Glycosylation profile of undifferentiated and chondrogenically differentiated human bone marrow mesenchymal stem cells

2.2.2.1 N-Glycome of mesenchymal stem cells and its changes during chondrogenic differentiation

It was an aim to investigate the N-glycosylation profile of MSCs during chondrogenic differentiation. The chondrogenically differentiated MSCs were isolated from their extracellular matrix (ECM) prior to N-glycan analysis, in order to obtain the N-glycosylation pattern of the pure cells without any contaminations from extracellular proteins of the ECM. Four different MSC preparations isolated from four different donors were used for the chondrogenic differentiation in order to obtain four biological replicates. The N-glycosylation profile of undifferentiated, early time point (day 5) and late time point (day 28) chondrogenically differentiated MSCs was investigated to monitor the changes of the N-glycosylation pattern during differentiation. The different cell samples were harvested and washed three times with PBS. Cell surface (glyco)proteins were digested with trypsin yielding to glycopeptides that were subjected to PNGase F-digestion. The released N-glycans were purified, desalted and derivatised. 60 % of the N-glycan pool was permethylated and measured by means of MALDI-TOF-MS. The rest of the N-glycan pool was labeled with the fluorophore APTS in order to detect the N-glycans by laser induced fluorescence detection through capillary electrophoresis. A representative mass spectrum of the resulting N-

glycosylation profile of human undifferentiated and day 28 chondrogenically differentiated MSCs is shown in Fig.2.18 A and B. About 85 different N-glycan signals were detected with MALDI-TOF-MS (Table 4).

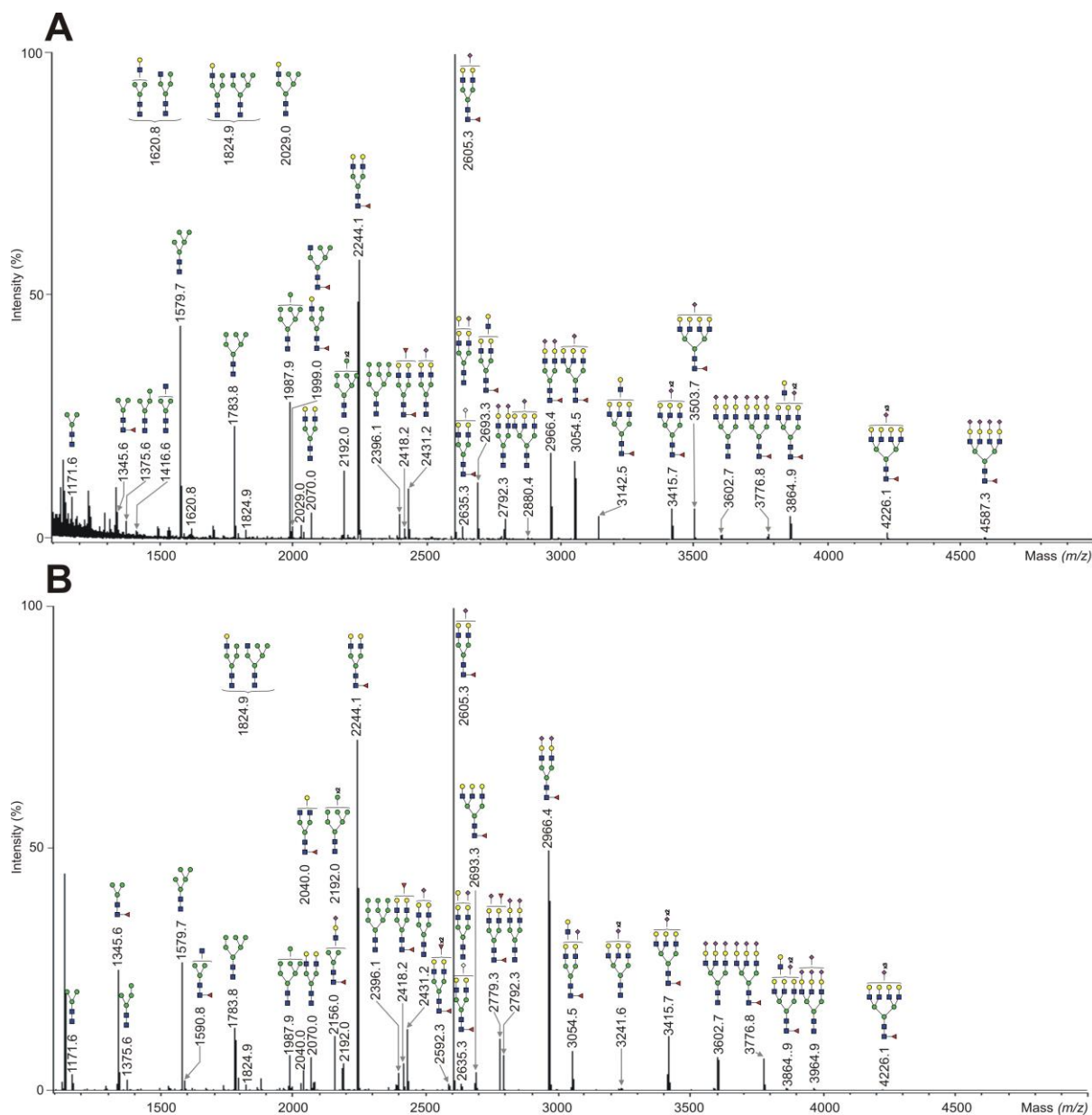


FIG. 2.18. MALDI-TOF-MS of PNGase F-released N-glycans of undifferentiated and chondrogenically differentiated human MSCs. Day 28 chondrogenically differentiated MSCs were isolated from their ECM prior to N-glycan analysis. Cell surface glycoproteins were directly digested from the cells with trypsin. N-glycans were enzymatically cleaved from glycopeptides with PNGase F, permethylated and measured by MALDI-TOF-MS. A representative mass spectrum of PNGase F-released N-glycans of undifferentiated (**A**) and chondrogenically differentiated human MSCs (**B**) is shown together with the 30 most abundant structures. Blue square represents N-acetylglucosamine, green circle mannose, yellow circle galactose, red triangle fucose and pink diamond N-acetylneuraminic acid.

The relative abundances of the 40 most abundant N-glycans derived from four (MSCs) and three (chondrogenically differentiated MSCs) different preparations are presented in Fig. 2.19 A and B. The diagrams represent the mean relative abundances of N-glycans from the different biological replicates. The N-glycan profiles of the different MSCs and chondrogenically differentiated cells analysed were highly similar, as can be determined from the small deviations within the observed glycan profiles.

Mass spectrometric profiling revealed that fucosylated biantennary complex-type N-glycans dominated the N-glycan profiles of undifferentiated MSCs and day 5 as well as day 28 of chondrogenically differentiated MSCs. The second major group was triantennary fucosylated structures. However, tetraantennary N-glycans were detected as well. High-mannose and hybrid type N-glycans were also detected. The amount of high-mannose N-glycans decreased by 11 % after day 5 of chondrogenic differentiation and increased again by 6 % after day 28. The high-mannose N-glycan H7N2 (m/z 1987.9) was found to be significantly underexpressed in day 28 of chondrogenic differentiated MSCs. Hybrid-type N-glycans were much less abundant than complex and high-mannose N-glycans and their amount stayed almost the same with chondrogenic differentiation. Neutral, sialylated as well as fucosylated hybrid N-glycans were detected in undifferentiated and day 5 and day 28 chondrogenically differentiated MSCs.

Evaluation of fucosylation. The amount of fucosylated N-glycans in day 5 chondrogenically differentiated cells was about 12 % higher than in MSCs but decreased again in day 28 chondrogenically differentiated cells by 8 %. In all, fucosylation increased just little after chondrogenic differentiation (3 %). The overall amount of mono- or biantennary fucosylated complex N-glycan increased. Some of these fucosylated N-glycans showed a significant increase after day 28 of chondrogenic differentiation such as H3N2F1 (m/z 1345.6), S1H4N3F1 (m/z 2156.0), S2H5N4F1 (m/z 2966.4) and S3H6N5F1 (m/z 3776.8). In contrast, the amount of the two biantennary fucosylated N-glycans H5N4F1 (m/z 2244.1) and S1H5N4F1 (m/z 2605.3) increased after day 5 of chondrogenic differentiation and decreased after day 28 of chondrogenic differentiation to a relative amount less than in undifferentiated MSCs. On the other hand, the overall amount of tri- and tetraantennary fucosylated structures decreased such as H6N5F1 (m/z 2693.3), S1H6N5F1 (m/z 3054.5), H7N6F1 (m/z 3142.5) and S1H7N6F1 (m/z 3503.7), which showed a significant decrease in day 28 of chondrogenically differentiated cells. Fucosylated structures were predominantly monofucosylated at the reducing GlcNAc residue. Besides, difucosylated N-glycans such as H4N4F2 (m/z 2214.1), H5N4F2 (m/z 2418.2) and S1H5N4F2 (m/z 2779.3) were found in undifferentiated and day 5 as well as in day 28 chondrogenically differentiated MSCs.

Evaluation of antennarity. The overall amount of N-glycans bearing one or two antennae increased in day 5 and day 28 chondrogenically differentiated MSCs. For example, the N-

glycans S1H4N3F1 (m/z 2156.0), S1H5N4F2 (m/z 2779.3) and S2H5N4F1 (m/z 2966.4) were significantly increased in day 28 chondrogenically differentiated cells. In contrast, the amount of N-glycans with three or four antennae decreased by about 7 %. The most abundant structures found in this group, showed a significant decrease after day 28 of chondrogenic differentiation such as triantennary N-glycans H3N5F1 (m/z 2081.0), H6N5F1 (m/z 2693.3), S1H6N5F1 (m/z 3054.5) and S3H6N5F1 (m/z 3776.8) as well as tetraantennary N-glycans H7N6F1 (m/z 3142.5), S1H7N6F1 (m/z 3503.7) and S2H7N6F1 (m/z 3864.9). Remarkably, the amount of fucosylated tetraantennary structures decreases from 4.4 to 0.6 % in day 28 of chondrogenically differentiated MSCs. Poly-LacNAc N-glycans were found in MSCs and chondrogenically differentiated cells such as H6N5F1 (m/z 2693.3), H7N6F1 (m/z 3142.5) and S2H7N6F1 (m/z 3864.9) in MSCs as well as S1H6N5F1 (m/z 3054.5) and S2H7N6F1 (m/z 3864.9) in chondrogenically differentiated MSCs. However, the poly-LacNAc signals were decreased in relative amount in day 28 of chondrogenically differentiated cells.

Evaluation of sialylation. Approximately half of the N-glycan structures were found to be sialylated. The overall amount of sialylated N-glycans increases by 6 % after day 28 of chondrogenic differentiation. Sialylated N-glycans were predominantly monosialylated although di-, tri- and tetrasialylated N-glycans were present as well. One third of the structures were found to be fully sialylated and the rest of the structures were just partially sialylated. In addition, the presence of fully sialylated structures decreased with increased antennarity.

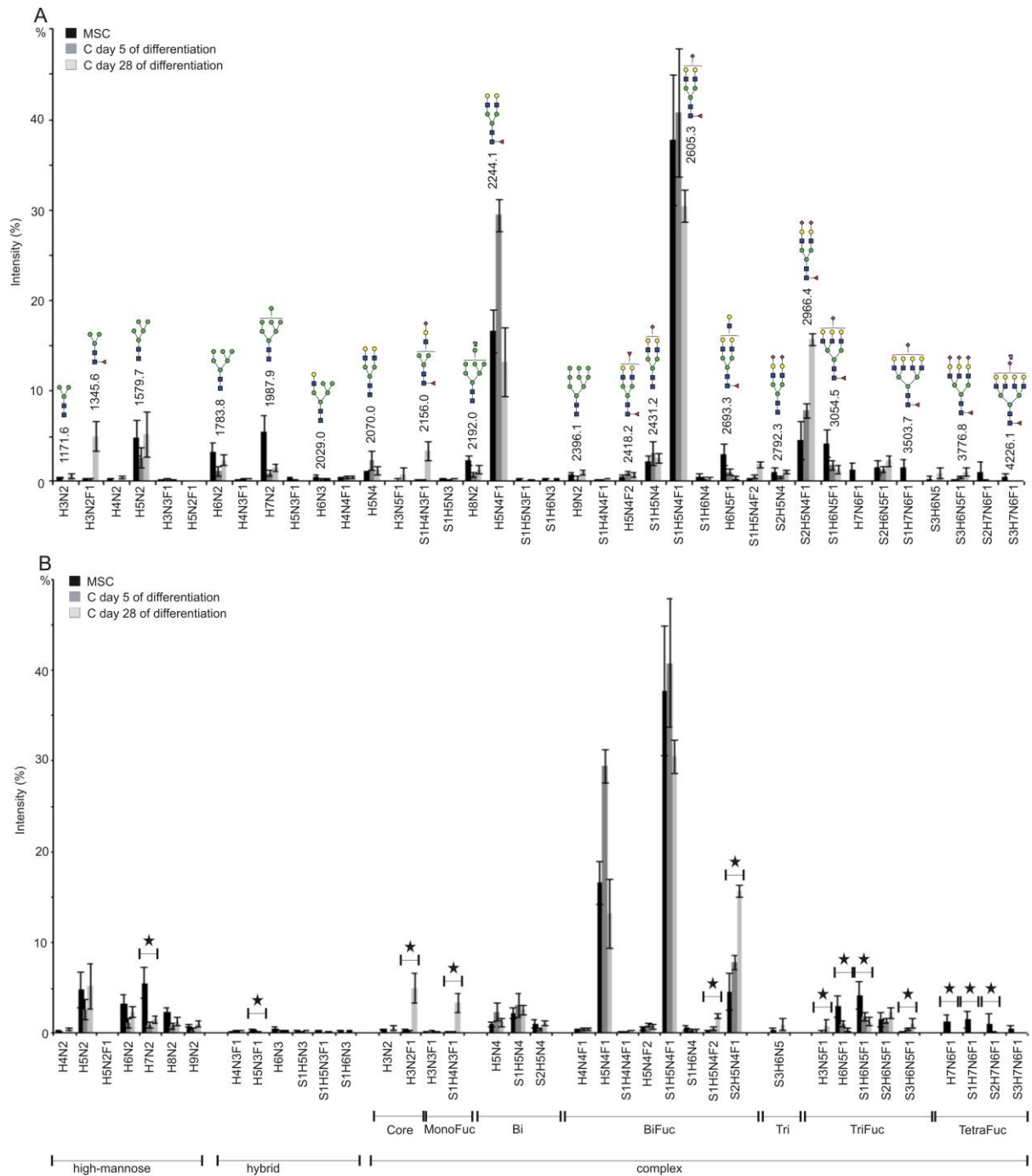


FIG. 2.19. Quantification of PNGase F-released N-glycans with MALDI-TOF-MS. **(A)** The average relative amounts of the 40 most abundant PNGase F-released N-glycans of undifferentiated human MSCs (black) and chondrogenically differentiated MSCs (C) at day 5 (dark grey) and day 28 (light grey) derived from four (MSCs, n=4) and three (chondrogenically differentiated MSCs, n=3) different preparations, **(B)** grouped according to their N-glycan type, antennarity and fucosylation. Day 5 and 28 chondrogenically differentiated MSCs were isolated from their ECM prior to N-glycan analysis. Statistical significant difference between the two sample groups undifferentiated MSCs and 28 days chondrogenically differentiated MSCs was assessed using Mann-Whitney U test (*p<0.05) and is marked with a star in **(B)**. Blue square represents N-acetylglucosamine, green circle mannose, yellow

circle galactose, red triangle fucose and pink diamond N-acetylneuraminic acid. H: hexose, N: N-acetylhexosamine, F: deoxyhexose, S: N-acetylneuraminic acid.

2.2.2.2 CE-LIF analysis of N-glycans from undifferentiated and chondrogenically differentiated human bone marrow mesenchymal stem cells

About 40 % of the N-glycan pool was analysed by means of CE-LIF in order to confirm the structure found by MALDI-TOF-MS. To this end, N-glycans were labeled with APTS and chemically desialylated by acetic acid hydrolysis, in order to convert the charged sialylated N-glycans into neutral molecules, and thus making separation independent from the charge of Neu5Ac. N-Glycans were then desalted on self-made graphite micro-columns and then subjected to CE-LIF analysis. Representative electropherograms of PNGase F-released N-glycans of undifferentiated and day 5 as well as day 28 chondrogenically differentiated MSCs without ECM are presented in Fig.2.23 A, B and D. N-glycans were assigned with the help of a standard table generated in our laboratory using N-glycans release from reference glycoproteins. In addition, MALDI-TOF-MS spectra of the desialylated N-glycan pools were used to assign the structures. The main structures were assigned to the electropherogram signals. In undifferentiated MSCs (Fig.2.23 A) the biantennary structures H5N4 (8.9 GU) and H5N4F1 (9.8 GU) comprised together the main part of the N-glycosylation profile, followed by the triantennary N-glycans H6N5 (11.0 GU) and H6N5F1 (12.0 GU) and tetraantennary fucosylated structure H7N6F1 (13.7 GU). High-mannose N-glycans such as H5N2 (GU) and H6N2 (GU) were detected as well. The relative amount of the biantennary structures H5N4 (8.9 GU) and H5N4F1 (9.8 GU) increased in day 5 and day 28 of chondrogenically differentiated cells without ECM (Fig.2.23 B and D) as can be seen from the peak height of the detected N-glycan signals. In contrast, the relative amount of the tri- and tetraantennary structures decreased drastically. Very similar distributions of the structures and changes during differentiation were obtained from the MALDI-TOF-MS data. Consequently, the CE-LIF electropherograms confirmed the mass spectrometric profiling.

2.2.2.3 Verification of the identified N-glycan structures in undifferentiated and chondrogenically differentiated mesenchymal stem cells with MALDI-TOF/TOF sequencing and exoglycosidase digestions

Verification of the most abundant N-glycan structures was done using specific exoglycosidases (see exoglycosidase digestion Table 7) in combination with MALDI-TOF/TOF-MS fragmentation that was performed in the positive-ion mode. A representative MALDI-TOF/TOF mass spectrum is presented in Fig. 2.20 A and B for the N-glycan signal

m/z 3142.5 of the composition H7N6F1 derived from human MSCs and of *m/z* 2418.2 of the composition H5N4F2 derived from day 28 chondrogenically differentiated MSCs. PNGase F-released N-glycans from undifferentiated and chondrogenically differentiated MSCs were consecutively digested using the following sequence of digestion: neuraminidase, $\beta(1-4)$ galactosidase, almond meal $\alpha(1-3,4)$ fucosidase, again $\beta(1-4)$ galactosidase, bovine kidney $\alpha(1-2,3,4,6)$ fucosidase and α -mannosidase in order to unravel the presence Lewis^X epitopes and core-fucosylated structures.

All sialylated N-glycans shifted after digestion with neuraminidase and no sialylated structures were detected any longer. All galactosylated N-glycans, except from Lewis^X-containing structures, were digested after addition of $\beta(1-4)$ galactosidase showing that all Gal residues are linked in $\alpha(1-4)$ -fashion to GlcNAc. Bifucosylated N-glycans such as H5N4F2 (*m/z* 2418.2), S1H5N4F2 (*m/z* 2779.3) and S1H6N5F2 (*m/z* 3228.6) were shown to contain one Lewis^X epitope because one fucosylated antennae containing a Gal residue remained after digestion with $\beta(1-4)$ galactosidase and shifted after addition of $\alpha(1-3,4)$ fucosidase and $\beta(1-4)$ galactosidase. Fucosylated structures shifted after addition of bovine kidney $\alpha(1-2,3,4,6)$ fucosidase, indicating that fucosylated N-glycans contained at least one core-Fuc that is $\alpha(1-6)$ -linked to the reducing GlcNAc residue. The presence of Man residues in high-mannose and hybrid type N-glycans was confirmed by α -mannosidase treatment. In addition, the detection of the diagnostic fragment ions N1F1 at *m/z* 474.0 and N2F1 at *m/z* 719.2 proved core-fucosylation for instance in the N-glycans H4N4F1 (*m/z* 2040.0), S1H4N3F1 (*m/z* 2156.0), H5N4F1 (*m/z* 2244.1), S1H5N4F1 (*m/z* 2605.3), H6N5F1 (*m/z* 2693.3), S1H5N4F2 (*m/z* 2779.3), S2H5N4F1 (*m/z* 2966.4), S1H6N5F1 (*m/z* 3054.5), S2H6N5F1 (*m/z* 3415.7) and S3H6N5F1 (*m/z* 3776.8) in undifferentiated and chondrogenically differentiated MSCs. The diagnostic fragment ions S1H1N1 at *m/z* 847.2 and S1H1 at *m/z* 620.1 confirmed the presence of a sialylated antenna in S1H5N4 (*m/z* 2431.2), S1H5N4F1 (*m/z* 2605.3) (Fig. 6), S2H5N4 (*m/z* 2792.3), S2H5N4F1 (*m/z* 2966.4), S1H6N5F1 (*m/z* 3054.5), S2H6N5F1 (*m/z* 3415.7), S1H7N6F1 (*m/z* 3503.7), S3H6N5 (*m/z* 3602.7), S3H6N5F1 (*m/z* 3776.8), S2H7N6F1 (*m/z* 3864.9), S3H7N6F1 (*m/z* 4226.1) and S4H7N6F1 (*m/z* 4587.3).

According to mass calculations, the N-glycan signals G1H5N4 (*m/z* 2461.2), G1H5N4F1 (*m/z* 2635.3), S1G1H5N4 (*m/z* 2822.4), S1G1H5N4F1 (*m/z* 2996.4) and G2H5N4F1 (*m/z* 3026.4) contained a Neu5Gc residue, which was verified by the diagnostic fragment ion G1H1N1 (*m/z* 877.2) for the N-glycan signals G1H5N4 (*m/z* 2461.2), G1H5N4F1 (*m/z* 2635.3), S1G1H5N4 (*m/z* 2822.4) and S1G1H5N4F1 (*m/z* 2996.4). However, the signal at *m/z* 2635.3 was found to correspond to a mix of two different structures, namely S1H6N4 and G1H5N4F1. Beside the Neu5Gc-containing N-glycan, the second structure contained an antenna with two Gal residues that are connected in linear fashion to each other as well as a

sialylated antenna. That was supported by the diagnostic fragment ions H2 m/z 463.0 and S1H1N1 m/z 847.2. Neu5Gc signals, such as G1H5N4 at m/z 2461.2 were also observed in previous studies (127, 151) as traces in MSCs. The Neu5Gc contamination is most likely stemming from cell culture media that contain animal-derived components (144, 152).

The signals at m/z 1620.8, 1794.9 and 1824.9 may present two different N-glycan isomeric structures, one may contain a galactosylated and the other one a non-galactosylated antenna (see exoglycosidase digestion Table 7).

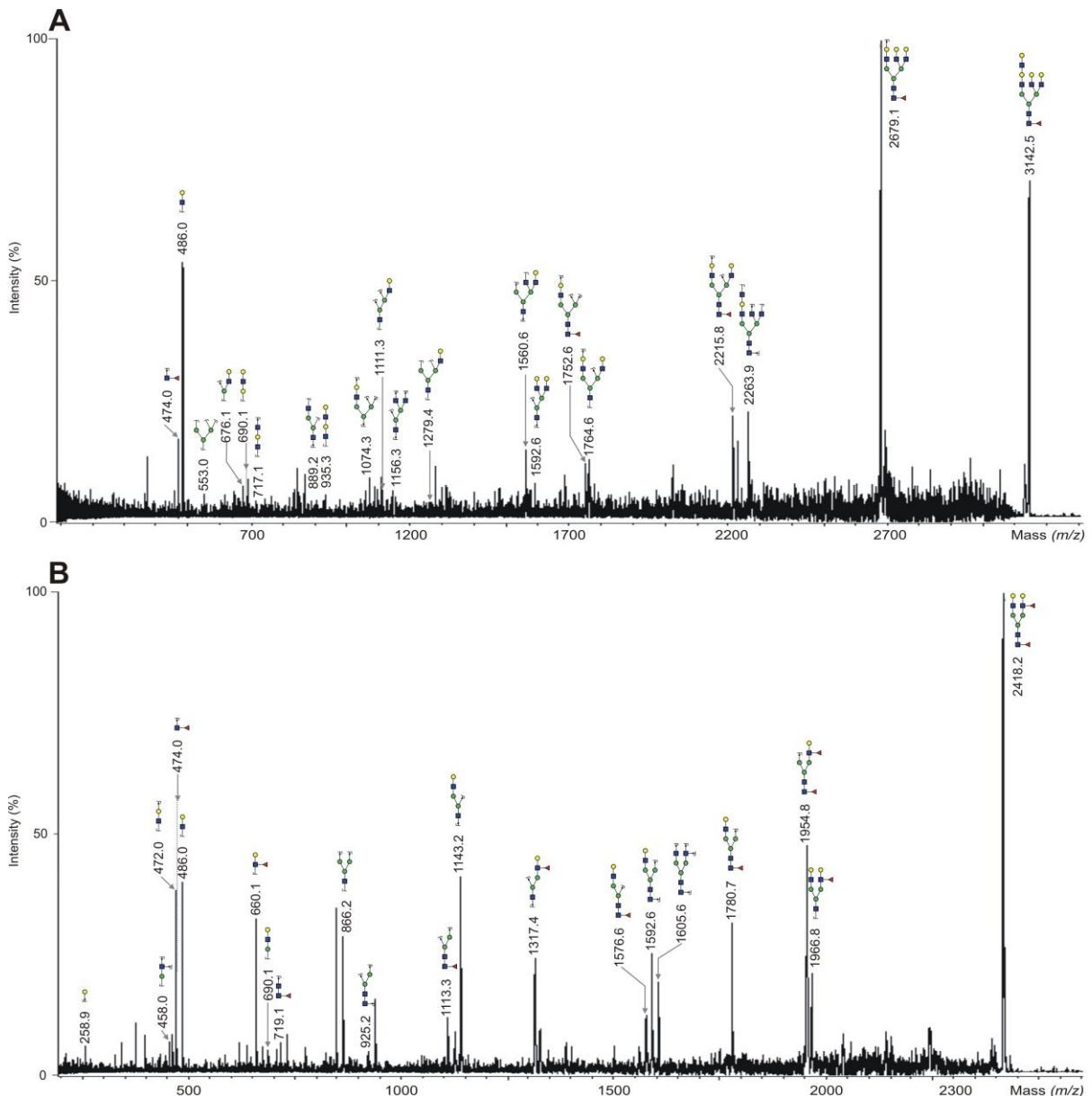


FIG. 2.20. MALDI-TOF/TOF mass spectrum of m/z 3142.5 of the composition H7N6F1 derived from human MSCs (**A**) and of m/z 2418.2 of the composition H5N4F2 derived from day 28 chondrogenically differentiated MSCs (**B**). Blue square represents N-acetylglucosamine, green circle mannose, yellow circle galactose, red triangle fucose and pink diamond N-acetylneuraminic acid.

MALDI-TOF/TOF fragmentation revealed that both isomeric forms were present in undifferentiated as well as day 28 chondrogenically differentiated MSCs, which was supported by the diagnostic fragment ions H1N1H1 m/z 690.1 and m/z 708.2 in case of the galactosylated N-glycan and by H2 m/z 445.0 and/ or N1H3 m/z 866.2 in case of the non-galactosylated structure. In contrast, the structures H5N3F1 (m/z 1999.0), H6N3 (m/z 2029.0) and H6N3F1 (m/z 2203.0) were identified as galactosylated hybrid-type N-glycans and this was verified by the fragment ion H1N1H1 at m/z 690.1 and m/z 708.2. In addition, this signals were sensitive to β (1-4) galactosidase.

The LacNAc motif was found in H6N5F1 (m/z 2693.3), H7N6F1 (m/z 3142.5) and S2H7N6F1 (m/z 3864.9) in undifferentiated MSCs as well as S1H6N5F1 (m/z 3054.5) and S2H7N6F1 (m/z 3864.9) in day 28 of chondrogenically differentiated MSCs. The presence of poly-LacNAc in these structures was verified by the diagnostic fragment ion H2N2 at m/z 935.2.

2.2.2.4 N-glycosylation profile of chondrogenically differentiated mesenchymal stem cells with their extracellular matrix (ECM)

In the previous paragraphs, the cell surface N-glycosylation profile of undifferentiated MSCs was presented and compared to the one of chondrogenically differentiated MSCs, which were isolated from their ECM prior to N-glycan analysis. In order to examine the influence of the ECM on the N-glycosylation profile of chondrogenically differentiated MSCs, day 5 and day 28 chondrogenically differentiated MSCs were harvested together with their ECM, washed three times with PBS and cell surface (glyco)proteins were digested with trypsin. N-glycans were then released with PNGase F, purified, desalted and derivatised. 60 % of the N-glycan pool was permethylated and measured by means of MALDI-TOF-MS and the rest was labeled with APTS for CE-LIF analysis (Fig.2.23 A, C and E). A representative mass spectrum of the resulting N-glycosylation profile of human undifferentiated and day 28 chondrogenically differentiated MSCs with ECM is shown in Fig.2.21 A and B. About 85 different N-glycan signals were detected with MALDI-TOF-MS (Table 4, see appendix). The mean averages of the relative abundances of the 40 most abundant N-glycans are presented in Fig. 2.22 A and B and were calculated from four different biological replicates ($n=4$). The cell surface N-glycosylation profile of undifferentiated MSCs was already described in detail in the previous paragraphs and will be compared with the profile of chondrogenically differentiated cells with their ECM in this section.

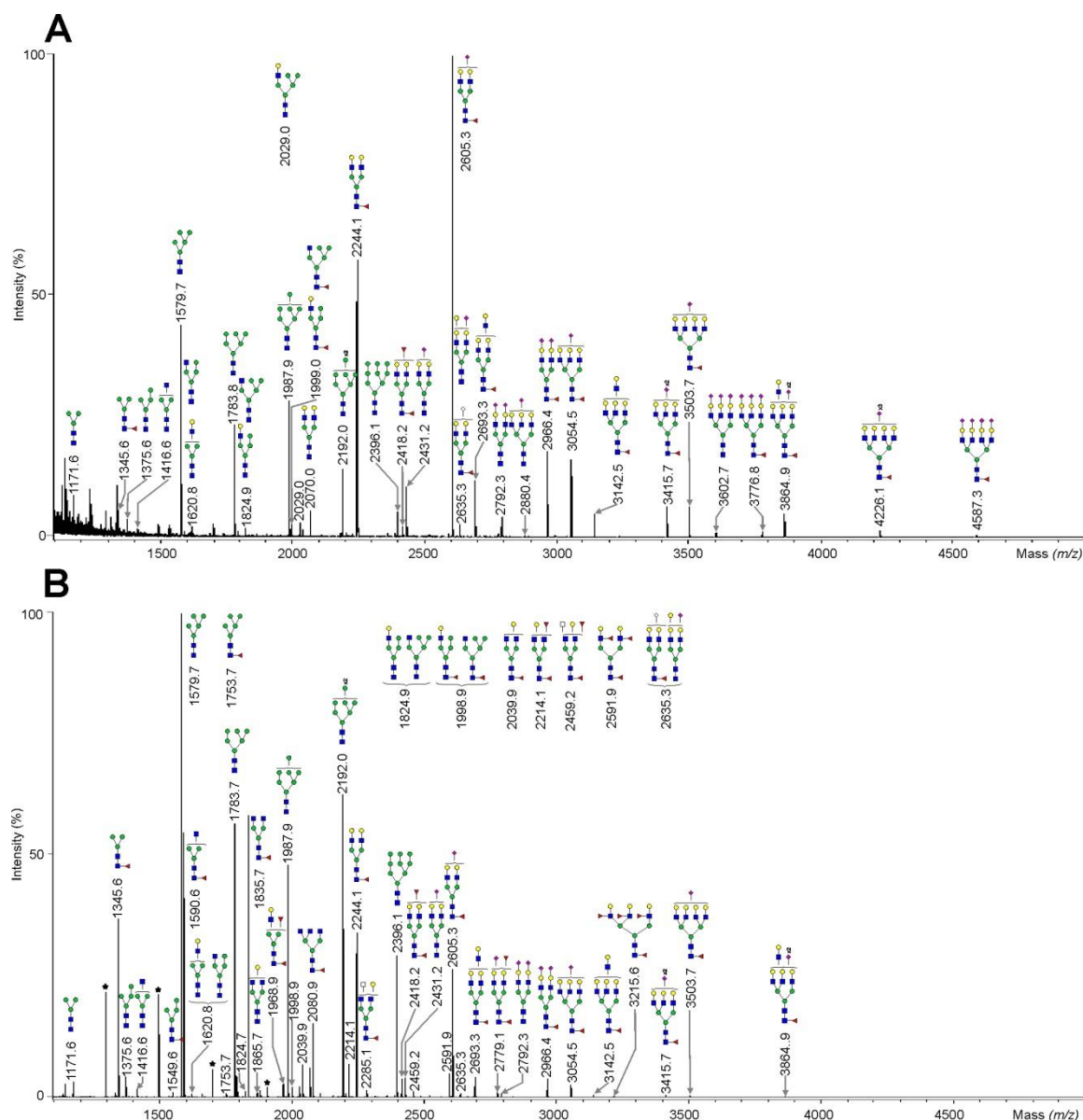


FIG. 2.21. MALDI-TOF-MS of PNGase F-released N-glycans of undifferentiated and day 28 chondrogenically differentiated MSCs. Day 28 chondrogenically differentiated MSCs were harvested with their ECM prior to N-glycan analysis. Cell surface glycoproteins were directly digested from the cells with trypsin. N-glycans were enzymatically cleaved from glycopeptides with PNGase F, permethylated and measured by MALDI-TOF-MS. A representative mass spectrum of PNGase F-released N-glycans of undifferentiated **(A)** and chondrogenically differentiated human MSCs **(B)** is shown together with the 30 most abundant structures. Blue square represents N-acetylglucosamine, green circle mannose, yellow circle galactose, red triangle fucose and pink diamond N-acetylneuraminic acid.

The mass spectrometric data revealed that the amount of high-mannose N-glycans increased drastically from 17 % in MSCs to 48 % in day 28 of chondrogenically differentiated cells with ECM. However, the increase was already observed in day 5 chondrogenically

differentiated cells with ECM, in which high-mannose N-glycans comprised about 43 % of the N-glycan pool. The increase of the high-mannose N-glycans H4N2 (*m/z* 1375.6), H5N2 (*m/z* 1579.7), H6N2 (*m/z* 1783.8), H8N2 (*m/z* 2192.0) and H9N2 (*m/z* 2396.1) was statistically significant.

The amount of hybrid-type N-glycans remained almost the same (about 2 %). Hybrid-type N-glycans were much less abundant than complex and high-mannose N-glycans and they stayed constant with chondrogenic differentiation. Neutral, sialylated as well as fucosylated hybrid N-glycans were detected in undifferentiated, day 5 and day 28 chondrogenically differentiated MSCs with ECM.

As the amount of high-mannose N-glycans increased drastically, the overall amount of complex N-glycans decreased from 80 % in MSCs to 48 % in day 28 of chondrogenically differentiated MSCs. Fucosylated tri- and tetraantennary N-glycans decreased in their relative amount by about 4 %, respectively. The decrease was statistically significant for fucosylated triantennary structures H6N5F1 (*m/z* 2693.3), S1H6N5F1 (*m/z* 3054.5) and S2H6N5F1 (*m/z* 3415.7) as well as tetraantennary N-glycans H7N6F1 (*m/z* 3142.5), S1H7N6F1 (*m/z* 3503.7), S2H7N6F1 (*m/z* 3864.9) and S3H7N6F1 (*m/z* 4226.1). However, the fucosylated triantennary structure H3N5F1 (*m/z* 2081.0) was absent in the profile of MSCs and present in day 5 and day 28 chondrogenically differentiated cells with an abundance of about 2 %. The relative amount of biantennary fucosylated N-glycans decreased dramatically from 61 % in MSCs to 30 % in day 28 chondrogenically differentiated cells with ECM. The decrease was significant for the structures H5N4F1 (*m/z* 2244.1), S1H5N4F1 (*m/z* 2605.3) and S2H5N4F1 (*m/z* 2966.4). In contrast, the fucosylated biantennary N-glycans H3N4F1 (*m/z* 1835.9), H4N4F1 (*m/z* 2040.0) and H4N4F2 (*m/z* 2214.1) showed a significant increase in relative amount in day 28 chondrogenically differentiated cells with ECM. Monoantennary complex N-glycans increased drastically in relative amount from 1 % in MSCs to 10 % in day 28 chondrogenically differentiated cells. The increase of the structures H3N2F1 (*m/z* 1345.6) and H3N3F1 (*m/z* 1590.8) was statistically significant. In addition, sialylation decreased drastically from 57 % in undifferentiated MSCs to 12 % in day 28 chondrogenically differentiated cells.

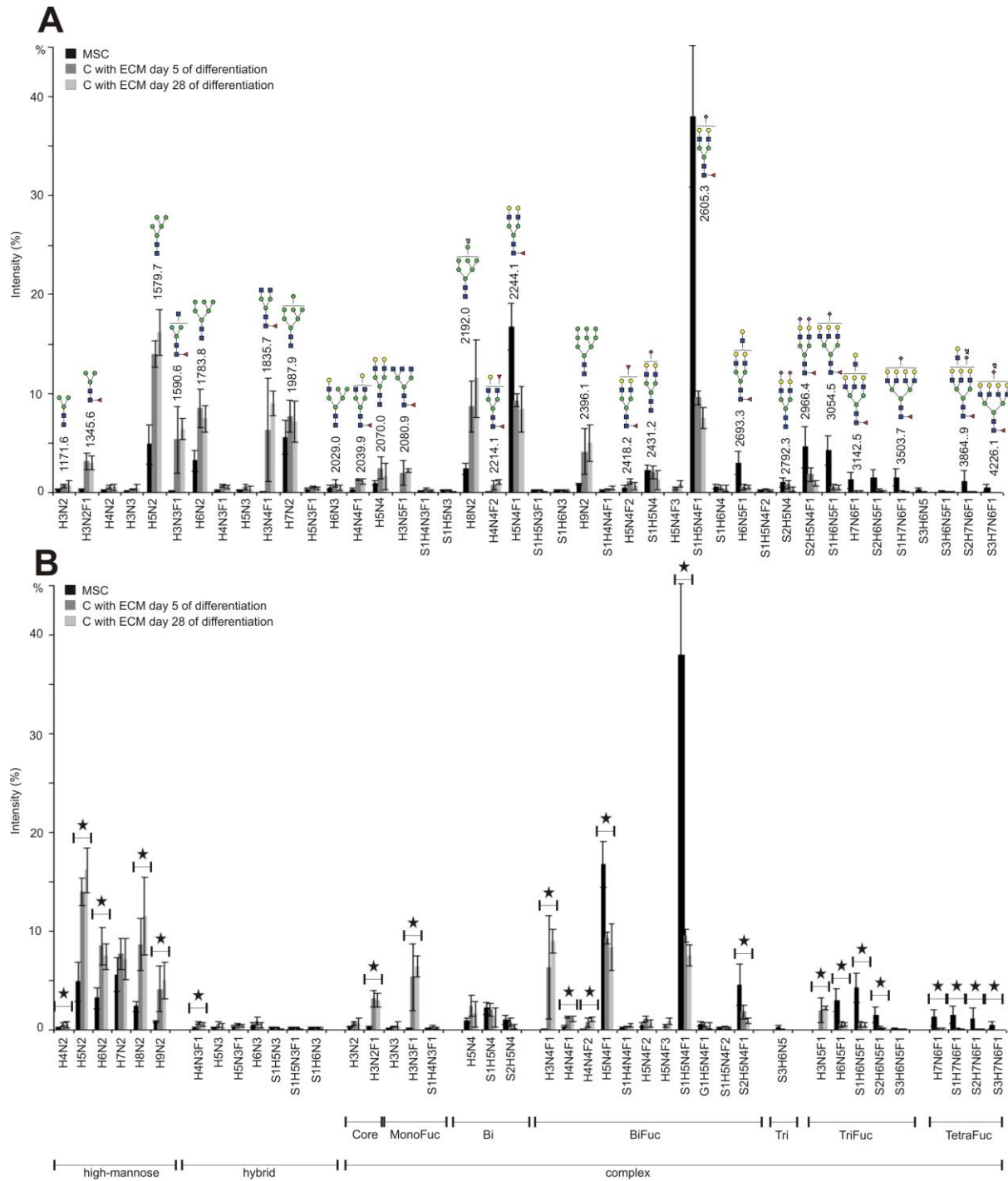


FIG. 2.22. Quantification of PNGase F-released N-glycans with MALDI-TOF-MS. **(A)** The average relative amounts of the 40 most abundant PNGase F-released N-glycans of undifferentiated human MSCs (black) and chondrogenically differentiated MSCs (C) at day 5 (dark grey) and day 28 (light grey) derived from four different preparations (n=4), **(B)** grouped according to their N-glycan type, antennarity and fucosylation. Day 5 and 28 chondrogenically differentiated MSCs were harvested with their ECM prior to N-glycan analysis. Statistical significance between the two sample groups undifferentiated MSCs and 28 days chondrogenically differentiated MSCs was assessed using Mann-Whitney U test ($*p \leq 0.05$) and is marked with a star in **(B)**. Blue square represents N-acetylglucosamine, green circle mannose, yellow circle galactose, red triangle fucose and pink

diamond N-acetylneuraminic acid. H: hexose, N: N-acetylhexosamine, F: deoxyhexose, S: N-acetylneuraminic acid.

2.2.2.5 CE-LIF analysis of N-glycans from undifferentiated and chondrogenically differentiated mesenchymal stem cells with their extracellular matrix (ECM)

N-glycans of undifferentiated and day 5 as well as day 28 chondrogenically differentiated MSCs with ECM were subjected to CE-LIF analysis (Fig.2.23 A, C and E).

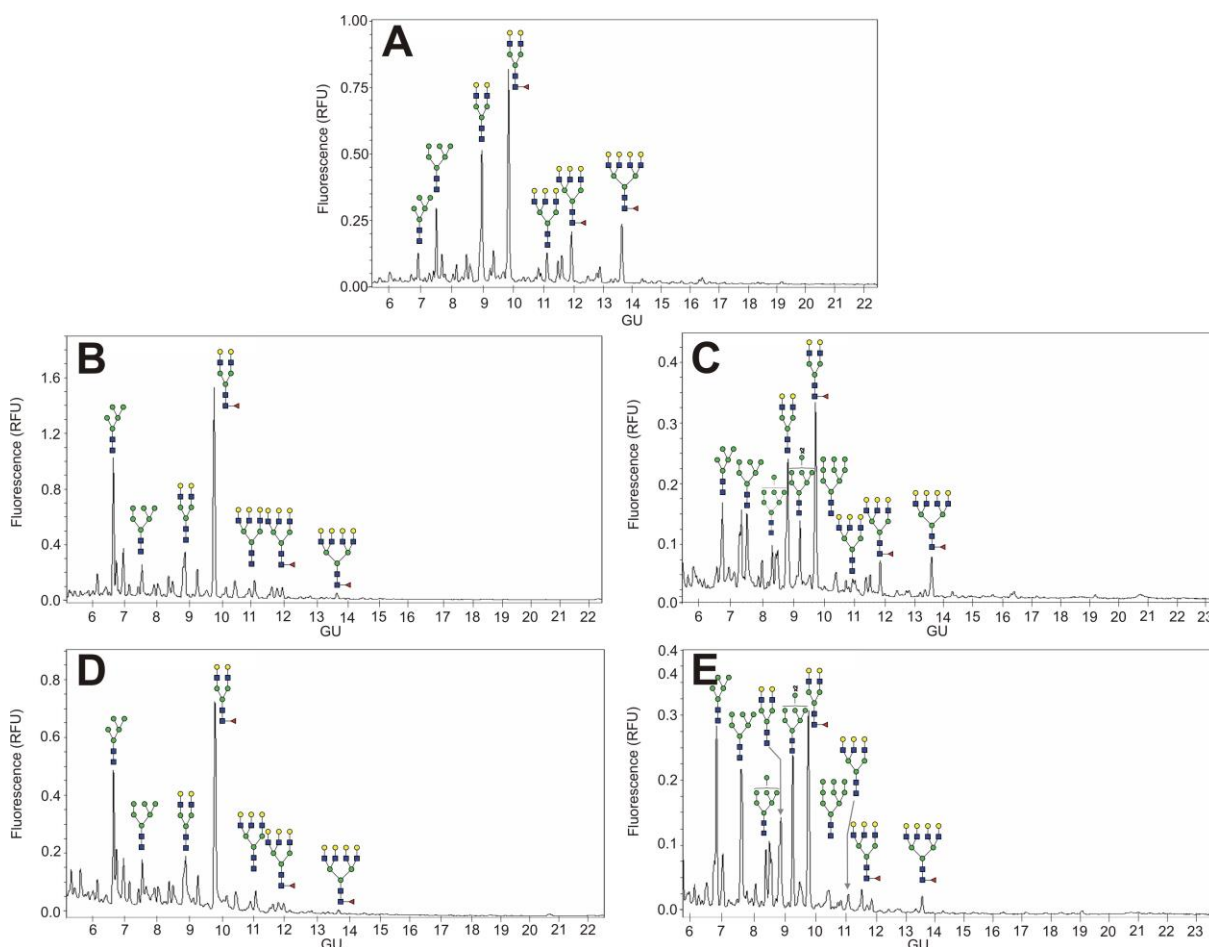


FIG. 2.23. CE-LIF electropherograms of PNGase F-released and desialylated complex-type N-glycans from undifferentiated (A), day 5 (B) as well as day 28 (D) chondrogenically differentiated human MSCs without ECM and day 5 (C) as well as day 28 (E) chondrogenically differentiated human MSCs with ECM. Cells were digested with trypsin in order to release cell surface (glyco)peptides. (Glyco)peptides were subjected to PNGase F digestion to release N-glycans, desialylated and measured by CE-LIF. Blue square represents N-acetylglucosamine, yellow square N-acetylgalactosamine, white square N-acetylhexosamine, green circle mannose, yellow circle galactose, red triangle fucose, white diamond N-glycolylneuraminic acid and pink diamond N-acetylneuraminic acid.

The relative abundances of complex-type N-glycans such as the triantennary fucosylated N-glycan H6N5F1 (12.0 GU) and tetraantennary fucosylated structure H7N6F1 (13.8 GU) decreased in day 28 of chondrogenically differentiated cells with ECM (Fig.2.23 E). In contrast, the amount of high-mannose N-glycans (6.7 – 10.5 GU) increased drastically after day 28 of chondrogenic differentiation in presence of ECM. Very similar distributions of the structures and changes during differentiation were obtained from the MALDI-TOF-MS data. Consequently, the CE-LIF electropherograms confirmed the mass spectrometric profiling.

2.2.3 N-Glycosylation profile of undifferentiated and osteogenically differentiated human bone marrow mesenchymal stem cells

2.2.3.1 N-Glycome of mesenchymal stem cells and its changes during osteogenic differentiation

Besides the adipogenic and chondrogenic potential of human bone marrow MSCs, they have the ability to differentiate into osteogenic direction. In the following paragraph, the N-glycosylation profile of undifferentiated and day 5 as well as day 28 osteogenically differentiated MSCs will be presented and compared. Early and late time stage osteogenically differentiated MSCs were isolated from their extracellular matrix in order to obtain the N-glycosylation profile of the pure cells. The procedure for N-glycan isolation and analysis was analogous to the one used for the chondrogenic differentiated MSCs. Briefly, MSCs and early time stage (day 5) as well as late time stage (day 28) osteogenically differentiated cells were harvested and washed three times with PBS. Cell surface (glyco)proteins were digested with trypsin yielding to glycopeptides that were subjected to PNGase F-digestion. Released N-glycans were purified, desalted and derivatised. 60 % of the N-glycan pool was permethylated and measured by means of MALDI-TOF-MS. The rest of the N-glycan pool was labeled with the fluorophore APTS in order to detect the N-glycans by laser induced fluorescence detection through capillary electrophoresis (CE-LIF). A representative mass spectrum of the resulting N-glycosylation profile of human undifferentiated and day 28 osteogenically differentiated MSCs is shown in Fig. 2.24 A and B. More than 100 different N-glycan signals were detected with MALDI-TOF-MS (Table 5, see appendix). The mean relative abundances of the 35 most abundant N-glycan signals calculated from three different biological replicates are presented in Fig. 2.25 A and B. Some samples were contaminated with N-glycans from cell culture medium, which were marked with a loop (Fig. 2.24) and excluded from the quantification presented in Fig. 2.25. The N-glycan profiles of the different MSCs and osteogenically differentiated cells analysed were highly similar, as can be determined from the small deviations within the observed glycan profiles. High-mannose N-glycans comprised about 16 % of the N-glycan pool of MSCs. The

overall amount of high-mannose N-glycans decreased in day 5 as well as day 28 of osteogenic differentiation by about 7 % and 5 %, respectively. In addition, the high-mannose structures H7N2 (m/z 1987.9) and H8N2 (m/z 2192.0) were significantly decreased in day 28 of osteogenically differentiated MSCs.

Moreover the amount of hybrid-type N-glycans remained almost the same (about 5 %). Neutral, sialylated as well as fucosylated hybrid N-glycans were detected in undifferentiated and day 5 and day 28 osteogenically differentiated MSCs.

Complex N-glycans comprised the major amount of the N-glycan pool of undifferentiated and day 5 as well as day 28 of osteogenically differentiated MSCs. The overall amount in MSCs was about 58 %, increased by 14 % in day 5 of osteogenic differentiation and decreased again by 5 % at day 28 of osteogenic differentiation.

Evaluation of antennarity. Biantennary complex N-glycans comprised about 7 % of the N-glycan pool of MSCs and no significant change was observed during osteogenic differentiation. In contrast, the amount of biantennary fucosylated structures increased dramatically from 30 % in MSCs to 44 % in day 5 and 49 % in day 28 of osteogenically differentiated MSCs. In addition, the structures H4N4F1 (m/z 2040.0), H5N4F1 (m/z 2244.1) and S1H5N4F1 (m/z 2605.3) were significantly increase after day 28 of osteogenic differentiation of MSCs. In contrast, the amount of larger complex-type N-glycans decreased during osteogenic differentiation of MSCs. The overall amount of triantennary fucosylated N-glycans decreased by 3 % in day 28 of osteogenically differentiated cells and the structures H6N5F1 (m/z 2693.3), S1H6N5 (m/z 2880.4), S1H6N5F1 (m/z 3054.5), S2H6N5F1 (m/z 3415.7) as well as S3H6N5F1 (m/z 3776.8) showed statistically significant decreases. The amount of tetraantennary fucosylated N-glycans decreased from 7 % in MSCs to 1 % in day 28 of osteogenically differentiated cells and the most abundant structures H7N6F1 (m/z 3142.5), S1H7N6F1 (m/z 3503.7), S2H7N6F1 (m/z 3864.9), S3H7N6F1 (m/z 4226.1) and S4H7N6F1 (m/z 4587.1) were significantly decreased after osteogenic differentiation. N-glycans with more than four antennae such as H7N8F1 (m/z 3632.8) and S1H8N7F2 (m/z 4128.0) were also present but comprised just a minor amount in undifferentiated and osteogenically differentiated MSCs (about 2 %). Consequently, the antennarity decreased after osteogenic differentiation of MSCs; the amount of biantennary N-glycans increased and the amount of tri- and tetraantennary decreased.

Evaluation of sialylation. The amount of sialylated structures was almost equal in undifferentiated MSCs and day 28 osteogenically differentiated cells and comprised about 35 % of the N-glycan pool. The most abundant sialylated structures were monosialylated but fully sialylated N-glycans were detected as well.

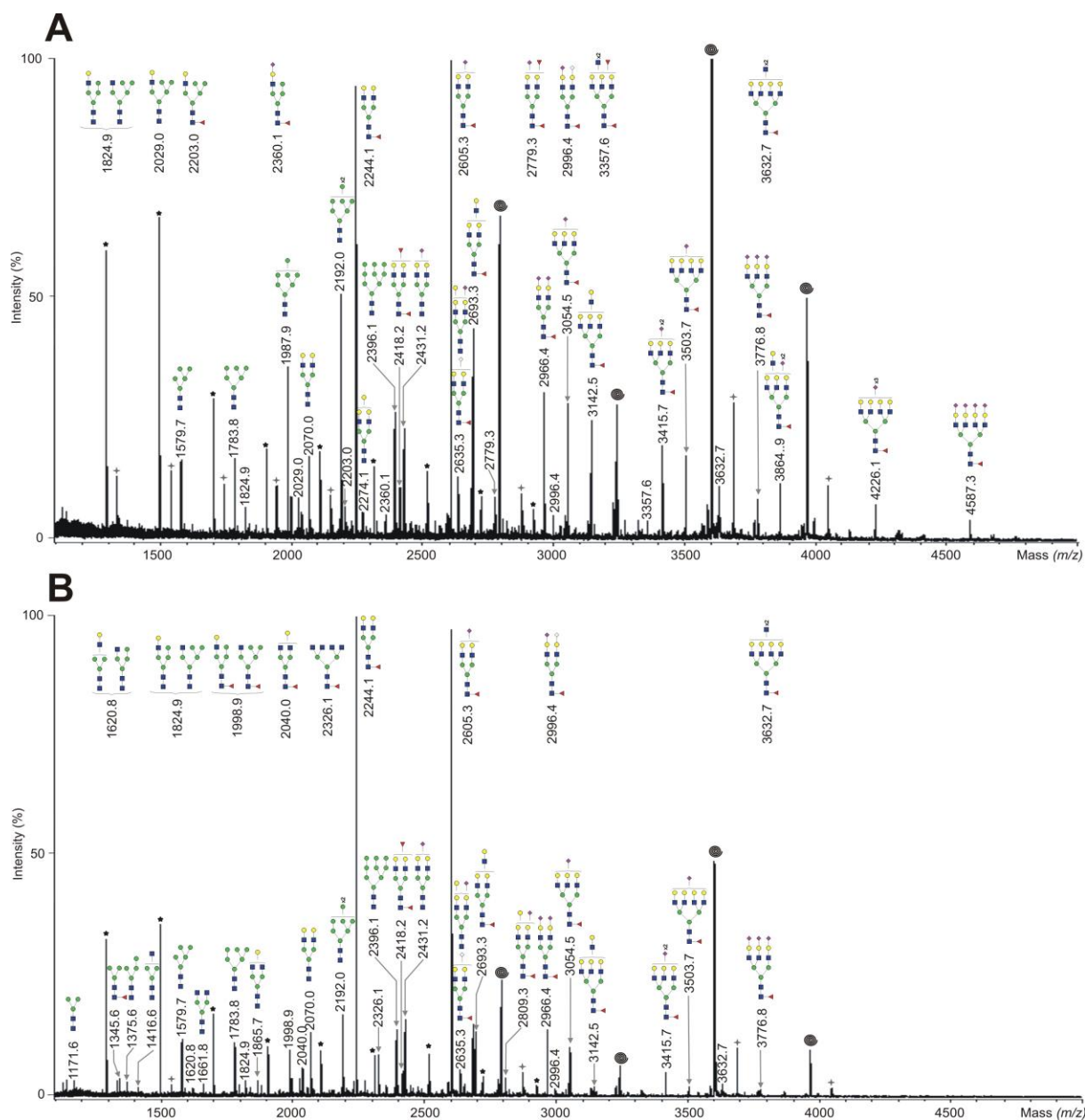


FIG. 2.24. MALDI-TOF-MS of PNGase F-released N-glycans of undifferentiated and osteogenically differentiated MSCs. Day 28 osteogenically differentiated MSCs were isolated from their ECM prior to N-glycan analysis. Cell surface glycoproteins were directly digested from the cells with trypsin. N-glycans were enzymatically cleaved from glycopeptides with PNGase F, permethylated and measured by MALDI-TOF-MS. A representative mass spectrum of PNGase F-released N-glycans of undifferentiated (**A**) and osteogenically differentiated human MSCs (**B**) is shown together with the 35 most abundant structures. Blue square represents N-acetylglucosamine, green circle mannose, yellow circle galactose, red triangle fucose and pink diamond N-acetylneuraminic acid. * Polyhexose contaminations are negligible. ✦ Non identified peaks. ● Cell culture contaminations.

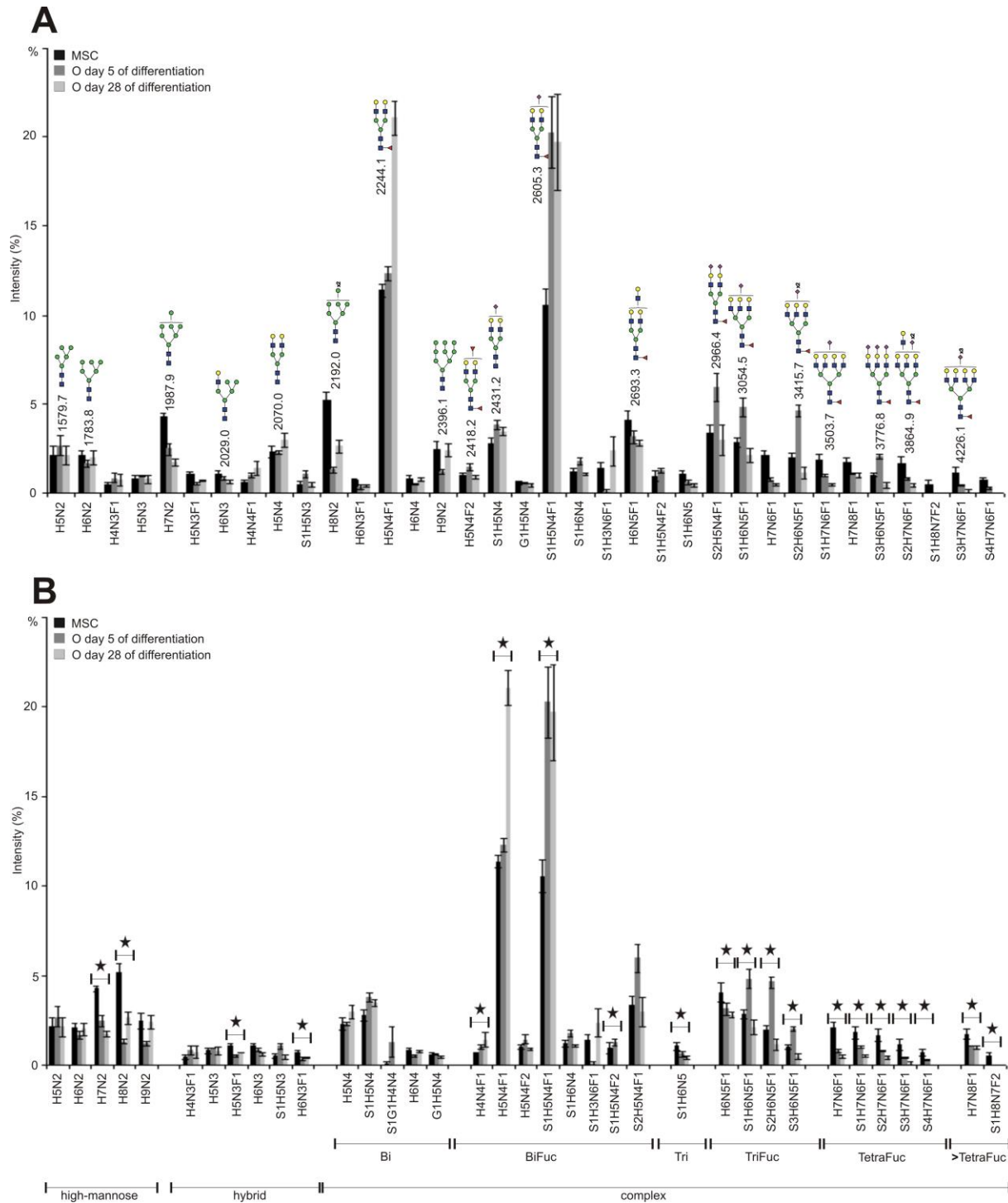


FIG. 2.25. Quantification of PNGase F-released N-glycans with MALDI-TOF-MS. **(A)** The average relative amounts of the 35 most abundant PNGase F-released N-glycans of undifferentiated human MSCs (black) and osteogenically differentiated MSCs (O) at day 5 (dark grey) and day 28 (light grey) derived from three different preparations (n=3), **(B)** grouped according to their N-glycan type, antennarity and fucosylation. Day 5 and 28 osteogenically differentiated MSCs were isolated from their ECM prior to N-glycan analysis. Statistical significant difference between the two sample groups undifferentiated MSCs and 28 days osteogenically differentiated MSCs was assessed using Mann-Whitney U test ($*p \leq 0.05$) and is marked with a star in **(B)**. Blue square represents N-

acetylglucosamine, green circle mannose, yellow circle galactose, red triangle fucose and pink diamond N-acetylneuraminic acid. H: hexose, N: N-acetylhexosamine, F: deoxyhexose, S: N-acetylneuraminic acid.

Evaluation of fucosylation. The most abundant fucosylated structures were monofucosylated at the reducing GlcNAc of the core structure (see 2.2.3.3). Some N-glycans bore two Fuc residues, namely H5N4F2 (m/z 2418.2), S1H5N4F2 (m/z 2779.3) and S1H8N7F2 (m/z 4128.0). Overall fucosylation increased from 53 % in MSCs to 61 % in day 28 of osteogenically differentiated cells. This was mainly affected by the significant increase of fucosylated biantennary N-glycans.

2.2.3.2 CE-LIF analysis of N-glycans from undifferentiated and osteogenically differentiated human bone marrow mesenchymal stem cells

About 40 % of the N-glycan pool was analysed by means of CE-LIF, in order to confirm the structures found by MALDI-TOF-MS.

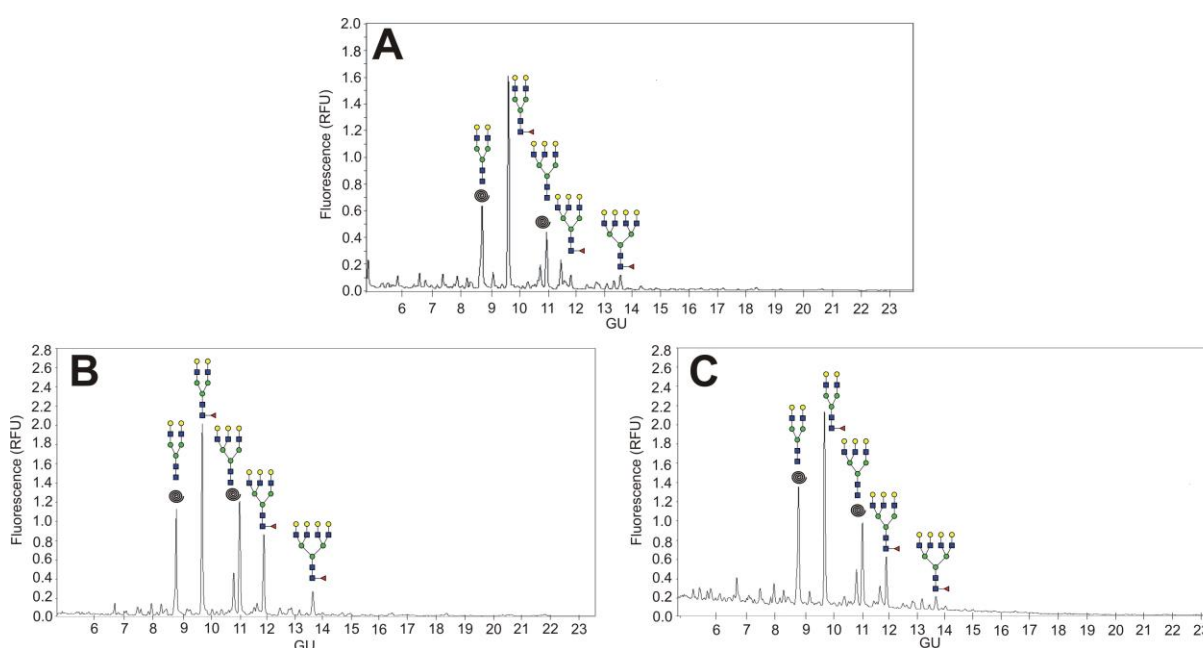


FIG. 2.26. CE-LIF electropherograms of PNGase F-released and desialylated N-glycans from undifferentiated (A), day 5 (B) as well as day 28 (C) osteogenically differentiated human MSCs without ECM. Cells were digested with trypsin in order to release cell surface (glyco)peptides. (Glyco)peptides were subjected to PNGase F digestion to release N-glycans, desialylated and measured by CE-LIF. Blue square represents N-acetylglucosamine, yellow square N-acetylgalactosamine, white square N-acetylhexosamine, green circle mannose, yellow circle galactose, red triangle fucose, white diamond N-glycolylneuraminic acid and pink diamond N-acetylneuraminic acid. ● Cell culture contaminations.

Representative electropherograms of PNGase F-released N-glycans of undifferentiated and day 5 as well as day 28 osteogenically differentiated MSCs without ECM are presented in Fig.2.26 A, B and C.

N-glycans were assigned with the help of a standard table generated in our laboratory using N-glycans release from reference glycoproteins. In addition, MALDI-TOF-MS spectra of the desialylated N-glycan pools were used to assign the structures. The overall distribution of the N-glycans was very similar to the one found in the MALDI-TOF mass spectra. The main structures were assigned to the electropherogram signals. In undifferentiated MSCs (Fig.2.26 A) the biantennary structures H5N4 (8.9 GU) and H5N4F1 (9.8 GU) comprised together the main part of the N-glycosylation profile, followed by the triantennary N-glycan H6N5F1 (12.0 GU) and tetraantennary fucosylated structure H7N6F1 (13.8 GU). The relative amount of the tri- and tetraantennary structures decreased in day 28 of osteogenically differentiated cells when compared with day 5 of osteogenic differentiation (Fig.2.26 B and C). The same distribution of the main structures was obtained from MALDI-TOF-MS data, which consequently was confirmed by the CE-LIF electropherograms.

2.2.3.3 Verification of identified N-glycan structures from undifferentiated and osteogenically differentiated mesenchymal stem cells with MALDI-TOF/TOF sequencing and exoglycosidase digestions

Verification of the most abundant N-glycan structures was done using MALDI-TOF/TOF-MS fragmentation that was performed in the positive-ion mode. A representative MALDI-TOF/TOF mass spectrum is presented in Fig. 2.27 A and B for the N-glycan signal m/z 2693.3 of the composition H6N5F1 derived from human MSCs and of m/z 2244.1 of the composition H5N4F1 derived from day 28 of osteogenically differentiated MSCs. The diagnostic fragment ions N1F1 at m/z 474.0, N2F1 at m/z 701.2 and/ or N2F1 at m/z 719.2 revealed core-fucosylation for instance in the N-glycans H5N3F1 (m/z 1999.0), H4N4F1 (m/z 2040.0), H5N4F1 (m/z 2244.1), H3N6F1 (m/z 2326.1), S1H5N4F1 (m/z 2605.3), H6N5F1 (m/z 2693.3), S2H5N4F1 (m/z 2966.4), S1H6N5F1 (m/z 3054.5), S2H6N5F1 (m/z 3415.7), S1H7N6F1 (m/z 3503.7) and S3H6N5F1 (m/z 3776.8) in undifferentiated and chondrogenically differentiated MSCs. The diagnostic fragment ions S1H1N1 at m/z 847.2 and/ or S1H2N1 at m/z 620.1 confirmed the presence of a sialylated antenna in S1H5N4 (m/z 2431.2), S1H5N4F1 (m/z 2605.3), S1H6N4 (m/z 2635.3), S1H6N4F1 (m/z 2809.3), S2H5N4F1 (m/z 2966.4), S1H6N5F1 (m/z 3054.5), S2H6N5F1 (m/z 3415.7), S1H7N6F1 (m/z 3503.7) and S3H6N5F1 (m/z 3776.8).

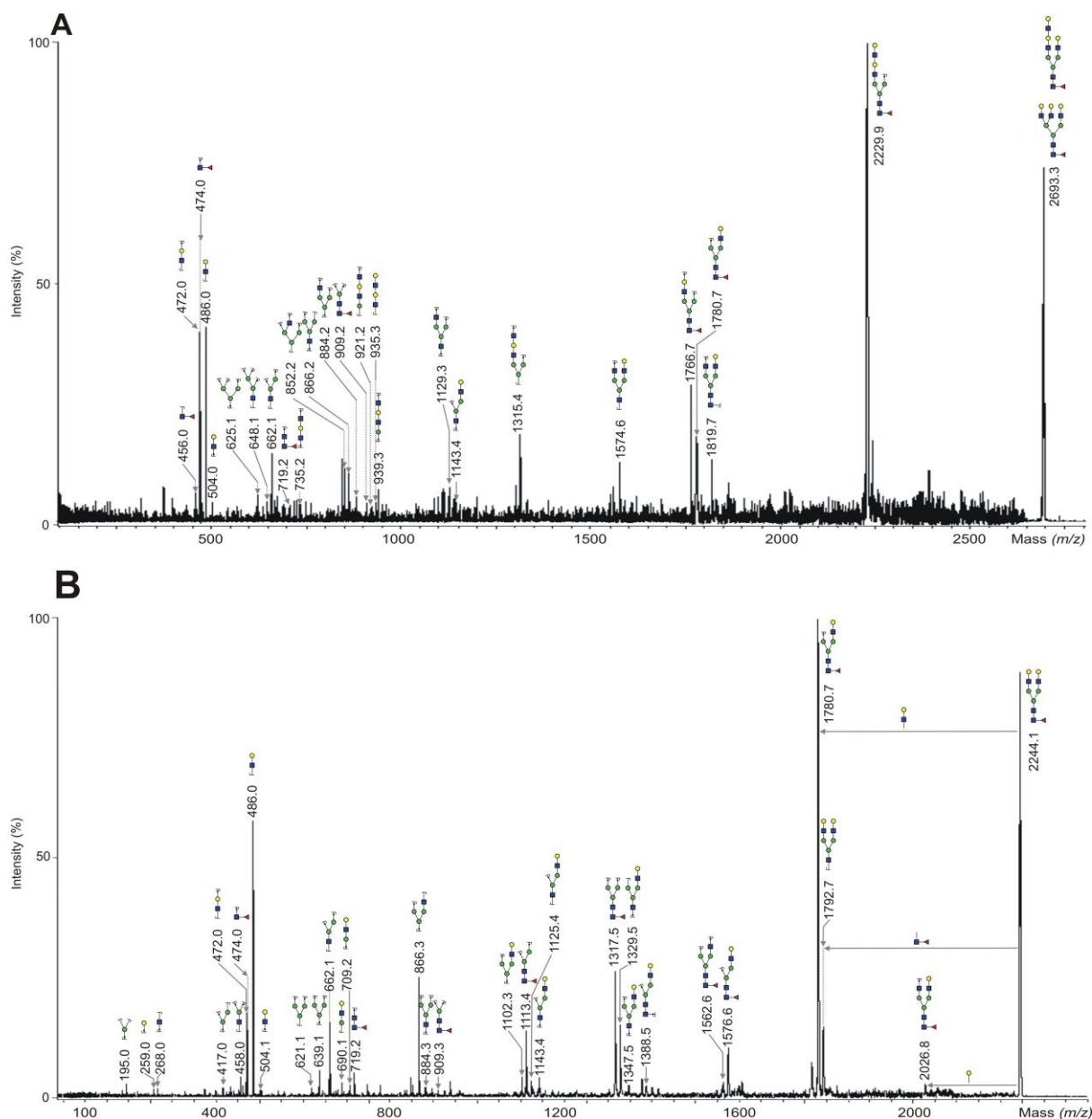


FIG. 2.27. MALDI-TOF/TOF mass spectrum of m/z 2693.3 of the composition H6N5F1 derived from human MSCs (**A**) and of m/z 2244.1 of the composition H5N4F1 derived from day 28 osteogenically differentiated MSCs (**B**). Blue square represents N-acetylglucosamine, green circle mannose, yellow circle galactose, red triangle fucose and pink diamond N-acetylneuraminic acid.

The two bifucosylated structures H5N4F2 (m/z 2418.2) and S1H5N4F2 (m/z 2779.3) contained one Fuc that is linked to the reducing GlcNAc of the core and one Fuc residue that is linked to a GlcNAc residue of one of the antenna. The diagnostic fragment ions N1F1 at m/z 474.0, N2F1 at m/z 701.2 and/ or N2F1 at m/z 719.2 revealed the core-linked Fuc and the diagnostic fragment ion H1N1F1 at m/z 660.1 the antennary-linked Fuc. Most probably, the two bifucosylated structures contain the Lewis^X epitope.

According to mass calculation the N-glycan signals G1H4N4 (m/z 2258.1), G1H5N4 (m/z 2461.2), S1G1H5N4 (m/z 2822.4) and S1G1H5N4F1 (m/z 2996.4) contain a Neu5Gc residue, which could not be verified by the MALDI-TOF/TOF fragmentation due to the low signal intensities of the peaks. However, the signal m/z 2635.3 was found to correspond to two different isomers, namely S1H6N4 and G1H5N4F1. Beside the Neu5Gc-containing N-glycan, which was verified by the diagnostic ion fragment N1H1G1 (m/z 877.2), the second structure contains an antenna with two Gal units that are connected to each other in linear fashion and a sialylated antenna, which was supported by the diagnostic ion fragment H2 m/z 463.0 and N1H1S1 m/z 847.2. Neu5Gc signals, such as G1H5N4 at m/z 2461.2 were also observed in previous studies (127, 151) in MSCs, but these glycans were only found as traces. The Neu5Gc contamination is most likely stemming from cell culture media that contain animal-derived components (144, 152).

The signals m/z 1824.9 and m/z 1999.0 may present two different hybrid N-glycan structures, either one with a galactosylated antenna or a non-galactosylated one. MALDI-TOF/TOF fragmentation revealed that they present two isomeric structures in day 28 of osteogenically differentiated MSCs, which was supported by the diagnostic fragment ions H1N1 at m/z 471.0. H2N1 and/ or m/z 708.2 in case of the galactosylated N-glycan and by H3 at m/z 648.1 and/ or H2N2 at m/z 938.2 in case of the non-galactosylated structure. In contrast, the structure H6N3 (m/z 2029.0) was identified as galactosylated hybrid-type N-glycan and this was verified by the fragment ions H1N1 at m/z 471.0 and m/z 708.2 as well as H3 at m/z 667.1.

The LacNAc motif was found in the structures H6N5F1 (m/z 2693.3), S1H6N5 (m/z 2880.4) and H7N6F1 (m/z 3142.5) in undifferentiated MSCs as well as in day 28 of osteogenically differentiated MSCs. The presence of poly-LacNAc in these structures was verified by the diagnostic fragment ion H2N2 at m/z 935.2.

2.2.3.4 N-glycosylation profile of osteogenically differentiated MSCs with their extracellular matrix (ECM)

The results obtained from chondrogenic differentiation of MSCs revealed that the ECM, which is secreted by the chondrogenically differentiated cells and typically found in connective tissues such as fibroblasts, bone, tendon and cartilage, seems to influence the N-glycosylation pattern of these cells. The N-glycosylation pattern of chondrogenically differentiated MSCs isolated from their ECM was significantly different from the one obtained from the same cells inclusively their ECM. Thus, the N-glycosylation pattern of day 5 osteogenically differentiated cells without ECM was investigated, presented in the previous section, and compared with the profile obtained from the same cells inclusively their ECM. A

representative mass spectrum of the resulting N-glycosylation profile of day 5 osteogenically differentiated MSCs with and without ECM is shown in Fig. 2.28 A and B. More than 100 different N-glycan signals were detected with MALDI-TOF-MS in day 5 osteogenically differentiated MSCs. The MALDI-TOF mass spectra showed some little quantitative differences in the N-glycosylation profile of day 5 osteogenically differentiated MSCs with and without ECM. The relative abundances of the 32 most abundant N-glycans derived from three different biological replicates are presented in Fig. 2.29 A and B. Some samples were contaminated with N-glycans from cell culture medium, which were marked with a loop (Fig. 2.28) and excluded from the quantification shown in Fig. 2.29. The main differences obtained from this data were that day 5 osteogenically differentiated MSCs with ECM contained less triantennary fucosylated N-glycans (about 4 %) and more biantennary fucosylated as well as tetraantennary fucosylated structures (3 % and 1 %, respectively) when compared with day 5 osteogenically differentiated cells without ECM. The overall amount of complex-type N-glycans as well as the amount of fucosylated structures was the same in day 5 osteogenically differentiated cells with and without ECM.

Sialylation was about 10 % lower in day 5 osteogenically differentiated MSCs with ECM. Based on these results the ECM seems to influence the N-glycosylation pattern of osteogenically differentiated cells mainly with respect to the sialylation. Antennarity and fucosylation stayed constant in day 5 osteogenically differentiated cells with and without ECM.

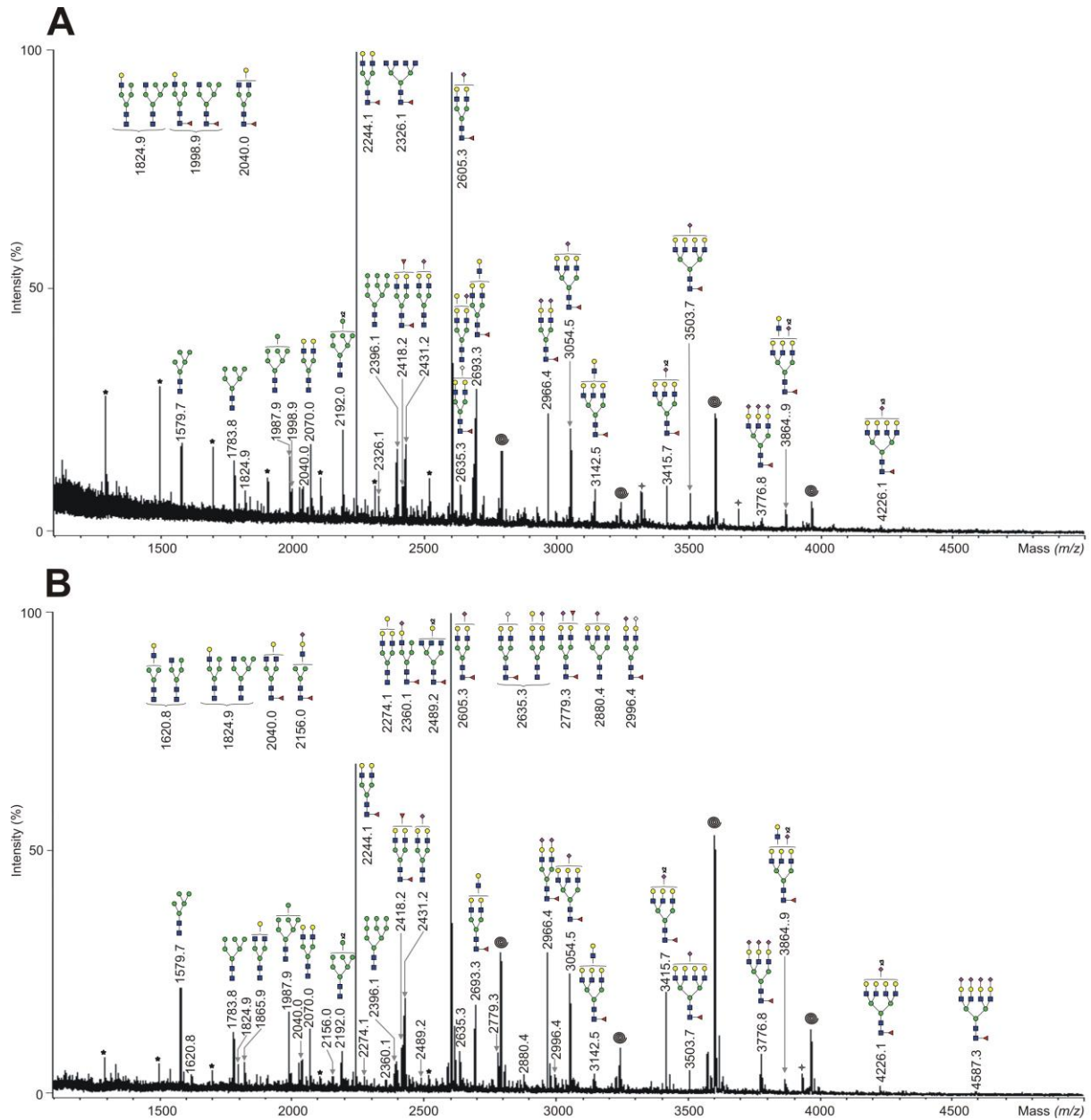


FIG. 2.28. MALDI-TOF-MS of PNGase F-released N-glycans of day 5 osteogenically differentiated MSCs. A representative mass spectrum of PNGase F-released N-glycans of day 5 osteogenically differentiated MSCs with ECM (**A**) and day 5 osteogenically differentiated MSCs without ECM (**B**) is shown together with the 40 most abundant structures. Cell surface glycoproteins were directly digested from the cells with trypsin. N-glycans were enzymatically cleaved from glycopeptides with PNGase F, permethylated and measured by MALDI-TOF-MS. Blue square represents N-acetylglucosamine, green circle mannose, yellow circle galactose, red triangle fucose and pink diamond N-acetylneuraminic acid. * Polyhexose contaminations are negligible. † Non identified peaks. ● Cell culture contaminations.

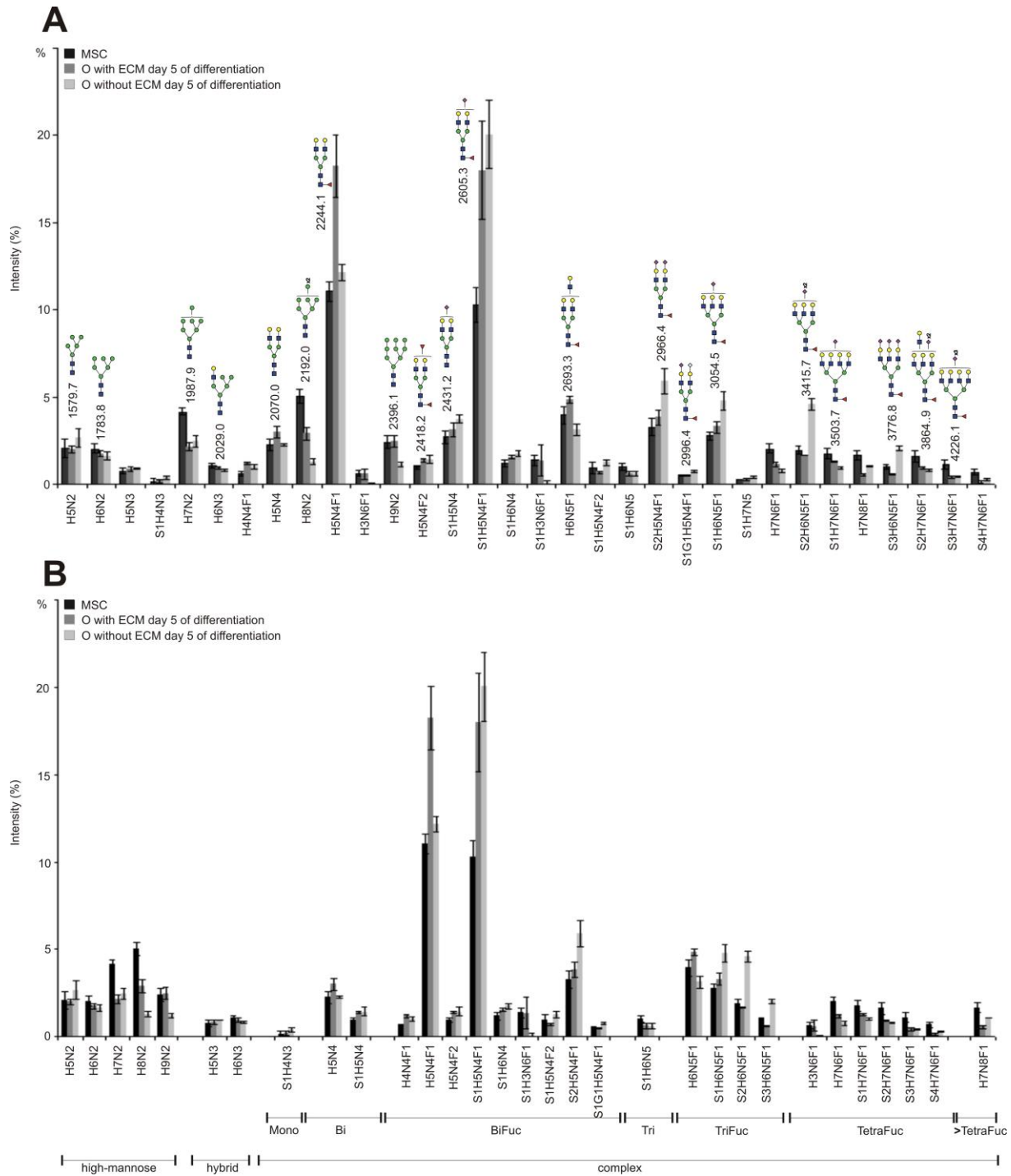


FIG. 2.29. Quantification of PNGase F-released N-glycans with MALDI-TOF-MS. **(A)** The average relative amounts of the 40 most abundant PNGase F-released N-glycans of undifferentiated human MSCs (black) and of day 5 osteogenically differentiated MSCs (O) with ECM (dark grey) and without ECM (light grey) derived from four (MSCs, n=4) and three (osteogenically differentiated MSCs, n=3) different preparations, **(B)** grouped according to their N-glycan type, antennarity and fucosylation. Blue square represents N-acetylglucosamine, green circle mannose, yellow circle galactose, red triangle fucose and pink diamond N-acetylneuraminic acid. H: hexose, N: N-acetylhexosamine, F: deoxyhexose, S: N-acetylneuraminic acid.

2.2.4 Glycan-based biomarkers of adipogenically, chondrogenically and osteogenically differentiated mesenchymal stem cells

PNGase F-released N-glycans of MSCs and their adipogenic, chondrogenic and osteogenic counterparts were characterised with MALDI-TOF-MS and CE-LIF and the relative abundance of each detected N-glycan signal was further quantified using MALDI-TOF-MS. The relative intensity for each detected glycan signal has been calculated and represents the percentage of total glycan profile, which has been given a value of 100 %. We and others have found that the percentages determined in this way are suitable for relative quantification of single glycan structures and thus comparison of changes in glycan profiles especially between closely related samples that are treated similarly (153-156). In addition, mean relative abundances were calculated from three different biological replicates. Statistical significant differences in relative abundance of N-glycans between the sample groups undifferentiated MSCs and day 15 adipogenically, day 28 chondrogenically or day 28 osteogenically differentiated cells were assessed using Mann-Whitney U test (* $p \leq 0.05$).

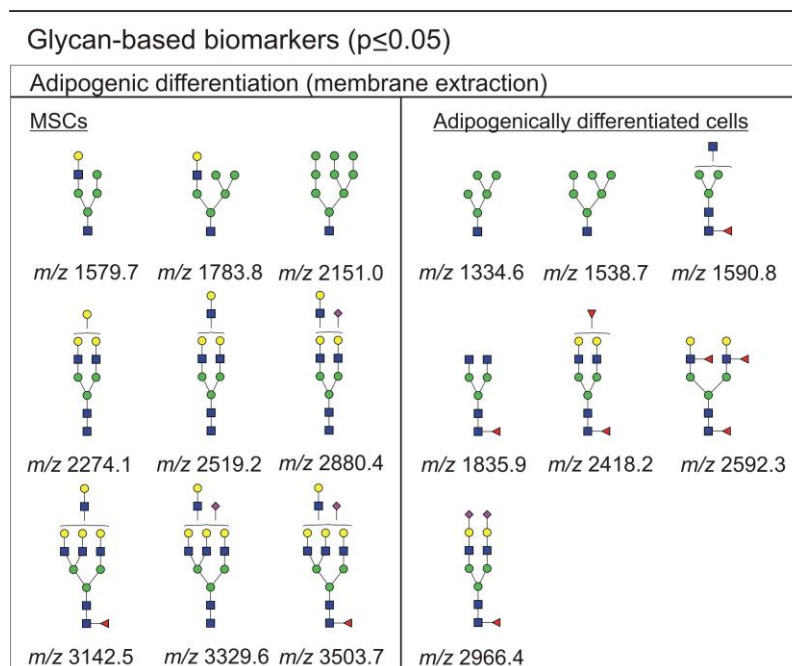


FIG. 2.30A Glycan-based biomarkers of undifferentiated and day 15 adipogenically differentiated MSCs. Statistical significance between the two sample groups undifferentiated MSCs and 15 days adipogenically differentiated MSCs was assessed using Mann-Whitney U test (* $p \leq 0.05$). Based on the test, the listed N-glycans were significantly overexpressed.

The N-glycans, which were significantly increased in undifferentiated MSCs and day 15 adipogenically differentiated cells are depicted in Fig.2.30A. In MSCs potential glycan-based biomarkers were mainly of complex-type and contained three to four antennae (m/z 2519.2,

2880.4, 3142.5, 3329.6 and 3503.7). In addition, two hybrid N-glycans and the high-mannose structure Man9 were statistically significant in MSCs (m/z 1579.7, 1783.8 and 2151.0, respectively). In contrast, glycan-based complex-type biomarkers of day 15 adipogenically differentiated cells possess maximum two antennae and at least one Fuc (m/z 1590.8, 1835.9, 2418.2, 2592.3 and 2966.4). Two were of high-mannose type (m/z 1334.6 Man5 and 1538.7 Man6).

Potential glycan-based biomarkers of undifferentiated and day 28 chondrogenically differentiated cells without their ECM are presented in Fig.30B. Complex-type N-glycan structures that were significantly increased in MSCs possess three to four antennae and were all core-fucosylated (m/z 2693.3, 3054.5, 3142.5, 3503.7 and 3864.9). One statistically significant structure was of the high-mannose N-glycan Man7 (m/z 1987.9). In contrast, significantly increased N-glycans of day 28 chondrogenically differentiated cells have one to two antennae (m/z 2156.0, 2779.3 and 2966.4), however, one triantennary and trisialylated structure m/z 3776.8 was determined as potential glycan-based biomarker as well. Significantly increased complex-type N-glycans of MSCs when compared to day 28 chondrogenically differentiated cells without ECM were also statistically significant when compared to day 28 chondrogenically differentiated cells with ECM (Fig. 2.30B). Glycan-based biomarkers determined for undifferentiated MSCs when compared to the sample group day 28 chondrogenically differentiated cells with ECM were all of complex-type, bi-, tri or tetraantennary and core-fucosylated (Fig. 2.30B). Most of them were sialylated and all of them were fully galactosylated structures.

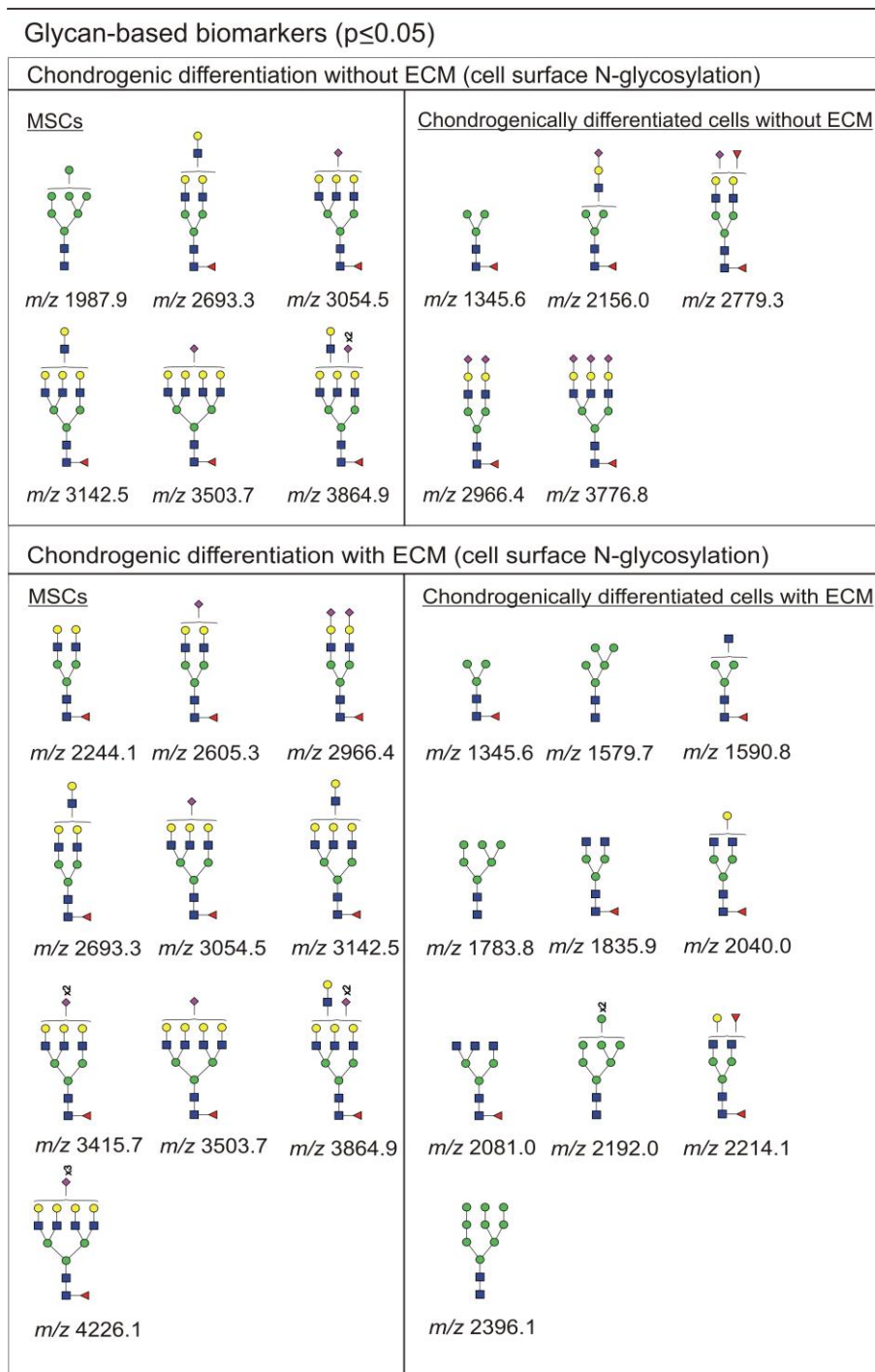


FIG. 2.30B Glycan-based biomarkers of undifferentiated and day 28 chondrogenically differentiated MSCs without and with their ECM. Statistical significance between the two sample groups undifferentiated MSCs and 28 days chondrogenically differentiated MSCs was assessed using Mann-Whitney U test ($*p \leq 0.05$). Based on the test, the listed N-glycans were significantly overexpressed.

In comparison, glycan-based biomarkers determined for day 28 chondrogenically differentiated cells with ECM possess just zero, one or two antennae and at least one Fuc that is attached to the reducing GlcNAc of the core (*m/z* 1345.6, 1590.8, 1835.9, 2040.0, 2081.0 and 2214.1). Four of the complex-type structures were agalactosylated and two of

them were partially galactosylated. In addition, the high-mannose structures Man5 (m/z 1579.7), Man6 (m/z 1783.8), Man8 (m/z 2192.0) and Man9 (m/z 2396.1) were significantly increased in day 28 chondrogenically differentiated cells with ECM.

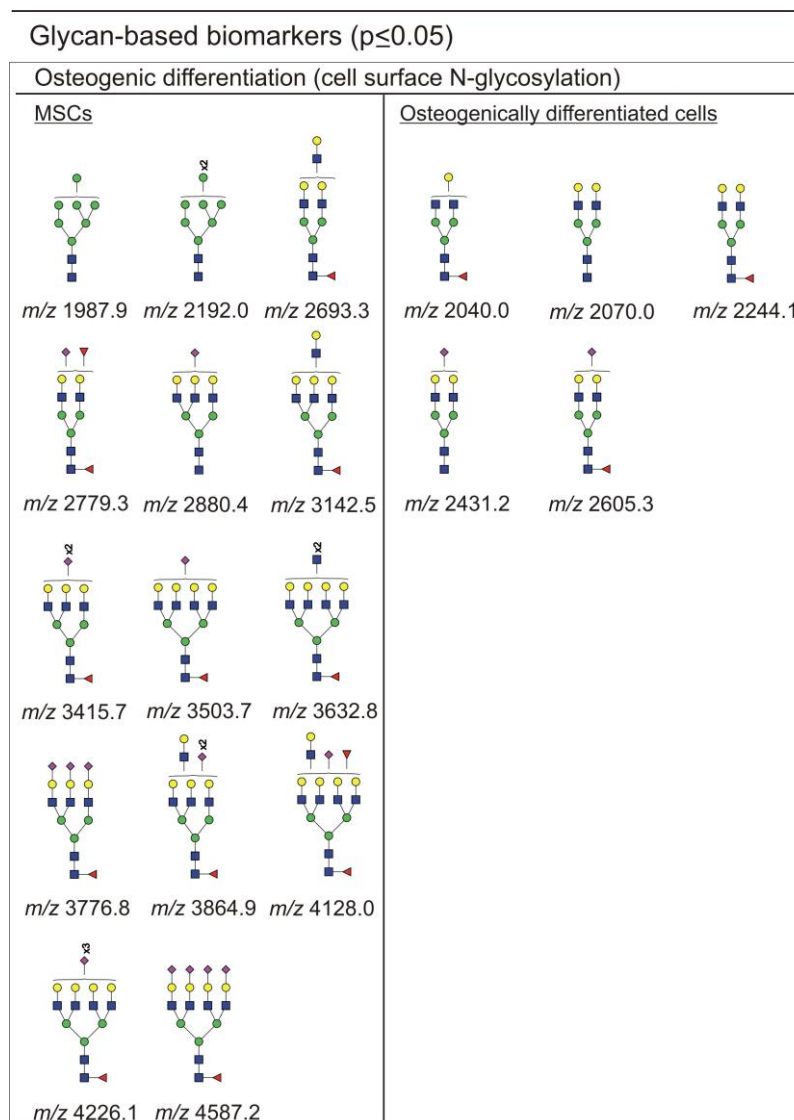


FIG. 2.30C Glycan-based biomarkers of undifferentiated and day 28 osteogenically differentiated MSCs. Statistical significant difference between the two sample groups undifferentiated MSCs and 28 days osteogenically differentiated MSCs was assessed using Mann-Whitney U test ($*p \leq 0.05$). Based on the test, the listed N-glycans were significantly overexpressed.

Glycan-based biomarkers that were determined for MSCs when compared to day 28 osteogenically differentiated cells contained three to five antennae and were fucosylated and/or sialylated (Fig. 2.30C). In addition, the two high-mannose N-glycans Man7 (m/z 1987.9) and Man8 (m/z 2192.0) were statistically significant in undifferentiated MSCs. N-glycans that were significantly increased in day 28 osteogenically differentiated cells without ECM were

exclusively complex-type, biantennary and galactosylated (m/z 2040.0, 2070.0, 2244.1, 2431.2 and 2605.3). Some of them contained a core-fucose and were sialylated.

In conclusion, N-glycan structures that were determined as glycan-based biomarkers for undifferentiated MSCs were mainly complex-type structures with three to five antennae. This was not the case when MSCs were differentiated into adipogenic, chondrogenic or osteogenic cells, in which statistically significant complex-type structures bore mostly just one or two antennae.

2.3 N-Glycosylation profile of mesenchymal stem cells depends on the passage number

As already mentioned in the introduction, the cell surface of SCs is covered with a dense layer, which is composed of complex glycans and they are the main components of the glycocalyx (60, 108). Different cell types express different glycan signatures making the carbohydrate structures, which are embedded in the glycocalyx, characteristic markers for a particular cell type. In this paragraph the stability of the cell surface N-glycosylation pattern of MSCs with regard to the passage number will be presented. The N-glycosylation profile presented in the previous sections was obtained from MSCs of the passage three, which will be compared with passage eight MSCs. A representative MALDI-TOF mass spectrum of MSCs of passage three and eight are presented in Fig.2.31 A and B, respectively. More than 90 different N-glycan signals were detected with MALDI-TOF-MS in undifferentiated MSCs of the passage three and eight. Based on the mass spectra it can be concluded that the N-glycosylation profiles were qualitatively very similar but some quantitative differences in the high-mannose and complex N-glycans existed. The relative abundances of the 50 most abundant N-glycans derived from four (passage three) and three (passage eight) different biological replicates are presented in Fig. 2.32. The high-mannose N-glycans H5N2 (m/z 1579.7), H8N2 (m/z 2192.0) and H9N2 (m/z 2396.1) were together increased by 6 % in passage eight MSCs. The complex-type N-glycans H5N4 (m/z 2070.0), H5N4F2 (m/z 2418.2) and S1H5N4 (m/z 2431.2) were increased in passage eight MSCs by about 7 %. In contrast, the complex-type N-glycans H5N4F1 (m/z 2244.1), S1H5N4F1 (m/z 2605.3), S2H5N4F1 (m/z 2966.4), S1H6N5F1 (m/z 3054.5), S2H6N5F1 (m/z 3415.7) and S1H7N6F1 (m/z 3503.7) were dramatically decreased in passage 8 MSCs by about 42 %. These results show that the passage number influenced the N-glycosylation profile of MSCs dramatically.

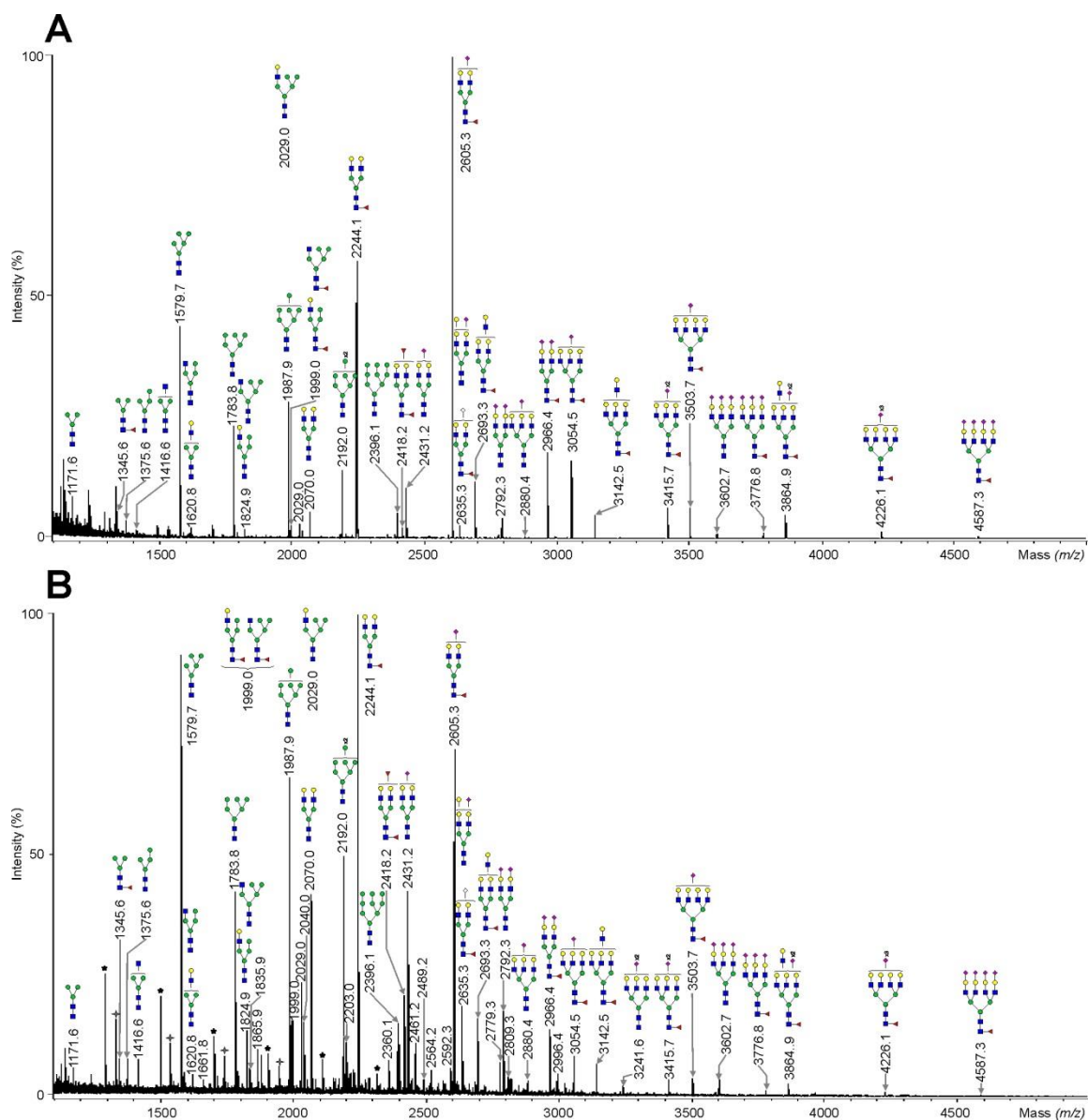


FIG. 2.31. MALDI-TOF-MS of PNGase F-released N-glycans of undifferentiated MSCs at different passages. A representative mass spectrum of undifferentiated MSCs at passage 3 (**A**) and passage 8 (**B**) is shown together with the 40 most abundant structures. Cell surface glycoproteins were directly digested from the cells with trypsin. N-glycans were enzymatically cleaved from glycopeptides with PNGase F, permethylated and measured by MALDI-TOF-MS. Blue square represents N-acetylglucosamine, green circle mannose, yellow circle galactose, red triangle fucose and pink diamond N-acetylneuraminic acid. * Polyhexose contaminations are negligible. † Non identified peaks.

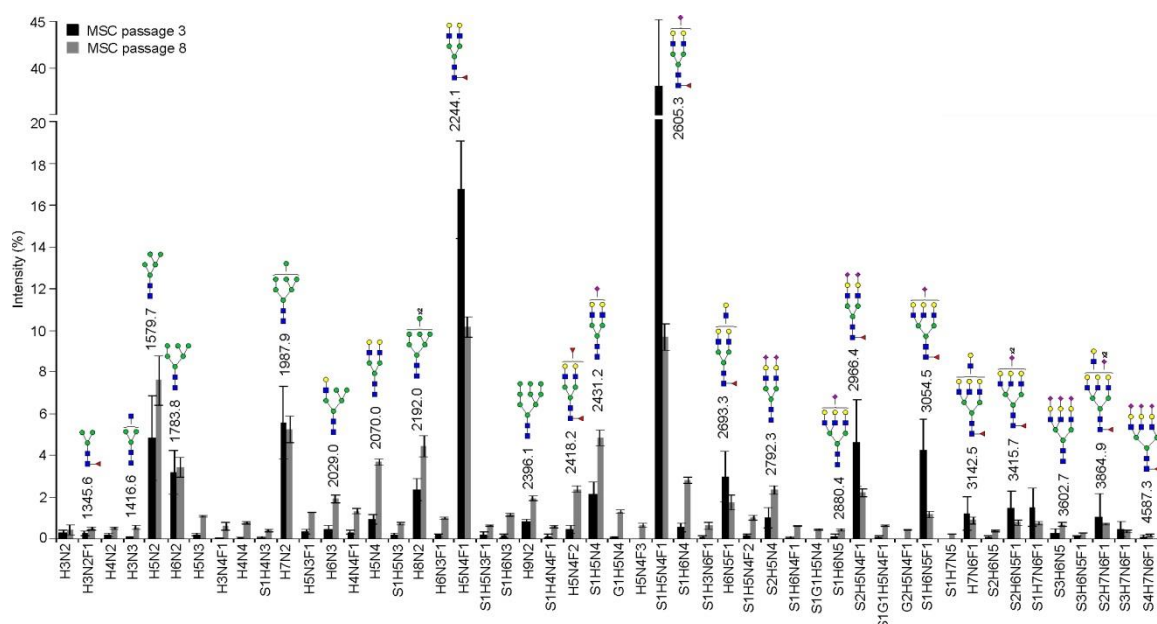


FIG. 2.32. Quantification of PNGase F-released N-glycans of MSCs with MALDI-TOF-MS. The average relative amounts of the 50 most abundant PNGase F-released N-glycans of undifferentiated human MSCs at passage 3 (black) and passage 8 (dark grey) derived from four (passage 3, n=4) and three (passage 8, n=3) different preparations. Blue square represents N-acetylglucosamine, green circle mannose, yellow circle galactose, red triangle fucose and pink diamond N-acetylneuraminic acid. H: hexose, N: N-acetylhexosamine, F: deoxyhexose, S: N-acetylneuraminic acid.

2.4 N-Glycosylation profile of chondrogenic dedifferentiated cells

The primary source of MSCs is bone marrow, but adipose tissue, synovium, periosteum, amniotic fluid, placenta and umbilical cord blood also contain MSCs and can therefore be used as alternative cell sources (157). Another possibility to obtain MSCs is the process of dedifferentiation, which describes a return of differentiated cells to an earlier stage with an extended differentiation potential. Studies by Woodbury et al. and Li et al. described the ability of MSC-derived neurons to revert back to MSC morphology (158, 159). But it was unknown whether these dedifferentiated MSCs were similar to MSCs. The process of dedifferentiation is an alternative way to assess SCs in a more simple and rapid way and is of great interest in the field of regenerative SC therapy. The glycosylation status of the cell can be used to determine its differentiation state. In the following section the N-glycosylation profile of undifferentiated MSCs will be compared to the one of chondrogenically dedifferentiated as well as chondrogenically differentiated cells to determine similarities or differences. A representative MALDI-TOF mass spectrum of undifferentiated MSCs and chondrogenically dedifferentiated cells are presented in Fig.2.33 A and B, respectively. More than 100 different N-glycan signals were detected with MALDI-TOF-MS in undifferentiated MSCs and chondrogenically dedifferentiated cells. The relative abundances of the 40 most

abundant N-glycans derived from four (undifferentiated MSCs and chondrogenically dedifferentiated cells) and three (chondrogenically differentiated MSCs) biological replicates are presented in Fig.2.34. Dedifferentiation of chondrogenically differentiated cells theoretically gives rise to MSCs with a similar N-glycosylation profile as found for undifferentiated MSCs. In fact, the N-glycosylation profiles of undifferentiated MSCs and chondrogenically dedifferentiated cells exhibited many similarities but differences were detected as well. Complex-type and high-mannose structures that were very similar in quantities were H5N2 (*m/z* 1579.7), H6N2 (*m/z* 1783.8), H7N2 (*m/z* 1987.9), S1H5N4 (*m/z* 2431.2), H6N5F1 (*m/z* 2693.3), H7N6F1 (*m/z* 3142.5), S2H6N5F1 (*m/z* 3415.7), S1H7N6F1 (*m/z* 3503.7) and S2H7N6F1 (*m/z* 3864.9) and accounted together 24 % in MSCs and 27 % in chondrogenically dedifferentiated cells. The presence of these structures with very similar relative amounts in undifferentiated MSCs and chondrogenically dedifferentiated cells indicated that the dedifferentiated cells possess a stem cell-like N-glycosylation pattern. On the other hand, some complex- and high-mannose-type N-glycans were quite different in quantities such as H5N4 (*m/z* 2070.0), H8N2 (*m/z* 2192.0), H5N4F1 (*m/z* 2244.1), H9N2 (*m/z* 2396.1), H6N5 (*m/z* 2519.2) and S1H5N4F1 (*m/z* 2605.3), which accounted together 59 % in MSCs and 39 % in chondrogenically dedifferentiated cells. In addition, some structures such as H3N4 (*m/z* 1661.8), H3N5F1 (*m/z* 2081.0), H5N3F1 (*m/z* 2173.0), H3N6F1 (*m/z* 2326.1), S1H4N5 (*m/z* 2472.2), H7N4 (*m/z* 2478.2), H6N5 (*m/z* 2519.2), S1H5N5 (*m/z* 2676.3), S1H6N6F1 (*m/z* 3299.6), H7N8F1 (*m/z* 3632.8), S1H8N7F1 (*m/z* 3952.9) and S3H8N7F1 (*m/z* 4676.1) were present as traces in chondrogenically dedifferentiated cells but not in undifferentiated MSCs and accounted together 9 %. Thus, the differences in the N-glycosylation profiles of MSCs and chondrogenically dedifferentiated cells were quantitative but qualitative as well.

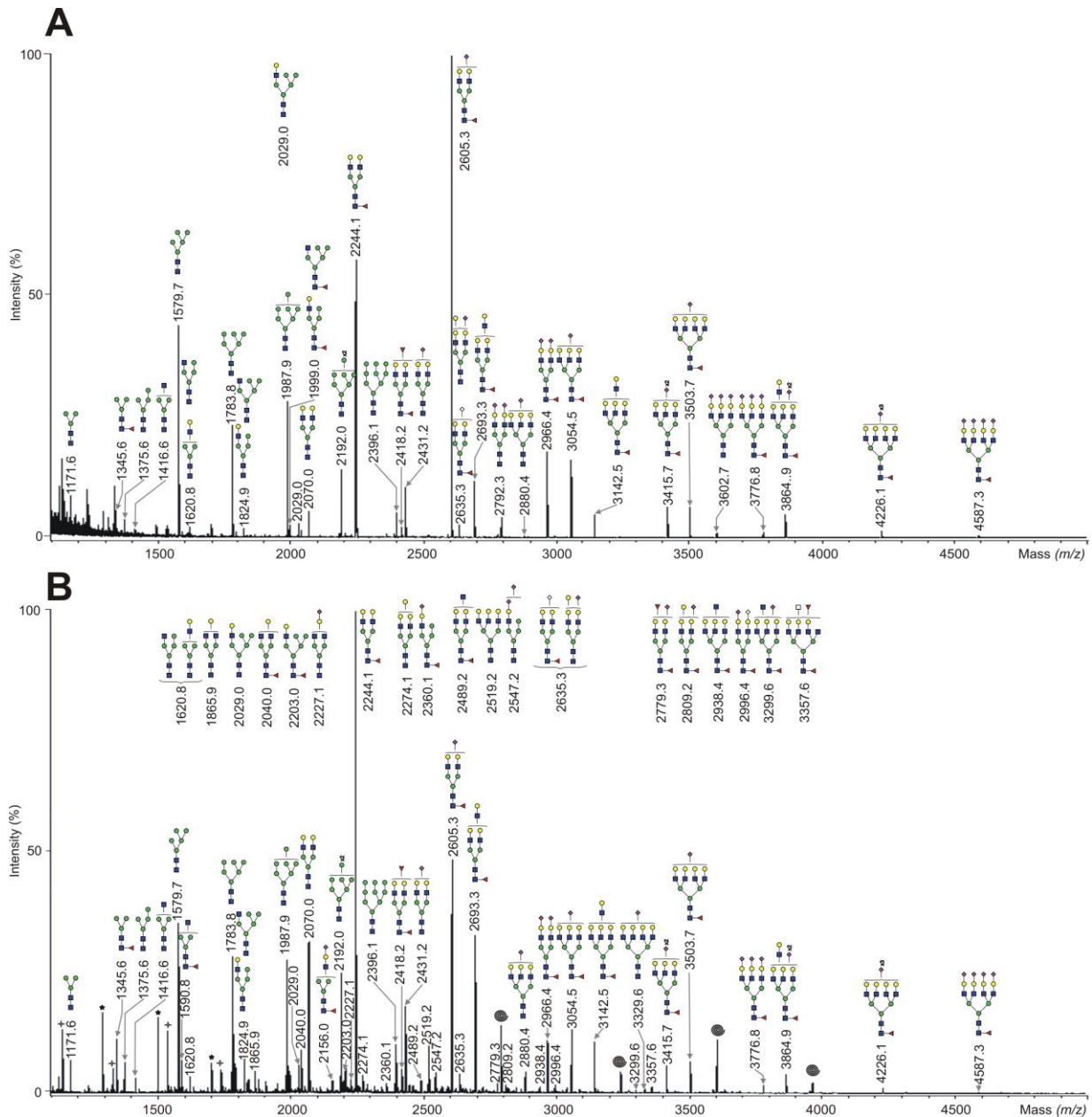


FIG. 2.33. MALDI-TOF-MS of PNGase F-released N-glycans. A representative mass spectrum of undifferentiated MSCs (**A**) and chondrogenic dedifferentiated MSCs (**B**) is shown together with the 55 most abundant structures. Cell surface glycoproteins were directly digested from the cells with trypsin. N-glycans were enzymatically cleaved from glycopeptides with PNGase F, permethylated and measured by MALDI-TOF-MS. Blue square represents N-acetylglucosamine, green circle mannose, yellow circle galactose, red triangle fucose and pink diamond N-acetylneuraminic acid. * Polyhexose contaminations are negligible. † Non identified peaks. ● Cell culture contaminations.

The N-glycosylation pattern of chondrogenically dedifferentiated cells and day 28 chondrogenically differentiated MSCs possess many similarities such as in the structures H5N2 (*m/z* 1579.7), H5N4F1 (*m/z* 2244.1), H5N4F2 (*m/z* 2418.2), S1H5N4 (*m/z* 2431.2), S1H6N5F1 (*m/z* 3054.5) and S2H6N5F1 (*m/z* 3415.7), which had the same relative

abundances and accounted together about 24 % in chondrogenically dedifferentiated cells and 25 % in chondrogenically differentiated MSCs. These results indicated that the chondrogenically dedifferentiated cells were still in a chondrogenic-like differentiation stage. The N-glycosylation profile of chondrogenically dedifferentiated cells possesses partial similarities with undifferentiated MSCs and at the same time with chondrogenically differentiated MSCs. The cells may be in a stage between undifferentiated MSCs and chondrogenically differentiated MSCs. Finally this example showed that the N-glycosylation profile can be used as an indicator of the differentiation stage for quality control of SCs.

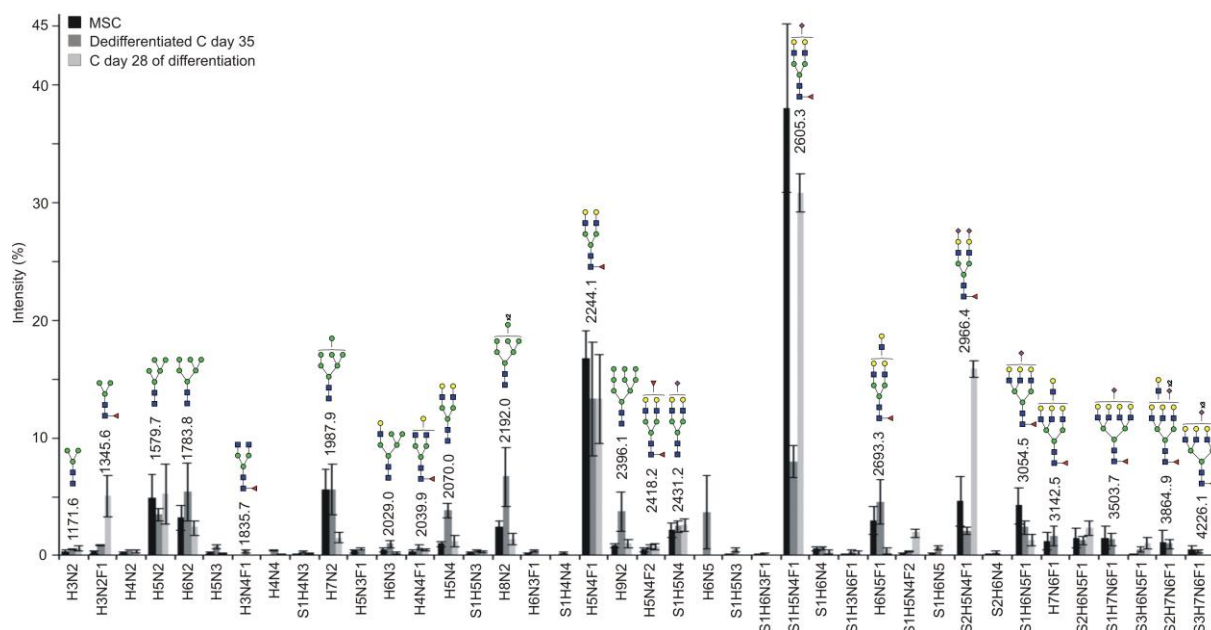


FIG. 2.34. Quantification of PNGase F-released N-glycans with MALDI-TOF-MS. The average relative amounts of the 44 most abundant PNGase F-released N-glycans of undifferentiated human MSCs (black), day 35 chondrogenic dedifferentiated cells (dark grey) and day 28 chondrogenically differentiated MSCs (light grey) derived from four (MSC and day 35 chondrogenic dedifferentiated cells, n=4) and three (day 29 chondrogenically differentiated MSCs, n=3) different preparations. Blue square represents N-acetylglucosamine, green circle mannose, yellow circle galactose, red triangle fucose and pink diamond N-acetylneuraminic acid. H: hexose, N: N-acetylhexosamine, F: deoxyhexose, S: N-acetylneuraminic acid.

2.5 N-Glycosylation Profile of Undifferentiated ESCs and its changes during endoderm differentiation into hepatocyte-like cells

2.5.1 N-Glycosylation Profile of ESCs before and after differentiation into hepatocyte-like cells

ESCs were differentiated into hepatocyte-like cells by the working group of Dr. Katrin Zeilinger (Charité-Universitätsmedizin Berlin, BCRT, Biomedizinisches Forschungszentrum). The cell surface N-glycosylation profile of undifferentiated human ESCs was investigated by MALDI-TOF-MS to identify the cell surface structures typical for ESCs. Seven different ESC preparations were used for the hepatogenic differentiation in order to obtain seven biological replicates. The N-glycosylation profile of undifferentiated, early time point (definitive endoderm) and late time point (hepatocyte-like cells) hepatogenically differentiated ESCs was investigated to monitor the changes of the N-glycosylation pattern during hepatogenic differentiation. The different cell samples were harvested and washed three times with PBS. Cell surface (glyco)proteins were digested with trypsin yielding to glycopeptides that were subjected to PNGase F-digestion. The released N-glycans were purified, desalted and derivatised. 60 % of the N-glycan pool was permethylated and measured by means of MALDI-TOF-MS. The rest of the N-glycan pool was labeled with the fluorophore APTS in order to detect the N-glycans by laser induced fluorescence detection through capillary electrophoresis. The N-glycosylation pattern of ESCs was compared to the one of definitive endoderm cells and hepatocyte-like cells that were obtained from differentiation of ESCs. A representative MALDI-TOF mass spectrum is presented in Fig.2.35 A and B.

High-mannose N-glycans comprised about 39 % of the N-glycan pool of ESCs, which had the form H4-9N2. The mass spectra revealed bi-, tri- and tetraantennary complex N-glycans. Fucosylated structures were predominantly monofucosylated but minor amounts of bi- and trifucosylated N-glycans were detected as well. The main part of the sialylated N-glycans were monosialylated and a minor part was bearing two or three terminal N-acetyl neuraminic acid residues (Neu5Ac).

Some complex N-glycans were fully galactosylated such as H5N4F1 (m/z 2244.1), S1H5N4 (m/z 2431.2), S1H5N4F1 (m/z 2605.3), H6N5F1 (m/z 2693.3), H7N6F1 (m/z 3142.5) and S1H7N6 (m/z 3330.6). In contrast, the N-glycans H3N4 (m/z 1661.7), H3N4F1 (m/z 1835.7), H4N4F1 (m/z 2040.0), H3N5F1 (m/z 2081.0), H4N5F1 (m/z 2285.1), H5N5F1 (m/z 2489.2), H4N6F1 (m/z 2530.2), H5N6F1 (m/z 2734.3) and H6N6F1 (m/z 2938.4) were just partially galactosylated.

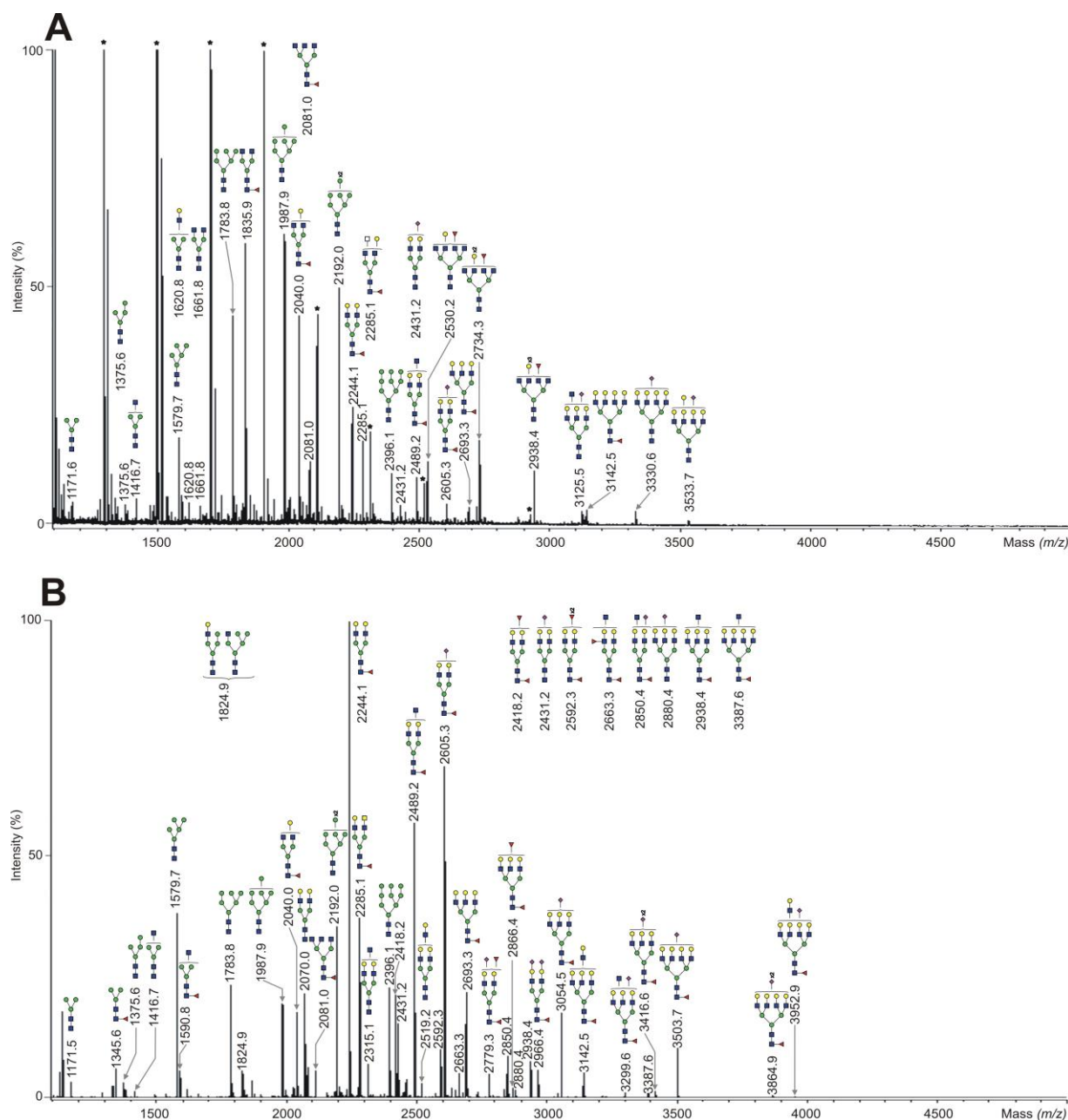


FIG. 2.35. MALDI-TOF-MS of PNGase F-released N-glycans. A representative mass spectrum of undifferentiated ESCs (**A**) and hepatocyte-like cells (**B**) is shown together with the 40 most abundant structures. Cell surface glycoproteins were directly digested from the cells with trypsin. N-glycans were enzymatically cleaved from glycopeptides with PNGase F, permethylated and measured by MALDI-TOF-MS. Blue square represents N-acetylglucosamine, green circle mannose, yellow circle galactose, red triangle fucose and pink diamond N-acetylneuraminic acid. * Polyhexose contaminations are negligible.

In hepatocyte-like cells, that were differentiated from ESCs, the high-mannose structures H4-9N2 were detected as well. Complex N-glycans were predominantly biantennary, followed by tri- and tetraantennary N-glycans as well as tetraantennary structures with one additional LacNAc chain. The major amount of complex N-glycans in hepatocyte-like cells was fully

galactosylated. Fucosylated N-glycans were mono- or bifucosylated and just partially sialylated with Neu5Ac. The relative abundances of the 30 most abundant N-glycans derived from seven (undifferentiated ESCs), four (definitive endoderm cells) and eight (hepatocyte-like cells) different biological replicates are presented in Fig.2.36 and the relative abundance of all detected signals were listed in table 6 (see appendix).

The amount of high-mannose structures were dramatically decreased from 39 % in ESCs to 18 % in hepatocyte-like cells. In addition, the high-mannose structures H6N2 (*m/z* 1783.7), H7N2 (*m/z* 1987.7), H8N2 (*m/z* 2191.8) and H9N2 (*m/z* 2396.1) were significantly decreased in hepatocyte-like cells.

Hybrid N-glycans were present as well but were minor in amount. It was possible to detect neutral and fucosylated hybrid-type structures in ESCs as well as in hepatocyte-like cells. In addition, sialylated hybrid N-glycans were present in hepatocyte-like cells. The amount of hybrid N-glycans was very low (about 3 % in ESCs) although the structures H4N3F1 (*m/z* 1794.9) and H5N3F1 (*m/z* 1999.0) were significantly decreased in hepatocyte-like cells.

The amount of biantennary N-glycans increased drastically from 11 % in ESCs to 49 % in hepatocyte-like cells and comprised the main part of complex-type N-glycans. Especially the fucosylated biantennary N-glycans were significantly more present in hepatocyte-like cells. The biantennary structures H5N4 (*m/z* 2069.8), S1H5N4 (*m/z* 2431.2) and fucosylated biantennary N-glycans H5N4F1 (*m/z* 2244.1), H5N4F2 (*m/z* 2418.2), S1H5N4F1 (*m/z* 2605.3) as well as S2H5N4F1 (*m/z* 2966.4) were significantly increased in hepatocyte-like cells. In addition, triantennary fucosylated N-glycans were increased in hepatocyte-like cells in which the N-glycans H6N5F1 and S1H6N5F1 were statistically significant.

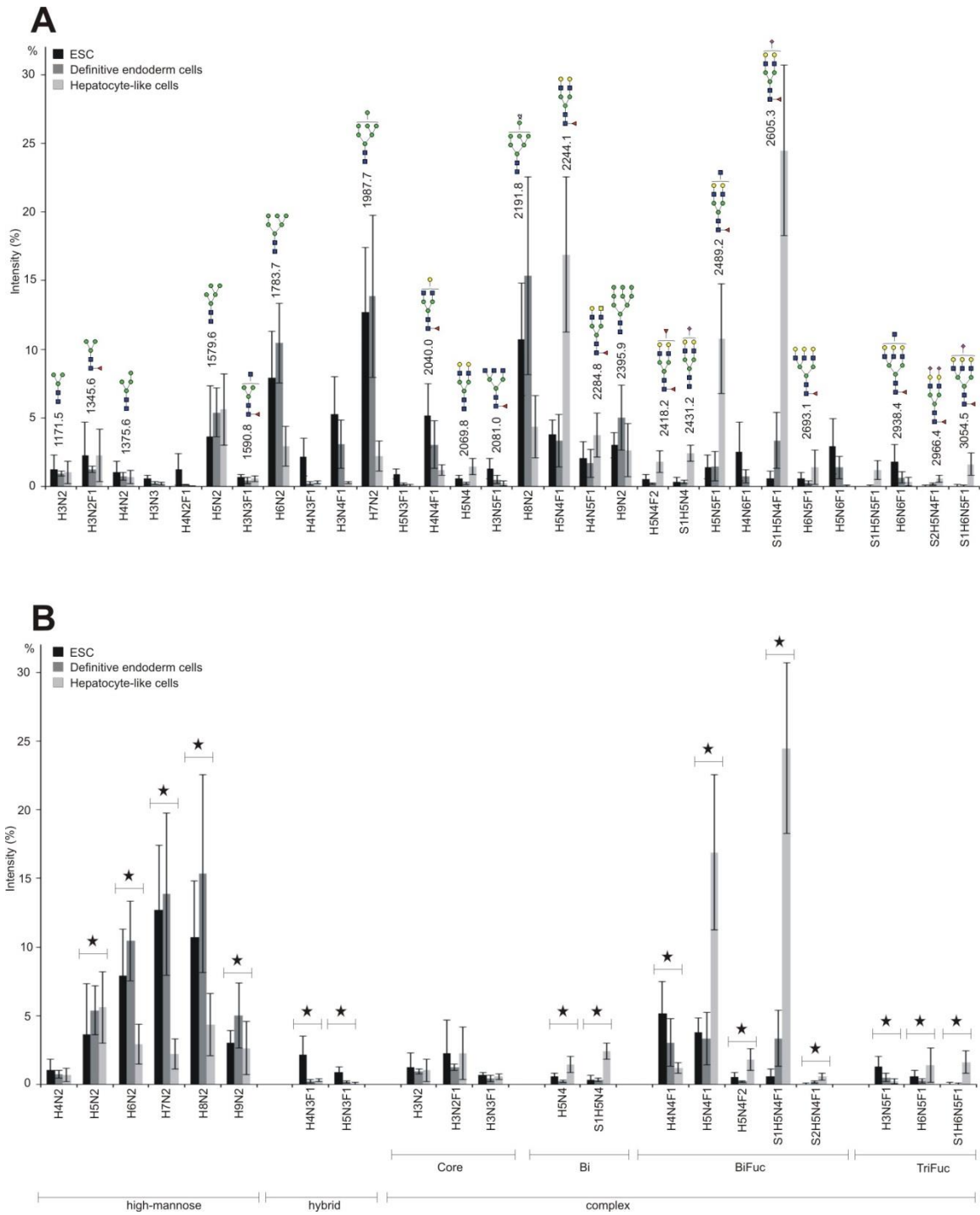


FIG. 2.36. Quantification of PNGase F-released N-glycans with MALDI-TOF-MS. The average relative amounts of the 30 most abundant PNGase F-released N-glycans of undifferentiated human ESCs (black), definitive endoderm cells (dark grey) and hepatocyte-like cells (light grey) derived from seven (ESC and hepatocyte-like cells, n=7) and four (definitive endoderm cells, n=4) different preparations. Statistical significant difference between the two sample groups undifferentiated ESCs and hepatocyte-like cells was assessed using Mann-Whitney U test (*p≤0.05) and is marked with a star in **(B)**. Blue square represents N-acetylglucosamine, green circle mannose, yellow circle galactose, red triangle fucose and pink diamond N-acetylneuraminic acid. H: hexose, N: N-acetylhexosamine, F: deoxyhexose, S: N-acetylneuraminic acid.

2.5.2 CE-LIF analysis of N-glycans from undifferentiated embryonic stem cells and hepatocyte-like cells

About 40 % of the N-glycan pool was analysed by means of CE-LIF, in order to confirm the structures found by MALDI-TOF-MS. Representative electropherograms of PNGase F-released N-glycans of undifferentiated ESCs and hepatocyte-like cells are presented in Fig.2.37 A and B. N-Glycans were assigned with the help of a standard table generated in our laboratory using N-glycans release from reference glycoproteins. In addition, MALDI-TOF-MS spectra of the desialylated N-glycan pools were used to assign the structures. The main structures were assigned to the electropherogram signals. In undifferentiated ESCs (Fig.2.37 A) high-mannose structures such as H5N2 (6.7 GU), H6N2 (7.5 GU) and H8N2 (9.3 GU) were detected. In addition, the biantennary structures H3N4F1 (7.6 GU), H5N4F1 (9.8 GU) and H5N5F1 (10.4 GU) were assigned to the electropherogram. Furthermore the partially galactosylated tetraantennary N-glycans H4N6F1 (10.9 GU), H5N6F1 (12.0 GU) and H6N6F1 (12.8 GU) as well as the fully galactosylated tetraantennary fucosylated structure H7N6F1 (13.8 GU) were detected.

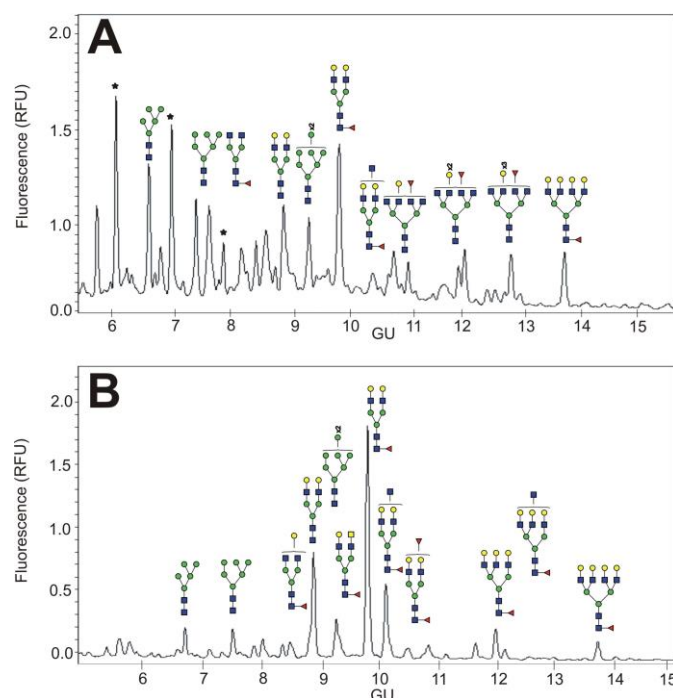


FIG. 2.37. CE-LIF electropherograms of PNGase F-released and desialylated N-glycans from undifferentiated ESCs **(A)** and hepatocyte-like cells **(B)**. Cells were digested with trypsin in order to release cell surface (glyco)peptides. (Glyco)peptides were subjected to PNGase F digestion to release N-glycans, desialylated and measured by CE-LIF. Blue square represents N-acetylglucosamine, yellow square N-acetylgalactosamine, white square N-acetylhexosamine, green circle mannose, yellow circle galactose, red triangle fucose, white diamond N-glycolylneuraminic acid and pink diamond N-acetylneuraminic acid. * Polyhexose contaminations are negligible.

In hepatocyte-like cells (Fig.2.37 B) the biantennary N-glycans H4N4F1 (8.5 GU), H5N4 (8.9 GU), H4N5F1 (9.2 GU), H5N4F1 (9.8 GU), H5N5F1 (10.2 GU) and H5N4F2 (10.5 GU) comprised the major part of complex N-glycans followed by triantennary structures such as H6N5F1 (12.0 GU) and tetraantennary N-glycan H7N6F1 (13.8 GU). High-mannose N-glycans such as H5N2 (6.7 GU), H6N2 (7.5 GU) and H8N2 (9.3 GU) were detected as well. Very similar distributions of the structures and changes during differentiation were obtained from the MALDI-TOF-MS data. Consequently, the CE-LIF electropherograms confirmed the mass spectrometric profiling.

2.5.3 Verification of identified N-glycan structures from undifferentiated embryonic stem cells and hepatocyte-like cells with MALDI-TOF/TOF sequencing and exoglycosidase digestions

Verification of the most abundant N-glycan structures was done using specific exoglycosidases (see exoglycosidase digestion Table 8) in combination with MALDI-TOF/TOF-MS fragmentation that was performed in the positive-ion mode. A representative MALDI-TOF/TOF mass spectrum is presented in Fig. 2.38 A and B for the N-glycan signal m/z 2938.4 of the composition H6N6F1 derived from human ESCs and of m/z 2285.0 of the composition H4N5F1 derived from hepatocyte-like cells. PNGase F-released N-glycans from hepatocyte-like cells were consecutively digested using the following sequence of digestion: neuraminidase, $\beta(1-4)$ galactosidase, almond meal $\alpha(1-3,4)$ fucosidase, again $\beta(1-4)$ galactosidase, bovine kidney $\alpha(1-2,3,4,6)$ fucosidase and α -mannosidase in order to unravel the presence Lewis^X epitopes and core-fucosylated structures.

All sialylated N-glycans shifted after digestion with neuraminidase and no sialylated structures were detected any longer. The diagnostic fragment ions S1H1N1 at m/z 847.2 and S1H2N1 at m/z 620.1 confirmed the presence of a sialylated antenna in S1H5N4F1 (m/z 2605.3), S1H5N4F2 (m/z 2779.3), S1H5N5F1 (m/z 2850.4), S2H5N4F1 (m/z 2966.4), S1H6N5F1 (m/z 3054.5), S2H6N5F1 (m/z 3415.7), S1H7N6F1 (m/z 3503.7) and S2H7N6F1 (m/z 3864.9) of hepatocyte-like cells.

Almost all N-glycans containing Gal residues were digested after addition of $\beta(1-4)$ galactosidase showing that almost all Gal residues were linked in $\alpha(1-4)$ -fashion to GlcNAc. Bifucosylated N-glycans of hepatocyte-like cells such as H4N4F2 (m/z 2214.1), H5N4F2 (m/z 2418.2), H4N5F2 (m/z 2459.2), H5N5F2 (m/z 2663.3), S1H5N4F2 (m/z 2779.3) and S1H6N5F2 (m/z 3228.6) were shown to contain one Lewis^X epitope since after digestion with $\beta(1-4)$ galactosidase one fucosylated antennae containing a Gal residue remained and this structure shifted after addition of $\alpha(1-3,4)$ fucosidase and $\beta(1-4)$ galactosidase. In addition, the diagnostic fragment ion H1N1F1 (m/z 660.1) revealed the presence of a fucosylated

antennae in hepatocyte-like cells and therefore confirmed the exoglycosidase results. Most of the fucosylated structures shifted after addition of bovine kidney $\alpha(1-2,3,4,6)$ fucosidase, indicating that fucosylated N-glycans contained at least one core-Fuc that is $\alpha(1-6)$ -linked to the reducing GlcNAc residue. In addition, the detection of the diagnostic fragment ions N1F1 at m/z 474.0 and N2F1 at m/z 719.2 proved core-fucosylation for instance in the N-glycans H4N4F1 (m/z 2040.0), H5N4F1 (m/z 2244.1), S1H5N4F1 (m/z 2605.3), H6N5F1 (m/z 2693.3), S1H5N4F2 (m/z 2779.3), S2H5N4F1 (m/z 2966.4), S1H6N5F1 (m/z 3054.5) and S2H6N5F1 (m/z 3415.7).

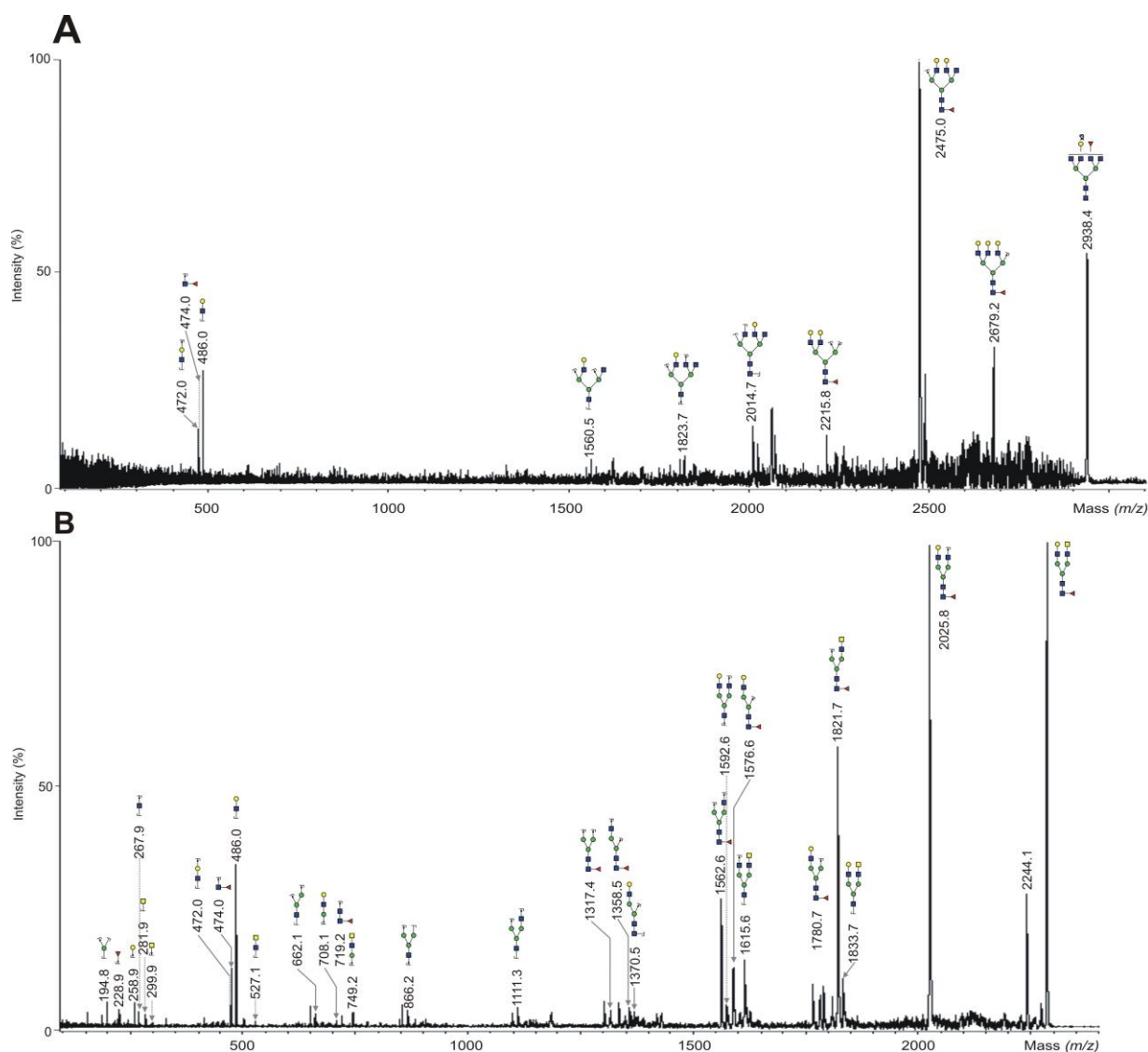


FIG. 2.38. MALDI-TOF/TOF mass spectrum of m/z 2938.4 of the composition H6N6F1 derived from human ESCs **(A)** and of m/z 2285.0 of the composition H4N5F1 derived from hepatocyte-like cells **(B)**. Blue square represents N-acetylglucosamine, green circle mannose, yellow circle galactose, red triangle fucose and pink diamond N-acetylneuraminic acid.

All high-mannose- and hybrid-type signals were sensitive to α -mannosidase treatment, which confirms the presence of Man residues in high-mannose and hybrid type N-glycans.

The signals m/z 1794.9, 1865.9 and 1824.9 in hepatocyte-like cells may present two different N-glycan structures, either one with a galactosylated antenna or a non-galactosylated one. MALDI-TOF/TOF fragmentation revealed that they present a mix of these two structures in hepatocyte-like cells, which was supported by the diagnostic fragment ions H1N1 m/z 472.0, H1N1 m/z 485.0 and/ or m/z 708.2 in case of the galactosylated N-glycan and by H2 m/z 445.0, H2N1 m/z 648.1 and/ or H3N1 m/z 866.2 in case of the non-galactosylated one. In contrast, the structures H4N3 (m/z 1620.8), H5N3F1 (m/z 1999.0) and H6N3 (m/z 2029.0) were identified as galactosylated complex or hybrid-type N-glycans in hepatocyte-like cells and this was verified by the fragment ions H2N1 m/z 690.1 and/ or m/z 708.2. In addition, this signals were sensitive to β (1-4) galactosidase. MALDI-TOF/TOF fragmentation of H6N4F1 (m/z 2448.2) revealed the presence of a digalactosylated antenna in ESCs. This was supported by the fragment ion H2N1 (m/z 690.2).

In hepatocyte-like cells, the structure H4N5F1 (m/z 2285.1) was found to contain GalNAc, which was verified by the diagnostic fragment ion N2 (m/z 527.1) (Fig. 2.38 B). Due to the high intensity of H5N4F1 (m/z 2244.1) and close position to H4N5F1 (m/z 2285.1), a relatively high signal was observed for H1N1 (m/z 486.0) when compared to the signal N2 (m/z 527.1) (Fig. 2.38 B).

2.5.4 Glycan-based biomarkers of undifferentiated embryonic stem cells and hepatocyte-like cells

As described for MSCs and their adipogenic, chondrogenic and osteogenic progeny, cell surface N-glycans of undifferentiated ESCs, definitive endoderm cells as well as hepatocyte-like cells that were obtained from differentiation of ESCs were qualified and quantified by MALDI-TOF-MS. The relative amounts of N-glycan structures found in the two sample groups ESCs and hepatocyte-like cells were compared and statistically evaluated using the Mann-Whitney U test (* $p \leq 0.05$). Four high-mannose N-glycans were significantly increased in ESCs, namely Man6, Man7, Man8 and Man9 (m/z 1783.8, 1987.9, 2192.0, 2396.1, respectively). The two hybrid-type structures H4N3F1 (m/z 1794.9) and H5N3F1 (m/z 1999.0) were also statistically significant in ESCs. In addition, the complex N-glycans H4N4F1 (m/z 2040.0) and H3N5F1 (m/z 2081.0) were significantly increased in ESCs. In contrast, one high-mannose N-glycan Man5 (m/z 1579.7) and eight complex-type structures were significantly overexpressed in hepatocyte-like cells when compared to undifferentiated ESCs. Six of them were biantennary (m/z 2070.0, 2244.1, 2418.2, 2431.2, 2605.3, 2966.4)

and two of them triantennary N-glycans (m/z 2693.3, 3054.5). Most of these structures were core-fucosylated and half of them sialylated.

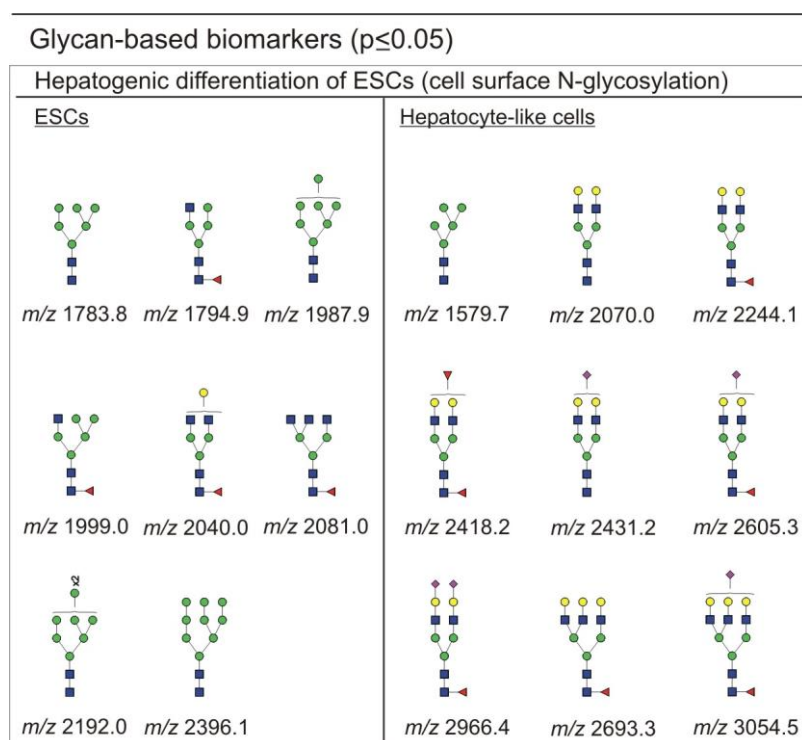


FIG. 2.39 Glycan-based biomarkers of undifferentiated ESCs and hepatocyte-like cells. Statistical significant difference between the two sample groups undifferentiated ESCs and hepatocyte-like cells was assessed using Mann-Whitney U test ($*p \leq 0.05$). Based on the test, the listed N-glycans were significantly overexpressed

3. Discussion

The dense layer composed of complex carbohydrate structures found on the cell surface, which is called glycocalyx, is cell lineage-specific and very sensitive towards biological processes such as differentiation. Thus, cell surface glycan structures present a powerful and diverse tool in the field of glycan-based biomarker discovery. Qualitative and quantitative changes of the cell surface glycosylation pattern can be used in the field of regenerative medicine to identify certain SC populations, to monitor SC differentiation as well as the loss of the SC behaviour. This study aimed at investigating the cell surface N-glycosylation decoration of SCs before and during differentiation into more specialised cells and therefore the first goal was to establish a rapid and sensitive method which allows the elucidation of the N-glycan structures that are embedded in the glycocalyx.

3.1 Rapid analysis of cell surface N-glycosylation of living cells

Located on the cell surface, N-glycans play important roles in various processes as they are directly involved in cell-cell or cell-protein interactions that trigger various biological responses. Thus, it is of paramount importance to have robust analytical methods to characterise them.

The classical cell membrane extraction protocol, which is used in many laboratories produces high levels of high-mannose N-glycans (122, 124) that stem from both membrane glycoproteins as well as glycoproteins from the ER. An et al. (122) confirmed with proteomic analysis the presence of plasma membrane proteins but also contamination from endoplasmic reticulum (ER) and other membranes when membrane extraction was applied, showing that N-glycans derived from the ER were included in the analysis of SCs N-glycome as well (122). In addition, Nakano et al. (124) isolated cell membrane proteins, which were dotted on polyvinylidene difluoride membrane prior to PNGase F digestion with the aim to characterise glycome alterations of human T-cell acute lymphoblastic leukemia. Although their study revealed the presence of high-mannose N-glycans as well as bi-, tri- and tetraantennary N-glycans (124), they obtained a high proportion of high-mannose type N-glycans on the cell membrane glycoproteins.

Such a high proportion of high-mannose N-glycans prevents a good detection and quantification of complex-type N-glycans. We recently published a protocol that overcomes this problem (127) using Endo H, which specifically cleaves high-mannose and hybrid-type N-glycans. Endo H-digested glycopeptides were isolated and then treated with PNGase F to release complex-type N-glycans. This protocol enabled the separation of the high abundant high-mannose N-glycans from complex-type N-glycans, which yielded in an improved

detection and quantification of complex-type N-glycans (127). The disadvantages of this method are that it is time-consuming and requires many steps.

Therefore, the aim was to develop a simple and reproducible protocol to analyse cell surface N-glycosylation. With the new established method the amount of high-mannose N-glycans had decreased from 90 % to 10 %. At the same time, the detection of complex-type N-glycans was drastically improved when compared to the membrane preparation method. With the new protocol, it was possible to detect 94 different N-glycan structures in HEK 293 cells. In addition, more than 20 of them were complex N-glycans that were not present in the N-glycan pool of HEK 293 cells when the membrane preparation method was applied. It was possible to detect nearly twice the number of structures as Nakano et al. (124) and Reinke et al. (126) who both used membrane extraction to isolate glyco(proteins). In addition, the abundance of high-mannose N-glycans found in HEK 293T cells in the study of Reinke et al. was remarkably high (126). Thus, the newly established method is more suitable for cell surface glycosylation profiling due to the fact that a higher number of complex-type N-glycans were present and their detection is enhanced.

The new approach requires about 4×10^6 cells to obtain a cell surface N-glycosylation profile without loss of N-glycan structures. When compared with the amounts used by other groups for cell membrane extraction, namely from 50 to 100×10^6 cells, the cell number used with the new method was much lower (122-124). In addition, the new approach is not time-consuming when compared with the membrane preparation protocol. It was possible to obtain cell surface glycopeptides in about an hour starting from the cell pellet instead of two working days with the cell membrane extraction protocol. This time is comparable with the time required by Nakano et al. and An et al. to isolate and denature membrane proteins (122, 124). Mi et al. (123) described an even more complex and time-consuming method to obtain glycopeptides from cell membranes. Besides the increased preparation time, the costs for N-glycan analysis through cell membrane extraction were higher since additional consumables and centrifugation steps were required.

The new method was applied to profile and compare the cell surface N-glycosylation profile of HEK 293, CHO-K1, AGE1.HN and Hep G2 cells. In addition, it was an aim to test the selectivity of the method towards different cell lines. Exoglycosidase digestions and MALDI-TOF/TOF fragmentation revealed the presence of core-fucosylated N-glycans and the GlcNAc-GalNAc motif in HEK 293 cells. These results confirmed previous studies of Reinke et al. (160), which reported the high expression level of the glycosyltransferase FucT-VIII and a high content of core-fucose in HEK 293T cells. In addition, studies on L-selectin and human protein C expressed in HEK 293 cells revealed that they contained the GalNAc motif (161) (143), which supports the assumption that the HEK 293 cell line specifically produces GalNAc epitopes in glycans.

In the N-glycome of CHO-K1 cells the presence of core-fucosylated N-glycans as well as traces of the antigenic Neu5Gc was found. These findings can be supported by literature published on the N-glycome of recombinant glycoproteins expressed in CHO-K1 cells (60, 92), namely anti-HER2 monoclonal antibodies (162), human plasminogen activator (57), human alpha-1-antitrypsin (A1AT) (163) and human erythropoietin (164).

AGE1.HN cells typically contained a high degree of core and antennary fucosylated N-glycans, which is in line with previous findings on recombinant A1AT (165). A1AT expressed in AGE1.HN contained core-fucosylated di-, tri and tetraantennary N-glycans and up to four Fuc residues were found on triantennary structures (165). Moreover, studies of Rudd et al. and Stimson et al. support our findings that core-fucosylation and Lewis^x epitopes are characteristic epitopes in neuronal N-glycosylation (166, 167). Their studies revealed the presence of the two mentioned types of Fuc linkages in N-glycans of the prion protein in mice and hamsters (166, 167).

Core-fucosylation was found to be characteristic for Hep G2 cells. These findings can be supported by studies on hepatoma cell glycoprotein glycosylation, in which $\alpha(1-6)$ -linked core-Fuc has been reported on α -fetoprotein and transferrin (168, 169). In parallel, Noda et al. successfully demonstrated that the $\alpha(1-6)$ -fucosyltransferase gene was expressed at high levels in hepatomas of rat models and hepatoma cell lines (170). Taken together, core-fucosylation seems to be a singular trait of Hep G2 cells. In addition to that, the presence of the GlcNAc-GalNAc motive in Hep G2 cells was verified, which was reported in glycans derived from hepatoma by Johnson et al. (171), namely on alpha-fetoprotein O-glycans of hepatocellular carcinoma patients.

Altogether, the cell surface N-glycome of the four cell lines studied here, namely HEK293, CHO-K1, AGE1.HN and Hep G2, possesses the same features which were previously described in the N-glycome found on recombinant proteins produced in these cell lines.

It was possible to establish a new glycomics method, which is able to profile specific cell surface N-glycosylation of living cells and at the same time is fast, robust, sensitive and reproducible. In addition, with the new method an increased number and amount of complex type N-glycans was detected. Characterisation of cell surface N-glycan structures generates informations, which are of great importance as they can directly predict the N-glycan profiles of recombinant glycoproteins and is of relevance to glycobiotechnologists. Furthermore, cell surface glycosylation profiling may be of help in glycomedicine, especially in the fields of biomarker discovery.

3.2 N-Glycosylation profile of undifferentiated and adipogenically, chondrogenically and osteogenically differentiated human bone marrow mesenchymal stem cells

In this study, MSCs were differentiated into adipogenic, chondrogenic and osteogenic direction by the working group of Dr. Jochen Ringe (Charité-Universitätsmedizin Berlin, BCRT, Labor für Tissue Engineering/ Klinik für Rheumatologie). For practical reasons, such as to verify homogeneous MSC cultures or to monitor the quality and progress of MSC differentiation during repair tissue formation, and to fulfill regulatory issues like therapy approval, knowledge of biomarkers describing MSCs and their development stages is of utmost importance. However, all known MSC markers, among them the most prominent ones like the cell surface proteins CD73 (5'-nucleotidase), CD90 (thy-1), CD105 (endoglin), CD166 (alcam) (172) and Stro-1 (173) are not specific. For instance, MSCs are usually identified as colony-forming unit-fibroblasts and Stro-1 negative cells are not capable of forming colonies (174). In contrast, Stro-1 positive cells are capable to become hematopoietic stem cell-supporting fibroblasts, smooth muscle cells, adipocytes, osteoblasts and chondrocytes, which support the functional role of MSCs. In addition, Stro-1 is not only expressed from MSCs and its expression is gradually lost during culture. Several other useful but unspecific markers for MSCs and their differentiated progeny have been identified in molecular profiling approaches for example focusing on the adipogenic lineage (175). Knowledge of markers for precise labeling and tracking of those cells would therefore strongly enhance their importance in regenerative medicine.

3.2.1 Adipogenic differentiation of human mesenchymal stem cells

With the aim to find glycan-based stage specific markers for undifferentiated and adipogenically differentiated MSCs, the N-glycosylation profile of human bone marrow-derived MSCs during adipogenic differentiation was investigated on qualitative and quantitative level. To our knowledge, this study describes the first report on the N-glycome of early (day 5) and late (day 15) adipogenically differentiated MSCs (127).

Adipogenesis of MSCs was performed using a standardised and reproducible assay, which induces stimulation of MSCs for up to 15 days using an adipogenic cocktail consisting of insulin, dexamethasone, indomethacin and 3-isobutyl-1-methylxanthine (172, 175). Afterwards cell membrane (glyco)proteins were isolated by membrane extraction and N-glycans were enzymatically released, purified and analysed by means of MALDI-TOF-MS. In addition, structural verification was performed with exoglycosidase digestions and MALDI-TOF/TOF fragmentation analysis.

Several high-mannose-type N-glycans were detected in human MSCs and their adipogenically differentiated progeny and dominated in the N-glycan profile of Endo H-released N-glycans. However, the amount of high-mannose N-glycans increased with differentiation resulting in a higher amount in adipogenically differentiated MSCs. Mainly small high-mannose-type N-glycans containing three to six Man residues were found to be overexpressed in adipogenically differentiated cells. This is also described in literature, in which studies revealed that besides human MSCs and their osteogenically counterparts (151), human embryonic (176) and hematopoietic stem and progenitor cells (177) contain high amounts of high-mannose-type N-glycans on their cell surface. Quantification with MALDI-TOF-MS revealed that short high-mannose-type N-glycans such as H5N1 and H6N1 were significantly enriched in adipogenically differentiated MSCs, while larger high-mannose-type N-glycan such as H9N1 was significantly underexpressed in adipogenically differentiated MSCs. Studies by Heiskanen et al. revealed that high-mannose-type N-glycans dominated the N-glycan profile of undifferentiated MSCs in comparison to their osteogenically differentiated counterparts, whereas N-glycans with more than six Man residues were enriched in osteogenically differentiated cells (151). In addition, Heiskanen et al. showed that smaller high-mannose-type N-glycans were increased in relative abundance in osteogenically differentiated MSCs (151). Thus, our data are in line with the studies of Heiskanen et al.; high-mannose-type N-glycans containing at least seven Man residues were more abundant in undifferentiated MSCs and seem to be a characteristic feature for undifferentiated human MSCs and less characteristic for osteogenically or adipogenically differentiated cells.

The monoglucosylated high-mannose-type N-glycan H10N1 was detected predominantly in undifferentiated MSCs, which is known to be a characteristic feature of improperly folded nascent glycoproteins in the endoplasmic reticulum. Glycoprotein precursors containing a monoglucosylated glycan moiety remain in the ER until proper folding is achieved within the calnexin/ calreticulin cycle (178). The monoglucosylated H10N1 high-mannose-type N-glycan was detected in human embryonic SCs as well (179) and may therefore be a typical feature of SCs.

Beside high-mannose N-glycans, hybrid-type N-glycans were detected as well but they were much less abundant when compared with the two other types of N-glycosylation. However, hybrid-type N-glycans were present in undifferentiated and adipogenically differentiated MSCs. Neutral, sialylated as well as fucosylated hybrid-type N-glycans were detected and quantification using MALDI-TOF-MS revealed that the two neutral hybrid-type N-glycans H5N2 and H6N2 were significantly overexpressed in undifferentiated MSCs. The opposite was described by studies from Heiskanen et al. which revealed that neutral hybrid-type N-glycans were more abundant in osteogenically differentiated MSCs (151). These differences

may arise from the fact, that MSCs were differentiated into osteogenic direction but also from the different digestion protocols, which consisted in our case of a tryptic digestion step followed by endoglycosidase digestion of the resulting (glyco)peptides. Tryptic digestion of (glyco)proteins improves the accessibility of endoglycosidases to the reducing end of glycans. However, Heiskanen et al. (151) did not describe how PNGase F digestion of (glyco)proteins was performed and therefore comparison is not possible.

The mass spectrometric quantification data revealed a decrease in fucosylation and branching of complex-type N-glycans in adipogenically differentiated MSCs. The biantennary fucosylated N-glycans H3N4F1, H5N4F3 and S2H5N4F1 were significantly increased in 15 days adipogenically differentiated MSCs, while triantennary N-glycans H6N5F1 and S1H6N5 as well as tetraantennary structures H7N6F1, S1H7N6 and S1H7N6F1 were significantly enriched in undifferentiated human MSCs when compared to adipogenically differentiated MSCs. These results are in line with the studies did by Morad et al. (180), which revealed a decreased level of antennarity of complex-type N-glycans, namely of tri- and tetraantennary structures, in adipogenically differentiated MSCs. This was proven using lectin staining of membrane extracts. Morad et al. showed also that the level of these structures was increased in osteogenically differentiated MSCs (180). Thus, according to the studies of Morad et al., the level of antennarity was decreasing during adipogenic differentiation and increasing during osteogenic differentiation of MSCs (180). While in our study N-glycans were analysed using MALDI-TOF-MS and CE-LIF, Morad et al. performed glycoanalysis of membrane proteins using lectin microarrays, showing that utilisation of different methods lead to similar results (180). In contrast, the studies of Heiskanen et al. described that the acidic N-glycan profile of MSCs contained an increased amount of the larger complex-type N-glycans (five GlcNAc or more) and of N-glycans with two or more Fuc residues when compared to osteogenically differentiated cells (151). Our mass spectrometric data revealed that fucosylated N-glycans bore at least one core-linked Fuc. In addition, the most abundant fucosylated N-glycans were monofucosylated with an $\alpha(1-6)$ -linked Fuc, which is bond to the Asn-linked GlcNAc residue of the N-glycan core.

Quantification of the mass spectrometric data showed that the overall sialylation was increased in adipogenically differentiated MSCs. In comparison, Heiskanen et al. found that complex-type N-glycans lacking Neu5Ac were enriched in osteogenically differentiated MSCs (151), showing that sialylation is increased in undifferentiated MSCs. Increase or decrease of the overall sialylation may be therefore influenced by the different routes of MSC differentiation, namely adipogenic or osteogenic differentiation.

The linear poly-LacNAc epitope was predominantly found in undifferentiated MSCs, which has been previously reported by Heiskanen et al. (151). Thus, linear poly-LacNAc may be a characteristic feature of undifferentiated MSCs. Literature describes the presence of high-

molecular weight poly-LacNAcs in human embryonal carcinoma cells, where they are supposed to play roles in the interactions on the same membrane. In addition, large branched poly-LacNAc, which are expressed in mouse embryonic SCs and early embryonic cells, are assumed to participate in cell survival by increasing the interaction of membrane molecules within the membrane (111). It has been also described that poly-LacNAcs can change their structure from linear chains in fetal blood cells into branched chains in the adult (181). Poly-LacNAc epitopes are able to interact with lectins in a multivalent fashion, such as with β -galactoside binding lectins. β -Galactoside binding lectins are galectins, which are known to be involved in many cell adhesion and signaling phenomena. Studies revealed that they have a higher affinity for poly-LacNAcs than for single LacNAc units, suggesting that the function of LacNAc epitopes is influenced by their structure (151, 182-184).

The overall distribution of N-glycans found in undifferentiated as well as adipogenically differentiated MSCs based on mass spectrometric profiling was confirmed with CE-LIF analysis. The main advantage of CE-LIF when compared with MALDI-TOF-MS is its ability to discriminate between isomeric structures, which appear in MALDI-TOF-MS as a single peak. Since CE-LIF separates the molecules according to their size, shape and charge, isomers will be detected at different migration times. In our laboratory a list of N-glycan structures isolated from standard glycoproteins was generated and the migration time based on sequential exoglycosidase experiments and fractionation of single N-glycan structures with HPAEC-PAD in combination with MALDI-TOF-MS and CE-LIF analysis was assigned. It was possible to identify the Man7 as well as Man8 N-glycans as isomeric structures. The terminal Man residues may be connected in three different ways to Man6GlcNAc2. The three isomers of Man7 and Man8 were already verified by studies from Frisch et al. (149) using HPAEC-PAD fractionation of each high-mannose N-glycan released from human blood serum and subsequent measurements by MALDI-TOF-MS and CE-LIF that revealed the migration times of each structure. In addition, based on studies in our laboratory it was possible to assign the two isomers of complex-type triantennary N-glycan Gal3Man3GlcNAc5 in MSCs and adipogenically differentiated cells in which the third antennae maybe linked in β (1-4)- or β (1-6)-fashion to the Man of the core structure. Lectin experiments by Cummings et al. (85) and enzyme digestions by Yamashita et al. (84) confirmed the difference between the two triantennary isomers. The triantennary N-glycan with the β (1-4)-linked antennae has a higher migration time than the one with the β (1-6)-linked antennae since the latter one needs less space and can therefore migrate faster. In MSCs the peak of the β (1-6)-isomer was higher than the peak signal for the β (1-4)-isomer. Studies in our laboratory revealed the same isomeric distribution of triantennary N-glycan of alpha-1 antitrypsin (A1AT) expressed in HEK-293 cells as well as literature dealing with recombinant proteins expressed in CHO cells (86, 87). In both cases, the amount of the β (1-6)-isomer dominated.

Based on the results and statistical analysis, the biantennary structures H5N4F2, H5N4F3 and S2H5N4F1 as well as the high-mannose N-glycans Man5 and Man6 were proposed as potential glycan-based biomarkers for adipogenically differentiated cells. These potential glycan-based biomarkers were significantly overexpressed in day 15 of adipogenically differentiated MSCs and may be used to monitor the loss of the SC status of MSCs.

3.2.2 Chondrogenic differentiation of human mesenchymal stem cells

The cell surface N-glycosylation profile of undifferentiated MSC and chondrogenically differentiated cells was investigated and compared on qualitative and quantitative level. In addition, early (day 5) and late (day 28) time point chondrogenically differentiated MSCs were subjected to N-glycan analysis before and after isolation from their ECM to clarify the impact of ECM on the N-glycosylation profile of chondrogenically differentiated MSCs. Chondrogenic differentiation of MSCs revealed a significantly increased amount of high-mannose N-glycans in day 5 as well as day 28 of chondrogenically differentiated MSCs. This was not the case, when chondrogenically differentiated cells were isolated from ECM prior to N-glycan analysis. In contrast, the abundance of high-mannose N-glycans was lower when the ECM was absent. Toegel et al. (185) studied the carbohydrate structures of the glycocalyx of primary human chondrocytes using a panel of lectins. N-linked glycans were profiled by *L. culinaris* agglutinin and *S. nigra* agglutinin, which identified the expression of high-mannose-type N-glycans and terminal sialyl- α (2-6)Gal epitopes, respectively (185). This supported the presence of high-mannose and sialylated N-glycans in primary chondrocytes. Furthermore, Toegel et al. (185) did the same lectin staining experiments on primary chondrocytes derived from patients with osteoarthritis (OA). Osteoarthritis is a disease which is accompanied by a breakdown of the cartilage matrix (extracellular matrix of chondrocytes). Interestingly, their studies revealed that chondrocytes from OA patients contained significantly increased amount of high-mannose N-glycans, when compared to normal primary chondrocytes (185). In addition, previous studies by Bernard et al. revealed that chondrocytes produce mature glycoproteins such as fibronectin bearing just high-mannose or hybrid N-glycans when compared to fibroblast fibronectin that bears just complex-type N-glycans (186). Pabst et al. studied the N-glycosylation of primary human chondrocytes and showed a very similar distribution of N-glycans, with high peak intensities of high-mannose N-glycans such as Man8 and Man9 (187). In all, this indicates a relationship between chondrocytes and the relatively high high-mannose N-glycan level, which is very probably influenced by the components of the ECM. In addition, the amount of complex N-glycans was drastically decreased after chondrogenic differentiation when the ECM was present; particularly biantennary N-glycans. In contrast, when the ECM was absent, the amount of

biantennary structures increased after differentiation. Larger complex N-glycans, such as triantennary structures decreased after differentiation into chondrogenic cells in both cases, when N-glycan analysis was done with and without their ECM. Furthermore small complex-type monoantennary structures increased with differentiation. Yang et al. (188) studied the biosynthetic pathway of glycoproteins in cultured human chondrocytes from OA patients and found that they have potential to synthesise biantennary N-glycans, which was verified by the presence of β 4Gal-transferase. The latter is able to extend the two terminal GlcNAc residues to form complex-type antennae (188). However, their studies revealed also that the activities of GlcNAc-transferases III and V were below detectable levels (188), suggesting the significantly lower amount of tri- and tetraantennary structures in human chondrocytes. In addition, these results are in line with studies by Richard et al. (189) who have investigated glycosyltransferase activities in chondrocytes from patients with OA and normal human cartilage.

Sialylation was more abundant in day 28 chondrogenically differentiated cells when ECM was absent but decreased drastically when ECM was present. Toegel et al. (185) showed that primary chondrocytes of OA patients contained increased amounts of terminally sialylated N-glycans when compared to normal primary chondrocytes, which was verified by lectin staining of the glycocalyx. Thus, it is very probably that sialylation of the glycocalyx is influenced by components of the ECM. In addition, literature revealed that the negative charge on sialic acids of cell surface glycans most probably contribute to anti-adhesive properties of glycoproteins (190, 191), which can be explained by the role of leukosialin in cell adhesion. Leukosialin (CD34) is a sialoglycoprotein, which is expressed in leucocytes and there avoids aggregation of leukocytes as well as non-specific attachment to endothelial cells (190, 191). Fuc was mainly connected to the reducing GlcNAc of the core but Lewis^X epitopes were verified as well. Heiskanen et al. [10] revealed the presence of sialyl-Lewis^X epitopes on human MSCs and on osteogenically differentiated cells derived from them. Sialyl-Lewis^X is known to mediate fucosylation-dependent homing of MSCs into bone marrow [70]. In addition, Rosen et al. discovered the significant role of fucosylated and sulfated glycans in the process of adhesion of lymphocytes to endothelial cells, where they are found to be the best inhibitors for this interaction (192). Our studies confirmed the data from Pabst et al., who studied the N-glycosylation of primary chondrocytes and revealed the presence of biantennary structures as the main group, followed by triantennary complex N-glycans (187). However, they released the N-glycans from proteins in-gel after a cell lysis and precipitation step and applied LC-ESI-MS analysis. Therefore their results slightly differ from ours (187). In undifferentiated MSCs and day 28 chondrogenically differentiated cells without ECM the LacNAc epitope was verified.

Based on these results the triantennary N-glycans H6N5F1 and S1H6N5F1 as well as tetraantennary structures H7N6F1, S1H7N6F1 and S2H7N6F1 were proposed as glycan-based biomarkers for undifferentiated MSCs. In addition, the biantennary structures S1H5N4F2 and S2H5N4F1 were proposed as potential glycan-based biomarkers for day 28 chondrogenically differentiated cells without ECM and the biantennary N-glycans H3N4F1, H4N4F1 and H4N4F2 as glycan-based biomarkers for day 28 chondrogenically differentiated cells with ECM. These potential glycan-based biomarkers were significantly overexpressed in the respective cells and may be used to monitor the loss of the SC status of MSCs and to discriminate between undifferentiated MSCs and their chondrogenic counterparts.

3.2.3 Osteogenic differentiation of human mesenchymal stem cells

MSCs were differentiated into osteogenic cells and cell surface N-glycosylation was investigated before and after early (day 5) and late (day 28) time point of osteogenic differentiation and subsequent isolation from their ECM. The mass spectrometric data revealed that biantennary fucosylated N-glycans increased drastically and larger complex N-glycans such as tri- and tetraantennary structures decreased in relative amount. In comparison, Heiskanen et al. reported that the acidic N-glycan profile of MSCs contained relatively more of the larger complex-type N-glycans (five GlcNAc or more) [10] which supports our findings, that small complex N-glycans are more abundant in osteogenically differentiated cells. In addition, Morad et al. (180) studied N-glycosylation of protein membrane extracts derived from MSCs before and after osteogenic induction by lectin microarrays. In contrast, their studies revealed that the level of antennarity in osteogenic MSCs is higher than that of the undifferentiated MSC population [43] which is not the case in our study and the one of Heiskanen et al. [10]. The different results may stem from the application of different glycan preparation methods as well as different N-glycan profiling techniques. In our study, cell surface (glyco)proteins were directly digested with trypsin and N-glycans were enzymatically released with PNGase F, but Morad et al. used protein membrane extracts and applied lectin microarrays to study the N-glycosylation [43]. Protein membrane extracts include intracellular (glyco)proteins as well, which may affect the N-glycosylation pattern. Furthermore the use of lectins instead of mass spectrometric profiling may influence the results qualitatively, since the specificity of lectins and antibodies are limited, which might lead to the loss of important structural information. In contrast, MALDI-TOF-MS, which is used here to profile cell surface N-glycosylation is a powerful tool to study the N-glycosylation of cells more accurately. Sialylation was slightly decreased which supports the findings of Heiskanen et al. [10], which revealed that complex-type N-glycans lacking Neu5Ac were enriched in osteogenically differentiated MSCs (151). In addition, they used

¹H NMR to verify the mass spectrometric data and thereby revealed that both $\alpha(2-6)$ - and $\alpha(2-3)$ -linked sialic acids but quantitation showed that $\alpha(2-3)$ -linked sialic acid was the predominant linkage type [10]. Takahata et al. (193) studied the changes in sialylation during osteoclast differentiation and its effect on differentiation. Their studies revealed that sialic acid is expressed in osteoclast precursors and then accumulates on the cell surface after RANKL (osteoclast differentiation factor) stimulation. In addition, cleavage of terminal sialic acids from cell surface glycoconjugates resulted in strong inhibition of osteoclast differentiation, which indicates that cell surface sialylation is involved in the osteoclast differentiation process (193). Fucosylation was increased in day 28 osteogenically differentiated cells. Fuc residues were mainly linked to the reducing GlcNAc of the core. In comparison, studies by Heiskanen et al. revealed that MSCs contained more N-glycans with two or more Fuc residues when compared to their osteogenically counterparts (151). In addition, the LacNAc motif was verified in bi- and triantennary N-glycans of undifferentiated MSCs and day 28 osteogenically differentiated cells and has been previously reported in undifferentiated MSCs (151). In addition the studies by Heiskanen et al. [10] revealed the abundance of sulfate or phosphate ester modifications of complex and hybrid N-glycans from osteogenically differentiated cells. However measurements of the N-glycan pool of undifferentiated as well as osteogenically differentiated cells in the negative ionization mode of MALDI-TOF-MS revealed no signals for sulfate or phosphate modifications. The amount of high-mannose N-glycans decreased during osteogenic differentiation of MSCs. High-mannose type N-glycans are known to mediate osteoclast cell-cell fusion (194, 195). To sum up, the biantennary structures H4N4F1, H5N4, H5N4F1, S1H5N4 and S1H5N4F1 were proposed as glycan-based biomarkers for osteogenically differentiated cells, which were significantly overexpressed in these cells and may be used to discriminate between undifferentiated MSCs and their osteogenically differentiated counterparts

3.3 N-Glycosylation profile of undifferentiated embryonic stem cells and hepatocyte-like cells

In this study, ESCs were differentiated into hepatocyte-like cells by the working group of Dr. Katrin Zeilinger (Charité-Universitätsmedizin Berlin, BCRT, Biomedizinisches Forschungszentrum). Human ESCs aggregate to form spheroid clumps of cells named embryoid bodies (EBs) when grown in suspension (14). The cells within the EBs express molecular markers that are specific for the three embryonic germ layers. EBs mature through the process of spontaneous differentiation and express molecular markers that are specific for differentiated cells. Dissociation of EBs and further plating differentiated cells as a monolayer has revealed many cell lineages (11). In addition, numerous growth factors are

used to facilitate the differentiation of human ESCs into specific cell types (196). Lavon et al. demonstrated that human ESCs are able to spontaneously differentiate into hepatic-like cells (197). In this study, N-glycosylation analysis was done for undifferentiated ESCs, definitive endoderm cells (early time point of differentiation) and hepatocyte-like cells (late time point of differentiation). The N-glycosylation pattern was profiled with MALDI-TOF-MS and each N-glycan structure was quantified. The cell-surface N-glycosylation of ESCs and hepatocyte-like cells were qualitatively and quantitatively significantly different from each other. ESCs had a high degree of high-mannose N-glycans, as judged from mass spectrometric data. Satoma et al. (156) studied the N-glycome of ESCs by MALDI-TOF-MS and their studies revealed that the five most abundant signals of the neutral N-glycan fraction were the high-mannose structures Man5, Man6, Man7, Man8 and Man9, which dominated the profile. However, Satoma et al. [15] did not specify how they prepared the cells prior to N-glycan detachment with PNGase F but it is very probably that they used membrane extracts of the cells. This would mean, that intracellular (glyco)proteins were included in the samples as well and this maybe the source of the high content of high-mannose N-glycans as discussed in section 3.1. In addition, Wearne et al. (198) used lectins to study the cell surface glycosylation of ESCs and day 12 Embryoid bodies (EBs) and revealed the presence of terminal and internally linked α -D-mannopyranosyl groups which indicated the presence of high-mannose structures. Furthermore An et al. (199) showed using mass spectrometry that cell membrane isolated from human embryonic SCs have high levels high-mannose N-glycans and that they present the most abundant glycans. In addition, they applied lectin staining to prove that the high-mannose structures are part of the cell surface glycosylation of ESCs [59].

Taken our results and the data from literature together, it is very probably that the high content of high-mannose N-glycans is characteristic for undifferentiated ESCs. In addition, the monoglucosylated H10N1 high-mannose-type N-glycan was detected in ESCs and it disappeared in hepatocyte-like cells. Others showed that the monoglucosylated H10N1 high-mannose-type N-glycan was found to be in human embryonic SCs as well (179). The presence of the monoglucosylated H10N1 may therefore be a typical feature of undifferentiated SCs. Studies have suggested that high-mannose N-glycans mediate cell-cell fusion, sperm-egg fusion, myoblast fusion and osteoclast formation (79, 80). Therefore, it is assumed that high-mannose N-glycans on human ESCs play a role in cellular binding and recognition. Studies have revealed that high-mannose N-glycans are predominantly on the cell surface of tumor cells when compared with normal cells (81, 82). To unravel the role of high-mannose glycans on ESCs may be helpful in the field of cancer biology, since tumor and SCs have some similar characteristics, such as the ability to self-renew, the expression of cell surface markers and the activation of signaling pathways (200).

N-glycans of human ESCs were predominantly neutral structures, a minor amount of sialylated N-glycans was detected as well. These findings are in line with the studies of Satoma et al. which revealed that neutral N-glycans comprised approximately two thirds of the pool of human ESCs [15]. Differentiation of ESCs into hepatocyte-like cells resulted in a completely different cell surface N-glycosylation pattern, which was qualitatively and quantitatively altered indicating a relationship between differentiation and cell surface N-glycosylation. Our results revealed that differentiation of ESCs into hepatocyte-like cells was accompanied by a significantly increased amount of biantennary complex-type N-glycans with and without Fuc residues as well as triantennary fucosylated structures. In addition, some complex N-glycans in ESCs were partially galactosylated but fully galactosylated structures were present as well. Exoglycosidase experiments and fragmentation analysis revealed the presence of Lewis^X epitopes in hepatocyte-like cells. In addition, core-fucosylation was verified in ESCs and hepatocyte-like cells. Studies by Satoma et al. [15] proved that the most common fucosylation was the $\alpha(1-6)$ -fucosylation, which was verified by NMR profiling. In addition, exoglycosidase experiments by Satoma et al. [15] indicated the presence of Lewis^X epitopes in ESCs. However, due to the low sample amount and intensity of the bifucosylated signals in the mass spectra of ESCs, it was not possible to sequence the structures enzymatically in our study.

According to our knowledge, N-glycosylation of hepatocytes derived from differentiation of ESCs is not reported in the literature but N-glycosylation studies dealing with the glycoproteins α -fetoprotein and transferrin expressed in hepatoma cells revealed $\alpha(1-6)$ -linked core-Fuc, suggesting that core-Fuc is a characteristic feature of hepatogenic cell lines (168, 169). In addition, N-glycan analysis of culture medium of chicken embryo hepatocytes revealed complex-type biantennary N-glycans with $\alpha(1-6)$ -linked Fuc (83). Moreover Noda et al. demonstrated that the $\alpha(1-6)$ -fucosyltransferase gene is highly expressed in hepatomas of rat models and hepatoma cell lines [39]. The GalNAc-GlcNAc motif was detected in hepatocyte-like cells. O-glycans of alpha-fetoprotein derived from hepatoma was shown to bear GalNAc as well (171), suggesting the specificity of the GalNAc epitope in hepatoma cells.

To sum up, the biantennary N-glycans H5N4, H5N4F1, H5N4F2, S1H5N4, S1H5N4F1 and S2H5N4F2 as well as the triantennary structures H6N5F1 and S1H6N5F1 were proposed as potential glycan-based biomarkers for hepatocyte-like cells and maybe used to monitor the loss of the SC status of ESCs and to discriminate between ESCs and hepatocyte-like cells.

3.4 Conclusion

In conclusion, several studies revealed that the glycosylation of SCs, such as pluripotent embryonic (176, 179, 201, 202) or multipotent adult SCs (151, 177), is changing during the process of differentiation. Most of these studies rely on staining of carbohydrates with lectins and antibodies in combination with techniques like FACS, western blotting, microarray and immunohistochemistry (203, 204). However, the specificity of lectins and antibodies is limited, which might lead to the loss of important structural information. MALDI-TOF-MS is a powerful tool to study the N-glycome of SCs and to search for differentiation associated glycan structures (144, 177). The N-glycosylation pattern of bone marrow MSCs and their adipogenically, chondrogenically as well as osteogenically differentiated progeny was investigated and verified with MALDI-TOF-MS in combination with exoglycosidase digestions. In addition, the cell surface N-glycosylation pattern of human ESCs before and after their differentiation into hepatocyte-like cells was profiled. The results showed that the N-glycome of adipogenically differentiated human MSCs was clearly less fucosylated and branched than the one of undifferentiated human MSCs. N-glycans like H6N5F1 and H7N6F1 were proposed as candidate MSC markers for undifferentiated MSCs and N-glycans like H3N4F1 and H5N4F3 as potential markers for adipogenically differentiated MSCs. In addition, N-glycans that are potential candidate markers to discriminate between 5 days and 15 days adipogenically differentiated MSCs were found. In the context of soft tissue engineering, markers are important to verify culture homogeneity of MSCs and their adipogenically differentiated progeny, to monitor the progress of MSC development during adipogenesis and to analyse quality parameter like cell distribution in new formed adipose tissue.

The N-glycosylation profile of chondrogenically differentiated MSCs contained more high-mannose and less complex N-glycans when the ECM was present. Differentiation was accompanied with an increased amount of biantennary N-glycans when the ECM was absent. In both cases, cell surface N-glycosylation of chondrogenically differentiated cells was less branched than the one of undifferentiated MSCs. N-glycans were found to contain core-linked Fuc as well as Lewis^x epitopes. The triantennary N-glycans H6N5F1 and S1H6N5F1 as well as tetraantennary structures H7N6F1, S1H7N6F1 and S2H7N6F1 were proposed as glycan-based biomarkers for undifferentiated MSCs. In addition, the biantennary structures S1H5N4F2 and S2H5N4F1 were proposed as potential glycan-based biomarkers for day 28 chondrogenically differentiated cells without ECM and the biantennary N-glycans H3N4F1, H4N4F1 and H4N4F2 as glycan-based biomarkers for day 28 chondrogenically differentiated cells with ECM.

Osteogenic differentiation of MSCs was accompanied by an increased amount of biantennary structures. In addition, cell surface N-glycosylation was less branched in differentiated MSCs. In contrast, the amount of fucosylated structures increased which contained mainly core-linked Fuc. The biantennary structures H4N4F2, H5N4, H5N4F1, S1H5N4 and S1H5N4F1 were proposed as potential glycan-based biomarkers for osteogenically differentiated cells.

These results are essential to study the process of osteogenic and chondrogenic differentiation and the function of N-glycans during these events. Glycan-based biomarkers may help to identify the differentiation status of MSCs in the field of regenerative medicine as well as to identify and isolate pure MSCs populations.

ESCs were differentiated into hepatocyte-like cells. The N-glycosylation profiles were qualitatively and quantitatively significantly different. ESCs contained a high amount of high-mannose N-glycans. In contrast, complex-type N-glycans such as biantennary and triantennary N-glycans were dominant in hepatocyte-like cells and fully-galactosylated structures were much more abundant than in undifferentiated ESCs. In addition, the GalNAc epitope was detected in hepatocyte-like cells. The biantennary N-glycans H5N4, H5N4F1, H5N4F2, S1H5N4, S1H5N4F1 and S2H5N4F2 as well as the triantennary structures H6N5F1 and S1H6N5F1 were proposed as potential glycan-based biomarkers for hepatocyte-like cells. These results may help to study the mechanisms essential for human development as well as the participation of N-glycans during this event.

Mass spectrometry is a useful tool to gain the exact structural information on glycosylation but one main disadvantage is that it requires lot of material to be used in the frame of routine quality control. Therefore, in future studies, it is an aim to generate specific antibodies that detect development stage specific N-glycans. In addition the obtained mass spectrometry results could be translated into a lectin assay, which allows an easier detection of N-glycans. Potential candidates are *Phaseolus vulgaris* Leukoagglutinin and *Datura stramonium* Agglutinin as they recognise specifically galactosylated tri- and tetraantennary N-glycans. Moreover, the next step to identify SC biomarkers is to investigate the proteins carrying the identified glycan-based biomarkers. This can be achieved by searching for the core peptides bearing a N-glycosylation site with the respective N-glycan structure for example by liquid chromatography coupled to a mass spectrometer (LC-ESI-MS). The nanoLC-ESI-MS technique requires small sample amounts and enables a chromatographic separation of peptides followed by mass detection, which is essential to unravel the target glycopeptides. To conclude, our results show that the shift of cell surface N-glycosylation during differentiation is a powerful SCs biomarker.

4 Material and Methods

4.1 Devices

4.1.1 Electrophoresis

- Blot-apparatus Mini Trans-Blot (Bio-Rad, München, Germany)
- Gel-scanner GS-800, *Calibrated Densitometer* (Bio-Rad, München, Germany)
- Gel-dryer mgD-5040 (VWR, Darmstadt, Germany)
- Power supply PowerPac TM 30000 (Bio-Rad, München, Germany)
- Vertical-electrophoresis system, Mini-Protean 3 System, Multi-Casting Chamber (Bio-Rad, München, Germany)

4.1.2 Cell culture

- Gas incubator CB (Binder, Tuttlingen, Germany)
- Incubator shaker Certomat BS-1 (Sartorius, Göttingen, Germany)
- Light microscope Leica DMIL (Leica, Wetzlar, Germany)
- Membrane vacuum pump (Vacuubrand, Wertheim, Germany)
- Sterile work bench HERAsafe KS 12 (Heraeus, Hanau, Germany)

4.1.3 Centrifuges

- Mini-fuge (VWR, Darmstadt, Germany)
- Table-centrifuge 5402 (Eppendorf, Hamburg, Germany)
- Ultra-centrifuge J2-21 (Beckman Coulter, Fullerton, USA)
- Vacuum-centrifuge CentriVac (Heraeus, Hanau, Germany)
- Vacuum-centrifuge Univapo 150 ECH (Uniequip, Planegg, Germany)
- Cell-centrifuge Multifuge 3S-R (Heraeus, Hanau, Germany)

4.1.4 Other devices

- Analysis scale (Sartorius, Göttingen, Germany)
- Dionex ISC-3000 (Dionex, Idstein, Germany)
- Heat block Digi-Block (Laboratory Devices Inc., USA)
- Horizontal mixer Unimax 1000 (Heidolph Instruments GmbH, Schwabach, Germany)
- Incubation hood Unimax 1010 (Heidolph, Kelheim, Germany)
- Incubator 1000 (Dionex, Idstein, Germany)

- Cooling trap Unicryo MC2 x 21-60 °C (Uniequip, Planegg, Germany)
- Laser-induced capillary electrophoresis CE-LIF P/ACE™ MDQ System (Beckman Coulter, Fullerton, CA, USA)
- MALDI-TOF/TOF mass spectrometer Ultraflex III with a *smartbeam-II*™ Laser (Bruker Daltonics, Bremen, Germany)
- Microplate photometer Infinite M200 (Tecan, Männedorf, Switzerland)
- pH meter pH211 (Hanna Instruments, Kehl am Rhein, Germany)
- Vacuum concentrator (Heraeus, Düsseldorf, Germany)
- Thermomixer comfort (Eppendorf, Hamburg, Germany)
- Ultrasonic bath, Sonorex TK52 (Bandelin, Berlin, Germany)
- Vacuum pump (Vacuubrand, Wertheim, Germany)
- Vortex Genie 2 (Scientific Industries, Bohemia, USA)
- Water preparation system MilliQ Plus (Millipore, Neu-Ilseburg, Germany)
- HPLC, Summit HPLC (Dionex, Idstein, Germany)

4.2 Consumables

4.2.1 Chemicals

- 1,4-Dithioerythriol (DTE) (Sigma-Aldrich, Steinheim, Germany)
- super 2,5-Dihydroxybenzoic acid (sDHB) (Sigma-Aldrich, Steinheim, Germany)
- 2-Aminobenzamid (2AB) (Sigma-Aldrich, Steinheim, Germany)
- 2-Mercaptoethanol (Roth, Karlsruhe, Germany)
- 6-Aza-2-thiothymin (ATT) (Sigma-Aldrich, Steinheim, Germany)
- 8-Aminopyrene-1,3,6-trisulfonic acid trisodium salt (APTS) (Sigma-Aldrich, Steinheim, Germany)
- α -Cyano-4-hydroxycinnamic acid (ACCA) (Sigma-Aldrich, Steinheim, Germany)
- Acetonitrile (ACN) (VWR, Darmstadt, Germany)
- Acetone (Sigma-Aldrich, Steinheim, Germany)
- Acetic acid (Roth, Karlsruhe, Germany)
- Acrylamide-bisacrylamide solution 30 % (37,5:1) (Merck, Darmstadt, Germany)
- Ammonia solution >25 % (Merck, Darmstadt, Germany)
- Ammonium persulfate (APS) (Bio-Rad, München, Germany)
- Bisacrylamide (AppliChem, Darmstadt, Germany)
- Bromophenol blue (AppliChem, Darmstadt, Germany)
- Calcium chloride (Roth, Karlsruhe, Germany)

- Chloroform (Merck, Darmsadt, Germany)
- Coomassie *Biosafe* (Bio-Rad, München, Germany)
- Dimethyl sulfoxide (DMSO) (Sigma-Aldrich, Steinheim, Germany)
- Formic acid (FA) (Sigma-Aldrich, Steinheim, Germany)
- Glucose (Fluka, Sigma, Steinheim, Germany)
- Glycerine (Glycerol) (Fluka, Buchs, Switzerland)
- Iodacetamide (Sigma-Aldrich, Steinheim, Germany)
- Potassium chloride (Roth, Karlsruhe, Germany)
- Methyl iodide (Sigma-Aldrich, Steinheim, Germany)
- Potassium acetate (Sigma-Aldrich, Steinheim, Germany)
- Potassium hydrogenphosphate (Merck, Darmstadt, Germany)
- Potassium hydroxide pads (Merck, Darmsadt, Germany)
- Sodium dodecylsulfate (SDS) (Serva, Heidelberg, Germany)
- Sodium hydroxide (Sigma-Aldrich, Steinheim, Germany)
- Sodium cyanoborohydride (Fluka/ Sigma-Aldrich, Steinheim, Germany)
- N,N,N',N'-Tetramethylethylenediamine (TEMED) (Merck, Darmstadt, Germany)
- Nonidet P-40 (Roche, Mannheim, Germany)
- Polyethylenoxid (PEO), molecular weight ~300 kDa (Sigma-Aldrich, Steinheim, Germany)
- Tetrahydrofuran (THF) (Sigma-Aldrich, Steinheim, Germany)
- Trifluoroacetic acid (TFA) (Merck, Darmstadt, Germany)
- TRIS (Base) (Roth, Karlsruhe, Germany)
- Trypan blue (Biochrom, Berlin, Germany)

4.2.2 Enzymes

- Endo H from *Escherichia coli* (Roche, Mannheim, Germany)
- PNGase F from *Flavobacterium meningosepticum* (Roche, Mannheim, Germany)
- Trypsin from bovine pancreas (Sigma-Aldrich, Steinheim, Germany)
- *Arthrobacter ureafaciens* neuraminidase (Roche Applied Science, Indianapolis, IN, USA)
- β (1-4) galactosidase from *Streptococcus pneumoniae* (Prozyme, CA, USA)
- β -N-acetylhexosaminidase recombinant from *S. pneumoniae* and expressed in *E. coli* (Prozyme, CA, USA)
- α -mannosidase from *Canavalia ensiformis* (Jack bean, Sigma-Aldrich, Germany)
- Bovine testes β -galactosidase (Prozyme, CA, USA)

- Bovine kidney α (1-2,3,4,6) fucosidase (Prozyme, CA, USA)
- β (1–3,6) galactosidase from *Xanthomonas manihotis* (Prozyme, CA, USA)
- Almond meal α (1–3,4) fucosidase (Prozyme, CA, USA)

4.2.3 Standards

- RNase B from bovine Pancreas (Sigma-Aldrich, Steinheim, Germany)
- Dextran hydrolysate (DH) (Oxford, UK)
- Protein standard *Precision Plus All Blue* (Bio-Rad, München, Germany)
- Internal maltose standard (Sigma-Aldrich, Steinheim, Germany)

4.2.4 Other consumables

- BCA protein assay (VWR, Darmstadt, Germany)
- C18 Reversed-Phase Extra-Clean Column (Grace Alltech, Deerfield, IL, USA)
- Carbograph Extra-Clean Column (Grace Alltech, Deerfield, IL, USA)
- Calbiosorb Adsorbent (Calbiochem, Darmstadt, Germany)
- Filter tips (Greiner Bio-One, Frickenhausen, Germany)
- Sterilfilter 0.2 μ m (VWR, Darmstadt, Germany)

4.2.5 Cell culture

- Dulbecco's Modified Eagle Medium (DMEM) (PAA, Pasching, Austria)
- Hams F12 (PAA, Pasching, Austria)
- RPMI (PAA, Pasching, Austria)
- L-glutamine (PAA, Pasching, Austria)
- Sodium pyruvate (PAA, Pasching, Austria)
- Phosphate-buffered saline (PBS) (PAA, Pasching, Austria)
- Penicillin (Biochrom AG, Berlin, Germany)
- Streptomycin (Biochrom AG, Berlin, Germany)
- Collagen A (Biochrom AG, Berlin, Germany)
- Fetal calf serum (FCS) (Biochrom AG, Berlin, Germany)
- Adenovirus Expression Medium (AEM) (Gibco, California, USA)
- Dimethyl sulfoxide (DMSO) (AppliChem, Darmstadt, Germany)
- Trypan blue (Biochrom AG, Berlin, Germany)
- Trypsin-EDTA (PAA, Pasching, Austria)

4.2.6 Cell lines

HEK-293, CHO-K1 and Hep G2 and cells were purchased from DSMZ (Braunschweig, Germany). AGE1.HN cells were a generous gift from ProBioGen AG (Berlin, Germany). MSCs were differentiated into adipogenic, chondrogenic and osteogenic direction by the working group of Dr. Jochen Ringe (Charité-Universitätsmedizin Berlin, BCRT, Labor für Tissue Engineering/ Klinik für Rheumatologie). ESCs were differentiated into hepatocyte-like cells by the working group of Dr. Katrin Zeilinger (Charité-Universitätsmedizin Berlin, BCRT, Biomedizinisches Forschungszentrum).

4.3 Cell biological methods

Cultivation of eukaryotic cells was done in a culture incubator at a temperature of 37 °C under 5 % CO₂ and 95 % humidity. All steps were done under a sterile bench. All materials used were sterile packed or sterilised prior to use at 120 °C for 20 min in water vapor. Cell counting was done in a Neubauer-counting chamber and vitality was tested using trypan blue staining.

4.4 Cell culture

4.4.1 Cell culture of HEK 293, CHO-K1, AGE1.HN and Hep G2

HEK 293 cells were cultivated in Dulbecco's Modified Eagle's Medium (DMEM) containing glucose (4.5 g/l), 10 % fetal calf serum (FCS), penicillin (100 U/mL), streptomycin (100 µg/mL), L-glutamine (200 mM) and sodium pyruvate (1 mM). AGE1.HN cells were cultured in adenovirus expression medium (AEM) containing penicillin (100 U/mL), streptomycin (100 µg/mL) and L-glutamine (2 mM). CHO-K1 cells were cultured in Ham's F12 containing 10 % FCS, penicillin (100 U/mL), streptomycin (100 µg/mL) and sodium pyruvate (1 mM). Hep G2 cells were cultured in RPMI containing 10 % FCS, penicillin (100 U/mL), streptomycin (100 µg/mL), L-glutamine (2 mM), sodium pyruvate (1 mM) and 0.32 % glucose. The adherent cell lines HEK 293, CHO-K1 and Hep G2 were cultured in 60.1 cm² dishes. Cell culture dishes used for Hep G2 cultivation were first incubated with 5 mL of 10 % collagen A in phosphate buffered saline (PBS) containing CaCl₂ (9 mM) and MgCl₂ (5 mM) for 30 min at 4 °C. They were subsequently washed twice with PBS and plated with Hep G2 cells. AGE1.HN suspension cells were cultured in 250 mL flasks. The medium was changed twice per week and adherent cell lines (HEK 293, CHO-K1 and Hep G2) were cultured until about 90 % confluence was reached.

4.4.2 Generation of cryocultures

For cell storage, about 5×10^6 cells were pelleted from the exponential growth phase by centrifugation (5 min, 900 rpm) and stored in 1 ml freezing media (90 % FCS, 10 % DMSO). Freezing was performed gradually (-20 °C, -80 °C, liquid nitrogen). Cell thawing was done at room temperature, after which cells were placed in 10 ml media, centrifuged (5 min, 900 rpm) and resuspended in medium.

4.5 Protein biochemical methods

4.5.1 Isolation of cell membrane glycoproteins

Approximately 4×10^6 cells per cell type were harvested for the isolation of cell membrane glycoproteins. AGE1.HN suspension cells were harvested, centrifuged for 15 min at 420 g, washed four times with PBS, resuspended in 100 μ l PBS and stored at -80 °C until the time of analysis. The adherent cell lines HEK 293, CHO-K1 and Hep G2 were washed with ice-cold PBS in the cell culture dish, suspended in PBS, centrifuged for 15 min at 420 g and additionally washed twice with PBS. Cells were subsequently resuspended in 100 μ l PBS and stored at -80 °C until the time of analysis. Cell membrane extraction was performed according to Lieke et al. (199) with slight modifications. Briefly, cell pellets were thawed and suspended in 2 mL of homogenisation buffer consisting of KCl (150 mM), CaCl_2 (2 mM), NaHCO_3 (1 mM) and protease inhibitors (complete EDTA-free, Roche Applied Science, Mannheim, Germany). Cell lysis was then performed by 30 strokes through a syringe having a narrow needle, and 20 mL of NaHCO_3 (1 mM) was subsequently added. The lysate was centrifuged at 1400 g for 30 min at 4°C and the pellet was discarded. The supernatant, which contains cellular membranes, was then collected and centrifuged at 48.000 g for 20 min at 4°C. The resulting pellet, which contains glycoproteins and other membrane proteins, was washed three times with 300 μ l of water (26.000 g, 15 min, 4°C). The pellet was resuspended in water, methanol and chloroform (3:8:4), and incubated for 30 min on ice in order to separate lipids from membrane glycoproteins. Proteins were finally precipitated by centrifugation at 26,000 g for 20 min at 4°C. The supernatant was discarded and proteins were washed twice with 400 μ l of ethanol (26.000 g, 10 min, 4°C) and then resuspended in 300 μ l $\text{NaH}_2\text{PO}_4/\text{Na}_2\text{HPO}_4$ buffer (20 mM), pH 7.0, containing 2 % SDS and 2 % NP-40 (Calbiochem). Detergents were removed overnight using Calbiosorb™ adsorbent beads (Merck; Darmstadt, Germany) and the supernatant was assayed for protein concentration by the bicinchoninic acid (BCA) assay (Thermo Scientific) and finally lyophilised.

4.5.2 Protein concentration determination by BCA assay

The BCA (bicinchoninic acid) assay was used to determine the protein concentration of cell membrane (glyco)proteins. The reduction of Cu^{2+} takes place in basic solution through the side chain of cysteine (Cys), cystin, tyrosin (Tyr), Trp and the peptide bond in which the Cu^+ ions generates with BCA a purple complex BCA (205, 206). This complex can be detected calorimetrically at 562 nm. 10 μl of the protein sample are mixed with 100 μl freshly prepared BCA reagent in a 96 well microplate and incubated for 30 min at 37 °C under slight agitation. The absorption is measured in a micro plate photometer at 562 nm and the protein concentration is determined with the help of a BSA standard curve.

4.5.3 SDS polyacrylamide gel electrophoresis (SDS-PAGE)

4.5.3.1 Preparation of stacking and separating gels

12 % gels were prepared for protein separation accorind to Laemmli (207). First, the separation gel was prepared and poured between the two glass plates. The separation gel was composed of 4.2 ml water, 1.7 ml separation gel buffer (1.5 M Tris/ HCl pH 8.8), 0.1 ml 10 % (w/v) SDS, 4 ml of a 30 % acrylamide/ 0.8 % bisacrylamide solution, 10 μl TEMED and 100 μl 10 % APS. For an optimal resolving line, the layer of the resolving gel was covered with water. When the gel was polymerised, the water layer was discarded. The stacking gel was poured above the separation gel and was composed of 2.95 ml water, 1.25 ml separation gel buffer (0.5 M Tris/HCl pH 6.8), 50 μl 10 % (w/v) SDS, 650 μl acrylamide-bisacrylamide (30 % turnkey solution), 5 μl TEMED and 50 μl 10 % (w/v) APS. A gel comb was inserted between the glass disks to create gel pockets and was taken out carefully after the polymerisation of the stacking gel. Gels were stored at 4 °C for maximum one week before being used.

4.5.3.2 Sample preparation and application on the gel

The SDS gel is positioned into the gel cassette and the gel chamber is filled with 1 x SDS running buffer (10 x SDS: 30.3 g/L tris, 144.1 g/L glycin, 10 g/L SDS, adjusted to 1 l with water). The gel pockets and the two electrodes should be thereby covered with the running buffer. 5 μl of SDS non reductive sample buffer (5.44 ml 1M Tris/HCl pH 6.8, 1.74 g SDS, 50 % (v/v) glycerol, 20 ml water, 0.015 % (w/v) bromphenol blue) was added to 15 μl of each sample, dissolved in 1x PBS. The reductive sample buffer contained additionally 8 % (v/v) 2-mercaptoethanol. Samples were heated at 99 °C for 5 min, cooled down to room temperature and centrifuged. Sample (20 μl) or protein standards (3 μl) were transferred to

the gel-pockets. The gel-cassette was connected to a power supply (BioRad Power PAC 3000) and the amperage was set to 20 mA per gel. The maximum voltage was set to 200V.

4.5.4 Coomassie staining

Coomassie brilliant blue is a triphenylmethane dye, which is able to stain proteins unspecifically by attachment to basic side chains of amino acids within the protein. Gels were first washed three times with water. After discarding the water, the coomassie staining solution was added to the gels and shaken for 1 h at room temperature. Afterwards, the staining solution was discarded and the gels were shaken overnight in water.

4.6 Analytical methods for glycan analysis

4.6.1 Tryptic digestion of cell membrane (glyco)proteins

Membrane glycoproteins were dissolved in 300 μ l of $\text{NaH}_2\text{PO}_4/\text{Na}_2\text{HPO}_4$ buffer (20 mM, pH 7.0). Trypsin (20 μ l, 1 μ g/ μ l) was then added and samples were incubated for 6 h at 37 °C. A freshly prepared aliquot of trypsin (20 μ l, 1 μ g/ μ l) was added to the mixture and samples were digested overnight at 37 °C.

4.6.2 Release of N-glycans from cell membrane glycoproteins by PNGase F

After trypsin deactivation (99 °C, 5 min), 1.5 U of peptide-N4-(N-acetyl- β -glucosaminyl) asparagine amidase F (PNGase F) from *Flavobacterium meningosepticum* (Roche Applied Science, Mannheim, Germany) was added to the glycopeptide samples and digestions were performed overnight at 37 °C. Digestions were continued for 8 h at 37 °C by addition of a second aliquot of 1 U PNGase F. Released N-glycans were isolated from the peptide moieties using C18 Extract-Clean™ cartridges. N-glycans were then desalted using carbograph Extract-Clean™ columns and evaporated to dryness.

4.6.3 Release of N-glycans from cell membrane (glyco)proteins by Endo H followed by PNGase F

After trypsin deactivation (99°C, 5 min), N-glycans of high-mannose- and hybrid-type were detached from glycopeptides using 7 mU endo- β -N-acetylglucosaminidase H (Endo H) recombinantly expressed in *Escherichia coli* (Roche Applied Science) and digestions were carried out in 200 μ l of 25 mM $\text{NaH}_2\text{PO}_4/\text{Na}_2\text{HPO}_4$ buffer at pH 5.6 and overnight at 37°C. Released N-glycans were isolated from the peptide moiety using C18 Extract-Clean™ cartridges (Alltech) and the N-glycan as well as the remaining glycopeptide fractions were

eluted and collected. N-Glycans were desalted with carbograph Extract-Clean™ columns (Alltech) and evaporated to dryness. Glycopeptides were also evaporated to dryness, dissolved in 300 µl of 20 mM NaH₂PO₄/Na₂HPO₄ (pH 7.0), and 1.5 U peptide-N4-(N-acetyl-β-glucosaminyl) asparagine amidase F (PNGase F, Roche Applied Science) from *Flavobacterium meningosepticum* expressed in *Escherichia coli* were added to this glycopeptide solution for 8 h at 37°C in order to detach complex-type N-glycans. Digestions were continued overnight by addition of a second aliquot of 1 U PNGase F. Released N-glycans were isolated from the peptide moieties using C18 Extract-Clean™ cartridges. N-Glycans were then desalted using carbograph Extract-Clean™ columns and evaporated to dryness.

4.6.4 Enzymatic release and isolation of cell surface N-glycans

Approximately 4x10⁶ cells were used for the digestion of cell surface (glyco)proteins. Cells were harvested and washed four times with PBS (15 min at 600 rpm). The resulting cell pellet was resuspended in 500 µl cold PBS containing trypsin (2.5 mg/mL) and shaken at 150 rpm for 15 min at 37 °C. Samples were then centrifuged at 15000 rpm and 4 °C for 15 min, and the supernatant, containing cell surface glycopeptides, was separated from the pellet. Trypsin was then deactivated at 99 °C for 5 min. Tryptic glycopeptides were digested overnight at 37° C with 0.5 U of PNGase F. Released N-glycans were isolated from the peptide moieties using C18 Extract-Clean™ cartridges (Alltech, Deerfield, IL). N-Glycans were subsequently desalted using carbograph Extract-Clean™ columns (Alltech, Deerfield, IL) and evaporated to dryness.

4.6.5 Purification of N-glycans

4.6.5.1 Calbiosorb

Calbiosorb was used to remove detergents that were used to solubilise membrane (glyco)proteins since it is able to adsorb organic compounds. Calbiosorb beads were carefully washed with water. Then the beads were suspended in water (beads:water = 1:2) and about 200 µl of the beads suspension were added to the samples. Samples were shaken for 5 min at room temperature and the supernatant was placed in a new vial.

4.6.5.2 C18 reversed phase chromatography

The hydrophobic stationary phase C18 is able to bind proteins and peptides reversibly. In contrast, free glycans don't bind to the column material. First, samples were acidified with 1

% TFA to a final pH value < 4. Columns were equilibrated with 3 x 400 µl of 80 % ACN in 0.1 % TFA followed by 0.1 % TFA in water, respectively. Samples were applied and columns were washed with 3 x 400 µl of 0.1 % TFA in water. The flow-through, which contained free glycans, was collected. When necessary, peptides were eluted from the C18 column with 3 x 400 µl of 50 % ACN in 0.1 % TFA. Samples were either dried under vacuum (peptides) or further desalted on Carbograph columns (glycans).

4.6.5.3 Carbograph

Carbograph is able to bind proteins and peptides irreversibly and glycans reversibly. Thus, free glycans can be separated from proteins or peptides as well as desalted. Columns were equilibrated with 3 x 400 µl of 80 % ACN in 0.1 % TFA followed by 0.1 % TFA in water, respectively. Glycan samples derived from C18 purification were directly applied to the carbograph column. Glycan samples resulting from enzymatic digestions were acidified with 1 % TFA to a final pH value < 4 prior to application on the carbograph column. After application of the samples, columns were washed with 3 x 400 µl of 0.1 % TFA in water in order to desalt glycans. Glycans were then eluted with 3 x 400 µl of 25 % ACN in 0.1 % TFA. Samples were dried under vacuum.

4.6.5.4 C18 reversed phase chromatography of permethylated N-glycans

When necessary, permethylated N-glycans were further purified with C18 reversed phase cartridges. The hydrophobic material is able to bind the non-polar permethylated N-glycans. C18 columns were equilibrated with 3 x 400 µl of methanol followed by water, respectively. Samples were dissolved in 200 µl methanol and applied to the column. They were then washed with 3 x 400 µl water followed by 10 % ACN, respectively. Glycans were eluted with 80 % ACN and evaporated to dryness.

4.6.5.5 Self-made graphite micro column

20 µl filter tips equipped with a filter were manually filled with graphite. The chromatographic principle is the same as carbograph but with smaller volumes. Filter tips were placed in a table centrifuge and equilibrated with 3 x 40 µl of 80 % ACN in 0.1 % TFA followed by 0.1 % TFA, respectively. The acidified samples (pH < 4) were applied to the cartridge. After centrifugation, bond glycans were washed with 3 x 40 µl 0.1 % TFA and finally eluted with 3 x 40 µl of 25 % ACN in 0.1% TFA. APTS-labeled glycans were eluted with 50 % ACN in 0.1 % TFA and 2AB-labeled glycans with 80 % ACN in 0.1 % TFA. Sample were evaporated to dryness.

4.6.5.6 Lyophilisation of samples

In order to minimise the volume of samples after purification or for buffer exchange prior to exoglycosidase digestions, samples were dried under vacuum and centrifugation.

4.6.6 Exoglycosidase digestions of N-glycans

Exoglycosidase digestions were performed to verify the monosaccharide types and glycosidic linkages.

Undifferentiated and adipogenically differentiated MSCs: High-mannose- and hybrid-type N-glycans derived after Endo H digestion were dissolved in 50 mM sodium acetate (pH 5.0, Merck) and digested for 18 h at 37°C using the following exoglycosidases consecutively with different concentrations: 3 U/ml *Arthrobacter ureafaciens* neuraminidase (Roche Applied Science), 0.2 U/ml β (1-4) galactosidase from *Streptococcus pneumoniae* (Prozyme), 4 U/ml β -N-acetylhexosaminidase recombinant from *S. pneumoniae* and expressed in *E. coli* (Prozyme), and 20 U/ml α -mannosidase from *Canavalia ensiformis* (Jack bean) (Sigma-Aldrich). Complex-type N-glycans were also dissolved in 50 mM sodium acetate (pH 5.0) and digested for 18 h at 37°C using the following exoglycosidases consecutively with different concentrations: 3 U/ml *A. ureafaciens* neuraminidase, 1 U/ml bovine testes β -galactosidase, 6 U/ml β -N-acetylhexosaminidase recombinant from *S. pneumoniae* and expressed in *E. coli*, and to determine core-fucosylated structures, 2.3 U/ml bovine kidney α (1-2,3,4,6) fucosidase (all Prozyme). After inhibition at 95°C for 5 min, samples were permethylated and lyophilised.

HEK 293, CHO-K1, AGE1.HN, Hep G2, undifferentiated and chondrogenically differentiated MSCs, hepatocyte-like cells: N-glycans, dissolved in sodium acetate (100 mM, pH 5.0), were digested for 18 h at 37 °C using different exoglycosidases with the following concentrations: 3 U/mL *Arthrobacter ureafaciens* neuraminidase (EC 3.2.1.18, Roche Applied Science, Indianapolis, IN); 0.8 U/mL β (1–4) galactosidase from *Streptococcus pneumoniae* (GKX-5014, Prozyme); 0.75 U/mL bovine kidney α (1–2,3,4,6) fucosidase (GKX-5006, Prozyme); 5.4 mU/mL almond meal α (1–3,4) fucosidase (GKX-5019, Prozyme); 12 U/mL β -N-acetylhexosaminidase, recombinant from *Streptococcus pneumoniae*, expressed in *E. coli* (GKX-80050, Prozyme, CA). After inhibition at 95 °C for 5 min, samples were desalted on self-made graphite micro-columns and lyophilised. The presence of Lewis^X epitopes and core-fucosylated structures was shown using the following sequence of digestions: β (1–4) galactosidase, β (1–3,6) galactosidase, α (1–3,4) fucosidase, β (1–4) galactosidase, and bovine kidney α (1-2,3,4,6) fucosidase.

4.6.7 Desialylation of N-glycans

Dried N-glycans were dissolved in 40 μ l of a acetic acid solution (0.5 M) and incubated at 80 °C for 3 h. Desialylated N-glycans were then desalted on self-made graphite micro-columns.

4.6.8 Derivatisation of N-glycans

4.6.8.1 Permethylation

Permethylation was performed in DMSO using sodium hydroxide and methyl iodide as described elsewhere (208, 209). Chloroform was then added and the chloroform phase was washed with water until the water phase became neutral. The chloroform phase was finally evaporated under reduced pressure and samples were dissolved in 75 % aqueous acetonitrile for MALDI-TOF measurements. Permethylated cell surface N-glycans were further desalted with C18 Extract-Clean™ cartridges.

4.6.8.2 2AB-labeling

2AB-labeling of N-glycans was performed as described elsewhere (58) (59). Dried N-glycans were incubated in 8 μ l of 2-aminobenzamide / sodium cyanoborohydride (0.35 M / 1 M) in acetic acid-dimethyl sulfoxide (3:7 v/v) for 2 h at 65 °C. Samples were then lyophilised and desalted on self-made graphite micro-columns.

4.6.8.3 APTS-labeling

100 pmol of maltose was added as internal standard to each of the desialylated N-glycan samples, which were then dried under vacuum. APTS was dissolved in a 15 % acetic acid solution to give a concentration of 100 mg/ml and then diluted with THF (1:1 v/v). 8-Aminopyrene-1,3,6-trisulfonic acid (APTS) was added in excess to the sample in order to achieve a complete reaction. Samples were dissolved in 3 μ l of a THF / acetic acid solution (1:1 v/v). Then, 0.5 μ l of 1M sodium cyanoborohydride solution in THF and 0.5 μ l of the APTS solution were added to the samples and incubated at 37 °C overnight. Samples were then diluted with 21 μ l water and stored at -20 °C.

4.6.9 MALDI-TOF-MS

N-glycans were analysed on an Ultraflex III TOF/TOF mass spectrometer (Bruker Daltonics, Bremen, Germany) equipped with a smartbeam-II™ laser and a LIFT-MS/MS facility. After a delayed extraction time of 10 ns, the ions were accelerated with a 25 kV voltage.

Measurements were carried out in the positive-ionization mode. External calibration was performed using a dextran ladder. Samples (0.5 μ l) were mixed on a ground steel target in a 1:1 ratio (v/v) with the matrix consisting of super-dihydroxybenzoic acid (10 mg/mL, Sigma-Aldrich) dissolved in 10 % acetonitrile. The acquisition of mass spectra was done with the software Flex Control (version 3.0, Bruker Daltonics) and data processing and annotation was performed with Flex Analysis (version 3.0, Bruker Daltonics). Spectra were evaluated using Glyco-Peakfinder (online version, EUROCarbDB) and assigned N-glycan structures were built with the GlycoWorkbench software (version 1.1, EUROCarbDB) (91, 210). Mass tolerance for precursor ions was set to 100 ppm. Individual spectra were accepted based on the signal to noise ratio of each signal, which was about 10 for the signal with the smallest intensity and about 9000 for the signal with the highest intensity. Mass peaks with an intensity below 0.01 % were not considered. MALDI-TOF/TOF fragmentation was performed to verify the monosaccharide type and linkage. The mass tolerance for fragment ions was about 0.2 Da. Polyhexose contamination, when present, was negligible and excluded from the quantification.

4.6.10 CE-LIF

The detection of N-glycans in CE was done with laser-induced fluorescence (λ_{exc} 488, λ_{em} 520). APTS-labeled samples (5 μ l) were diluted with 20 μ l of water and injected into the CE-LIF. Separations were achieved with reversed polarity on a polyvinyl alcohol (PVA)-coated capillary (50 nm id, 40 cm effective length to the window, 50.2 cm total length). Glycans were separated in an acetate buffer (25mM, pH 4.75) with 0.4 % polyethylenoxide (PEO). The capillary was first rinsed for 2 min and 30 psi with buffer. Then the sample was injected (0.5 psi, 4s) and finally separated at 30 kV and a runtime of 30 min. APTS-labeled maltose was used as the internal standard to normalise the detected migration times.

4.6.11 Sialic acid determination using HPLC

Enzymatically released and purified cell surface N-glycans were subjected to sialic acid analysis (211). Sialic acids were hydrolysed in 3 M acetic acid for 3 h at 80 °C. After the reaction, samples were neutralised with 25 % ammonia and then evaporated. Samples were dissolved in 20 μ l of water. The internal standard, 2-keto-3-deoxy-nonulosonic acid (KDN), was added and sialic acids were specifically labeled with 1,2-diamino-4,5-methylene dioxybenzene (DMB, Sigma-Aldrich, St. Louis, MO) for 2.5 h at 56 °C using 100 μ l of a solution containing 7 mM DMB, 18 mM sodium hydrosulfite, 0.75 M β -mercaptoethanol. The reaction products were analysed using RP-HPLC on a Gemini C18 column (4.6 mm x 250

mm, 5 μ , Phenomemex, Torrance, CA) by applying a gradient of water (A) and acetonitrile/methanol (6/4; v/v; B) at 0.5 mL/min. Elution started with 17 % B for 10 min followed by an increase to 35 % B in 60 min. Labeled sialic acids were monitored by fluorescence detection (λ_{exc} 373 nm, λ_{em} 448 nm).

4.7 Statistical analysis

Data were expressed as mean and standard error of mean. Student t-test was performed with SigmaStat software (Systat), to test expressed genes for their statistical significance, ($*p<0.05$, $**p<0.01$, $***p<0.001$). Mann-Whitney U test was used to assess statistically significant changes of N-glycan structures during differentiation using SPSS 18.0 software (SPSS), ($*p\leq 0.05$).

4.8 Softwares

- 32 Karat 8.0 (Beckman Coulter, Krefeld, Germany)
- Adobe Photoshop 12.0 x 32 (Adobe Systems, USA)
- Biotoools 3.1 (Bruker Daltonics, Bremen, Germany)
- CorelDraw 11 (Corel)
- Endnote X5 (Thomson Reuters, USA)
- ExPASy (Swiss Institut of Bioinformatics, Switzerland)
- FlexAnalysis 3.0 (Bruker Daltonics, Bremen, Germany)
- FlexControl 3.0 (Bruker Daltonics, Bremen, Germany)
- GlycoPeakfinder (EuroCarbDB)
- GlycoWorkbench 1.1 (EuroCarbDB)
- Mascot (Matrix Science CE-LIF, London, UK)
- Microsoft (Word and Excel, Windows)
- Quantity One 4.6.3 (Bio-Rad, München)

5 References

1. Weissman, I. L., Anderson, D. J., and Gage, F. (2001) Stem and progenitor cells: Origins, Phenotypes, Lineage Commitments, and Transdifferentiations. *Annual Review of Cell and Developmental Biology* 17, 387-403
2. Smith, A. G. (2001) Embryo-derived stem cells: Of Mice and Men. *Annual Review of Cell and Developmental Biology* 17, 435-462
3. McCulloch, E. A., and Till, J. E. (2005) Perspectives on the properties of stem cells. *Nat Med* 11, 1026-1028
4. Moore, K. E., Mills, J. F., and Thornton, M. M. (2006) Alternative sources of adult stem cells: A possible solution to the embryonic stem cell debate. *Gender Medicine* 3, 161-168
5. Pessina, A., and Gribaldo, L. (2006) The key role of adult stem cells: therapeutic perspectives. *Current Medical Research and Opinion* 22, 2287-2300
6. Evans, M. J., and Kaufman, M. H. (1981) Establishment in culture of pluripotential cells from mouse embryos. *Nature* 292, 154-156
7. Martin, G. R. (1981) Isolation of a pluripotent cell line from early mouse embryos cultured in medium conditioned by teratocarcinoma stem cells. *Proceedings of the National Academy of Sciences* 78, 7634-7638
8. Lanza, R., Gearhart, J., Hogan, B., Melton, D., Pederson, R., Thomas, J., and West, M. (2004) *Handbook of Stem Cells-Embryonic Stem Cells*, Elsevier Academic Press, USA
9. Saitou, M., Barton, S. C., and Surani, M. A. (2002) A molecular programme for the specification of germ cell fate in mice. *Nature* 418, 293-300
10. Amit, M., Carpenter, M. K., Inokuma, M. S., Chiu, C.-P., Harris, C. P., Waknitz, M. A., Itskovitz-Eldor, J., and Thomson, J. A. (2000) Clonally Derived Human Embryonic Stem Cell Lines Maintain Pluripotency and Proliferative Potential for Prolonged Periods of Culture. *Developmental Biology* 227, 271-278
11. Sullivan, S., Cowan, C. A., and Eggan, K. (2007) *Human Embryonic Stem Cells: The Practical Handbook*, Wiley, England
12. Ambrosetti, D.-C., Schöler, H. R., Dailey, L., and Basilico, C. (2000) Modulation of the Activity of Multiple Transcriptional Activation Domains by the DNA Binding Domains Mediates the Synergistic Action of Sox2 and Oct-3 on the Fibroblast Growth Factor-4Enhancer. *Journal of Biological Chemistry* 275, 23387-23397
13. Dushnik-Levinson, M., and Benvenisty, N. (1995) Embryogenesis in vitro: Study of Differentiation of Embryonic Stem Cells. *Neonatology* 67, 77-83
14. Itskovitz-Eldor J, Schuldiner M, Karsenti D, Eden A, Yanuka O, Amit M, Soreq H, and N, B. (2000) Differentiation of human embryonic stem cells into embryoid bodies compromising the three embryonic germ layers. *Molecular Medicine* 6, 88-95
15. Dressel R, Schindehütte J, Kuhlmann T, Elsner L, Novota P, Baier PC, Schillert A, Bickeböller H, Herrmann T, Trenkwalder C, Paulus W, and A., M. (2008) The tumorigenicity of mouse embryonic stem cells and in vitro differentiated neuronal cells is controlled by the recipients' immune response. *PLoS One* 3, e2622
16. Stachelscheid, H., Wulf-Goldenberg, A., Eckert, K., Jensen, J., Edsbagge, J., Björquist, P., Rivero, M., Strehl, R., Jozefczuk, J., Prigione, A., Adjaye, J., Urbaniak, T., Bussmann, P., Zeilinger, K., and Gerlach, J. C. (2013) Teratoma formation of human embryonic stem cells in three-dimensional perfusion culture bioreactors. *Journal of Tissue Engineering and Regenerative Medicine* 7, 729-741
17. Horslen, S. P., and Fox, I. J. (2004) Hepatocyte Transplantation. *Transplantation* 77, 1481-1486.
18. Brunt, K. R., Weisel, R. D., and Li, R.-K. (2012) Stem cells and regenerative medicine — future perspectives. *Canadian Journal of Physiology and Pharmacology* 90, 327-335

REFERENCES

19. Lanza, R., Blau, H., Melton, D., Moore, M., Thomas, E. D., Verfaillie, C., Weissman, I., and West, M. (2004) *Handbook of Stem Cells-Adult and fetal stem cells*, Elsevier Academic Press, USA
20. (2006) The key role of adult stem cells: therapeutic perspectives. *Current Medical Research and Opinion* 22, 2287-2300
21. Marshak, R. D., Gardner, L. R., and Gottlieb, D. (2001) *Stem Cell Biology*, Cold Spring Harbor, USA
22. Pittenger, M. F., Mackay, A. M., Beck, S. C., Jaiswal, R. K., Douglas, R., Mosca, J. D., Moorman, M. A., Simonetti, D. W., Craig, S., and Marshak, D. R. (1999) Multilineage Potential of Adult Human Mesenchymal Stem Cells. *Science* 284, 143-147
23. Sanchez-Ramos, J., Song, S., Cardozo-Pelaez, F., Hazzi, C., Stedeford, T., Willing, A., Freeman, T. B., Saporta, S., Janssen, W., Patel, N., Cooper, D. R., and Sanberg, P. R. (2000) Adult Bone Marrow Stromal Cells Differentiate into Neural Cells in Vitro. *Experimental Neurology* 164, 247-256
24. Ji, J. F., He, B. P., Dheen, S. T., and Tay, S. S. W. (2004) Interactions of Chemokines and Chemokine Receptors Mediate the Migration of Mesenchymal Stem Cells to the Impaired Site in the Brain After Hypoglossal Nerve Injury. *Stem cells* 22, 415-427
25. Yu, J., Li, M., Qu, Z., Yan, D., Li, D., and Ruan, Q. (2010) SDF-1/CXCR4-Mediated Migration of Transplanted Bone Marrow Stromal Cells Toward Areas of Heart Myocardial Infarction Through Activation of PI3K/Akt. *Journal of Cardiovascular Pharmacology* 55, 496-505 410.1097/FJC.1090b1013e3181d1097a1384
26. Caplan, Arnold I., and Correa, D. (2011) The MSC: An Injury Drugstore. *Cell stem cell* 9, 11-15
27. Giordano, A., Galderisi, U., and Marino, I. R. (2007) From the laboratory bench to the patient's bedside: An update on clinical trials with mesenchymal stem cells. *Journal of Cellular Physiology* 211, 27-35
28. Singh Mohal, J., D. Tailor, H., and S. Khan, W. (2012) Sources of Adult Mesenchymal Stem Cells and their Applicability for Musculoskeletal Applications. *Current Stem Cell Research & Therapy* 7, 103-109
29. Gronthos, S., Graves, S., Ohta, S., and Simmons, P. (1994) The STRO-1+ fraction of adult human bone marrow contains the osteogenic precursors. *Blood* 84, 4164-4173
30. Kolf, C., Cho, E., and Tuan, R. (2007) Mesenchymal stromal cells. Biology of adult mesenchymal stem cells: regulation of niche, self-renewal and differentiation. *Arthritis Research & Therapy* 9, 204
31. Menssen, A., Haupl, T., Sittinger, M., Delorme, B., Charbord, P., and Ringe, J. (2011) Differential gene expression profiling of human bone marrow-derived mesenchymal stem cells during adipogenic development. *BMC Genomics* 12, 461
32. Langston, J. W. (2005) The promise of stem cells in Parkinson disease. *The Journal of Clinical Investigation* 115, 23-25
33. Lindvall, O., Kokaia, Z., and Martinez-Serrano, A. (2004) Stem cell therapy for human neurodegenerative disorders—how to make it work. *Nature Medicine* 10, S42–S50
34. Zeng, X., Cai, J., Chen, J., Luo, Y., You, Z.-B., Fötter, E., Wang, Y., Harvey, B., Miura, T., Backman, C., Chen, G.-J., Rao, M. S., and Freed, W. J. (2004) Dopaminergic Differentiation of Human Embryonic Stem Cells. *Stem cells* 22, 925-940
35. Cho, Y. H., Kim, D.-S., Kim, P. G., Hwang, Y. S., Cho, M. S., Moon, S. Y., Kim, D.-W., and Chang, J. W. (2006) Dopamine neurons derived from embryonic stem cells efficiently induce behavioral recovery in a Parkinsonian rat model. *Biochemical and Biophysical Research Communications* 341, 6-12
36. Martinat, C., Bacci, J.-J., Leete, T., Kim, J., Vanti, W. B., Newman, A. H., Cha, J. H., Gether, U., Wang, H., and Abeliovich, A. (2006) Cooperative transcription activation by Nurr1 and Pitx3 induces embryonic stem cell maturation to the midbrain dopamine neuron phenotype. *Proceedings of the National Academy of Sciences of the United States of America* 103, 2874-2879

37. Wang, Q., Matsumoto, Y., Shindo, T., Miyake, K., Shindo, A., Kawanishi, M., Kawai, N., Tamiya, T., and Nagao, S. (2006) Neural stem cells transplantation in cortex in a mouse model of Alzheimer's disease. *The Journal of Medical Investigation* 53, 61-69
38. Chinzei, R., Tanaka, Y., Shimizu-Saito, K., Hara, Y., Kakinuma, S., Watanabe, M., Teramoto, K., Arii, S., Takase, K., Sato, C., Terada, N., and Teraoka, H. (2002) Embryoid-body cells derived from a mouse embryonic stem cell line show differentiation into functional hepatocytes. *Hepatology* 36, 22-29
39. Wu, C. D., Boyd, S. A., and Wood, J. K. (2007) Embryonic stem cell transplantation: potential applicability in cell replacement therapy and regenerative medicine. *Frontiers in Bioscience* 1, 4525-4535
40. Kofidis, T., de Bruin, J. L., Hoyt, G., Ho, Y., Tanaka, M., Yamane, T., Lebl, D. R., Swijnenburg, R.-J., Chang, C.-P., Quertermous, T., and Robbins, R. C. (2005) Myocardial Restoration With Embryonic Stem Cell Bioartificial Tissue Transplantation. *The Journal of heart and lung transplantation : the official publication of the International Society for Heart Transplantation* 24, 737-744
41. Paek, H. J., Morgan, J. R., and Lysaght, M. J. (2005) Sequestration and Synthesis: The Source of Insulin in Cell Clusters Differentiated from Murine Embryonic Stem Cells. *Stem cells* 23, 862-867
42. Zhan, X., Dravid, G., Ye, Z., Hammond, H., Shambloot, M., Gearhart, J., and Cheng, L. Functional antigen-presenting leucocytes derived from human embryonic stem cells in vitro. *The Lancet* 364, 163-171
43. Caplan, Arnold I. (2000) Tissue Engineering Designs for the Future: New Logics, Old Molecules. *Tissue Engineering* 6, 1-8
44. Saito, T., Dennis, J. E., Lennon, D. P., Young, R. G., and Caplan, A. I. (1996) Myogenic Expression of Mesenchymal Stem Cells within Myotubes of mdx Mice in Vitro and in Vivo. *Tissue Engineering* 1, 327-344
45. Shake, J. G., Gruber, P. J., Baumgartner, W. A., Senechal, G., Meyers, J., Redmond, J. M., Pittenger, M. F., and Martin, F. J. (2002) In vivo mesenchymal stem cell grafting in a swine myocardial infarct model: molecular and physiologic consequences. *The Annals Thoracic Surgery*, 1919-1926
46. Huang, L., and Burd, A. (2012) An update review of stem cell applications in burns and wound care. *Indian Journal of Plastic Surgery* 45, 229-236
47. Rademacher, T. W., Parekh, R. B., and Dwek, R. A. (1988) Glycobiology. *Annual Review of Biochemistry* 57, 785-838
48. Ohtsubo, K., and Marth, J. D. (2006) Glycosylation in Cellular Mechanisms of Health and Disease. *Cell* 126, 855-867
49. Nieuwdorp, M., Meuwese, M. C., Vink, H., Hoekstra, J. B., Kastelein, J. J., and Stoes, E. S. (2005) The endothelial glycocalyx: a potential barrier between health and vascular disease. *Current Opinion in Lipidology* 16, 507-511
50. Hossler, P., Mulukutla, B. C., and Hu, W.-S. (2007) Systems Analysis of N-Glycan Processing in Mammalian Cells. *PLoS ONE* 2, e713
51. Spiro, R. G. (2002) Protein glycosylation: nature, distribution, enzymatic formation, and disease implications of glycopeptide bonds. *Glycobiology* 12, 43R-56R
52. Gabius, H.-J. (2009) *The Sugar Code*, WILEY-VCH, Weinheim
53. Varki, A., Cummings, R. D., Esko, J. D., Freeze, H. H., Stanley, P., Bertozzi, C. R., Hart, G. W., and Etzler, M. E. (2009) *Essentials of Glycobiology*, 2 Ed., Cold Spring Harbor (NY): Cold Spring Harbor Laboratory Press, New York
54. Furmanek A , and ., H. J. (2000) protein c-mannosylation facts and questions. *Acta Biochimica Polonica* 47, 781-789
55. Tateno, H., Uchiyama, N., Kuno, A., Togayachi, A., Sato, T., Narimatsu, H., and Hirabayashi, J. (2007) A novel strategy for mammalian cell surface glycome profiling using lectin microarray. *Glycobiology* 17, 1138-1146
56. Kornfeld, R., and Kornfeld, S. (1985) Assembly of Asparagine-Linked Oligosaccharides. *Annual Review of Biochemistry* 54, 631-664

57. Bergwerff, A. A., van Oostrum, J., Asselbergs, F. A. M., Bürgi, R., Hokke, C. H., Kamerling, J. P., and Vliegenthart, J. F. G. (1993) Primary structure of N-linked carbohydrate chains of a human chimeric plasminogen activator K2tu-PA expressed in Chinese hamster ovary cells. *European Journal of Biochemistry* 212, 639-656
58. Bigge, J. C., Patel, T. P., Bruce, J. A., Goulding, P. N., Charles, S. M., and Parekh, R. B. (1995) Nonselective and Efficient Fluorescent Labeling of Glycans Using 2-Amino Benzamide and Anthranilic Acid. *Analytical Biochemistry* 230, 229-238
59. Blanchard, V., Gadkari, R., Gerwig, G., Leeflang, B., Dighe, R., and Kamerling, J. (2007) Characterization of the N-linked oligosaccharides from human chorionic gonadotropin expressed in the methylotrophic yeast *Pichia pastoris*. *Glycoconjugate Journal* 24, 33-47
60. Borys, M. C., Dalal, N. G., Abu-Absi, N. R., Khattak, S. F., Jing, Y., Xing, Z., and Li, Z. J. (2010) Effects of culture conditions on N-glycolylneuraminic acid (Neu5Gc) content of a recombinant fusion protein produced in CHO cells. *Biotechnology and Bioengineering* 105, 1048-1057
61. Priatel, J. J., Chui, D., Hiraoka, N., Simmons, C. J. T., Richardson, K. B., Page, D. M., Fukuda, M., Varki, N. M., and Marth, J. D. (2000) The ST3Gal-I Sialyltransferase Controls CD8+ T Lymphocyte Homeostasis by Modulating O-Glycan Biosynthesis. *Immunity* 12, 273-283
62. Gagneux, P., and Varki, A. (1999) Evolutionary considerations in relating oligosaccharide diversity to biological function. *Glycobiology* 9, 747-755
63. Lau, K. S., and Dennis, J. W. (2008) N-Glycans in cancer progression. *Glycobiology* 18, 750-760
64. Hahn, T. J., and Goochee, C. F. (1992) Growth-associated glycosylation of transferrin secreted by HepG2 cells. *Journal of Biological Chemistry* 267, 23982-23987
65. Stanley, P., and Ioffe, E. (1995) Glycosyltransferase mutants: key to new insights in glycobiology. *The FASEB Journal* 9, 1436-1444
66. Saitoh, O., Wang, W. C., Lotan, R., and Fukuda, M. (1992) Differential glycosylation and cell surface expression of lysosomal membrane glycoproteins in sublines of a human colon cancer exhibiting distinct metastatic potentials. *Journal of Biological Chemistry* 267, 5700-5711
67. Dennis, J. W., Granovsky, M., and Warren, C. E. (1999) Glycoprotein glycosylation and cancer progression. *Biochimica et Biophysica Acta (BBA) - General Subjects* 1473, 21-34
68. Hakomori, S.-i. (1985) Aberrant Glycosylation in Cancer Cell Membranes as Focused on Glycolipids: Overview and Perspectives. *Cancer Research* 45, 2405-2414
69. Kim, Y., and Varki, A. (1997) Perspectives on the significance of altered glycosylation of glycoproteins in cancer. *Glycoconjugate Journal* 14, 569-576
70. Lanctot, P. M., Gage, F. H., and Varki, A. P. (2007) The glycans of stem cells. *Current Opinion in Chemical Biology* 11, 373-380
71. Haltiwanger, R. S., and Lowe, J. B. (2004) Role of glycosylation in development. *Annual review of biochemistry* 73, 491-537
72. Varki, A. (1993) Biological roles of oligosaccharides: all of the theories are correct. *Glycobiology* 3, 97-130
73. Rudd, P. M., Wormald, M. R., Stanfield, R. L., Huang, M., Mattsson, N., Speir, J. A., DiGennaro, J. A., Fetrow, J. S., Dwek, R. A., and Wilson, I. A. (1999) Roles for glycosylation of cell surface receptors involved in cellular immune recognition. *Journal of Molecular Biology* 293, 351-366
74. Perillo, N. L., Marcus, M. E., and Baum, L. G. (1998) Galectins: versatile modulators of cell adhesion, cell proliferation, and cell death. *J Mol Med (Berl)* 76, 402-412
75. Rudd, P. M., Wormald, M. R., Stanfield, R. L., Huang, M., Mattsson, N., Speir, J. A., DiGennaro, J. A., Fetrow, J. S., Dwek, R. A., and Wilson, I. A. (1999) Roles for glycosylation of cell surface receptors involved in cellular immune recognition. *Journal of molecular biology* 293, 351-366

76. Helenius, A., and Aebi, M. (2004) Roles of N-linked glycans in the endoplasmic reticulum. *Annual review of biochemistry* 73, 1019-1049
77. Lanctot, P. M., Gage, F. H., and Varki, A. P. (2007) The glycans of stem cells. *Current opinion in chemical biology* 11, 373-380
78. Singh, A., Satchell, S. C., Neal, C. R., McKenzie, E. A., Tooke, J. E., and Mathieson, P. W. (2007) Glomerular Endothelial Glycocalyx Constitutes a Barrier to Protein Permeability. *Journal of the American Society of Nephrology* 18, 2885-2893
79. Danielli, J. F. (1940) Capillary permeability and oedema in the perfused frog. *The Journal of Physiology* 98, 109-129
80. Luft, J. H. (1966) Fine structures of capillary and endocapillary layer as revealed by ruthenium red. *Federation proceedings* 25, 1773-1783
81. Chappell, D., Jacob, M., Hofmann-Kiefer, K., Bruegger, D., Rehm, M., Conzen, P., Welsch, U., and Becker, B. F. (2007) Hydrocortisone Preserves the Vascular Barrier by Protecting the Endothelial Glycocalyx. *Anesthesiology* 107, 776-784.
82. Rehm, M., Zahler, S., Lötsch, M., Welsch, U., Conzen, P., Jacob, M., and Becker, B. F. (2004) Endothelial Glycocalyx as an Additional Barrier Determining Extravasation of 6% Hydroxyethyl Starch or 5% Albumin Solutions in the Coronary Vascular Bed. *Anesthesiology* 100, 1211-1223
83. Vink, H., and Duling, B. R. (2000) Capillary endothelial surface layer selectively reduces plasma solute distribution volume. *American Journal of Physiology - Heart and Circulatory Physiology* 278, H285-H289
84. Pries, A. R., and Kuebler, W. M. (2006) Normal Endothelium. In: Moncada, S., and Higgs, A., eds. *The Vascular Endothelium I*, pp. 1-40, Springer Berlin Heidelberg
85. Pries, A. R., Secomb, T. W., and Gaehtgens, P. (2000) The endothelial surface layer. *Eur J Physiol* 440, 653-666
86. Jacob, M., Bruegger, D., Rehm, M., Welsch, U., Conzen, P., and Becker, B. F. (2006) Contrasting Effects of Colloid and Crystalloid Resuscitation Fluids on Cardiac Vascular Permeability. *Anesthesiology* 104, 1223-1231
87. Nieuwdorp, M., van Haefen, T. W., Gouverneur, M. C. L. G., Mooij, H. L., van Lieshout, M. H. P., Levi, M., Meijers, J. C. M., Holleman, F., Hoekstra, J. B. L., Vink, H., Kastelein, J. J. P., and Stroes, E. S. G. (2006) Loss of Endothelial Glycocalyx During Acute Hyperglycemia Coincides With Endothelial Dysfunction and Coagulation Activation In Vivo. *Diabetes* 55, 480-486
88. Nelson, A., Berkestedt, I., Schmidtchen, A., Ljunggren, L., and Bodelsson, M. (2008) Increased Levels of Glycosaminoglycans During Septic Shock: Relation to Mortality and the Antibacterial Actions of Plasma. *Shock* 30, 623-627
610.1097/SHK.1090b1013e3181777da3181773
89. Vlodavsky, I., Ilan, N., Nadir, Y., Brenner, B., Katz, B.-Z., Naggi, A., Torri, G., Casu, B., and Sasisekharan, R. (2007) Heparanase, heparin and the coagulation system in cancer progression. *Thrombosis Research* 120, Supplement 2, S112-S120
90. Luo, X., Yang, H., Liang, C., and Jin, S. (2010) Structural characterization of N-linked oligosaccharides of Defibrase from *Agikistronodon acutus* by sequential exoglycosidase digestion and MALDI-TOF mass spectrometry. *Toxicon* 55, 421-429
91. Ceroni, A., Maass, K., Geyer, H., Geyer, R., Dell, A., and Haslam, S. M. (2008) GlycoWorkbench: A Tool for the Computer-Assisted Annotation of Mass Spectra of Glycans. *Journal of Proteome Research* 7, 1650-1659
92. Costa, A. R., Withers, J., Rodrigues, M. E., McLoughlin, N., Henriques, M., Oliveira, R., Rudd, P., and Azeredo, J. (2013) The impact of microcarrier culture optimization on the glycosylation profile of a monoclonal antibody. *SpringerPlus* 2, 25
93. Jenkins, N., Parekh, R. B., and James, D. C. (1996) Getting the glycosylation right: Implications for the biotechnology industry. *Nature Biotechnology* 14, 975-981
94. Lis, H., and Sharon, N. (1993) Protein glycosylation. *European Journal of Biochemistry* 218, 1-27
95. Helenius, A., and Aebi, M. (2004) Roles of n-linked glycans in the endoplasmic reticulum. *Annual Review of Biochemistry* 73, 1019-1049

REFERENCES

96. Mills, K., Mills, P. B., Clayton, P. T., Mian, N., Johnson, A. W., and Winchester, B. G. (2003) The underglycosylation of plasma α 1-antitrypsin in congenital disorders of glycosylation type I is not random. *Glycobiology* 13, 73-85
97. Christlet, T. H. T., and Veluraja, K. (2011) Database analysis of O-glycosylation sites in proteins. *Biophysical Journal* 80, 952-960
98. (1998) Concepts and Principles of O-Linked Glycosylation. *Critical Reviews in Biochemistry and Molecular Biology* 33, 151-208
99. Ten Hagen, K. G., Fritz, T. A., and Tabak, L. A. (2003) All in the family: the UDP-GalNAc:polypeptide N-acetylgalactosaminyltransferases. *Glycobiology* 13, 1R-16R
100. Tarp, M. A., and Clausen, H. (2008) Mucin-type O-glycosylation and its potential use in drug and vaccine development. *Biochimica et Biophysica Acta (BBA) - General Subjects* 1780, 546-563
101. Hart, G. W. (1997) Dynamic o-linked glycosylation of nuclear and cytoskeletal proteins. *Annual Review of Biochemistry* 66, 315-335
102. Gospodarowicz, D. (1974) Localisation of a fibroblast growth factor and its effect alone and with hydrocortisone on 3T3 cell growth. *Nature* 249, 123-127
103. Zhang, X., Ibrahim, O. A., Olsen, S. K., Umemori, H., Mohammadi, M., and Ornitz, D. M. (2006) Receptor Specificity of the Fibroblast Growth Factor Family: The complete mammalian fgf family. *Journal of Biological Chemistry* 281, 15694-15700
104. Barrett, A. J., Davies, M. E., and Grubb, A. (1984) The place of human γ -trace (cystatin C) amongst the cysteine proteinase inhibitors. *Biochemical and Biophysical Research Communications* 120, 631-636
105. Taupin, P., Ray, J., Fischer, W. H., Suhr, S. T., Hakansson, K., Grubb, A., and Gage, F. H. (2000) FGF-2-Responsive Neural Stem Cell Proliferation Requires CcG, a Novel Autocrine/Paracrine Cofactor. *Neuron* 28, 385-397
106. Moloney, D. J., Shair, L. H., Lu, F. M., Xia, J., Locke, R., Matta, K. L., and Haltiwanger, R. S. (2000) Mammalian Notch1 Is Modified with Two Unusual Forms of O-Linked Glycosylation Found on Epidermal Growth Factor-like Modules. *Journal of Biological Chemistry* 275, 9604-9611
107. Moloney, D. J., Panin, V. M., Johnston, S. H., Chen, J., Shao, L., Wilson, R., Wang, Y., Stanley, P., Irvine, K. D., Haltiwanger, R. S., and Vogt, T. F. (2000) Fringe is a glycosyltransferase that modifies Notch. *Nature* 406, 369-375
108. Haltiwanger, R. S., and Lowe, J. B. (2004) Role of glycosylation in development. *Annual Review of Biochemistry* 73, 491-537
109. Yu, R. K., and Yanagisawa, M. (2006) Glycobiology of neural stem cells. *CNS & neurological disorders drug targets* 5, 415-423
110. Yanagisawa, M., and Yu, R. K. (2007) The expression and functions of glycoconjugates in neural stem cells. *Glycobiology* 17, 57R-74R
111. Muramatsu, T., and Muramatsu, H. (2004) Carbohydrate antigens expressed on stem cells and early embryonic cells. *Glycoconjugate journal* 21, 41-45
112. Badcock, G., Pigott, C., Goepel, J., and Andrews, P. W. (1999) The Human Embryonal Carcinoma Marker Antigen TRA-1-60 Is a Sialylated Keratan Sulfate Proteoglycan. *Cancer Research* 59, 4715-4719
113. Close, B. E., Mendiratta, S. S., Geiger, K. M., Broom, L. J., Ho, L. L., and Colley, K. J. (2003) The minimal structural domains required for neural cell adhesion molecule polysialylation by PST/ST8Sia IV and STX/ST8Sia II. *The Journal of biological chemistry* 278, 30796-30805
114. Kim, D. S., Lee, D. R., Kim, H. S., Yoo, J. E., Jung, S. J., Lim, B. Y., Jang, J., Kang, H. C., You, S., Hwang, D. Y., Leem, J. W., Nam, T. S., Cho, S. R., and Kim, D. W. (2012) Highly pure and expandable PSA-NCAM-positive neural precursors from human ESC and iPSC-derived neural rosettes. *PloS one* 7, e39715
115. Patsos, G., André, S., Roeckel, N., Gromes, R., Gebert, J., Kopitz, J., and Gabius, H.-J. (2009) Compensation of loss of protein function in microsatellite-unstable colon cancer cells (HCT116): A gene-dependent effect on the cell surface glycan profile. *Glycobiology* 19, 726-734

116. Tao, S.-C., Li, Y., Zhou, J., Qian, J., Schnaar, R. L., Zhang, Y., Goldstein, I. J., Zhu, H., and Schneck, J. P. (2008) Lectin microarrays identify cell-specific and functionally significant cell surface glycan markers. *Glycobiology* 18, 761-769
117. Hirabayashi, J., Yamada, M., Kuno, A., and Tateno, H. (2013) Lectin microarrays: concept, principle and applications. *Chemical Society Reviews* 42, 4443-4458
118. Kuno, A., Uchiyama, N., Koseki-Kuno, S., Ebe, Y., Takashima, S., Yamada, M., and Hirabayashi, J. (2005) Evanescent-field fluorescence-assisted lectin microarray: a new strategy for glycan profiling. *Nature Methods* 2
119. Rosenfeld, R., Bangio, H., Gerwig, G. J., Rosenberg, R., Aloni, R., Cohen, Y., Amor, Y., Plaschkes, I., Kamerling, J. P., and Maya, R. B.-Y. (2007) A lectin array-based methodology for the analysis of protein glycosylation. *Journal of Biochemical and Biophysical Methods* 70, 415-426
120. Zheng, T., Peelen, D., and Smith, L. M. (2005) Lectin Arrays for Profiling Cell Surface Carbohydrate Expression. *Journal of the American Chemical Society* 127, 9982-9983
121. Ebe, Y., Kuno, A., Uchiyama, N., Koseki-Kuno, S., Yamada, M., Sato, T., Narimatsu, H., and Hirabayashi, J. (2006) Application of Lectin Microarray to Crude Samples: Differential Glycan Profiling of Lec Mutants. *Journal of Biochemistry* 139, 323-327
122. An, H. J., Gip, P., Kim, J., Wu, S., Park, K. W., McVaugh, C. T., Schaffer, D. V., Bertozzi, C. R., and Lebrilla, C. B. (2012) Extensive Determination of Glycan Heterogeneity Reveals an Unusual Abundance of High Mannose Glycans in Enriched Plasma Membranes of Human Embryonic Stem Cells. *Molecular & Cellular Proteomics* 11
123. Mi, W., Jia, W., Zheng, Z., Wang, J., Cai, Y., Ying, W., and Qian, X. (2012) Surface glycoproteomic analysis of hepatocellular carcinoma cells by affinity enrichment and mass spectrometric identification. *Glycoconjugate Journal* 29, 411-424
124. Nakano, M., Saldanha, R., Göbel, A., Kavallaris, M., and Packer, N. H. (2011) Identification of Glycan Structure Alterations on Cell Membrane Proteins in Desoxyepothilone B Resistant Leukemia Cells. *Molecular & Cellular Proteomics* 10
125. Jervis, A. J., Langdon, R., Hitchen, P., Lawson, A. J., Wood, A., Fothergill, J. L., Morris, H. R., Dell, A., Wren, B., and Linton, D. (2010) Characterization of N-Linked Protein Glycosylation in *Helicobacter pullorum*. *Journal of Bacteriology* 192, 5228-5236
126. Reinke, S. O., Bayer, M., Berger, M., Blanchard, V., and Hinderlich, S. (2011) Analysis of Cell Surface N-glycosylation of the Human Embryonic Kidney 293T Cell Line. *Journal of Carbohydrate Chemistry* 30, 218-232
127. Hamouda, H., Ullah, M., Berger, M., Sittinger, M., Tauber, R., Ringe, J., and Blanchard, V. (2013) N-Glycosylation Profile of Undifferentiated and Adipogenically Differentiated Human Bone Marrow Mesenchymal Stem Cells: Towards a Next Generation of Stem Cell Markers. *Stem Cells and Development* 22
128. Kuhn, P., Guan, C., Cui, T., Tarentino, A. L., Plummer, T. H., and Van Roey, P. (1995) Active Site and Oligosaccharide Recognition Residues of Peptide-N4-(N-acetyl- β -D-glucosaminyl)asparagine Amidase F. *Journal of Biological Chemistry* 270, 29493-29497
129. Blanchard, V., Frank, M., Leeftang, B. R., Boelens, R., and Kamerling, J. P. (2008) The Structural Basis of the Difference in Sensitivity for PNGase F in the De-N-glycosylation of the Native Bovine Pancreatic Ribonucleases B and BS \dagger . *Biochemistry* 47, 3435-3446
130. Kamerling, J. P., and Boons, G. J. (2007) *Comprehensive Glycoscience: From Chemistry to Systems Biology*, Elsevier Science Limited
131. Maley, F., Trimble, R. B., Tarentino, A. L., and Plummer Jr, T. H. (1989) Characterization of glycoproteins and their associated oligosaccharides through the use of endoglycosidases. *Analytical Biochemistry* 180, 195-204
132. Tarentino, A. L., Gomez, C. M., and Plummer, T. H. (1985) Deglycosylation of asparagine-linked glycans by peptide:N-glycosidase F. *Biochemistry* 24, 4665-4671

133. Nuck, R. (2002) *Methods in Molecular Biology-Post-translational Modifications of Proteins*, Humana Press, Totowa New Jersey
134. Chu, F. K. (1986) Requirements of cleavage of high mannose oligosaccharides in glycoproteins by peptide N-glycosidase F. *Journal of Biological Chemistry* 261, 172-177
135. Rademaker, G. J., Pergantis, S. A., Blok-Tip, L., Langridge, J. I., Kleen, A., and Thomas-Oates, J. E. (1998) Mass Spectrometric Determination of the Sites of O-Glycan Attachment with Low Picomolar Sensitivity. *Analytical Biochemistry* 257, 149-160
136. Hanisch, F.-G., Jovanovic, M., and Peter-Katalinic, J. (2001) Glycoprotein Identification and Localization of O-Glycosylation Sites by Mass Spectrometric Analysis of Deglycosylated/Alkylaminylated Peptide Fragments. *Analytical Biochemistry* 290, 47-59
137. Mechref, Y., Baker, A. G., and Novotny, M. V. (1998) Matrix-assisted laser desorption/ionization mass spectrometry of neutral and acidic oligosaccharides with collision-induced dissociation. *Carbohydrate Research* 313, 145-155
138. Reinhold, V. N., Reinhold, B. B., and Costello, C. E. (1995) Carbohydrate Molecular Weight Profiling, Sequence, Linkage, and Branching Data: ES-MS and CID. *Analytical Chemistry* 67, 1772-1784
139. Briggs, J. B., Keck, R. G., Ma, S., Lau, W., and Jones, A. J. S. (2009) An analytical system for the characterization of highly heterogeneous mixtures of N-linked oligosaccharides. *Analytical Biochemistry* 389, 40-51
140. Guttman, A., and Pritchett, T. (1995) Capillary gel electrophoresis separation of high-mannose type oligosaccharides derivatized by 1-aminopyrene-3,6,8-trisulfonic acid. *Electrophoresis* 16, 1906-1911
141. Guttman, A., Chen, F.-T. A., Evangelista, R. A., and Cooke, N. (1996) High-Resolution Capillary Gel Electrophoresis of Reducing Oligosaccharides Labeled with 1-Aminopyrene-3,6,8-trisulfonate. *Analytical Biochemistry* 233, 234-242
142. Laroy, W., Contreras, R., and Callewaert, N. (2006) Glycome mapping on DNA sequencing equipment. *Nature Protocols* 1, 397-405
143. Wedepohl, S., Kaup, M., Riese, S. B., Berger, M., Dervedde, J., Tauber, R., and Blanchard, V. r. (2010) N-Glycan Analysis of Recombinant L-Selectin Reveals Sulfated GalNAc and GalNAc-GalNAc Motifs. *Journal of Proteome Research* 9, 3403-3411
144. Heiskanen, A., Satomaa, T., Tiitinen, S., Laitinen, A., Mannelin, S., Impola, U., Mikkola, M., Olsson, C., Miller-Podraza, H., Blomqvist, M., Olonen, A., Salo, H., Lehenkari, P., Tuuri, T., Otonkoski, T., Natunen, J., Saarinen, J., and Laine, J. (2007) N-glycolylneuraminic acid xenoantigen contamination of human embryonic and mesenchymal stem cells is substantially reversible. *Stem Cells* 25, 197-202
145. Martin, M. J., Muotri, A., Gage, F., and Varki, A. (2005) Human embryonic stem cells express an immunogenic nonhuman sialic acid. *Nat Med* 11, 228-232
146. Wedepohl, S., Kaup, M., Riese, S. B., Berger, M., Dervedde, J., Tauber, R., and Blanchard, V. (2010) N-glycan analysis of recombinant L-Selectin reveals sulfated GalNAc and GalNAc-GalNAc motifs. *Journal of proteome research* 9, 3403-3411
147. Reinke, S. O., Bayer, M., Berger, M., Hinderlich, S., and Blanchard, V. (2012) The analysis of N-glycans of cell membrane proteins from human hematopoietic cell lines reveals distinctions in their pattern. *Biological chemistry* 393, 731-747
148. Frisch, E., Kaup, M., Egerer, K., Weimann, A., Tauber, R., Berger, M., and Blanchard, V. (2011) Profiling of Endo H-released serum N-glycans using CE-LIF and MALDI-TOF-MS--application to rheumatoid arthritis. *Electrophoresis* 32, 3510-3515
149. Frisch, E., Kaup, M., Egerer, K., Weimann, A., Tauber, R., Berger, M., and Blanchard, V. (2011) Profiling of Endo H-released serum N-glycans using CE-LIF and MALDI-TOF-MS – Application to rheumatoid arthritis. *Electrophoresis* 32, 3510-3515

150. Risch, S. (2012) Serumglykom-Charakterisierung und automatisierte Strukturaufklärung der N-Glykane beim Ovarialkarzinom. *Charité Universitätsmedizin Berlin / Fachbereich Biologie, Chemie, Pharmazie der Freien Universität Berlin*, p. 174, Freie Universität Berlin, Berlin
151. Heiskanen, A., Hirvonen, T., Salo, H., Impola, U., Olonen, A., Laitinen, A., Tiitinen, S., Natunen, S., Aitio, O., Miller-Podraza, H., Wuhrer, M., Deelder, A. M., Natunen, J., Laine, J., Lehenkari, P., Saarinen, J., Satomaa, T., and Valmu, L. (2009) Glycomics of bone marrow-derived mesenchymal stem cells can be used to evaluate their cellular differentiation stage. *Glycoconjugate journal* 26, 367-384
152. Martin, M. J., Muotri, A., Gage, F., and Varki, A. (2005) Human embryonic stem cells express an immunogenic nonhuman sialic acid. *Nature medicine* 11, 228-232
153. Hemmoranta, H., Satomaa, T., Blomqvist, M., Heiskanen, A., Aitio, O., Saarinen, J., Natunen, J., Partanen, J., Laine, J., and Jaatinen, T. (2007) N-glycan structures and associated gene expression reflect the characteristic N-glycosylation pattern of human hematopoietic stem and progenitor cells. *Experimental Hematology* 35, 1279-1292
154. Kyselova, Z., Mechref, Y., Kang, P., Goetz, J. A., Dobrolecki, L. E., Sledge, G. W., Schnaper, L., Hickey, R. J., Malkas, L. H., and Novotny, M. V. (2008) Breast Cancer Diagnosis and Prognosis through Quantitative Measurements of Serum Glycan Profiles. *Clinical Chemistry* 54, 1166-1175
155. Aoki, K., Perlman, M., Lim, J.-M., Cantu, R., Wells, L., and Tiemeyer, M. (2007) Dynamic Developmental Elaboration of N-Linked Glycan Complexity in the Drosophila melanogaster Embryo. *Journal of Biological Chemistry* 282, 9127-9142
156. Satomaa, T., Heiskanen, A., Mikkola, M., Olsson, C., Blomqvist, M., Tiittanen, M., Jaatinen, T., Aitio, O., Olonen, A., Helin, J., Hiltunen, J., Natunen, J., Tuuri, T., Otonkoski, T., Saarinen, J., and Laine, J. (2009) The N-glycome of human embryonic stem cells. *BMC Cell Biology* 10, 42
157. Mohal, J. S., Tailor, H. D., and Khan, W. S. (2012) Sources of adult mesenchymal stem cells and their applicability for musculoskeletal applications. *Current stem cell research & therapy* 7, 103-109
158. Li, T. Y., Shu, C., Wong, C. H. Y., Lo, P. S., Zhu, H., Lau, M. C., Chan, M. Y., Tsang, L. L., Gou, Y. L., Chung, Y. W., and Chan, H. C. (2004) Plasticity of rat bone marrow-derived 5-hydroxytryptamine-sensitive neurons: dedifferentiation and redifferentiation. *Cell Biology International* 28, 801-807
159. Woodbury, D., Reynolds, K., and Black, I. B. (2002) Adult bone marrow stromal stem cells express germline, ectodermal, endodermal, and mesodermal genes prior to neurogenesis. *Journal of Neuroscience Research* 69, 908-917
160. Reinke, S. O., Bayer, M., Berger, M., Blanchard, V. r., and Hinderlich, S. Analysis of Cell Surface N-glycosylation of the Human Embryonic Kidney 293T Cell Line. *Journal of Carbohydrate Chemistry* 30, 218-232
161. Yan, S. B., Chao, Y. B., and van Halbeek, H. (1993) Novel Asn-linked oligosaccharides terminating in GalNAc β (1-4)[Fuc α (1-3)]GlcNAcB(1 \rightarrow .) are present in recombinant human Protein C expressed in human kidney 293 cells. *Glycobiology* 3, 597-608
162. Ho, S. C. L., Koh, E. Y. C., van Beers, M., Mueller, M., Wan, C., Teo, G., Song, Z., Tong, Y. W., Bardor, M., and Yang, Y. (2013) Control of IgG LC:HC ratio in stably transfected CHO cells and study of the impact on expression, aggregation, glycosylation and conformational stability. *Journal of Biotechnology* 165, 157-166
163. Lee, K., Lee, S., Gil, J., Kwon, O., Kim, J., Park, S., Chung, H.-S., and Oh, D.-B. (2013) N-glycan analysis of human α 1-antitrypsin produced in Chinese hamster ovary cells. *Glycoconjugate Journal* 30, 537-547
164. Hokke, C. H., Bergwerff, A. A., Van Dedem, G. W. K., Kamerling, J. P., and Vliegthart, J. F. G. (1995) Structural Analysis of the Sialylated N- and O-Linked Carbohydrate Chains of Recombinant Human Erythropoietin Expressed in Chinese Hamster Ovary Cells. *European Journal of Biochemistry* 228, 981-1008

165. Blanchard, V., Liu, X., Eigel, S., Kaup, M., Rieck, S., Janciauskiene, S., Sandig, V., Marx, U., Walden, P., Tauber, R., and Berger, M. N-glycosylation and biological activity of recombinant human alpha1-antitrypsin expressed in a novel human neuronal cell line. *Biotechnology and Bioengineering* 108, 2118-2128
166. Rudd, P. M., Endo, T., Colominas, C., Groth, D., Wheeler, S. F., Harvey, D. J., Wormald, M. R., Serban, H., Prusiner, S. B., Kobata, A., and Dwek, R. A. (1999) Glycosylation differences between the normal and pathogenic prion protein isoforms. *Proceedings of the National Academy of Sciences* 96, 13044-13049
167. Stimson, E., Hope, J., Chong, A., and Burlingame, A. L. (1999) Site-Specific Characterization of the N-Linked Glycans of Murine Prion Protein by High-Performance Liquid Chromatography/Electrospray Mass Spectrometry and Exoglycosidase Digestions. *Biochemistry* 38, 4885-4895
168. Hutchinson, W. L., Du, M.-Q., Johnson, P. J., and Williams, R. (1991) Fucosyltransferases: Differential plasma and tissue alterations in hepatocellular carcinoma and cirrhosis. *Hepatology* 13, 683-688
169. Matsumoto, K., Maeda, Y., Kato, S., and Yuki, H. (1994) Alteration of asparagine-linked glycosylation in serum transferrin of patients with hepatocellular carcinoma. *Clinica Chimica Acta* 224, 1-8
170. Noda, K., Miyoshi, E., Uozumi, N., Gao, C.-X., Suzuki, K., Hayashi, N., Hori, M., and Taniguchi, N. (1998) High expression of α -1-6 fucosyltransferase during rat hepatocarcinogenesis. *International Journal of Cancer* 75, 444-450
171. Johnson, P. J., Poon, T. C. W., Hjelm, N. M., Ho, C. S., Ho, S. K. W., Welby, C., Stevenson, D., Patel, T., Parekh, R., and Townsend, R. R. (1999) Glycan composition of serum alpha-fetoprotein in patients with hepatocellular carcinoma and non-seminomatous germ cell tumour. *Br J Cancer* 81, 1188-1195
172. Pittenger, M. F., Mackay, A. M., Beck, S. C., Jaiswal, R. K., Douglas, R., Mosca, J. D., Moorman, M. A., Simonetti, D. W., Craig, S., and Marshak, D. R. (1999) Multilineage potential of adult human mesenchymal stem cells. *Science* 284, 143-147
173. Gronthos, S., Graves, S. E., Ohta, S., and Simmons, P. J. (1994) The STRO-1+ fraction of adult human bone marrow contains the osteogenic precursors. *Blood* 84, 4164-4173
174. Kolf, C. M., Cho, E., and Tuan, R. S. (2007) Mesenchymal stromal cells. Biology of adult mesenchymal stem cells: regulation of niche, self-renewal and differentiation. *Arthritis research & therapy* 9, 204
175. Menssen, A., Haupl, T., Sitterling, M., Delorme, B., Charbord, P., and Ringe, J. (2011) Differential gene expression profiling of human bone marrow-derived mesenchymal stem cells during adipogenic development. *BMC Genomics* 12, 461
176. Wearne, K. A., Winter, H. C., O'Shea, K., and Goldstein, I. J. (2006) Use of lectins for probing differentiated human embryonic stem cells for carbohydrates. *Glycobiology* 16, 981-990
177. Hemmoranta, H., Satomaa, T., Blomqvist, M., Heiskanen, A., Aitio, O., Saarinen, J., Natunen, J., Partanen, J., Laine, J., and Jaatinen, T. (2007) N-glycan structures and associated gene expression reflect the characteristic N-glycosylation pattern of human hematopoietic stem and progenitor cells. *Experimental hematology* 35, 1279-1292
178. Parodi, A. J. (2000) Protein glucosylation and its role in protein folding. *Annual review of biochemistry* 69, 69-93
179. An, H. J., Gip, P., Kim, J., Wu, S., Park, K. W., McVaugh, C. T., Schaffer, D. V., Bertozzi, C. R., and Lebrilla, C. B. (2012) Extensive determination of glycan heterogeneity reveals an unusual abundance of high mannose glycans in enriched plasma membranes of human embryonic stem cells. *Molecular & cellular proteomics : MCP* 11, M111 010660

180. Morad, V., Pevsner-Fischer, M., Barnees, S., Samokovlisky, A., Rousso-Noori, L., Rosenfeld, R., and Zipori, D. (2008) The myelopoietic supportive capacity of mesenchymal stromal cells is uncoupled from multipotency and is influenced by lineage determination and interference with glycosylation. *Stem Cells* 26, 2275-2286
181. Fukuda, M., Fukuda, M. N., and Hakomori, S. (1979) Developmental change and genetic defect in the carbohydrate structure of band 3 glycoprotein of human erythrocyte membrane. *The Journal of biological chemistry* 254, 3700-3703
182. Leffler, H., Carlsson, S., Hedlund, M., Qian, Y., and Poirier, F. (2004) Introduction to galectins. *Glycoconjugate journal* 19, 433-440
183. Stowell, S. R., Arthur, C. M., Mehta, P., Slanina, K. A., Blixt, O., Leffler, H., Smith, D. F., and Cummings, R. D. (2008) Galectin-1, -2, and -3 exhibit differential recognition of sialylated glycans and blood group antigens. *The Journal of biological chemistry* 283, 10109-10123
184. Stowell, S. R., Dias-Baruffi, M., Penttila, L., Renkonen, O., Nyame, A. K., and Cummings, R. D. (2004) Human galectin-1 recognition of poly-N-acetylglucosamine and chimeric polysaccharides. *Glycobiology* 14, 157-167
185. Toegel, S., Plattner, V. E., Wu, S. Q., Goldring, M. B., Chiari, C., Kolb, A., Unger, F. M., Nehrer, S., Gabor, F., Viernstein, H., and Wirth, M. (2009) Lectin binding patterns reflect the phenotypic status of in vitro chondrocyte models. *In Vitro Cell.Dev.Biol.-Animal* 45, 351-360
186. Bernard, B. A., De Luca, L. M., Hassell, J. R., Yamada, K. M., and Olden, K. (1984) Retinoic acid alters the proportion of high mannose to complex type oligosaccharides on fibronectin secreted by cultured chondrocytes. *Journal of Biological Chemistry* 259, 5310-5315
187. Pabst, M., Grass, J., Toegel, S., Liebming, E., Strasser, R., and Altmann, F. (2012) Isomeric analysis of oligomannosidic N-glycans and their dolichol-linked precursors. *Glycobiology* 22, 389-399
188. Yang, X., Yip, J., Anastassiades, T., Harrison, M., and Brockhausen, I. (2007) The action of TNF α and TGF β include specific alterations of the glycosylation of bovine and human chondrocytes. *Biochimica et Biophysica Acta (BBA) - Molecular Cell Research* 1773, 264-272
189. Richard, M., Vignon, E., Peschard, M., Broquet, P., Carret, J., and Louisot, P. (1990) Glycosyltransferase activities in chondrocytes from osteoarthritic and normal human articular cartilage. *Biochemistry International* 3, 535-542
190. Fukuda, M., and Hindsgaul, O. (2000) *Molecular and Cellular Glycobiology*, Oxford University Press, New York
191. Ardmann, B., and Staunton, D. E. (1999) CD34 interferes with t-lymphocyte adhesion. *Proceedings of the National Academy of Sciences*, 5001
192. Rosen, S., Singer, M., Yednock, T., and Stoolman, L. (1985) Involvement of sialic acid on endothelial cells in organ-specific lymphocyte recirculation. *Science* 228, 1005-1007
193. Takahata, M., Iwasaki, N., Nakagawa, H., Abe, Y., Watanabe, T., Ito, M., Majima, T., and Minami, A. (2007) Sialylation of cell surface glycoconjugates is essential for osteoclastogenesis. *Bone* 41, 77-86
194. Morishima, S., Morita, I., Tokushima, T., Kawashima, H., Miyasaka, M., Omura, K., and Murota, S. (2003) Expression and role of mannose receptor/terminal high-mannose type oligosaccharide on osteoclast precursors during osteoclast formation. *Journal of Endocrinology* 176, 285-292
195. Kurachi, T., Morita, I., Oki, T., Ueki, T., Sakaguchi, K., Enomoto, S., and Murota, S. (1994) Expression on outer membranes of mannose residues, which are involved in osteoclast formation via cellular fusion events. *Journal of Biological Chemistry* 269, 17572-17576

196. Schuldiner, M., Yanuka, O., Itskovitz-Eldor, J., Melton, D. A., and Benvenisty, N. (2000) Effects of eight growth factors on the differentiation of cells derived from human embryonic stem cells. *Proceedings of the National Academy of Sciences* 97, 11307-11312
197. Lavon, N., Yanuka, O., and Benvenisty, N. (2004) Differentiation and isolation of hepatic-like cells from human embryonic stem cells. *Differentiation* 72, 230-238
198. Wearne, K. A., Winter, H. C., O'Shea, K., and Goldstein, I. J. (2006) Use of lectins for probing differentiated human embryonic stem cells for carbohydrates. *Glycobiology* 16, 981-990
199. Lieke, T., Gröbe, D., Blanchard, V., Grunow, D., Tauber, R., Zimmermann-Kordmann, M., Jacobs, T., and Reutter, W. (2011) Invasion of *Trypanosoma cruzi* into host cells is impaired by N-propionylmannosamine and other N-acylmannosamines. *Glycoconjugate Journal* 28, 31-37
200. Reya, T., Morrison, S. J., Clarke, M. F., and Weissman, I. L. (2001) Stem cells, cancer, and cancer stem cells. *Nature* 414
201. Satomaa, T., Heiskanen, A., Mikkola, M., Olsson, C., Blomqvist, M., Tiittanen, M., Jaatinen, T., Aitio, O., Olonen, A., Helin, J., Hiltunen, J., Natunen, J., Tuuri, T., Otonkoski, T., Saarinen, J., and Laine, J. (2009) The N-glycome of human embryonic stem cells. *BMC cell biology* 10, 42
202. Venable, A., Mitalipova, M., Lyons, I., Jones, K., Shin, S., Pierce, M., and Stice, S. (2005) Lectin binding profiles of SSEA-4 enriched, pluripotent human embryonic stem cell surfaces. *BMC developmental biology* 5, 15
203. Tao, S. C., Li, Y., Zhou, J., Qian, J., Schnaar, R. L., Zhang, Y., Goldstein, I. J., Zhu, H., and Schneck, J. P. (2008) Lectin microarrays identify cell-specific and functionally significant cell surface glycan markers. *Glycobiology* 18, 761-769
204. Tateno, H., Uchiyama, N., Kuno, A., Togayachi, A., Sato, T., Narimatsu, H., and Hirabayashi, J. (2007) A novel strategy for mammalian cell surface glycome profiling using lectin microarray. *Glycobiology* 17, 1138-1146
205. Smith, P. K., Krohn, R. I., Hermanson, G. T., Mallia, A. K., Gartner, F. H., Provenzano, M. D., Fujimoto, E. K., Goeke, N. M., Olson, B. J., and Klenk, D. C. (1985) Measurement of protein using bicinchoninic acid. *Analytical Biochemistry* 150, 76-85
206. Lottspeich, F., and Engels, J. W. (2006) *Bioanalytik*, Elsevier, Spektrum Akademischer Verlag
207. LAEMMLI, U. (1970) Cleavage of Structural Proteins during the Assembly of the Head of Bacteriophage T4. *Nature* 227, 680-685
208. Dell, A., Reason, A. J., Khoo, K.-H., Panico, M., McDowell, R. A., and Morris, H. R. (1994) [8] Mass spectrometry of carbohydrate-containing biopolymers. In: William J. Lennarz, G. W. H., ed. *Methods in Enzymology*, pp. 108-132, Academic Press
209. Wada, Y., Azadi, P., Costello, C. E., Dell, A., Dwek, R. A., Geyer, H., Geyer, R., Kakehi, K., Karlsson, N. G., Kato, K., Kawasaki, N., Khoo, K.-H., Kim, S., Kondo, A., Lattova, E., Mechref, Y., Miyoshi, E., Nakamura, K., Narimatsu, H., Novotny, M. V., Packer, N. H., Perreault, H., Peter-Katalinić, J., Pohlentz, G., Reinhold, V. N., Rudd, P. M., Suzuki, A., and Taniguchi, N. (2007) Comparison of the methods for profiling glycoprotein glycans—HUPO Human Disease Glycomics/Proteome Initiative multi-institutional study. *Glycobiology* 17, 411-422
210. Maass, K., Ranzinger, R., Geyer, H., von der Lieth, C.-W., and Geyer, R. (2007) "Glyco-peakfinder" – de novo composition analysis of glycoconjugates. *Proteomics* 7, 4435-4444
211. Hara, S., Yamaguchi, M., Takemori, Y., Furuhata, K., Ogura, H., and Nakamura, M. (1989) Determination of mono-O-acetylated N-acetylneuraminic acids in human and rat sera by fluorometric high-performance liquid chromatography. *Analytical Biochemistry* 179, 162-166

6. Appendix

APPENDIX

Proposed N-glycan structures		Cell type				Proposed N-glycan structures		Cell type					
m/z	Composition	% in HEK-293 MP CS		% in CHO-K1	% in AGE1. HN	% in Hep G2	m/z	Composition	% in HEK-293 MP CS		% in CHO-K1	% in AGE1. HN	% in Hep G2
1171.5	H3N2	0.73	0.50	0.07	1.86	2.47	2839.1	S1H7N4			0.03		
1345.5	H3N2F1	1.05	0.34	2.52	0.83	1.84	2850.1	S1H5N5F1	0.16	2.37	0.02		0.14
1375.6	H4N2	0.43	0.14	3.03	0.54	1.06	2852.1	G2H5N4			0.05		
1416.6	H3N3	0.09	0.15	1.25	0.61	0.57	2861.1	S1H3N6F2		0.14			0.01
1549.6	H4N2F1	0.04	0.01			0.11	2867.1	H6N5F2	0.04			0.09	0.01
1579.6	H5N2	8.34	5.15	8.89	9.34	5.78	2880.1	S1H6N5	0.20	0.24	0.20		0.30
1590.6	H3N3F1	0.18	0.22	0.19	0.50	0.41	2897.1	H7N5F1			0.14		
1620.7	H4N3	0.09	0.03	0.57	0.43	0.25	2908.1	H5N6F2		0.06			
1661.7	H3N4	0.12	0.05	0.07	0.16	0.06	2938.1	H6N6F1	0.05	0.08			0.05
1753.7	H5N2F1	0.08	0.00			0.13	2966.1	S2H5N4F1	0.93	6.24	3.06	0.65	19.9
1783.7	H6N2	12.9	2.83	7.28	2.70	3.08	2979.1	H5N7F1			0.06		
1794.7	H4N3F1	0.13	0.10	0.65	0.56	0.23	2996.1	S1G1H5N4F1	0.08	0.14	0.14		0.43
1824.7	H5N3	0.15	0.21	0.73	0.65	0.18	3007.1	S2H4N5F1		0.50			0.42
1835.7	H3N4F1	0.42	0.62	0.59	0.67	0.17	3024.1	S1H5N5F2		0.21			0.06
1865.7	H4N4	0.18	0.20	0.91	0.73	0.26	3026.1	G2H5N4F1			0.07		0.13
1968.7	H4N3F2				0.16		3037.1	S2H5N5		0.03			0.04
1981.7	S1H4N3					0.15	3041.1	H6N5F3	0.04			0.34	
1987.7	H7N2	7.74	1.38	6.36	1.23	1.86	3048.1	S2H3N6F1		0.01			0.19
1998.7	H5N3F1	0.12	0.08	0.17	0.32	0.06	3054.1	S1H6N5F1	0.43	1.30	0.60	0.13	0.94
2028.8	H6N3	0.20	0.20	0.49	0.62	0.16	3082.1	H5N6F3					
2039.8	H4N4F1	0.22	0.61	1.01	1.14	0.27	3084.1	G1H6N5F1 / S1H7N5			0.06		0.07
2069.8	H5N4	0.29	2.06	5.29	5.50	1.28	3112.1	H6N6F2		0.10			
2080.8	H3N5F1	0.25	0.50	0.06	0.38	0.08	3140.1	S2H5N4F2					0.52
2155.8	S1H4N3F1	0.25	0.06	0.08	0.13	0.10	3142.1	H7N6F1	0.04		0.07		
2185.8	S1H5N3	0.43	0.18	0.13	0.36	0.34	3153.1	H5N7F2					0.12
2191.8	H8N2	21.6	2.34	11.87	2.79	2.84	3170.1	S2H6N4F1					0.03
2202.8	H6N3F1	0.10	0.01	0.09	0.33		3211.1	S2H5N5F1	0.04	0.26			0.13
2213.8	H4N4F2	0.09	0.40	0.19	0.28	0.05	3215.1	H6N5F4				2.75	
2215.8	G1H5N3			0.01			3228.1	S1H6N5F2	0.05	0.11		0.12	0.48
2226.8	S1H4N4		0.06	0.14	0.15	0.10	3241.1	S2H6N5	0.07	0.21	0.31		0.85
2243.8	H5N4F1	0.39	6.24	12.25	10.58	2.40	3256.1	H5N6F4			0.13	0.11	
2256.8	G1H4N4			0.04			3269.1	S1H5N6F2		0.06			
2273.8	H6N4		0.03	0.21	0.07	0.03	3299.1	S1H6N6F1	0.03	0.15			0.00
2284.8	H4N5F1	0.24	3.01	0.05	0.18	0.08	3316.1	H7N6F2	0.01				
2314.8	H5N5	0.27	0.18	0.05	0.10	0.01	3329.1	S1H7N6	0.03				0.06
2325.8	H3N6F1	0.11	0.23	0.02	0.08	0.01	3385.1	S2H5N5F2					0.00
2359.9	S1H5N3F1	0.29	0.11	0.01	0.13	0.10	3403.1	S1H6N5F3	0.03	0.01		0.81	0.19
2389.9	S1H6N3	0.53	0.18	0.16	0.31	0.40	3416.1	S2H6N5F1	0.30	1.51	1.26	0.04	1.21
2395.9	H9N2	30.9	1.83	4.67	1.70	0.94	3457.1	S2H5N6F1		0.11			
2400.9	S1H4N4F1		0.18	0.08	0.30	0.19	3461.1	H6N6F4				0.09	
2417.9	H5N4F2	0.24	1.01	0.70	3.24	0.45	3474.1	S1H6N6F2		0.07			0.03
2430.9	S1H5N4	1.07	4.24	4.78	5.01	4.04	3491.1	H7N6F3				0.08	
2447.9	H6N4F1			1.08	0.36	0.30	3504.1	S1H7N6F1	0.09	0.16	0.08		0.35
2458.9	H4N5F2	0.33	6.19				3590.1	S2H6N5F2	0.04	0.14		0.13	1.60
2460.9	G1H5N4			0.44		0.24	3602.1	S3H6N5	0.03	0.71	0.26		3.59
2471.9	S1H4N5		0.12			0.05	3620.1	S2H7N5F1			0.20		
2477.9	H7N4			0.01			3633.1	H7N8F1					0.11
2488.9	H5N5F1	0.19	1.63	0.13	0.16	0.10	3661.1	S2H6N6F1		0.13			
2499.9	H3N6F2		1.34				3665.1	H7N6F4				0.62	
2518.9	H6N5	0.11	0.11	0.17		0.01	3678.1	S1H7N6F2	0.03			0.06	0.18
2529.9	H4N6F1		0.05				3691.1	S2H7N6	0.04		0.02		0.07
2546.9	S2H5N3	0.09		0.03		0.11	3749.1	S1H7N7F1		0.03			
2563.9	S1H6N3F1	0.10		0.03		0.06	3763.2	S2H6N5F3					0.25
2574.9	S1H4N4F2					0.02	3776.2	S3H6N5F1	0.15	1.45	0.66		2.37
2587.9	H4N4S2						3806.2	S2G1H6N5F1					0.10
2591.9	H5N4F3	0.16	0.16		8.70	0.17	3839.2	H7N6F5				5.93	
2599.9	H10N2	1.03	0.02	0.02	0.02	0.01	3852.2	S1H7N6F3				0.62	0.17
2604.9	S1H5N4F1	2.59	18.2	9.31	10.17	10.3	3864.2	S2H7N6F1	0.22	0.67	0.15	0.01	0.44
2632.9	H4N5F3		0.93		0.53		3951.2	S3H6N5F2					3.60
2634.9	G1H5N4F1	0.19	2.20	1.61	3.54	0.63	3964.2	S4H6N5		0.10	0.04		0.92
2645.9	S1H4N5F1	0.19	2.21			0.23	4026.2	S1H7N6F4				4.74	0.01
2652.0	H7N4F1			0.24		0.12	4039.2	S2H7N6F2	0.02	0.12		0.23	0.67
2663.1	H5N5F2	0.08	0.72		0.12	0.06	4069.3	S2H8N6F1			0.02		
2674.1	H3N6F3	0.29			0.07	0.06	4125.3	S3H6N5F3					0.14
2676.1	S1H5N5		2.02	0.02			4213.3	S2H7N6F3	0.01	0.01		0.98	0.37

APPENDIX

2687.1	S1H3N6F1		0.21			0.04	4226.3	S3H7N6F1	0.09	1.28	0.11	0.01	0.37
2693.1	H6N	0.13	0.23	0.40	0.09	0.10	4314.3	S2H8N7F1			0.02		0.05
2723.1	H7N5	0.07		0.03			4400.4	S3H7N6F2		0.05		0.11	0.57
2734.1	H5N6F1		0.10				4574.4	S3H7N6F3					0.51
2779.1	S1H5N4F2	0.30	1.01	0.16	2.16	2.79	4587.4	S4H7N6F1	0.08	0.85	0.08	0.01	0.15
2792.1	S2H5N4	0.19	1.37	1.41	0.41	6.84	4662.4	S2H8N7F3					0.10
2809.1	S1H6N4F1			1.24	0.11	0.65	4675.4	S3H8N7F1			0.03		
2820.1	S1H4N5F2	0.21	5.58		0.06	0.16	4761.5	S4H7N6F2					0.78
2822.1	S1G1H5N4			0.07		0.11	4849.5	S3H8N7F2					0.11
2833.1	S2H4N5					0.09	4935.6	S4H7N6F3					0.31
2837.1	H5N5F3		0.24		0.17	0.01							

Table 1. The average relative amounts of all PNGase F-released N-glycans of HEK 293 from cell membrane preparation (MP) and cell surface (CS) as well as of CHO, AGE1.HN and HEP G2 cells (4 repetitions for HEK 293, 3 repetitions for CHO, AGE1.HN and HEP G2). H: hexose, N: N-acetylhexosamine, F: deoxyhexose, S: N-acetylneuraminic acid.

Endo H-released N-glycans				
m/z	Composition	% in MSCs	% in A day 5	% in A day 15
926.4	H3N1	0.61	0.76	0.81
1130.5	H4N1	0.20	0.34	0.49
1334.6	H5N1	6.63	18.53	13.93
1538.7	H6N1	18.48	26.20	25.89
1579.7	H5N2	1.65	0.87	0.61
1742.8	H7N1	12.14	9.61	10.62
1783.8	H6N2	4.14	1.63	0.98
1940.9	H5N2S1	0.51	0.33	0.20
1946.9	H8N1	27.17	22.43	28.20
2145.0	H6N2S1	1.12	0.67	0.56
2151.0	H9N1	26.70	18.44	17.56
2355.1	H10N1	0.63	0.20	0.14

Table 2. The average relative amounts of Endo H-released N-glycans of undifferentiated and adipogenically differentiated (A) human MSCs on day 5 and day 15 of differentiation derived from three different donors. H: hexose, N: N-acetylhexosamine, F: deoxyhexose, S: N-acetylneuraminic acid.

PNGase F-released N-glycans									
m/z	Composition	% in MSCs	% in A day 5	% in A day 15	m/z	Composition	% in MSCs	% in A day 5	% in A day 15
1171.6	H3N2	0.21	0.30	0.26	2751.3	S2H6N3	0.04	0.02	0.00
1334.6	H5N1	0.16	0.20	0.11	2779.3	S1H5N4F2	0.10	0.13	0.27
1345.6	H3N2F1	0.68	0.70	0.83	2792.3	S2H5N4	0.79	0.86	1.21
1375.6	H4N2	0.05	0.06	0.04	2809.3	S1H6N4F1	0.05	0.04	0.04
1416.7	H3N3	0.07	0.14	0.21	2839.4	S1H7N4	0.02	0.01	0.00
1538.7	H6N1	0.38	0.34	0.34	2850.4	S1H5N5F1	0.08	0.04	0.09
1579.7	H5N2	0.12	0.11	0.07	2867.4	H6N5F2	0.04	0.07	0.07
1590.8	H3N3F1	0.25	0.54	0.90	2880.4	S1H6N5	1.69	0.79	0.48
1620.8	H4N3	0.08	0.12	0.12	2938.4	H6N6F1	0.06	0.04	0.06
1661.8	H3N4	0.01	0.02	0.04	2953.4	S1H5N4F3	0.04	0.12	0.24
1742.8	H7N1	0.23	0.13	0.16	2966.4	S2H5N4F1	4.11	7.27	9.09
1783.8	H6N2	0.10	0.03	0.03	2996.4	S2H6N4	0.28	0.73	0.51
1794.9	H4N3F1	0.40	0.29	0.19	3054.5	S1H6N5F1	8.77	5.86	5.24
1824.9	H5N3	0.83	2.00	0.62	3084.5	S1H7N5	0.47	0.33	0.23
1835.9	H3N4F1	0.24	0.71	1.87	3112.5	N6H6F2	0.01	0.01	0.00
1865.9	H4N4	0.04	0.06	0.11	3142.5	H7N6F1	5.58	0.64	0.43
1940.9	S1H5N2	0.13	0.23	0.14	3200.5	S2H7N4	0.01	0.01	0.00
1946.9	H8N1	0.65	0.40	0.59	3215.6	H6N5F4	0.01	0.00	0.00
1968.9	H4N3F2	0.01	0.02	0.02	3228.6	S1H6N5F2	0.02	0.04	0.07
1981.9	S1H4N3	0.03	0.05	0.07	3241.6	S2H6N5	0.44	0.28	0.41
1999.0	H5N3F1	0.16	0.05	0.05	3257.6	S1H7N5F1	0.00	0.00	0.06
2029.0	H6N3	0.05	0.05	0.03	3299.6	S1H6N6F1	0.08	0.02	0.02
2040.0	H4N4F1	0.23	0.22	0.26	3316.6	H7N6F2	0.02	0.00	0.00
2070.0	H5N4	2.12	3.62	2.52	3329.6	S1H7N6	0.58	0.15	0.07
2081.0	H3N5F1	0.02	0.07	0.19	3357.6	H6N7F2	0.03	0.12	0.18
2145.0	S1H6N2	0.08	0.07	0.08	3415.7	S2H6N5F1	2.10	3.87	4.04
2151.0	H9N1	0.45	0.25	0.30	3445.7	S2H7N5	0.27	0.30	0.20
2156.0	S1H4N3F1	0.22	0.27	0.30	3503.7	S1H7N6F1	5.29	1.03	0.96
2186.0	S1H5N3	0.89	2.92	1.47	3591.7	H8N7F1	0.37	0.04	0.11
2214.1	H4N4F2	0.05	0.04	0.06	3602.7	S3H6N5	0.14	0.34	2.08
2227.1	S1H4N4	0.02	0.03	0.06	3660.8	S2H6N6F1	0.02	0.00	0.00
2244.1	H5N4F1	16.81	18.42	12.41	3690.8	S2H7N6	0.19	0.03	0.05
2274.1	H6N4	0.56	0.62	0.31	3776.8	S3H6N5F1	0.36	0.27	1.91
2285.1	H4N5F1	0.01	0.02	0.01	3806.8	S3H7N5	0.06	0.09	0.16
2360.1	S1H5N3F1	0.09	0.03	0.07	3864.9	S2H7N6F1	2.19	0.59	1.22
2390.1	S1H6N3	0.04	0.08	0.05	3894.9	S2H8N6	0.05	0.02	0.04
2401.1	S1H4N4F1	0.09	0.12	0.17	3952.9	S1H8N7F1	0.14	0.02	0.17
2418.2	H5N4F2	0.16	0.34	0.53	3964.9	S4H6N5	0.00	0.02	0.22
2431.2	S1H5N4	2.91	4.33	5.41	4041.0	H9N8F1	0.07	0.00	0.00
2448.2	H6N4F1	0.03	0.04	0.04	4052.0	S3H7N6	0.03	0.00	0.00
2461.2	G1H5N4	0.03	0.05	0.10	4140.0	S2H8N7	0.01	0.00	0.00
2478.2	H7N4	0.01	0.01	0.00	4226.1	S3H7N6F1	0.82	0.17	0.98
2489.2	H5N5F1	0.09	0.14	0.15	4314.1	S2H8N7F1	0.15	0.01	0.10
2519.2	H6N5	2.40	0.74	0.30	4402.2	S1H9N8F1	0.05	0.00	0.03
2592.3	H5N4F3	0.24	0.71	1.45	4587.3	S4H7N6F1	0.15	0.03	0.41
2605.3	S1H5N4F1	20.36	30.85	32.31	4675.4	S3H8N7F1	0.04	0.00	0.08
2635.3	S1H6N4	0.86	1.62	1.10	4764.4	S2H9N8F1	0.00	0.00	0.08
2693.3	H6N5F1	10.52	3.43	2.10					

Table 3. The average relative amounts of all PNGase F-released N-glycans of undifferentiated and adipogenically differentiated (A) human MSCs on day 5 and day 15 of differentiation derived from three different donors. H: hexose, N: N-acetylhexosamine, F: deoxyhexose, S: N-acetylneuraminic acid.

PNGase F-released N-glycans													
m/z	Compo- sition	% in MSC	% in C day 5		% in C day 28		m/z	Compo- sition	% in MSC	% in C day 5		% in C day 28	
			-	+	-	+				-	+		
			ECM	ECM	ECM	ECM				ECM	ECM		
1171.6	H3N2	0.32	0.07	0.67	0.60	0.60	2461.2	G1H5N4	0.09	0.05	0.30	0.06	0.27
1345.6	H3N2F1	0.27	0.17	3.14	5.04	3.00	2489.2	H5N5F1	0.07	0.02	0.06	0.02	0.06
1375.6	H4N2	0.21	0.07	0.52	0.39	0.54	2519.2	H6N5	0.00	0.04	0.05	0.02	0.03
1416.7	H3N3	0.11	0.03	0.32	0.07	0.37	2547.2	S1H5N3	0.07	0.02	0.10	0.06	0.00
1549.7	H4N2F1	0.00	0.00	0.14	0.08	0.07	2564.2	S1H6N3F1	0.07	0.01	0.05	0.02	0.01
1579.7	H5N2	4.84	2.64	13.97	5.23	16.17	2592.3	H5N4F3	0.01	0.00	0.44	0.00	0.86
1590.8	H3N3F1	0.12	0.20	5.34	0.19	6.38	2599.3	H10N2	0.00	0.02	0.04	0.00	0.00
1620.8	H4N3	0.06	0.06	0.26	0.07	0.21	2605.3	S1H5N4F1	38.00	40.81	9.54	30.83	7.48
1661.8	H3N4	0.00	0.00	0.07	0.02	0.19	2635.3	S1H6N4	0.57	0.28	0.51	0.29	0.39
1753.8	H5N2F1	0.00	0.00	0.09	0.04	0.07	2646.3	S1H4N5F1	0.00	0.05	0.02	0.02	0.00
1783.8	H6N2	3.21	1.14	8.49	2.35	7.45	2693.3	H6N5F1	2.98	1.09	0.54	0.41	0.57
1794.9	H4N3F1	0.15	0.22	0.72	0.29	0.54	2779.3	S1H5N4F2	0.17	0.48	0.33	1.90	0.19
1824.9	H5N3	0.22	0.22	0.55	0.17	0.33	2792.3	S2H5N4	1.02	0.44	0.78	1.11	0.32
1835.9	H3N4F1	0.05	0.02	6.32	0.04	8.98	2809.3	S1H6N4F1	0.06	0.03	0.03	0.03	0.00
1865.9	H4N4	0.07	0.11	0.33	0.10	0.30	2822.4	S1G1H5N4	0.01	0.01	0.02	0.02	0.00
1968.9	H4N3F2	0.00	0.00	0.19	0.07	0.42	2850.4	S1H5N5F1	0.06	0.01	0.03	0.02	0.02
1981.9	S1H4N3	0.07	0.03	0.08	0.20	0.00	2866.4	H6N5F2	0.01	0.00	0.01	0.00	0.02
1987.9	H7N2	5.57	0.86	7.73	1.52	7.18	2880.4	S1H6N5	0.14	0.03	0.04	0.03	0.02
1999.0	H5N3F1	0.34	0.15	0.55	0.08	0.36	2938.4	H6N6F1	0.02	0.00	0.00	0.00	0.00
2029.0	H6N3	0.48	0.22	0.89	0.21	0.43	2966.4	S2H5N4F1	4.60	7.81	1.79	15.85	0.89
2040.0	H4N4F1	0.33	0.43	1.28	0.46	1.08	2979.4	H5N7F1	0.00	0.00	0.00	0.02	0.00
2070.0	H5N4	0.97	2.35	2.45	1.23	1.61	2996.4	S2H6N4	0.09	0.03	0.04	0.05	0.01
2081.0	H3N5F1	0.00	0.10	1.94	0.79	2.23	3026.4	G2H5N4F1	0.02	0.01	0.01	0.01	0.00
2156.0	S1H4N3F1	0.10	0.12	0.32	3.39	0.16	3054.5	S1H6N5F1	4.22	1.80	0.57	1.30	0.51
2186.0	S1H5N3	0.20	0.15	0.22	0.32	0.05	3084.5	S1H7N5	0.02	0.00	0.00	0.00	0.00
2192.0	H8N2	2.38	0.73	8.66	1.36	11.51	3142.5	H7N6F1	1.22	0.07	0.08	0.03	0.09
2203.0	H6N3F1	0.18	0.03	0.23	0.03	0.10	3211.5	S2H5N5F1	0.00	0.00	0.00	0.01	0.00
2214.1	H4N4F2	0.04	0.01	0.72	0.03	1.09	3228.6	S1H6N5F2	0.00	0.02	0.01	0.05	0.00
2227.1	S1H4N4	0.04	0.04	0.05	0.05	0.00	3241.6	S2H6N5	0.08	0.02	0.02	0.06	0.01
2244.1	H5N4F1	16.74	29.46	9.29	13.31	8.37	3402.6	S1H6N5F3	0.00	0.00	0.00	0.01	0.00
2274.1	H6N4	0.03	0.05	0.02	0.03	0.04	3415.7	S2H6N5F1	1.50	1.33	0.24	2.31	0.09
2285.1	H4N5F1	0.02	0.08	0.11	0.05	0.29	3503.7	S1H7N6F1	1.52	0.09	0.09	0.06	0.06
2326.1	H3N6F1	0.00	0.03	0.02	0.02	0.03	3591.7	H8N7F1	0.04	0.02	0.01	0.08	0.00
2360.1	S1H5N3F1	0.22	0.08	0.26	0.12	0.03	3602.7	S3H6N5	0.28	0.06	0.06	0.91	0.01
2390.1	S1H6N3	0.15	0.07	0.22	0.24	0.15	3776.8	S3H6N5F1	0.13	0.41	0.06	1.07	0.02
2396.1	H9N2	0.82	0.30	4.12	1.02	4.98	3864.9	S2H7N6F1	1.09	0.11	0.05	0.08	0.06
2401.1	S1H4N4F1	0.14	0.12	0.36	0.28	0.41	4226.1	S3H7N6F1	0.46	0.02	0.02	0.08	0.02
2418.2	H5N4F2	0.49	0.91	1.10	0.73	0.63	4314.1	S2H8N7F1	0.03	0.00	0.00	0.00	0.00
2431.2	S1H5N4	2.17	3.15	2.01	2.58	1.28	4587.3	S4H7N6F1	0.09	0.01	0.01	0.01	0.00
2448.2	H6N4F1	0.02	0.03	0.02	0.02	0.00							

Table 4. The average relative amounts of all PNGase F-released N-glycans of undifferentiated and chondrogenically differentiated (C) human MSCs on day 5 and day 28 of differentiation. Chondrogenically differentiated MSCs with and without their extracellular matrix (ECM) were used for the analysis. Data were derived from three (C without ECM) or four (undifferentiated MSCs and C with ECM) different replicates. H: hexose, N: N-acetylhexosamine, F: deoxyhexose, S: N-acetylneuraminic acid. – ECM: without ECM, + ECM: with ECM.



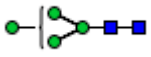


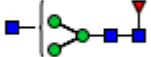
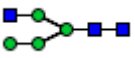
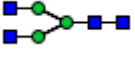
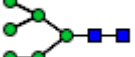

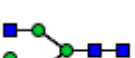




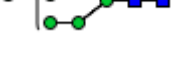

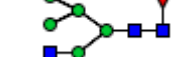
APPENDIX

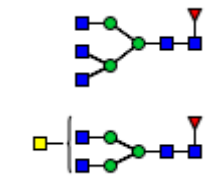
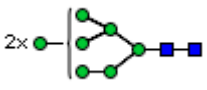















PNGase F-released N-glycans									
m/z	Composition	% in MSC	% in O day 5 -ECM	% in O day 28 -ECM	m/z	Composition	% in MSC	% in O day 5 -ECM	% in O day 28 -ECM
1171.6	H3N2	0.11	0.05	0.51	2676.3	S1H5N5	0.05	0.04	0.00
1345.6	H3N2F1	0.57	0.28	0.62	2693.3	H6N5F1	4.40	3.20	2.99
1375.6	H4N2	0.19	0.40	0.48	2749.3	S1H4N4F3	0.00	0.04	0.00
1416.7	H3N3	0.11	0.23	0.34	2762.3	S2H4N4F1	0.00	0.06	0.00
1579.7	H5N2	2.31	2.73	2.25	2779.3	S1H5N4F2	1.02	1.27	0.00
1590.8	H3N3F1	0.27	0.53	0.57	2809.3	S1H6N4F1	0.60	0.51	0.77
1620.8	H4N3	0.35	0.40	0.42	2822.4	S1G1H5N4	0.50	0.48	0.40
1661.8	H3N4	0.07	0.00	0.31	2839.4	S1H7N4	0.08	0.00	0.19
1783.8	H6N2	2.28	1.69	2.12	2850.4	S1H5N5F1	0.33	0.46	0.19
1794.9	H4N3F1	0.48	0.84	0.76	2866.4	H6N5F2	0.29	0.35	0.08
1824.9	H5N3	0.85	0.95	0.82	2880.4	S1H6N5	1.12	0.62	0.46
1835.9	H3N4F1	0.30	0.30	0.41	2938.4	H6N6F1	0.00	0.03	0.00
1865.9	H4N4	0.53	0.38	0.77	2952.4	G1H5N6	0.06	0.08	0.00
1981.9	S1H4N3	0.15	0.39	0.33	2966.4	S2H5N4F1	3.63	6.06	3.18
1987.9	H7N2	4.65	2.53	1.84	2979.4	H5N7F1	0.00	0.52	0.00
1999.0	H5N3F1	1.15	0.51	0.74	2996.4	S1G1H5N4F1	0.57	0.76	0.36
2029.0	H6N3	1.18	0.84	0.66	3026.4	G2H5N4F1	0.18	0.05	0.00
2040.0	H4N4F1	0.68	1.03	1.50	3037.4	S2H5N5	0.41	0.33	0.45
2070.0	H5N4	2.50	2.34	3.16	3054.5	S1H6N5F1	3.08	4.90	2.25
2081.0	H3N5F1	0.31	0.18	0.44	3084.5	S1H7N5	0.28	0.41	0.00
2156.0	S1H4N3F1	0.31	0.42	0.36	3136.5	S1H4N7F1	0.48	0.00	0.44
2186.0	S1H5N3	0.54	1.06	0.49	3142.5	H7N6F1	2.28	0.77	0.48
2192.0	H8N2	5.64	1.34	2.81	3211.5	S2H5N5F1	0.00	0.05	0.00
2203.0	H6N3F1	0.77	0.35	0.44	3228.6	S1H6N5F2	0.25	0.46	0.56
2227.1	S1H4N4	0.30	0.36	0.43	3258.6	S1H7N5F1	0.00	0.00	0.23
2244.1	H5N4F1	12.31	12.50	22.42	3299.6	S1H6N6F1	0.00	0.05	0.00
2258.1	G1H4N4	0.00	0.00	0.24	3323.6	S2H4N7	0.78	0.00	0.32
2274.1	H6N4	0.88	0.51	0.79	3329.6	S1H7N6	0.09	0.00	0.00
2285.1	H4N5F1	0.51	0.36	0.30	3358.6	H6N7F2	0.39	0.09	0.24
2326.1	H3N6F1	0.69	0.04	0.97	3415.7	S2H6N5F1	2.15	0.10	0.00
2360.1	S1H5N3F1	0.63	0.35	0.40	3428.6	H6N8F1	0.00	4.70	1.21
2390.1	S1H6N3	0.61	0.58	0.47	3445.6	S2H7N5	0.26	0.40	0.00
2396.1	H9N2	2.66	1.20	2.59	3474.6	S1H6N6F2	0.08	0.43	0.00
2401.1	S1H4N4F1	0.49	0.69	0.44	3503.7	S1H7N6F1	1.99	0.99	0.49
2418.2	H5N4F2	1.07	1.47	0.94	3632.8	H7N8F1	1.86	1.08	1.03
2431.2	S1H5N4	3.03	3.87	3.68	3766.8	H8N7F2	1.00	0.00	0.31
2448.2	H6N4F1	0.45	0.21	0.50	3776.8	S3H6N5F1	1.10	2.08	0.48
2461.2	G1H5N4	0.61	0.58	0.47	3807.8	G1H8N7	0.00	0.17	0.00
2472.2	S1H4N5	0.39	0.00	0.29	3864.9	S2H7N6F1	1.80	0.81	0.43
2478.2	H7N4	0.25	0.00	0.36	3952.9	S1H8N7F1	0.32	0.07	0.00
2489.2	H5N5F1	0.36	0.40	0.40	3976.9	S2H6N8	0.00	0.66	0.00
2547.2	S1H5N3	0.26	0.43	0.30	4046.0	unknown	0.60	0.00	0.61
2564.2	S1H6N3F1	0.22	0.00	0.25	4128.0	S1H8N7F2	0.55	0.00	0.00
2588.2	S2H4N4	0.09	0.06	0.00	4226.1	S3H7N6F1	1.23	0.44	0.10
2592.3	H5N4F3	0.00	0.00	0.00	4314.1	S2H8N7F1	0.39	0.12	0.00
2605.3	S1H5N4F1	11.43	20.57	21.01	4326.1	S5H6N5	0.12	0.04	0.00
2635.3	S1H6N4/	1.31	1.80	1.15	4587.1	S4H7N6F1	0.75	0.30	0.00
2663.3	H5N5F2	0.00	0.09	0.22	4676.1	S3H8N7F1	0.10	0.07	0.00


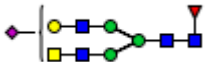










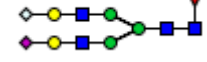



Table 5. The average relative amounts of all PNGase F-released N-glycans of undifferentiated and osteogenically differentiated (O) human MSCs on day 5 and day 28 of differentiation derived from three different preparations. Day 5 and 28 osteogenically differentiated MSCs were isolated from their ECM prior to N-glycan analysis. H: hexose, N: N-acetylhexosamine, F: deoxyhexose, S: N-acetylneuraminic acid, -ECM: without ECM.

PNGase F-released N-glycans									
m/z	Composition	% in ESC	% in DEC	% in HLC	m/z	Composition	% in ESC	% in DEC	% in HLC
1171.6	H3N2	1.49	1.64	1.08	2500.2	H3N6F2			0.01
1345.6	H3N2F1	2.64	2.22	2.36	2519.2	H6N5	0.08		0.14
1375.6	H4N2	1.23	1.52	0.72	2530.2	H4N6F1	2.93	0.79	
1416.7	H3N3	0.69	0.45	0.23	2547.2	S1H5N3			0.01
1549.7	H4N2F1	1.48	0.22	0.04	2560.2	H5N6	0.11		
1579.7	H5N2	4.43	10.67	5.78	2592.3	H5N4F3	0.23	0.13	0.52
1590.8	H3N3F1	0.82	0.62	0.59	2599.3	H10N2	0.14	0.06	
1620.8	H4N3	0.57	0.20	0.34	2605.3	S1H5N4F1	0.70	3.84	25.23
1661.8	H3N4	0.43	0.15	0.07	2635.3	S1H6N4/ G1H5N4F1	0.16	0.10	0.18
1753.8	H5N2F1	1.12	0.07	0.03	2646.3	S1H4N5F1		0.08	0.18
1783.8	H6N2	9.21	14.36	3.02	2652.3	H7N4F1	0.11		
1794.9	H4N3F1	2.54	0.35	0.30	2663.3	H5N5F2	0.12	0.05	0.27
1824.9	H5N3	0.45	0.19	0.31	2676.3	S1H5N5	0.07	0.06	0.07
1835.9	H3N4F1	6.07	3.36	0.30	2687.3	S1H3N6F1		0.02	0.09
1865.9	H4N4	0.59	0.20	0.23	2693.3	H6N5F1	0.71	0.29	1.40
1968.9	H4N3F2	0.78		0.01	2734.3	H5N6F1	3.43	1.50	0.06
1981.9	S1H4N3			0.08	2764.3	H6N6	0.08		
1987.9	H7N2	14.60	16.97	2.28	2779.3	S1H5N4F2	0.19	0.53	0.44
1999.0	H5N3F1	1.08	0.23	0.09	2792.3	S2H5N4			0.06
2029.0	H6N3	0.14	0.12	0.14	2809.3	S1H6N4F1			0.01
2040.0	H4N4F1	5.98	3.34	1.22	2820.3	S1H4N5F2		0.02	0.01
2070.0	H5N4	0.71	0.31	1.49	2837.4	H5N5F3	0.02		0.09
2081.0	H3N5F1	1.49	0.55	0.25	2850.4	S1H5N5F1		0.05	1.23
2156.0	S1H4N3F1		0.09	0.16	2866.4	H6N5F2	0.07		0.06
2173.0	H5N3F2	0.06		0.01	2880.4	S1H6N5	0.15	0.06	0.10
2186.0	S1H5N3	0.01	0.10	0.14	2921.4	S1H5N6	0.06		
2192.0	H8N2	12.33	18.38	4.48	2938.4	H6N6F1	2.08	0.71	0.36
2203.0	H6N3F1	0.17	0.04	0.03	2966.4	S2H5N4F1	0.03	0.23	0.59
2214.1	H4N4F2	0.47	0.11	0.07	2979.4	H5N7F1	0.02		
2216.1	G1H5N3	0.03			3026.4	G2H5N4F1			0.01
2227.1	S1H4N4			0.06	3041.4	H6N5F3			0.02
2244.1	H5N4F1	4.48	3.72	17.28	3054.5	S1H6N5F1	0.05	0.06	1.66
2255.1	H3N5F2			0.01	3084.5	S1H7N5	0.08		0.01
2274.1	H6N4	0.25	0.10	0.10	3112.5	H6N6F2	0.01		0.01
2285.1	H4N5F1	2.38	1.81	3.82	3125.5	S1H6N6	0.31	0.09	
2315.1	H5N5			0.32	3142.5	H7N6F1	0.61	0.15	0.19
2326.1	H3N6F1	0.73	0.20	0.02	3183.5	H6N7F1	0.06		
2330.1	S1H4N3F2	0.49			3211.5	S2H5N5F1			0.02
2360.1	S1H5N3F1		0.03	0.07	3215.5	H6N5F4			0.01
2390.1	S1H6N3			0.05	3228.6	S1H6N5F2			0.02
2396.1	H9N2	3.54	6.28	2.70	3299.6	S1H6N6F1			0.05
2401.1	S1H4N4F1			0.21	3316.6	H7N6F2	0.02		
2418.2	H5N4F2	0.65	0.31	1.86	3330.6	S1H7N6	0.34	0.10	
2431.2	S1H5N4	0.38	0.43	2.49	3346.6	H8N6F1	0.05		
2448.2	H6N4F1	0.55	0.12	0.06	3387.6	H7N7F1			0.03
2459.2	H4N5F2		0.07	0.26	3416.6	S2H6N5F1			0.09
2461.2	G1H5N4	0.02			3503.7	S1H7N6F1			0.52
2478.2	H7N4	0.12			3533.7	S1H8N6	0.13		
2489.2	H5N5F1	1.64	1.55	11.06	3864.9	S2H7N6F1			0.02

Table 6. The average relative amounts of all PNGase F-released N-glycans of undifferentiated ESCs, definitive endoderm cells (DEC) and hepatocyte-like cells (HLC) derived from seven (ESCs and HLCs) and four (DECs) different preparations. H: hexose, N: N-acetylhexosamine, F: deoxyhexose, S: N-acetylneuraminic acid.

Proposed N-glycan structure			Consecutive Enzymatic Digestions				
m/z	Composition	Proposed Structure	N	G4	F3,4	G4	F
1171.5	H3N2		ud	ud	ud	ud	ud
1345.5	H3N2F1		ud	ud	ud	ud	d
1375.6	H4N2		ud	ud	ud	ud	ud
1416.6	H3N3		ud	ud	ud	ud	ud
1579.6	H5N2		ud	ud	ud	ud	ud
1590.6	H3N3F1		ud	ud	ud	ud	d
1620.7	H4N3		ud	ud	ud	ud	ud
1661.7	H3N4		ud	ud	ud	ud	ud
1783.7	H6N2		ud	ud	ud	ud	ud
1794.7	H4N3F1		ud	ud	ud	ud	d
1824.7	H5N3		ud	ud	ud	ud	ud
1835.7	H3N4F1		ud	ud	ud	ud	d
1865.7	H4N4		ud	d	ud	ud	ud
1987.7	H7N2		ud	ud	ud	ud	ud
1998.7	H5N3F1		ud	d	ud	ud	d
2028.8	H6N3		ud	d	ud	ud	ud
2039.8	H4N4F1		ud	d	ud	ud	d
2069.8	H5N4		ud	d	ud	ud	ud

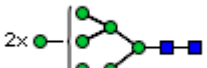
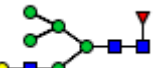



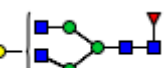
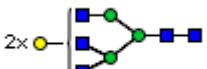


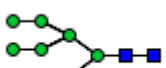

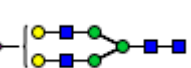
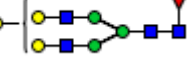
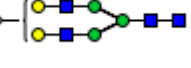




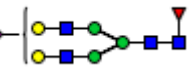
2080.8	H3N5F1		ud	ud	ud	ud	d
2191.8	H8N2		ud	ud	ud	ud	ud
2213.8	H4N4F2		ud	ud	d	d	d
2226.8	S1H4N4		d	d	ud	ud	ud
2243.8	H5N4F1		ud	d	ud	ud	d
2284.8	H4N5F1		ud	d	ud	ud	d
2314.8	H5N5		ud	d	ud	ud	ud
2325.8	H3N6F1		ud	ud	ud	ud	d
2389.9	S1H6N3		d	d	ud	ud	ud
2395.9	H9N2		ud	ud	ud	ud	ud
2417.9	H5N4F2		ud	d	d	d	d
2430.9	S1H5N4		d	d	ud	ud	ud
2458.9	H4N5F2		ud	ud	d	d	d
2488.9	H5N5F1		ud	d	ud	ud	d
2499.9	H3N6F2		ud	ud	d	ud	d
2518.9	H6N5		ud	d	ud	ud	ud
2604.9	S1H5N4F1		d	d	ud	ud	d

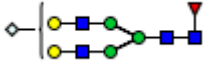
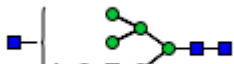
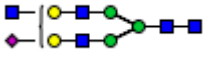
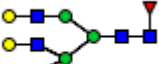

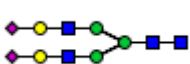
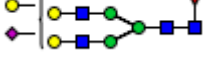

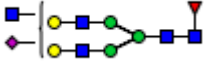
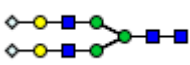



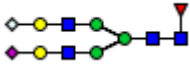
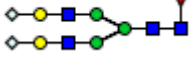


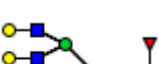
2634.9	S1H6N4		d	d	ud	ud	ud
2645.9	S1H4N5F1		d	d	ud	ud	d
2663.1	H5N5F2		ud	d	d	d	d
2674.1	H3N6F3		ud	ud	d	ud	d
2693.1	H6N5F1		ud	d	ud	ud	d
2779.1	S1H5N4F2		d	d	d	d	d
2792.1	S2H5N4		d	d	ud	ud	ud
2820.1	S1H4N5F2		d	d	d	d	d
2850.1	S1H5N5F1		d	d	ud	ud	d
2880.1	S1H6N5		d	d	ud	ud	ud
2938.1	H6N6F1		ud	d	ud	ud	d
2966.1	S2H5N4F1		d	d	ud	ud	d
2996.1	S1G1H5N4F1		d	d	ud	ud	d
3007.1	S2H4N5F1		d	d	ud	ud	d
3024.1	S1H5N5F2		d	d	d	d	d
3054.1	S1H6N5F1		d	d	ud	ud	d


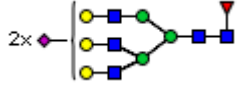






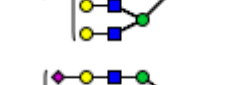
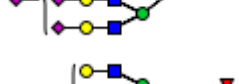

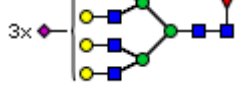
3228.1	S1H6N5F2		d	d	d	d	d
3241.1	S2H6N5	2x	d	d	ud	ud	ud
3299.1	S1H6N6F1		d	d	ud	ud	d
3416.1	S2H6N5F1	2x	d	d	ud	ud	d
3504.1	S1H7N6F1		d	d	ud	ud	d
3590.1	S2H6N5F2	2x	d	d	d	d	d
3602.1	S3H6N5		d	d	ud	ud	ud
3678.1	S1H7N6F2		d	d	d	d	d
3776.2	S3H6N5F1		d	d	ud	ud	d
3864.2	S2H7N6F1	2x	d	d	ud	ud	d
3964.2	S4H6N5		d	d	ud	ud	ud
4039.2	S2H7N6F2	2x	d	d	d	d	d
4226.3	S3H7N6F1	3x	d	d	ud	ud	d
4400.4	S3H7N6F2	3x	d	d	d	d	d
4587.4	S4H7N6F1		d	d	ud	ud	d

Exoglycosidase digestion Table 1. Exoglycosidase digestions of PNGase F-released N-glycans derived from HEK 293 cells. N: *Arthrobacter ureafaciens* neuraminidase, G4: $\beta(1-4)$ galactosidase from *Streptococcus pneumoniae*, F3,4: almond meal $\alpha(1-3,4)$ fucosidase, F: Bovine kidney $\alpha(1-2,3,4,6)$ fucosidase. The presence of Lewis^x antennae was demonstrated by exoglycosidase digestions. The cartoons imply neither a specific glycan isomer nor allocation of the Lewis^x motif to a distinct antenna. Note that some low abundant structures were not observed in the mass spectrum after exoglycosidase digestion and were therefore not listed here. d: digested, ud: undigested, H: hexose, N: N-acetylhexosamine, F: deoxyhexose, S: N-acetylneuraminic acid, G: N-glycolylneuraminic acid. Blue square represents N-acetylglucosamine, yellow square N-acetylgalactosamine, white square N-acetylhexosamine, green circle mannose, yellow circle galactose, red triangle fucose, pink diamond N-acetylneuraminic acid and white diamond N-glycolylneuraminic acid.

Proposed N-glycan structure			Consecutive Enzymatic Digestions				
m/z	Composition	Proposed Structure	N	G4	F3,4	G4	F
1171.5	H3N2		ud	ud	ud	ud	ud
1345.5	H3N2F1		ud	ud	ud	ud	d
1375.6	H4N2		ud	ud	ud	ud	ud
1416.6	H3N3		ud	ud	ud	ud	ud
1579.6	H5N2		ud	ud	ud	ud	ud
1590.6	H3N3F1		ud	ud	ud	ud	d
1620.7	H4N3		ud	ud	ud	ud	ud
1661.7	H3N4		ud	ud	ud	ud	ud
1783.7	H6N2		ud	ud	ud	ud	ud
1794.7	H4N3F1		ud	ud	ud	ud	d
1824.7	H5N3		ud	ud	ud	ud	ud
1835.7	H3N4F1		ud	ud	ud	ud	d
1865.7	H4N4		ud	d	ud	ud	ud
1981.7	S1H4N3		d	d	ud	ud	ud
1987.7	H7N2		ud	ud	ud	ud	ud
1998.7	H5N3F1		ud	d	ud	ud	d
2028.8	H6N3		ud	d	ud	ud	ud
2039.8	H4N4F1		ud	d	ud	ud	d
2069.8	H5N4		ud	d	ud	ud	ud
2080.8	H3N5F1		ud	ud	ud	ud	d

2191.8	H8N2		ud	ud	ud	ud	ud
2202.8	H6N3F1		ud	d	ud	ud	d
2226.8	S1H4N4		d	d	ud	ud	ud
2243.8	H5N4F1		ud	d	ud	ud	d
2273.8	H6N4		ud	d	ud	ud	ud
2284.8	H4N5F1		ud	d	ud	ud	d
2314.8	H5N5		ud	d	ud	ud	ud
2359.9	S1H5N3F1		d	d	ud	ud	d
2389.9	S1H6N3		d	d	ud	ud	ud
2395.9	H9N2		ud	ud	ud	ud	ud
2417.9	H5N4F2		ud	d	d	d	d
2430.9	S1H5N4		d	d	ud	ud	ud
2447.9	H6N4F1		ud	d	ud	ud	d
2460.9	G1H5N4		d	d	ud	ud	ud
2477.9	H7N4		ud	d	ud	ud	ud
2488.9	H5N5F1		ud	d	ud	ud	d
2518.9	H6N5		ud	d	ud	ud	ud
2563.9	S1H6N3F1		d	d	ud	ud	d
2604.9	S1H5N4F1		d	d	ud	ud	d

2634.9	G1H5N4F1		d	d	ud	ud	ud
2665.1	G1H6N4		d	d	ud	ud	ud
2676.1	S1H5N5		d	d	ud	ud	ud
2693.1	H6N5F1		ud	d	ud	ud	d
2779.1	S1H5N4F2		d	d	d	d	d
2792.1	S2H5N4		d	d	ud	ud	ud
2809.1	S1H6N4F1		d	d	ud	ud	d
2822.1	S1G1H5N4		d	d	ud	ud	ud
2850.1	S1H5N5F1		d	d	ud	ud	d
2852.1	G2H5N4		d	d	ud	ud	ud
2880.1	S1H6N5		d	d	ud	ud	ud
2897.1	H7N5F1		ud	d	ud	ud	d
2966.1	S2H5N4F1		d	d	ud	ud	d
2996.1	S1G1H5N4F 1		d	d	ud	ud	d
3026.1	G2H5N4F1		d	d	ud	ud	d
3054.1	S1H6N5F1		d	d	ud	ud	d
3084.1	G1H6N5F1		d	d	ud	ud	d
3142.1	H7N6F1		ud	d	ud	ud	d

3241.1	S2H6N5		d	d	ud	ud	ud
3416.1	S2H6N5F1		d	d	ud	ud	d
3504.1	S1H7N6F1		d	d	ud	ud	d
3602.1	S3H6N5		d	d	ud	ud	ud
3620.1	S2H7N5F1		d	d	ud	ud	d
3691.1	S2H7N6		d	d	ud	ud	ud
3776.2	S3H6N5F1		d	d	ud	ud	d
3864.2	S2H7N6F1		d	d	ud	ud	d
3964.2	S4H6N5		d	d	ud	ud	ud
4069.3	S2H8N6F1		d	d	ud	ud	d
4226.3	S3H7N6F1		d	d	ud	ud	d
4587.4	S4H7N6F1		d	d	ud	ud	d

Exoglycosidase digestion Table 2. Exoglycosidase digestions of PNGase F-released N-glycans derived from CHO cells. N: *Arthrobacter ureafaciens* neuraminidase, G4: $\beta(1-4)$ galactosidase from *Streptococcus pneumoniae*, F3,4: almond meal $\alpha(1-3,4)$ fucosidase, F: Bovine kidney $\alpha(1-2,3,4,6)$ fucosidase. The presence of Lewis^x antennae was demonstrated by exoglycosidase digestions. The cartoons imply neither a specific glycan isomer nor allocation of the LewisX motif to a distinct antennae. Note that some low abundant structures were not observed in the mass spectrum after exoglycosidase digestion and were therefore not listed here. d: digested, ud: undigested, H: hexose, N: N-acetylhexosamine, F: deoxyhexose, S: N-acetylneuraminic acid, G: N-glycolylneuraminic acid. Blue square represents N-acetylglucosamine, green circle mannose, yellow circle galactose, red triangle fucose, pink diamond N-acetylneuraminic acid and white diamond N-glycolylneuraminic acid.


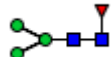
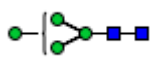
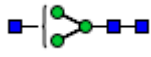
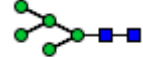
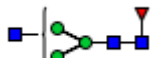
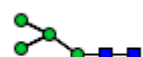



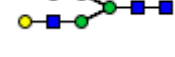


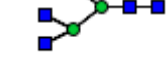
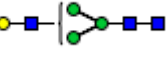
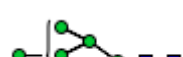
Proposed N-glycan structure			Consecutive Enzymatic Digestions				
m/z	Composition	Proposed Structure	N	G4	F3,4	G4	F
1171.5	H3N2		ud	ud	ud	ud	ud
1345.5	H3N2F1		ud	ud	ud	ud	d
1375.6	H4N2		ud	ud	ud	ud	ud
1416.6	H3N3		ud	ud	ud	ud	ud
1579.6	H5N2		ud	ud	ud	ud	ud
1590.6	H3N3F1		ud	ud	ud	ud	d
1620.7	H4N3		ud	ud	ud	ud	ud
1783.7	H6N2		ud	ud	ud	ud	ud
1794.7	H4N3F1		ud	ud	ud	ud	d
1824.7	H5N3		ud	ud	ud	ud	ud
1835.7	H3N4F1		ud	ud	ud	ud	d
1865.7	H4N4		ud	d	ud	ud	ud
1987.7	H7N2		ud	ud	ud	ud	ud
1998.7	H5N3F1		ud	d	ud	ud	d
2028.8	H6N3		ud	d	ud	ud	ud
2039.8	H4N4F1		ud	d	ud	ud	d
2069.8	H5N4		ud	d	ud	ud	ud
2191.8	H8N2		ud	ud	ud	ud	ud

2202.8	H6N3F1		ud	d	ud	ud	d
2226.8	S1H4N4		d	d	ud	ud	ud
2243.8	H5N4F1		ud	d	ud	ud	d
2256.8	G1H4N4		d	d	ud	ud	ud
2284.8	H4N5F1		ud	d	ud	ud	d
2314.8	H5N5		ud	d	ud	ud	ud
2359.9	S1H5N3F1		d	d	ud	ud	d
2389.9	S1H6N3		d	d	ud	ud	ud
2395.9	H9N2		ud	ud	ud	ud	ud
2400.9	S1H4N4F1		d	d	ud	ud	d
2417.9	H5N4F2		ud	d	d	d	d
2430.9	S1H5N4		d	d	ud	ud	ud
2460.9	H5N4G1		d	d	ud	ud	ud
2488.9	H5N5F1		ud	d	ud	ud	d
2591.9	H5N4F3		ud	ud	d	d	d
2604.9	S1H5N4F1		d	d	ud	ud	d
2634.9	S1H6N4		d	d	ud	ud	d
2693.1	H6N5F1		ud	d	ud	ud	d

2779.1	S1H5N4F2		d	d	d	d	d
2792.1	S2H5N4		d	d	ud	ud	ud
2867.1	H6N5F2		ud	d	d	d	d
2966.1	S2H5N4F1		d	d	ud	ud	d
3041.1	H6N5F3		ud	d	d	d	d
3054.1	S1H6N5F1		d	d	ud	ud	d
3215.1	H6N5F4		ud	ud	d	d	d
3228.1	S1H6N5F2		d	d	d	d	d
3403.1	S1H6N5F3		d	d	d	d	d
3416.1	S2H6N5F1		d	d	ud	ud	d
3491.1	H7N6F3		ud	d	d	d	d
3590.1	S2H6N5F2		d	d	d	d	d
3665.1	H7N6F4		ud	d	d	d	d

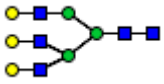
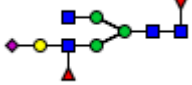
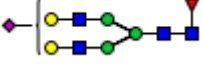
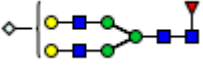

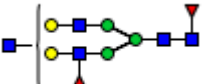
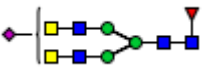
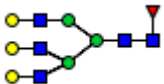
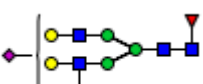





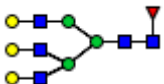
3678.1	S1H7N6F2		d	d	d	d	d
3839.2	H7N6F5		ud	ud	d	d	d
3852.2	S1H7N6F3		d	d	d	d	d
3864.2	S2H7N6F1	2x	d	d	ud	ud	d
4026.2	S1H7N6F4		d	d	d	d	d
4039.2	S2H7N6F2	2x	d	d	d	d	d
4213.3	S2H7N6F3	2x	d	d	d	d	d
4226.3	S3H7N6F1	3x	d	d	ud	ud	d
4400.4	S3H7N6F2	3x	d	d	d	d	d

Exoglycosidase digestion Table 3. Exoglycosidase digestions of PNGase F-released N-glycans derived from AGE1.HN cells. N: *Arthrobacter ureafaciens* neuraminidase, G4: $\beta(1-4)$ galactosidase from *Streptococcus pneumoniae*, F3,4: almond meal $\alpha(1-3,4)$ fucosidase, F: Bovine kidney $\alpha(1-2,3,4,6)$ fucosidase. The presence of Lewis^x antennae was demonstrated by exoglycosidase digestions. The cartoons imply neither a specific glycan isomer nor allocation of the LewisX motif to a distinct antennae. Note that some low abundant structures were not observed in the mass spectrum after exoglycosidase digestion and were therefore not listed here. d: digested, ud: undigested, H: hexose, N: N-acetylhexosamine, F: deoxyhexose, S: N-acetylneuraminic acid, G: N-glycolylneuraminic acid. Blue square represents N-acetylglucosamine, green circle mannose, yellow circle galactose, red triangle fucose, pink diamond N-acetylneuraminic acid and white diamond N-glycolylneuraminic acid.

Proposed N-glycan structures			Consecutive Enzymatic Digestions				
m/z	Composition	Proposed Structure	N	G4	F3,4	G4	F
1171.5	H3N2		ud	ud	ud	ud	ud
1345.5	H3N2F1		ud	ud	ud	ud	d
1375.6	H4N2		ud	ud	ud	ud	ud
1416.6	H3N3		ud	ud	ud	ud	ud
1579.6	H5N2		ud	ud	ud	ud	ud
1590.6	H3N3F1		ud	ud	ud	ud	d
1783.7	H6N2		ud	ud	ud	ud	ud
1794.7	H4N3F1		ud	ud	ud	ud	d
1824.7	H5N3		ud	ud	ud	ud	ud
1835.7	H3N4F1		ud	ud	ud	ud	d
1865.7	H4N4		ud	ud	ud	ud	ud
1981.7	S1H4N3		d	d	ud	ud	ud
1987.7	H7N2		ud	ud	ud	ud	ud
1998.7	H5N3F1		ud	d	ud	ud	d
2028.8	H6N3		ud	d	ud	ud	ud
2039.8	H4N4F1		ud	d	ud	ud	d

2069.8	H5N4		ud	d	ud	ud	ud
2080.8	H3N5F1		ud	ud	ud	ud	d
2155.8	S1H4N3F1		d	d	ud	ud	d
2185.8	S1H5N3		d	d	ud	ud	ud
2191.8	H8N2		ud	ud	ud	ud	ud
2213.8	H4N4F2		ud	ud	d	d	d
2226.8	S1H4N4		d	d	ud	ud	ud
2243.8	H5N4F1		ud	d	ud	ud	d
2314.8	H5N5		ud	d	ud	ud	ud
2325.8	H3N6F1		ud	ud	ud	ud	d
2359.9	S1H5N3F1		d	d	ud	ud	d
2389.9	S1H6N3		d	d	ud	ud	ud
2395.9	H9N2		ud	ud	ud	ud	ud
2400.9	S1H4N4F1		d	ud	ud	d	d
2417.9	H5N4F2		ud	d	d	d	d
2430.9	S1H5N4		d	d	ud	ud	ud
2460.9	G1H5N4		d	d	ud	ud	ud
2488.9	H5N5F1		ud	d	ud	ud	d

APPENDIX

2518.9	H6N5		ud	d	ud	ud	ud
2574.9	S1H4N4F2		d	ud	d	d	d
2604.9	S1H5N4F1		d	d	ud	ud	d
2634.9	G1H5N4F1		d	d	ud	ud	d
2645.9	S1H4N5F1		d	d	ud	ud	d
2663.1	H5N5F2		ud	d	d	d	d
2687.1	S1H3N6F1		d	ud	ud	ud	d
2693.1	H6N5F1		ud	d	ud	ud	d
2779.1	S1H5N4F2		d	d	d	d	d
2792.1	S2H5N4		d	d	ud	ud	ud
2820.1	S1H4N5F2		d	ud	d	d	d
2822.1	S1G1H5N4		d	d	ud	ud	ud
2833.1	S2H4N5		d	d	ud	ud	ud
2850.1	S1H5N5F1		d	d	ud	ud	d
2867.1	H6N5F2		ud	d	d	d	d

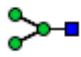
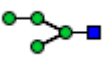
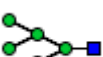
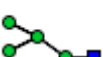



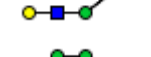

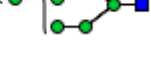

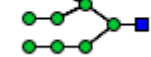
2880.1	S1H6N5		d	d	ud	ud	ud
2966.1	S2H5N4F1		d	d	ud	ud	d
2996.1	S1G1H5N4F1		d	d	ud	ud	d
3007.1	S2H4N5F1		d	d	ud	ud	d
3024.1	S1H5N5F2		d	d	d	d	d
3026.1	G2H5N4F1		d	d	ud	ud	d
3037.1	S2H5N5		d	d	ud	ud	ud
3048.1	S2H3N6F1		d	ud	ud	ud	d
3054.1	S1H6N5F1		d	d	ud	ud	d
3140.1	S2H5N4F2		d	d	d	d	d
3170.1	S1G1H5N4F2		d	d	d	d	d
3211.1	S2H5N5F1		d	d	ud	ud	d
3228.1	S1H6N5F2		d	d	d	d	d
3241.1	S2H6N5		d	d	ud	ud	ud
3403.1	S1H6N5F3		d	d	d	d	d
3416.1	S2H6N5F1		d	d	ud	ud	d

3504.1	S1H7N6F1		d	d	ud	ud	d
3590.1	S2H6N5F2	2x	d	d	d	d	d
3602.1	S3H6N5		d	d	ud	ud	ud
3678.1	S1H7N6F2		d	d	d	d	d
3691.1	S2H7N6	2x	d	d	ud	ud	ud
3763.2	S2H6N5F3	2x	d	d	d	d	d
3776.2	S3H6N5F1		d	d	ud	ud	d
3806.2	S2G1H6N5F1	2x	d	d	ud	ud	d
3852.2	S1H7N6F3		d	d	d	d	d
3864.2	S2H7N6F1	2x	d	d	ud	ud	d
3951.2	S3H6N5F2		d	d	d	d	d
3964.2	S4H6N5		d	d	ud	ud	ud
4039.2	S2H7N6F2	2x	d	d	d	d	d

4125.3	S3H6N5F3		d	d	d	d	d
4213.3	S2H7N6F3		d	d	d	d	d
4226.3	S3H7N6F1		d	d	ud	ud	d
4400.4	S3H7N6F2		d	d	d	d	d
4574.4	S3H7N6F3		d	d	d	d	d
4587.4	S4H7N6F1		d	d	ud	ud	d
4761.5	S4H7N6F2		d	d	d	d	d
4935.6	S4H7N6F3		d	d	d	d	d
5025.6	S1G3H7N6F3		d	d	d	d	d


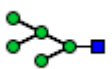

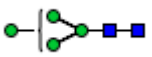
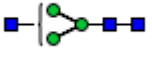
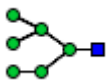

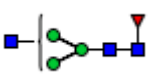
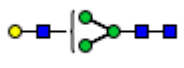

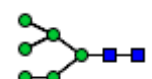





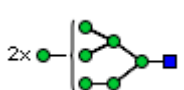


Exoglycosidase digestion Table 4. Exoglycosidase digestions of PNGase F-released N-glycans derived from HEP G2 cells. N: *Arthrobacter ureafaciens* neuraminidase, G4: $\beta(1-4)$ galactosidase from *Streptococcus pneumoniae*, F3,4: almond meal $\alpha(1-3,4)$ fucosidase, F: Bovine kidney $\alpha(1-2,3,4,6)$ fucosidase. The presence of Lewis^x antennae was demonstrated by exoglycosidase digestions. The cartoons imply neither a specific glycan isomer nor allocation of the Lewis^x motif to a distinct antennae. Note that some low abundant structures were not observed in the mass spectrum after exoglycosidase digestion and were therefore not listed here. d: digested, ud: undigested, H:

hexose, N: N-acetylhexosamine, F: deoxyhexose, S: N-acetylneuraminic acid, G: N-glycolylneuraminic acid. Blue square represents N-acetylglucosamine, yellow square N-acetylgalactosamine, white square N-acetylhexosamine, green circle mannose, yellow circle galactose, red triangle fucose, pink diamond N-acetylneuraminic acid and white diamond N-glycolylneuraminic acid.

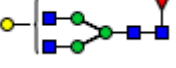
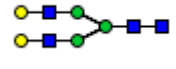

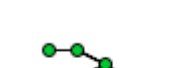
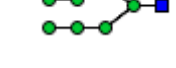
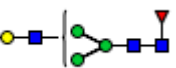
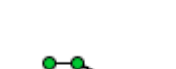
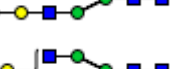
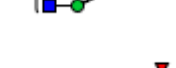

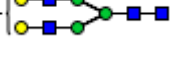

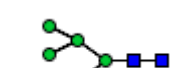
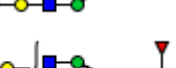




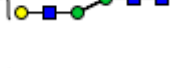
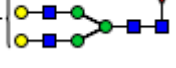
Found N-glycan structures			Cell type			Consecutive Enzymatic Digestions			
m/z	Composition	Proposed Structure	MSC	A day 5	A day 15	N	G4	H	M
926.4	H3N1		x	x	x	ud	ud	ud	ud
1130.5	H4N1		x	x	x	ud	ud	ud	ud
1334.6	H5N1		x	x	x	ud	ud	ud	d
1538.7	H6N1		x	x	x	ud	ud	ud	d
1579.7	H5N2		x	x	x	ud	d	d	d
1742.8	H7N1		x	x	x	ud	ud	ud	d
1783.8	H6N2		x	x	x	ud	d	d	d
1940.9	S1H5N2		x	x	x	d	d	d	d
1946.9	H8N1		x	x	x	ud	ud	ud	d
2145.0	S1H6N2		x	x	x	d	d	d	d
2151.0	H9N1		x	x	x	ud	ud	ud	d
2355.1	H10N1		x	x	x	ud	ud	ud	d

Exoglycosidase digestion Table 5. Exoglycosidase digestions of Endo H-released N-glycans derived from undifferentiated and adipogenically differentiated bone marrow MSCs. N: *Arthrobacter ureafaciens* neuraminidase; G4: $\beta(1-4)$ galactosidase from *Streptococcus pneumoniae*, H: β -N-acetylhexosaminidase recombinant from *Streptococcus pneumoniae*, expressed in *Escherichia coli*, M: α Mannosidase from *Canavalia ensiformis*. X denotes the presence of a peak in the MALDI-TOF mass spectra of the corresponding N-glycome of MSCs or adipogenically differentiated MSCs (A) day 5 and 15 of differentiation. d: digested, ud: undigested. H: hexose, N: N-acetylhexosamine, S: N-acetylneuraminic acid. Blue square represents N-acetylglucosamine, green circle mannose, yellow circle galactose, red triangle fucose and pink diamond N-acetylneuraminic acid.

APPENDIX

Found N-glycan structure			Cell type			Consecutive Enzymatic Digestions			
m/z	Composition	Proposed Structure	MSC	A day 5	A day 15	N	G	H	F
1171.6	H3N2		x	x	x	ud	ud	ud	ud
1334.6	H5N1		x	x	x	ud	ud	ud	ud
1345.6	H3N2F1		x	x	x	ud	ud	ud	d
1375.6	H4N2		x	x	x	ud	ud	ud	ud
1416.7	H3N3		x	x	x	ud	ud	d	ud
1538.7	H6N1		x	x	x	ud	ud	ud	ud
1579.7	H5N2		x	x	x	ud	ud	ud	ud
1590.8	H3N3F1		x	x	x	ud	ud	d	d
1620.8	H4N3		x	x	x	ud	d	d	ud
1742.8	H7N1		x	x	x	ud	ud	ud	ud
1783.8	H6N2		x	x	x	ud	ud	ud	ud
1794.9	H4N3F1		x	x	x	ud	d	d	d
1824.9	H5N3		x	x	x	ud	d	d	ud
1835.9	H3N4F1		x	x	x	ud	ud	d	d
1865.9	H4N4		x	x	x	ud	ud	d	ud
1940.9	S1H5N2		x	x	x	d	d	d	ud
1946.9	H8N1		x	x	x	ud	ud	ud	ud
1981.9	S1H4N3		x	x	x	d	d	d	ud
1999.0	H5N3F1		x	x	x	ud	d	d	d

APPENDIX

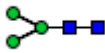
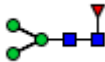
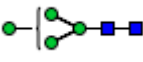
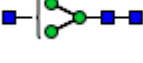
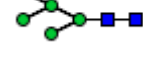
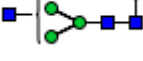
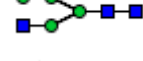

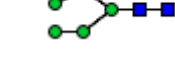
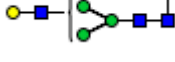




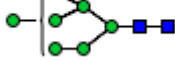

2040.0	H4N4F1		x	x	x	ud	d	d	d
2070.0	H5N4		x	x	x	ud	d	d	ud
2145.0	S1H6N2		x	x	x	d	d	d	ud
2151.0	H9N1		x	x	x	ud	ud	ud	ud
2156.0	S1H4N3F1		x	x	x	d	d	d	d
2186.0	S1H5N3		x	x	x	d	d	d	ud
2227.1	S1H4N4		x	x	x	d	d	d	ud
2244.1	H5N4F1		x	x	x	ud	d	d	d
2274.1	H6N4		x	x	x	ud	d	d	ud
2360.1	S1H5N3F1		x	x	x	d	d	d	d
2390.1	S1H6N3		x	x	x	d	d	d	ud
2401.1	S1H4N4F1		x	x	x	d	d	d	d
2431.2	S1H5N4		x	x	x	d	d	d	ud
2461.2	G1H5N4		x	x	x	d	d	d	ud
2489.2	H5N5F1		x	x	x	ud	d	d	d
2519.2	H6N5		x	x	x	ud	d	d	ud
2605.3	S1H5N4F1		x	x	x	d	d	d	d
2635.3	S1H6N4		x	x	x	d	d	d	d
2693.3	H6N5F1		x	x	x	ud	d	d	d
2751.3	S2H6N3		x	x		d	d	d	ud

APPENDIX

2792.3	S2H5N4		x	x	x	d	d	d	ud
2850.4	S1H5N5F1		x	x	x	d	d	d	d
2880.4	S1H6N5		x	x	x	d	d	d	ud
2966.4	S2H5N4F1		x	x	x	d	d	d	d
2996.4	S2H6N4		x	x	x	d	d	d	d
3054.5	S1H6N5F1		x	x	x	d	d	d	d
3084.5	H7N5S1		x	x	x	d	d	d	d
3142.5	H7N6F1		x	x	x	ud	d	d	d
3329.6	S1H7N6		x	x	x	d	d	d	ud
3415.7	S2H6N5F1		x	x	x	d	d	d	d
3445.7	S2H7N5		x	x	x	d	d	d	d
3503.7	S1H7N6F1		x	x	x	d	d	d	d
3602.7	S3H6N5		x	x	x	d	d	d	ud
3690.8	S2H7N6		x	x	x	d	d	d	ud
3776.8	S3H6N5F1		x	x	x	d	d	d	d
3806.8	S3H7N5		x	x	x	d	d	d	d
3864.9	S2H7N6F1		x	x	x	d	d	d	d
3894.9	S2H8N6		x	x		d	d	d	d

3964.9	S4H6N5			x	x	d	d	d	ud
4052.0	S3H7N6		x			d	d	d	ud
4226.1	S3H7N6F1		x	x	x	d	d	d	d
4587.3	S4H7N6F1		x	x	x	d	d	d	d

Exoglycosidase digestion Table 6. Exoglycosidase digestions of PNGase F-released N-glycans derived from undifferentiated and adipogenically differentiated bone marrow MSCs. N: *Arthrobacter ureafaciens* neuraminidase, G: Bovine testes β -galactosidase, H: β -N-acetylhexosaminidase recombinant from *Streptococcus pneumoniae*, expressed in *Escherichia coli*, F: Bovine kidney α (1-2,3,4,6) fucosidase. X denotes the presence of a peak in the MALDI-TOF mass spectra of the corresponding N-glycome of MSCs or adipogenically differentiated MSCs (A) day 5 and 15 of differentiation. Note that some low abundant structures were not observed in the mass spectrum after exoglycosidase digestion and were therefore not listed here. d: digested, ud: undigested. H: hexose, N: N-acetylhexosamine, F: deoxyhexose, S: N-acetylneuraminic acid. Blue square represents N-acetylglucosamine, yellow square N-acetylgalactosamine, white square N-acetylhexosamine, green circle mannose, yellow circle galactose, red triangle fucose, pink diamond N-acetylneuraminic acid and white diamond N-glycolylneuraminic acid.

Found N-glycan structures			Cell type		Consecutive Enzymatic Digestions					
m/z	Composition	Proposed Structure	MSC	C day 28	N	G4	F3,4	G4	F	M
1171.6	H3N2		x	x	ud	ud	ud	ud	ud	d
1345.6	H3N2F1		x	x	ud	ud	ud	ud	d	d
1375.6	H4N2		x	x	ud	ud	ud	ud	ud	d
1416.7	H3N3		x	x	ud	ud	ud	ud	ud	d
1579.7	H5N2		x	x	ud	ud	ud	ud	ud	d
1590.8	H3N3F1		x	x	ud	ud	ud	ud	d	d
1620.8	H4N3		x	x	ud	ud	ud	ud	ud	ud
1783.8	H6N2		x	x	ud	ud	ud	ud	ud	d
1794.9	H4N3F1		x	x	ud	ud	ud	ud	d	d
1824.9	H5N3		x	x	ud	ud	ud	ud	ud	d
1865.9	H4N4		x	x	ud	ud	ud	d	ud	ud
1987.9	H7N2		x	x	ud	ud	ud	ud	ud	d
1999.0	H5N3F1		x	x	ud	d	ud	ud	d	d
2029.0	H6N3		x	x	ud	d1	ud	ud	ud	d
2040.0	H4N4F1		x	x	ud	ud	ud	ud	d	ud
2070.0	H5N4		x	x	ud	d	ud	ud	ud	ud

APPENDIX

2081.0	H3N5F1			x	ud	ud	ud	ud	d	ud
2192.0	H8N2		x	x	ud	ud	ud	ud	ud	d
2203.0	H6N3F1		x	x	ud	d	ud	ud	d	d
2244.1	H5N4F1		x	x	ud	d	ud	ud	d	ud
2360.1	S1H5N3F1		x	x	d	d	ud	ud	d	d
2390.1	S1H6N3		x	x	d	d	ud	ud	ud	d
2396.1	H9N2		x	x	ud	ud	ud	ud	ud	d
2401.1	S1H4N4F1		x	x	d	ud	ud	ud	d	ud
2418.2	H5N4F2		x	x	ud	d	d	d	d	ud
2431.2	S1H5N4		x	x	d	d	ud	ud	ud	ud
2461.2	G1H5N4		x	x	d	d	ud	ud	ud	ud
2489.2	H5N5F1		x	x	ud	d	ud	ud	d1	ud
2519.2	H6N5			x	ud	d	ud	ud	ud	ud
2605.3	S1H5N4F1		x	x	d	d	ud	ud	d	ud
2693.3	H6N5F1		x	x	ud	d	ud	ud	d	ud
2779.3	S1H5N4F2		x	x	d	d	d	d	d	ud
2792.3	S2H5N4		x	x	d	d	ud	ud	ud	ud
2822.4	S1G1H5N4		x	x	d	d	ud	ud	ud	ud

APPENDIX

2850.4	S1H5N5F1		x	x	d	d	ud	ud	d	ud
2880.4	S1H6N5		x	x	d	d	ud	ud	ud	ud
2966.4	S2H5N4F1		x	x	d	d	ud	ud	d	ud
2996.4	S1G1H5N4F1		x	x	d	d	ud	ud	d	ud
3026.4	G2H5N4F1		x	x	d	d	ud	ud	d	ud
3054.5	S1H6N5F1		x	x	d	d	ud	ud	d	ud
3142.5	H7N6F1		x	x	ud	d	ud	ud	d	ud
3228.6	S1H6N5F2			x	d	d	d	d	d	ud
3241.6	S2H6N5		x	x	d	d	ud	ud	ud	ud
3415.7	S2H6N5F1		x	x	d	d	ud	ud	d	ud
3503.7	S1H7N6F1		x	x	d	d	ud	ud	d	ud
3602.7	S3H6N5		x	x	d	d	ud	ud	ud	ud
3776.8	S3H6N5F1		x	x	d	d	ud	ud	d	ud
3864.9	S2H7N6F1		x	x	d	d	ud	ud	d	ud
4226.1	S3H7N6F1		x	x	d	d	ud	ud	d	ud
4587.3	S4H7N6F1		x	x	d	d	ud	ud	d	ud

Exoglycosidase digestion Table 7. Exoglycosidase digestions of PNGase F-released N-glycans derived from undifferentiated MSCs and day 28 of chondrogenically differentiated MSCs. N: *Arthrobacter ureafaciens* neuraminidase, G4: $\beta(1-4)$ galactosidase from *Streptococcus pneumoniae*, F3,4: almond meal $\alpha(1-3,4)$ fucosidase, F: Bovine kidney $\alpha(1-2,3,4,6)$ fucosidase, M: α Mannosidase from *Canavalia ensiformis*. The presence of LewisX antenna was established by exoglycosidase digestions. The cartoons imply neither a specific glycan isomer nor allocation of the LewisX motif to a distinct antennae. Note that some low abundant structures were not observed in the mass spectrum after exoglycosidase digestion and were therefore not listed here. d: digested, ud: undigested, H: hexose, N: N-acetylhexosamine, F: deoxyhexose, S: N-acetylneuraminic acid, G: N-glycolylneuraminic acid. Blue square represents N-acetylglucosamine, yellow square N-acetylgalactosamine, white square N-acetylhexosamine, green circle mannose, yellow circle galactose, red triangle fucose, pink diamond N-acetylneuraminic acid and white diamond N-glycolylneuraminic acid.

APPENDIX

m/z	Composition	Proposed Structure	N	G4	F3,4	G4	F	M
1171.6	H3N2		ud	ud	ud	ud	ud	d
1345.6	H3N2F1		ud	ud	ud	ud	d	d
1375.6	H4N2		ud	ud	ud	ud	ud	d
1416.7	H3N3		ud	ud	ud	ud	ud	d
1579.7	H5N2		ud	ud	ud	ud	ud	d
1590.8	H3N3F1		ud	ud	ud	ud	d	d
1620.8	H4N3		ud	d	ud	ud	ud	d
1661.8	H3N4		ud	ud	ud	ud	ud	ud
1783.8	H6N2		ud	ud	ud	ud	ud	d
1794.9	H4N3F1		ud	ud	ud	ud	d	d
1824.9	H5N3		ud	ud	ud	ud	ud	d
1835.9	H3N4F1		ud	ud	ud	ud	d	ud
1865.9	H4N4		ud	ud	ud	ud	ud	d
1987.9	H7N2		ud	ud	ud	ud	ud	d
1999.0	H5N3F1		ud	d	ud	ud	d	d
2029.0	H6N3		ud	d	ud	ud	ud	d
2040.0	H4N4F1		ud	d	ud	ud	d	ud
2070.0	H5N4		ud	d	ud	ud	ud	ud

APPENDIX

2081.0	H3N5F1		ud	ud	ud	ud	d	ud
2192.0	H8N2		ud	ud	ud	ud	ud	d
2214.1	H4N4F2		ud	ud	d	d	d	ud
2227.1	S1H4N4		d	d	ud	ud	ud	ud
2244.1	H5N4F1		ud	d	ud	ud	d	ud
2285.1	H4N5F1		ud	d	d	d	d	ud
2315.1	H5N5		ud	d	ud	ud	ud	ud
2390.1	S1H6N3		d	d	ud	ud	ud	d
2396.1	H9N2		ud	ud	ud	ud	ud	d7
2401.1	S1H4N4F1		d	d	ud	ud	d	ud
2418.2	H5N4F2		ud	d	d	d	d	ud
2431.2	S1H5N4		d	d	ud	ud	ud	ud
2459.2	H4N5F2		ud	ud	d	d	d	ud
2489.2	H5N5F1		ud	d	ud	ud	d	ud
2519.2	H6N5		ud	d	ud	ud	ud	ud
2605.3	S1H5N4F1		d	d	ud	ud	d	ud

APPENDIX

2646.3	S1H4N5F1		d	d	ud	ud	d	ud
2663.3	H5N5F2		ud	d	d	d	d	ud
2693.3	H6N5F1		ud	d	ud	ud	d	ud
2779.3	S1H5N4F2		d	d	d	d	d	ud
2792.3	S2H5N4		d	d	ud	ud	ud	ud
2850.4	S1H5N5F1		d	d	ud	ud	d	ud
2880.4	S1H6N5		d	d	ud	ud	ud	ud
2938.4	H6N6F1		ud	d	ud	ud	d	ud
2966.4	S2H5N4F1		d	d	ud	ud	d	ud
3054.5	S1H6N5F1		d	d	ud	ud	d	ud
3142.5	H7N6F1		ud	d	ud	ud	d	ud
3228.6	S1H6N5F2		d	d	d	d	d	ud
3299.6	S1H6N6F1		d	d	ud	ud	d	ud
3416.6	S2H6N5F1		d	d	ud	d	d	ud
3503.7	S1H7N6F1		d	d	ud	ud	d	ud
3864.9	S2H7N6F1		d	d	ud	ud	d	ud

Exoglycosidase digestion Table 8. Exoglycosidase digestions of PNGase F-released N-glycans derived from hepatocyte-like cells. N: *Arthrobacter ureafaciens* neuraminidase, G4: $\beta(1-4)$ galactosidase from *Streptococcus pneumoniae*, F3,4: almond meal $\alpha(1-3,4)$ fucosidase, F: Bovine kidney $\alpha(1-2,3,4,6)$ fucosidase, M: α Mannosidase from *Canavalia ensiformis*. The presence of LewisX antenna was established by exoglycosidase digestions. The cartoons imply neither a specific glycan isomer nor allocation of the LewisX motif to a distinct antennae. Note that some low abundant structures were not observed in the mass spectrum after exoglycosidase digestion and were therefore not listed here. d: digested, ud: undigested, H: hexose, N: N-acetylhexosamine, F: deoxyhexose, S: N-acetylneuraminic acid, G: N-glycolylneuraminic acid. Blue square represents N-acetylglucosamine, yellow square N-acetylgalactosamine, white square N-acetylhexosamine, green circle mannose, yellow circle galactose, red triangle fucose, pink diamond N-acetylneuraminic acid and white diamond N-glycolylneuraminic acid.